BY

29 OCTOBER 1979   YU. P. SAFRONOV AND YU. G. ANDRIANOV   1 OF 3

Translation

INFRARED TECHNOLOGY AND OUTER SPACE

By

Yu. P. Safronov and Yu. G. Andrianov

NOTE

JPRS publications contain information primarily from foreign
newspapers, periodicals and books, but also from news agency
transmissions and broadcasts. Materials from foreign-language
sources are translated; those from English-language sources
are transcribed or reprinted, with the original phrasing and
other characteristics retained.

Headlines, editorial reports, and material enclosed in brackets
[] are supplied by JPRS. Processing indicators such as [Text]
or [Excerpt] in the first line of each item, or following the
last line of a brief, indicate how the original information was
processed. Where no processing indicator is given, the infor-
mation was summarized or extracted.

Unfamiliar names rendered phonetically or transliterated are
enclosed in parentheses. Words or names preceded by a ques-
tion mark and enclosed in parentheses were not clear in the
original but have been supplied as appropriate in context.
Other unattributed parenthetical notes within the body of an
item originate with the source. Times within items are as
given by source.

The contents of this publication in no way represent the poli-
cies, views or attitudes of the U.S. Government.

For further information on report content
call (703) 351-2938 (economic); 3468
(political, sociological, military); 2726
(life sciences); 2725 (physical sciences).

FOR OFFICIAL USE ONLY

INFRARED TECHNOLOGY AND OUTER SPACE

CONTENTS   PAGE

- a -   [I - USSR - E FOUO]

l

FOR OFFICIAL USE ONLY

Page

CONTENTS (Continued)

- b -

FOR OFFICIAL USE ONLY

FOR OFFICIAL USE ONLY

FOR OFFICIAL USE ONLY

PUBLICATION DATA

English title   : INFRARED TECHNOLOGY AND OUTER SPACE

Russian title   : INFRAKRASNAYA TEKHNIKA I KOSMOS

Author (s)   : Yu. P. Safronov and Yu. G. Andrianov

Editor (s)   :

Publishing House   : Soviet Radio

Place of Publication   : Moscow

Date of Publication   : 1978

Signed to press   : 4 July 1978

Copies   : 5150

- d -

UDC 621.384.3:629.78

INFRARED TECHNOLOGY AND OUTER SPACE

Moscow INFRAKRASNAYA TEKHNIKA I KOSMOS in Russian 1978 pp signed to press
4 Jul 78 pp 1-248

[Book by Yu. P. Safronov, Sovetskoye Publishing House, 248 pages, 5,150
copies]

[Text] A study is made of the prospective areas of application of infrared
technology: space navigation, range measurements, tracking of targets in
outer space, space communications, astrophysical research and investigation
of the earth's resources.

The book is intended for specialists in the field of infrared engineering
and a broad class of readers interested in its application in the national
economy.

1

FOR OFFICIAL USE ONLY

FOREWORD

After the first artificial earth satellite was launched on 4 October 1957,
significant means were invested in the exploitation of space. In turn,
the development of space research is yielding ever newer perceptible,
at times entirely unexpected results with every passing year which confirm
the validity of the selected path and justify the expenditures on the
creation of space equipment and the development of cosmonautics. The great
progress which has been made both in the exploitation and discovery of the
secrets of the earth and in investigating the planets of the solar system
are evidence of this.

The space systems and objects are equipped with sensitive receptor elements,
by means of which information is picked up from the environment. These
include radio engineering, optical, barometric, magnetic, radiation and
other sensors which permit us to obtain a concept of the corresponding
characteristics of the outside world. Sensitive elements and systems
operating in the infrared range are playing an ever greater role in this
large complex of varied space receptors.

As is known, the instruments of infrared technology were used in a number
of areas in the national economy before the conquest of outer space began.
In industry the comparatively high penetrating capacity of infrared radia-
tion is used to dry paint and wood, which offers the possibility of improv-
ing the quality of products. Infrared instruments permit remote detection
of significant (to 0.01°C) local overheating of parts of various devices
by the infrared radiation (engines, electronic equipment, and so on).
Spectral measurements in the infrared range offer the possibility of chemical
analysis of materials. When using infrared photography it is possible to
read inscriptions and detect fingerprints which are not visible to the
naked eye and also to discover pictures hidden under a layer of paint.
Infrared technology has found application also in medicine, navigation and
other areas.

Along with its use in science and engineering, infrared technology has been
more and more widely introduced into military science, and, in the opinion
of foreign authors, there is every possibility of increasing its role and
significance in military engineering. By using infrared devices -- heat

2

FOR OFFICIAL USE ONLY

FOR OFFICIAL USE ONLY

direction finders -- it is possible to determine the directions of ships, aircraft, tanks and other targets which constitute heated bodies. The heat direction finders make it possible to detect targets also by the negative thermal contrast, for example, icebergs against the background of the ocean. Some forms of missiles are equipped with heat-sensitive homing devices. Communications systems have been developed on the basis of infra- red radiation which permit secret transmission of a variety of information.

The conquest of space is opening up new areas of application of infrared technology. They include the following: weather forecasting on the earth, space communications, the study of life on other planets, the investigation of the earth's resources, orientation of satellites and spacecraft, tracking of missiles and satellites and the solution of problems connected with the application of equipment for military purposes.

The various areas of application of infrared technology do not, however, mean that it holds a privileged position among other types of technology. By using infrared devices it is technically simpler to solve certain problems at the same time as other problems are better solved, for example, by using television or radar equipment.

In this book a study is made of the basic areas of the application of infra- red technology connected with the conquest of space. The book was written by published Soviet and foreign materials.

Yu. G. Andrianov wrote §1.2, 1.3, Chapter 2, §3.1-3.4, 4.4, 4.5, 7.4 and 7.5; Yu. P. Safronov wrote 4.3, Chapter 5, Chapter 6 and Chapter 8. The fore- word to the book was written by the authors jointly. The scientific editor of the book, A. S. Batrakov, wrote §1.1, 3.5, 4.1, 4.2, 7.1-7.3.

Let us take this opportunity to express our appreciation to candidates of technical sciences G. I. Leshev and A. S. Batrakov for careful examination of the manuscript and valuable suggestions.

3

FOR OFFICIAL USE ONLY

CHAPTER 1. BASIC AREAS OF APPLICATION AND OPERATING CHARACTERISTICS OF INFRARED SYSTEMS IN SPACE

1.1. Basic Areas of Use of Infrared Engineering in Space

In infrared equipment the information about the targets is obtained by analyzing the polarization intensity and the spectrum of their emission or the measurement of optical characteristics (integral and spectral radiation, reflection and transmission coefficients) in the infrared part of the spectrum.

The majority of infrared devices are passive type devices and record the characteristic thermal emission of the targets or the radiation of natural sources reflected by them (the sun, moons, stars) in the infrared range.

The characteristic thermal emission of bodies is most completely described by Planck's law characterizing the radiation distribution with respect to the spectrum as a function of the temperature of the emitter:

$$r_{\lambda,T} = \varepsilon_{\lambda,T} \frac{C_1}{\lambda^5} \frac{1}{\exp(C_2/\lambda T) - 1}, \tag{1.1}$$

where $r_{\lambda,T}$ is the spectral density of the radiation power, watts-m^{-2}-micron^{-1}; λ is the wave length, microns; T is the absolute temperature, K; $\varepsilon_{\lambda,T}$ is the spectral radiation coefficient; C_1 and C_2 are constants; $C_1 = 3.74 \cdot 10^{12}$ watts-microns^4-m^{-2}; $C_2 = 14385$ microns-deg.

For an absolutely black body ($\varepsilon_{\lambda,T} = 1$) and "gray" bodies ($\varepsilon_{\lambda,T} = \varepsilon < 1$) the maximum spectral density $r_{\lambda,T}$ is observed on a wave length of λ_m determined by Wien's law:

$$\lambda_m T = 2898 \text{ micron-deg} \tag{1.2}$$

About 71% of the energy emitted by a body is concentrated in the range of $0.5\lambda_m$ to $2.0\lambda_m$.

4

The total radiation power emitted by a body per unit surface is defined by the Stefan-Boltzmann law

$$R = \int_0^\infty r_{\lambda, T} d\lambda = \varepsilon \sigma T^4, \qquad (1.3)$$

where ε is the integral radiation coefficient; $\sigma = 5.7 \cdot 10^{-8}$ watts-m^{-2}-deg^{-4} is the Stefan-Boltzmann constant.

The measurement of the total radiation power (intensity) in a wide spectral range in accordance with (1.3) makes remote determination of the temperature of the targets possible, isolation of them with respect to positive or negative thermal contrast with respect to the background, and it makes it possible to obtain thermal pictures of the terrain by scanning. The intensity is measured using various types of infrared radiometers [1.2]. The intrared radiometers are used in scientific research to obtain thermal pictures of the moon and the planets of the solar system, to investigate the infrared radiation of galactic sources, terrestrial and solar space. Artificial earth satellites are oriented by the infrared emission of the earth's horizon. In military engineering infrared radiometers are used for thermal reconnaissance of military targets, above-water ships by the radiation of the hull, the power plant and superstructures, submarines in the submerged state by the thermal contrast of the wake, to obtain thermal pictures of the earth's surface, for detection of launches of intercontinental ballistic missiles (ICBM's) [1.2, 1.3].

Infrared surveying of the earth's surface and the cloud cover from meteorological satellites is one of the most important areas of applied use of infrared equipment. The Nimbus, ESSA and other American satellites make surveys in the 2.4-4.2 micron range. This range is convenient for night surveys, for the thermal emission of the earth's surface and the clouds in the daytime is distorted sharply by the reflected solar radiation.

The Soviet satellites of the Meteor system received infrared patterns in the 8-12 micron range. Since the temperature of the earth's surface on the average is 288 K, in accordance with (1.2) and (1.1) for a range of 8-12 microns we have a maximum of the thermal radiation emitted by the earth and the atmosphere. The reflected solar radiation for the Meteor satellite in practice has no effect on the quality of the image. The outgoing thermal radiation is surveyed around the clock, the equipment is switched on by special onward devices on command from the earth. The on-board infrared equipment is a narrow-angled scanning radiometer with instantaneous field of view of 1.5°x1.5°, and it records the strip of about 1100 km wide on each orbit. The threshold sensitivity is 0.5-0.6°C at a temperature of 20-25°C. The data is transmitted from the satellite in the radio visibility zone of ground receivers in the form of a brightness image of the thermal field and simultaneously in the form of a digital picture of the equivalent radiation temperature [1.4]. As a rule, the infrared survey is made for meteorological purposes. By the infrared images it is possible to study

5

the cloud distribution over large sections of the earth simultaneously,
to recognize and estimate the degree of development of cyclones and
atmospheric activity. The analysis of a large number of infrared images
transmitted from the satellites has demonstrated that when there are few
clouds it is possible to record thermal nonuniformities of the earth's
surface. This offers the possibility of using them in geological and
geographic studies. The coastline and hydrographic network are clearly
visible on infrared pictures taken from space. Thermal nonuniformities of
water surfaces are well recorded in the infrared range [1.4].

The observation of ground targets from space and space targets from the
earth is influenced significantly by clouds which cover the targets and
the attenuation of the infrared radiation of the earth's atmosphere as a
result of absorption by water vapor, carbon dioxide and ozone and, to a
lesser degree, as a result of scattering on dust and moisture particles.
The transmission coefficient of the atmosphere, depending on the effective
amount of water vapor and carbon dioxide, usually is presented in the
published tables [1.2, 1.3]. Observations can be made through the earth's
atmosphere in sections of the spectrum of relatively good transparency,
in the so-called "windows of transparency": 0.95-1.05; 1.2-1.3; 1.5-1.8;
2.1-2.4; 3.3-4.2; 4.5-5.1; 8-13 microns. The selection of the window
transparency for observation is determined by the mean value of the tempera-
ture of the targets in accordance with (1.1) and (1.2) or the emission
spectrum of sources illuminating the object. Windows of transparency up to
3 microns permit solar radiation in the infrared range reflected by the
targets to be recorded where it predominates over the natural thermal
emission of the targets.

The significant leap in the application of infrared equipment is connected
with studies of the natural resources of the earth from spacecraft. Informa-
tion from photographic, television, infrared and radar systems is used for
overall evaluation of the natural resources.

In the USSR the studies of the resources of the earth have been performed
on the Soyuz, Kosmos and Meteor spacecraft, and the Salyut orbital stations
[1.1]. A special spacecraft was launched on 3 June 1977 to obtain informa-
tion on the natural resources of the planet. This is the Meteor-Priroda
spacecraft with an inclination of 98°. Experimental scientific equipment
was installed on board the satellite which will provide for taking photo-
graphs in several spectral bands, recording of the thermal emission of the
earth's surface in the infrared range, sounding of the atmosphere with
determination of the temperature profiles with respect to altitude. The
information from the satellite will be useful for studying soils, the
vegetation and planted fields, soil structural surveys, and so on. The
study of soil moisture, erosion of river banks and lake shores, photographic
surveys of snow, ice, floods, and marine navigational conditions are
important problems [1.5]. The systematic purposeful study of natural
resources from the Meteor-Priroda satellite is necessary for agriculture
and forestry, the fishing and maritime fleets, geology, and so on.

6

FOR OFFICIAL USE ONLY

The study of the natural resources in the United States was performed from the ERTS-1 artificial earth satellite (1972-1973) by the Skylab orbital stations (1973-1974). At the present time the Landsat satellite which is analogous to the ERTS-1, is being used for these purposes. It is proposed that a Landsat C and Landsat D satellite with improved equipment be launched in 1977-1980.

The HCMM (AEM-A) satellite has been developed in the United States to map the earth in the infrared range in order to search for outcrops of useful minerals and groundwater. It is proposed that a two-channel infrared radiometer be installed on it, one channel of which is designed to record the characteristic thermal radiation and the other, to record reflected solar radiation in the infrared range [1.7].

Broad-scale oceanographic research will be performed by the Seasat A satellite [1.8]. The basic goals of this satellite are as follows: mapping ice fields, the study of the topographic characteristics of the ocean surface caused by currents, tides, and storms; recording of the altitude and direction of the waves and winds at the surface of the ocean, marine currents and temperature of the sea surface on a global scale. Jointly with radar and a microwave scanning radiometer, the set of equipment will also include an infrared scanning radiometer operating in the visible and infrared bands and recording energy emitted and reflected by the ocean surface.

In space engineering wide use is made of infrared spectrometric equipment. The infrared spectra for any chemical compound has an entirely defined nature and is the same type of characteristic of the compound as, for example, the melting point, index of refraction and other physical constants. The determination of the spectral coefficient $\varepsilon_{\lambda,T}$ (and the spectral absorption coefficient $\alpha_{\lambda,T}$ which is equal to it with respect to magnitude) in a broad spectral range will permit qualitative chemical analyses to be performed. By the absolute values of $\varepsilon_{\lambda,T}$ or $\alpha_{\lambda,T}$ the concentration of the individual components is determined, and with known chemical composition it is possible to characterize the state of the surface of the target. The methods of infrared spectrometry are especially effective when analyzing materials in the gaseous state.

The spectral studies are performed using infrared spectrometers, spectrometer telescopes and infrared interference spectrometers. In the infrared spectrometers, the spectral analysis is realized using a prism or diffraction gratings, and the spectrum obtained either is recorded on a photographic plate (in the near infrared region) or it is scanned in front of the exit slit beyond which the infrared photoreceiver is placed. The highest resolution is obtained by the interference infrared spectrometers in which the intensity-modulated radiant flux goes to a Michelson interferometer, it is split into two beams which on being combined at the output interfere with each other. The difference in path of the beams in the interferometer is continuously varied by periodic displacement of one of the mirrors of the interferometer. The interferogram is recorded by a radiation receiver. The signal obtained in this way is a Fourier transformation of the spectrum.

7

FOR OFFICIAL USE ONLY

FOR OFFICIAL USE ONLY

In order to obtain the spectrum itself the inverse Fourier transformation
is made by a computer. The resolution of the interference spectrometer
in practice is two orders higher than the best instruments with diffraction
gratings [1.2].

The space infrared spectrometers are used to solve astrophysical problems
(to study the composition of the atmosphere of the planets, the vertical
distribution of the components and the temperature, the condition of the
surface of the moon and the planets), in meteorology and when studying
natural resources (the analysis of atmospheric pollution, CO_2 and water
vapor distribution, temperature with respect to altitude, determination of
areas of accumulation of plankton in the ocean, and so on). The analysis of
the radiation spectrum of the targets is realized by multispectral systems
simultaneously forming the images in several spectral bands. The spectral
attributes are used for target selection in the infrared devices for military
purposes.

The spectrometric infrared equipment is used on all automatic interplanetary
stations (AMS) to study the moon, Mars and Venus. On the American inter-
planetary station, Voyager 1 and 2 launched in August and September of 1977
and intended to study the Jupiter and Saturn from a fly-by trajectory will
provide a significant part of the information by an interference infrared
spectrometer/radiometer. This combination instrument is planned for use
in investigating the composition of the atmosphere of Jupiter, Saturn and
their satellites while recording the components contained in the atmosphere
in small amounts, to study the energy balances on global and local scales,
the diurnal gradients and variations in temperature, the dynamics and
composition of the "red spot" of Jupiter, and determine the sizes of the
bodies forming Saturn's rings [1.9].

A broad, important spectrometric research program was carried out in 1976-
1977 on the Soviet Salyut-5 orbital station by two crews of cosmonauts,
B. V. Volynov and V. M. Zholovov, V. V. Gorbatko and Yu. N. Glazkov, and
also in the automatic mode. More than 300 astrogeophysical, technological,
medical-biological and other studies and experiments were performed during
flight in the automated and manned modes [1.10].

The astrophysical studies were performed using the ITS-K infrared spectrometer-
telescope (see Chapter 3) in the 2-15 micron band. The infrared intra-
atmospheric spectrum of the sun and solar space was obtained for the first
time. Preliminary analysis demonstrated that in the 4-8 micron range varia-
tions in intensity of the solar radiation are observed which have not been
detected during ground spectroscopy. Infrared spectroscopy was performed
on the surface of the moon and infrared galactic sources. Valuable spectra
of the terrestrial space were obtained. An infrared telescope was used to
perform infrared spectroscopy of the earth's surface for the first time
in such a broad range on passing through it. On the basis of the trans-
mission spectra in the 2-15 micron band, the altitude distribution of
carbon dioxide, carbon monoxide, ozone and other components was determined

8

FOR OFFICIAL USE ONLY

FOR OFFICIAL USE ONLY

which will permit judgment of how the industrial activity influences the atmosphere.

A photographic and spectrographic set of equipment was installed on board the Salyut-5 station to study natural resources. Photographs were made of a significant part of the territory of the Soviet Union and also the Indian, Pacific and Atlantic Oceans.

Several hundreds of spectrograms of different types of natural formations and landscapes were obtained in various parts of the earth: forests, agricultural areas, steppes and arid regions, surface of water and clouds. They were used as a basis for the experimental catalogs of spectral characteristics of natural formations. This will permit us to develop methods of monitoring the condition of foreign, water resources, agricultural crops, to solve the problems connected with land improvement and harvest forecasting.

A new element in the spectral studies of the natural environment was measurement of the degree of polarization of the solar radiation reflected by the clouds, the water surfaces and other natural formations of our planet. These measurements are needed to develop methods of estimating the degree of contamination of the water surface with petroleum and petroleum products, to estimate the moisture of the surface layer of the ground and determine the structure and state of clouds.

In future space programs of the United States for 1980 to the year 2000 [1.11] the plan calls for creating orbital stations in a near-earth orbit, bases on the moon and the planets, launching spacecraft for studying the moon (1980), Mars (1981), a landing on Mars and delivery of an automatic Mars exploration vehicle; in 1984 -- a study from polar orbit, 1989 -- delivery of samples of Martian soil, Venus (1978-1983), Mercury (1983), Jupiter from orbit (1985 to 1986), Jupiter and Uranus from the fly-by trajectory (1979), Saturn (1982-1984, 1985-1990). Studies are planned in the areas of astrophysics and natural resources of the earth, commercial utilization of space and solar energy.

Significant changes in the technology for performing space research are expected after the creation of a space transport system [1.12]. The basic element of this system is a reusable space transport vehicle (RSTV). New possibilities are being opened up as a result of reducing the restrictions on mass and volume of the payload, organization of servicing and repair in orbit, return of the payload to the earth for inspection, repair and repeated insertion. The plan calls for future conversion to building spacecraft from standardized modules, which will make it possible to increase the operativeness of performing new experiments.

One of the first payloads of the RSTV will be the Large Space Telescope (LST) with a 2.4 meter aperture for operation in the range from far ultraviolet to near infrared. The use of the LST will increase the precision by comparison with ground astronomy by at least tenfold.

9

FOR OFFICIAL USE ONLY

FOR OFFICIAL USE ONLY

Since 1973 work has been done on designing the Spacelab orbital space station which will be installed in the cargo compartment of the RSTV. It is planned that the Spacelab orbital space station will be inserted into orbit at the beginning of the 1980's. The research program includes experiments in such areas as astronomy, physics of the sun, astrophysics, the investigation of natural resources, space biology and medicine, technological research and so on. For Spacelab provision has been made for the development of an infrared telescope [1.13] with a mirror diameter of 1.10 meters and cooling to a temperature of about 20°K. By using this telescope studies will be made of remote or gas-clouded galaxies, atmospheres and surfaces of the planets, asteroids, the study of interstellar gas and cosmic dust, and the atmospheres of cold stars. The infrared telescope will include a photometer, a photopolarimeter, a Michelson interferometer, a large mosaic photoreceiver for receiving pictures of the stellar sky in the selected spectral range. The telescope can be controlled either automatically or by astronauts. It is proposed that the optical elements of the telescope be made from pressed beryllium which has high ratio of thermal conductivity to its coefficient of thermal expansion. The power surface very well reflects the infrared radiation without additional coating. The total mass of the telescope is reduced to 2 tons (without helium tanks weighing 300 kg used for cooling). The field of view of the telescope is 15'. The orientation system permits the telescope to be sighted on a star with an accuracy of $\pm 1"$. The gyroscopic system provides for stabilizing the position of the telescope access with a precision of $\pm 0.25"$.

In the future, expansion of the scales of application of infrared systems in space engineering should be expected. With improvement of the parameters of lasers, the volume of research using active infrared systems will increase significantly. By laser sounding it is proposed to study the spatial distribution of cirrus clouds and the composition of aerosols in the lower stratosphere, the composition of the atmosphere and atmospheric pollution, to obtain spectrozonal images of the earth's surface. Laser rangefinding equipment and space communications systems in the infrared band will receive further development.

1.2. Operating Characteristics of Infrared Systems in Space

The basic operating characteristics of infrared devices in on-board space systems include a deep vacuum, radiation cooling and the effect of cosmic radiation. The effect of a deep vacuum is felt in the high evaporation rate of various materials, especially various lubricants. Accordingly, the provision of lubrication of various moving parts in the on-board instruments is complicated. The solution to this problem proceeds along the path of the development of equipment without moving working parts, the sealing of the moving parts and the development of various film lubricants.

FOR OFFICIAL USE ONLY

At the same time, the rapid evaporation of various materials under vacuum conditions and under the effect of solar radiation, including gas evolution from various synthetic materials will lead to contamination of the optical parts and sensitive elements of the infrared devices as a result of condensation of the evaporated materials and evolved gases. Thus, soon after inserting the Nimbus 4 meteorological satellite into orbit on 8 April 1970, its SWS infrared spectrometer with wedge optical filters failed [1.14]. The spectrometer was intended for measurement of the intensity of the earth's emission as a function of wave length in the ranges of 1.2-2.4 and 3.2-6.4 microns. After the fifth orbit the sensitivity in the first channel dropped completely, and in the second it was significantly diminished. After analysis of the possible causes of the failure, the conclusion was drawn that the most probable cause was the formation of ice on the sensitive element cooled to a temperature of 176°K. In order to check out this conclusion, laboratory experiments were performed with respect to the simulation of the temperature and vacuum conditions characteristic of the orbital conditions in a liquid nitrogen-cooled vacuum chamber. The experimental results demonstrated that a layer of ice could be formed on the infrared detector, the thickness of which was equivalent to a layer of water 0.28 mm thick.

As a result of gas evolution from certain synthetic materials under vacuum conditions and the effect of solar radiation, the optical parts can be contaminated. Thus, on board the Apollo 8 spacecraft it was not possible to make television observations through the large window as a result of severe contamination of it [1.15]. The contamination of other optical parts -- mirrors, diffraction gratings, prisms and so on -- is also possible. The contamination of the optical parts is also possible when testing infrared equipment and the entire spacecraft in test chambers simulating space conditions.

The performed studies [1.16] demonstrated that the concentration of the contaminating gases depends essentially on the orbital altitude and distance from the surface of the artificial earth satellite. The concentration decreases by ten times at an altitude of 100 km at a distance of 10 cm from the surface of the spacecraft, and at an altitude of 500 km, at a distance of 2 cm. The self-contamination conditions decrease sharply with an increase in orbital altitude. The ratio of the return flow of gases to the released flow varies from 0.5 at an altitude of 160-170 km to $1 \cdot 10^{-6}$ at an altitude of 1000 km. On the other hand, the self-contamination in the chamber can be greater or less than in orbit depending on the ratio of the chamber and spacecraft sizes. The conditions in ordinary vacuum chambers correspond to the orbital conditions at an altitude of about 400 km. At greater altitude the orbital contamination conditions are lower than in the chamber.

In addition, the contamination of the equipment also takes place as a result of operation of the on-board rocket engines, in particular, operating on a mixture of monomethylhydrazine and nitrogen dioxide. The contamination of spacecraft is controlled basically by selecting materials having minimum gas evolution and condensation of evaporated materials.

11

FOR OFFICIAL USE ONLY

The effect of space radiation on infra-red devices reduces to darkening of
some of the optical materials and a reduction in sensitivity of certain
infrared receivers. For successful control of this effect it is necessary
to select optical materials and receivers, least subject to the effect of
radiation and in some cases, shielding it out.

The low level of radiation of the stellar sky (radiation temperature about
4°K) and absence of an atmosphere (and, consequently, convection heat
exchange) permit us to use the methods of radiation cooling of the infra-
red radiation receivers and the equipment itself on oriented spacecraft,
which is needed to increase the sensitivity of the instruments. The
instruments and radiation receivers are cooled by using a darkened, cooled
area which is inside the reflecting cone which is the collimator for it
(see Fig 1.1). The two-stage cooling using two cones (cone in cone) is
possible.

The cooled area must have defined orientation in space. The Nimbus E
satellite, for example, had a 6-hour heliosynchronous orbit with an altitude
of 1450 km. In this orbit maximum illumination of the solar cells is
insured, and the platform of the cooler is hidden from the sun. Only the
night side of the earth and the horizon sensor are observed from the apex
of the cone. The horizon sensor is not visible from the platform itself;
in addition, its angular dimensions are small, and the effect on the
cooler temperature is low. The cooler is separated from the spacecraft by
multilayer thermal insulation and it is attached using tubes with low
thermal conductivity. The platform dimensions are 2.5x10 cm^2. The platform
temperature is 184°K. On reducing the thermal conductivity of the heat
insulators to zero the temperature will reach 154°K. The emissivity of
the cone walls has little influence on the platform temperature. Thus,
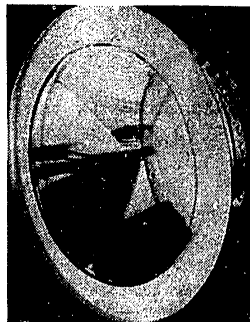with an increase in emissivity by 20% the temperature increases by only
1.2%.

Figure 1.1. Radiation cooler of infrared equipment

FOR OFFICIAL USE ONLY

FOR OFFICIAL USE ONLY

On the Nimbus 1, 2, 3 satellite, a simple single-stage cooler was used
which provides a temperature of 200°K in the Pb-Fe receivers of the infra-
red radiometers with high HRIR type resolution. The cone temperature is
about 290°K. The size of the area in the cooler is 9.8 cm. The cone is
coated with gold and has a viewing angle of ±30° in the vertical plane
and ±40° in the horizontal plane. The spectrometer with wedge filters
SWS developed for the Nimbus-4 satellite will contain a more complex
single-stage cooler which maintains a temperature of 175°K in the Pb-Fe
receiver.

There is a two-stage cooler maintaining a temperature of about 85°K in the
HgCdDe receiver in the VHRR spectrometer with very high resolution on the
TOS satellite.

During laboratory testing of the models of a two-stage cooler, the possi-
bility of radiation cooling to 80°K was demonstrated for actual thermal
and mechanical conditions. In addition, the low radiation level of the
cosmic background permits its use for reference measurements (the origin
of the coordinates) for on-board calibration of various measuring instru-
ments. A number of other requirements are imposed on equipment used in
space, including the infrared equipment: resistance to large vibration
overloads on being inserted into orbit and also rigid requirements on
dimensions, mass and energy consumption.

1.3. Technical Experiments in the Infrared Range and Support of the
Operation of On-Board Systems

In a number of cases infrared systems are used to support the operation
of on-board systems and also to perform technical experiments under space
conditions.

The large volume of technical experiments using infrared equipment have
been performed in order to control the stability of the spectral reflecting
properties of heat regulating coatings of the spacecraft and the
characteristics of optical materials and the parts of various on-board
optical instruments under space conditions.

The stability of the spectral reflecting properties of the heat regulating
coatings is important to maintain given temperature conditions of the
spacecraft during prolonged time in orbit under conditions of ultraviolet
radiation and cosmic radiation.

Thus, as a result of the tests run on board the Lunar orbiter [1,17] on
heat regulating coatings, a significant increase in the absorption of
solar radiation was detected and, as a result, an increase in the steady
state temperature above the calculated limits. After detection of this
situation, a series of tests were run on the heat regulating coatings
which included laboratory tests under ultraviolet radiation performed
under deep vacuum conditions, and flight tests on the Lunar orbiter 4 and 5.

13

FOR OFFICIAL USE ONLY

The tests of coatings during the flight experiments demonstrated more noticeable increase in the absorption of solar radiation than in similar tests run on the coatings in the laboratory. The results of the flight tests agree well with the data obtained during the Mariner 5 spacecraft flight, but they differ from the flight experiments on the OSO-2 and 3 satellites. It is considered that this difference is connected with the fact that beyond the limits of the magnetosphere, the rate of variation of the external conditions is higher, and in the laboratory all the environmental conditions characteristic of space flight were not simulated. Accordingly, it is considered very important to test the materials directly on board spacecraft.

Measurements of the reflecting properties of materials used as heat regulating coatings [1.18] and also materials used in the optical systems of on-board equipment (aluminum and silver plated mirrors with different coatings) were performed on board the ATS-3 satellite inserted into synchronous orbit with an altitude of 38,780 km over South America on 5 November 1967. The measurements were performed by the reflectometer built by the Electro-Optical Systems Company located outside the rotating satellite. The mechanically simulated radiation flux from a tube with a tungsten filament was incident on the samples along the normal. The reflectometer recorded the reflected flux within the limits to 5° from normal. Two photomultipliers, two lead sulfide photoresistors and one silicon photoelement were used as the radiation receivers. The following sections of the spectrum were isolated by optical filters: 0.3-0.4; 0.3-0.65; 0.65-1.20; 1.2-3.0; 0.6-3.0 microns. The radiation receivers were placed on an integrating sphere collecting the reflected flux. The rotating mirror realized successive irradiation of the samples and the measurement of the reflecting characteristics. In all, 18 tested samples and two standard samples (with high and low reflection coefficients) located along the arc of a circle were installed. Eight of the tested samples were protected by discs made of fused quartz 1.5 cm thick from protons with an energy to 18 Mev, electrons with an energy to 0.8 Mev, ultraviolet radiation with a wave length shorter than 0.16 microns and all of the dust particles. A rotary device was used to select these discs to measure the reflecting properties of them. These samples were exposed a total of 15 hours during the course of 24 months. There were 8 similar unprotected samples. A mirror with internal aluminum plating on a plate of used quartz 0.15 cm thick was used as the standard with high reflection, and black anodized aluminum with V grooves closed with a piece of fused quartz 0.15 cm thick was used as the standard with low reflection. Both standard samples were shielded and were exposed only during the measurement times. The temperature of the platform on which the samples were placed fluctuated within the limits of 12 to 19°C, and during the 6 months of dark the temperature dropped to 5°C. The precision of the measurements using the on-board reflectometer was within the limits of 1-5%, and for the majority of measurements, 2-3%. The tests made it possible to discover the thermal regulating coatings having the most stable characteristics.

14

It was discovered that among the mirror coatings used in optical devices, aluminum coatings with a protective SiO_2 and Al_2O_3 layer are more stable than with other dielectric coatings, in spite of the fact that a more significant decrease in reflecting properties was observed for them than under laboratory conditions.

In a number of the on-board devices, infrared systems are used as auxiliary units supporting the operation of the basic devices. An automatic system for regulating the frequency pass band using an incandescent tube as the radiation source and a photoresistor as the radiation receiver was used on the Mariner-Venus spacecraft according to the 1967 design in the on-board equipment for precise measurement of the distance to the planet [1.19]. For precise measurement of distance it is necessary to insure a spectral frequency of the radius signal from a remote rubidium standard of 1 megahertz in the 0.02 hertz band. In order to isolate the signal, a circuit with a phase filter is used. The photoresistor is connected to one circuit with two resistances regulating the frequency band. The photoresistor is illuminated by an incandescent tube. If the circuit falls out of adjustment, a voltage is fed to the tube, the tube illuminates the photoresistor, the resistance of which can vary from 300 megohms to 2 kilohms. Expansion of the band from 0.02 to 0.08 hertz takes place, and the signal is transmitted through the circuit. After tuning to the signal frequency the voltage is disconnected from the tube, the resistance of the photoresistor increases, and the band becomes more narrow. For the entire adjustment only about 3 minutes are required. Field transistors and the Clairex CL703C antimony-indium photoresistor are used in the circuit. The described system was tested during the Mariner spacecraft flight at a distance of 400 km from the planet Venus.

On board the Apollo spacecraft, infrared gas analyzers were used in the Lunar and command modules in the life support system to determine the carbon dioxide content in the air [1.20]. The infrared sensors are a single-beam photometer having interference filters that transmit radiation on wave lengths of 4.3 and 4.0 microns. Oscillations of the filters are realized by using a dipole, and modulation of the radiant flux at $\lambda=4.3$ microns with respect to the flux at $\lambda=4.0$ microns is insured. The carbon dioxide content is determined by the magnitude of the signal.

15

CHAPTER 2. SPACE NAVIGATION

2.1. Space Navigation Problems

The determination of the location of the spacecraft or aircraft in the
coordinate system in which its displacement is investigated and also the
realization of fully defined orientation of the vehicle with respect to this
system of coordinates achieved by turning the entire vehicle around axes
passing through its center of mass, are space flight navigational problems.
The orientation of the spacecraft is required both for determination of its
location and to insure normal operation of its devices independently of
whether determination of its location is required or not.

The methods of astronomical navigation based on determining the position
of known heavenly bodies with respect to a selected coordinate system are
finding broad application in space navigation. During space flights, in
contrast to ground navigation, the astronomical measurements are used not
only to calculate the angular coordinates of the target, but also to find
the flight altitude of the vehicle above the surface of the base body. For
artificial earth satellites, the earth is this body, and for interplanetary
communications, the sun.

During navigation of spacecraft, along with other means, infrared equipment
is used which permits determination of the direction of the heavenly bodies
by their emission in the infrared range of the spectrum and measurement of
the distance to them.

The orientation of the spacecraft in space reduces to finding the direction
of the heavenly bodies, the sun or planets, the positions of which in the
given coordinate system are known and realization of the required stabiliza-
tion of the equipment itself or its separate units with respect to the
selected directions. In the absence of stabilizers, the body can rotate
around three of its axes passing through its center of mass. In order to
insure defined orientation of the body in space, an orientation system
must have position control channels for the body with respect to each axis.
The orientation systems make it possible to decrease or exclude the
undesirable rotation of the spacecraft around their own center of masses,

16

to maintain fixed orientation with respect to a given coordinate system
and realize reorientation on command.

Without an orientation system, the spacecraft undergoes arbitrary rotations
(tumbling) around its center of mass as a result of the presence of a
number of sources of disturbances which, upon acting on it, create rotational
moment. The rotation of artificial earth satellites can occur under the
effect of a rotational moment on separation from the booster as a result
of the effect of the internal moving parts of the satellite itself and also
as a result of various external physical effects: magnetic and electric
fields of the earth, aerodynamic forces, the pressure of the solar radiation,
and encounters with meteor microparticles, and so on.

Entirely defined orientation of the spacecraft or its separate units is
required, for example, during operation of the engines with changing flight
trajectory and landing, to conduct observations of the surface of the earth
from on board the satellites, for the performance of astronomical observa-
tions and measurements from research rockets and space laboratories, to
provide for the operation of narrowly directional antennas and telemetric
systems of spacecraft and also to solve a number of other problems.

Orientation of the satellites or determination of the coordinates by the
on-board navigational systems were not required for scientific research
using the first Soviet artificial earth satellites.

In order to take the next steps in the conquest of space, it was necessary
to build spacecraft orientation systems. Thus, the Soviet interplanetary
automatic station "Luna-3" launched on 4 October 1959, and permitting the
first photographic image of the surface of the back side of the moon to be
taken, had an automatic system which provided for its orientation relative
to the sun and the moon required to photograph the moon [2.1].

The orientation system of the second Soviet automatic interplanetary station
following the interplanetary route to Venus made it possible to solve the
following problems during flight [2.2]:

To eliminate the arbitrary rotation of the station occurring on separation
from the booster rocket launched from a heavy artificial earth satellite;

To provide for search for the sun from any position of the station and
realize orientation of the solar cells on the sun during the entire flight
time;

To provide for any required spatial rotation of the station and stabilized
station;

To provide for orientation near Venus of the parabolic radio antenna having
an acute radiation pattern, in the direction of the earth to obtain high
speed transmission of scientific information and data on the operation
of the on-board equipment to the ground.

17

The orientation system of the interplanetary automatic station had sensors for orientation on the earth, the sun and a star.

The Soviet spacecraft "Vostok" also had an orientation system. In order for the command module with the astronaut to descend to the ground in a given area, before switching on the braking engine, completely defined orientation of the satellite in space was insured [2.3]. This problem was solved by orienting one of the axes of the spacecraft in the direction of the sun. The measuring elements of the system were optical and gyroscopic sensors. The signals coming from them were converted in the electronic module to instructions controlling the system of servoelements. The orientation system provides for automatic search for the sun, the correspond-ing rotation of the spacecraft and holding of it in the required position with great precision.

The orientation systems of the spacecraft are also needed to fulfill the missions with respect to the conquest of space such as observation of the earth surface from artificial satellites, the performance of astrophysical observations from research rockets and space observatories, the control of interplanetary flights, and so on.

The systems for orientation of the spacecraft are automatic control systems which control their position with respect to the given coordinate system. In general form each control channel can include a measuring device (sensor), an amplifying conversion circuit and servoelements (see Fig 2.1). The measuring device or the sensor of the orientation system generates mis-match signals with respect to the given direction which depend on the position of the axis of the sensor with respect to the direction of orienta-tion. The optical sensors permit determination of the directions of the heavenly bodies by their emission in the optical spectrum of frequencies, including the infrared part. The infrared sensors usually have an objective which focuses the infrared beams from the heavenly body on the radiation receiver. In the radiation receiver the infrared energy is converted to electric signals containing information about the position of the heavenly body with respect to the optical axis. The various methods of formation and generation of mismatch signals will be considered when describing specific orientation systems. The amplifying conversion devices amplify and convert the mismatch signals generated by the sensors to signals which control the servoelements. The servoelements of the orientation system generate control moments which act on a spacecraft. For the creation of control moments in astronautics, gas jet engines or rotating flywheels and also combination servoelements are used.

As interplanetary communications develop, the necessity for determining the position of the spacecraft using on-board navigational systems will acquire greater and greater significance. The infrared tracking systems permit determination of the position of the heavenly bodies with respect to the selected coordinate system, and the computers convert the measured elements to the coordinates of the spacecraft. The choice of reference directions
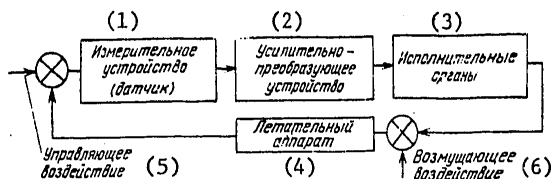
Figure 2.1. Functional diagram of an orientation system with respect to one axis

Key:
1. Measuring device (sensor)
2. Amplifying-conversion device
3. Servoelement
4. Spacecraft
5. Control input
6. Disturbance

used for orientation or determination of the location of the spacecraft and also the composition of the navigational equipment depend on the purpose of the spacecraft and its flight trajectory.

One of the necessary elements of the navigation of artificial earth satellites is determination of the local vertical, that is, the direction of the center of the terrestrial sphere from the point at which the satellite is located at a given point in time. On orientation with respect to the local vertical of the earth, the satellite is stabilized with respect to the pitch and bank angles. The determination of the local vertical by finding the center of the observed disc of the earth is the simplest method of constructing the vertical. This procedure resembles the determination of the local vertical with respect to the horizon in marine navigation. In view of the large angular dimensions of the earth on observation from artificial satellites, the instruments determining the direction of the center of the earth's disc (the vertical plotters) have peculiarities which distinguish them from solar or stellar sensors.

2.2. Sensors for Sensing the Horizon of the Planet Operating by Thermal Emission

In order to find the edge of the earth's disc (the horizon), it is possible to use any part of the optical spectrum of the earth's radiation: ultraviolet (UV), visible or infrared (IR), for the optical contrast between the earth and less bright background of outer space surrounding it exist in any part of the spectrum. However, it is less convenient to use the solar energy in the ultraviolet visible or shortwave infrared part of the spectrum reflected from the earth, for in this case the conditions of constructing the vertical when finding the satellite on the side of the earth illuminated and not illuminated by the sun differ sharply. In addition, the boundary between the illuminated and not illuminated sides can be perceived as a false horizon.

19

The method of constructing the vertical using the natural infrared (thermal) radiation of the earth permitting observation of the earth's disc independently of the position of the sun has become more widespread. This method of constructing the vertical with respect to the infrared horizon of the earth has come to be called the infrared vertical.

The design of the infrared horizon sensors in the United States has been based on measuring infrared radiation of the earth's atmosphere in 1958 using the measuring equipment installed on board ballistic missiles. The measurements were performed during day and night flights of two missiles. The processing of the measurement results made it possible to establish the contrast existing between the infrared radiation of the earth's atmosphere and outer space. On observation through a layer of the atmosphere from a satellite the earth has an average effective radiation temperature of about 250°K, and the effective radiation temperature of outer space is 4°K [2.4].

In spite of the fact that the earth's atmosphere spreads out above the surface of the earth to altitudes measured in hundreds of kilometers, its density decreases sharply with an increase in altitude so that approximately 85% of the atmospheric mass is below an altitude of 15 km. The basic part of the water vapor contained in the atmosphere and playing a large role in its radiation and about 60% of the atmospheric mass are in the layer below 6 km. The altitude of the infrared horizon and the stability of its position depend on the spectral section in which the observation is performed. High altitudes and higher stability pertain to sections of the spectrum corresponding to the absorption bands in the atmosphere; the lower altitudes and stability, to the measurements in the "windows of transparency" of the atmosphere. The angular and spectral distribution of the infrared radiation of the earth in space near the horizon were investigated by means of a diffraction spectrometer on the Kosmos series of earth satellites [2.5].

The graphs for the spectral intensities of the emission F as a function of altitude θ (in degrees) of the line of sight above the line of the visible horizon for different wave lengths are presented in Fig 2.2. The measurements were performed for a satellite altitude of 250 km. The effective horizon of the earth when observed in the intense absorption band of CO_2 of about 15 microns during measurements on the 0.5 level of the radiation intensity in the nadir lies approximately 27 km higher than for observations on a wave length of 11 microns. Consequently, the infrared horizon on the 15 micron wave length is appreciably higher than the clouds, and in its position does not depend on the cloud altitude and meteorological conditions. At the same time, in the "window of transparency" of the atmosphere at 8–12 microns the altitude of the horizon depends on the cloud altitude. The variations of the altitude of the horizon on a wave length of 15 microns [2.6] are estimated at 5-8 km and at 23 microns (the rotational absorption band of water vapor), 4-8 km. For wave lengths of 12 and 18 microns in the vicinity of the "windows of transparency" the variations encompass the entire troposphere (approximately to 18 km at the

20

equator). Accordingly, in order to obtain the minimum error in determining
the local vertical caused by instability of the horizon, sensors are used
which operate, as a rule, in the spectral band of 14-16 microns.
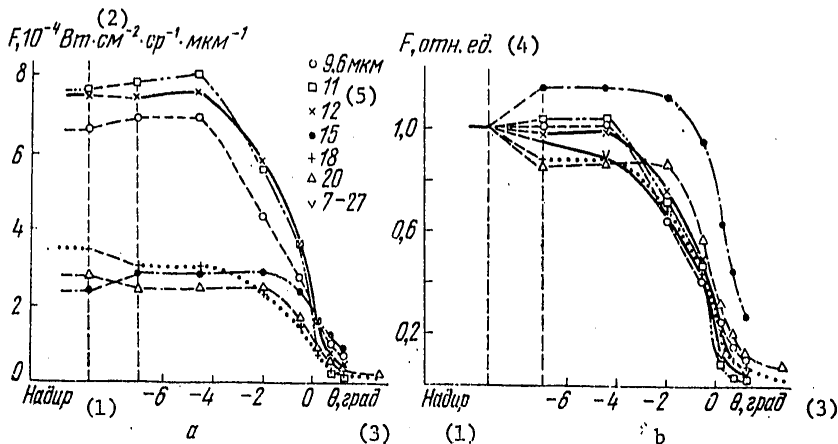
Figure 2.2.   Spectral radiation intensities of the earth as
a function of the altitude of the line of
sight above the line of the apparent horizon
for different wave lengths:
a -- in absolute units; b -- in relative units

Key:
1. Nadir
2. Watts-cm^{-2}-steradian^{-1}-micron^{-1}
3. Degrees
4. F, relative units
5. Microns

There are several types of horizon sensors used to construct a vertical
[2.7]: scanning, tracking and radiation-balance. In the scanning horizon
sensors, scanning is used with a narrow instantaneous viewing angle along
the scanning trajectory, usually conical and intersecting the horizon.
The scanning diagram is shown in Fig 2.3, a. In order to obtain informa-
tion about the orientation with respect to two axes, two optical scanning
heads are used which are oriented with respect to these two axes. On
passage of the instantaneous field of view through the infrared horizon,
pulses occur. The control signals are formed by processing the durations
or phases of the pulses formed compared with the reference pulses.

21

On the artificial earth satellites stabilized by rotation, sensors of the investigated type can be used, but they do not have rotating parts. The scanning diagram of such sensors is shown in Fig 2.3, b. The scanning by the instantaneous viewing was realized as a result of rotation of the artificial earth satellite itself, In the scanning type sensors, usually thermistor bolometers or pyroelectric detectors are used which have a small time constant (1-5 milliseconds) and a narrow noise level (equivalent noise power $1.5 \cdot 10^{-10}$ watts at a scanning frequency of 15 hertz). In the standard wide-angle scanning sensor built by the Barnes Engineering Company operating by the schematic depicted in Fig 2.3, a, the scanning is realized using a germanium prism rotated by a synchronous motor, with respect to a cone with the angle of aperture of 410° with an instantaneous viewing angle of 2x8°. The rotation rate of the prism is 30 rpm. The radiation receiver is an immersion thermistor bolometer.

When the line of sight passes through the Earth's horizon, the sensitive elements generate pulsed signals caused by the thermal constrast between the Earth's radiation and the cosmic background. In one rotation of the mirror the line of sight of the sensor passes through the horizon twice. Both sensors generate mismatch signals proportional to the angles between the perpendiculars to the centers of the chords connecting the points of intersection of the line of sight with the horizon line and the axis of the aircraft which must coincide with the local vertical.

A structural diagram of the vertical sensor with respect to one angle is presented in Fig 2.4. Rectangular pulses from the sensitive elements are fed after amplification and limiting to a phase detector in which they are compared with the phase pulses of the reference pulse generator. The pulses from the reference voltage generator are synchronized on rotation of the mirror by the pulses of the electromagnetic recording device. After the phase detector the mismatch signal is amplified by a DC amplifier. In the diagram provision is made for blocking of the sensor in the case where the sun falls in its field of view. The mass of the sensors is 1.5 kg, the intake power is 4 watts, and the orientation accuracy is ±0.5°.

The scanning sensor [2.8] for operation in stationary orbit was developed by Lockheed Missiles and Space Company. Scanning is realized within the limits of the angle of 50° simultaneously and parallel by two instantaneous fields of view separated by 12°. The scanning system is shown in Fig 2.3, c, and the schematic diagram of the sensor, in Fig 2.5,a. The scanning is realized by both instantaneous fields of view as a result of rocking of the plane mirror using a dipole with electromagnetic drive. Compensation of the nonlinearity of the law of motion by the instantaneous viewing fields with time takes place as a result of processing of the signal with respect to the angle of rotation of the scanning disc with Moire raster from which the readings are taken proportional to the angle of rotation of the scanning mirror at the time of transition of the instantaneous field of view through the infrared horizon. The output signals are determined as a result of comparing the time intervals $\Delta t = t_2 = t_1$ between the pulses occurring on entry and exit of the field of view from the earth's

22

FOR OFFICIAL USE ONLY

(5)
Мгновенный
угол
зрения
Линия
сканиро
вания
(6)
Ось
враще-
ния
(7)
Тепловой горизонт Земли
(8) b

(1)
Мгновенный
угол зрения

Направление
сканирования (2)

Направление
полета
Тепловой горизонт Земли
(4) (3)
a

(11)
Среднее
положение
линии
визирования

Угол
качания
(12)

Линия
сканирования
(13) d
Тепловой
горизонт Земли
(14)

50°

12°

Мгновенный
угол зрения
(1)

Отклоне-
ние по
тангажу
(10)

Отклонение
по крену
(9)

c

Поля зрения
фотоэле-
ментов
(15)

B
C
A

e

Ось тангажа
(16)

Поле зрения
детектора (17)

A

Тепловой горизонт
Земли
(18)

B

B'

A
Местная
вертикаль

Ось крена
(19)

(20)

A'

f

Поле
зрения
основного
детектора
(21)

Поле зрения
компенсацион-
го детектора (22)

g

Figure 2.3. Scanning diagrams and arrangement of the fields of
view of the infrared horizon sensors:
a -- sensors with conical scanning; b -- rotation-stabilized
satellite sensor; c -- sensor built by Lockheed Missiles and Space
Company for a synchronous artificial earth satellite; d -- tracking
type sensors; e -- sensors built by the Barnes Engineering Company;
f -- sensors of the radiation-balance type at inconstant orbital
altitude; g -- the same at constant orbital altitude.
Key:
1. Instantaneous viewing angle; 2 -- scanning direction; 3 -- flight
direction; 4 -- thermal horizon of the earth; 5 -- instantaneous viewing
angle; 6 -- scanning line; 7 -- axis of rotation; 8 -- thermal horizon
of the earth; 9 -- bank deflection; 10 -- pitch deflection; 11 --
mean position of the viewing line; 12 -- rocking angle; 13 -- scanning
line; 14 -- thermal horizon of the earth; 15 -- fields of view of the

23
FOR OFFICIAL USE ONLY

FOR OFFICIAL USE ONLY

photoelement; 16 -- pitch axis; 17 -- detector field of view;
18 -- thermal horizon of the earth; 19 -- bank axis; 20 -- local
vertical; 21 -- field of view of the l sic detector; 22 -- field of
view of the compensation detector
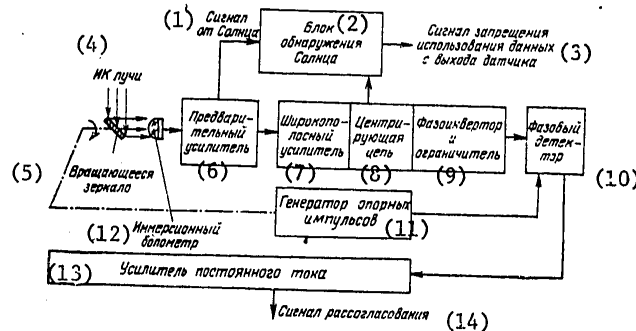
Figure 2.4. Structural diagram of the sensor determining the
deviation from the vertical in one direction

Key:
1. Signal from the sun
2. Sun detection unit
3. Signal forbidding the use of data from the sensor output
4. Infrared beams
5. Rotating mirror
6. Preamplifier
7. Wide-band amplifier
8. Aligning circuit
9. Phase inverter and limiter
10. Phase detector
11. Reference pulse generator
12. Immersion bolometer
13. DC amplifier
14. Mismatch signal

disc, with a standard pulse (deviation with respect to pitch) and also
comparison of the intervals between the two pulses for the two fields of
view (deviation with respect to bank). The sensor is 10.8x11.4x17.8 cm^3
in size, it weighs 1.8 kg. The intake power is 5 watts. The entrance
pupil of the objective is 38 mm in diameter. The instantaneous field of
view is 1.1x1.1°. The operating spectral range is 14.1 to 15.8 microns.
The linear operating zone of the sensor with respect to pitch is +10°,
and with respect to bank, 2.5°. The accuracy of determining the vertical
(in the vicinity of 0) is +0.05° (three mean square deviations).

24

FOR OFFICIAL USE ONLY
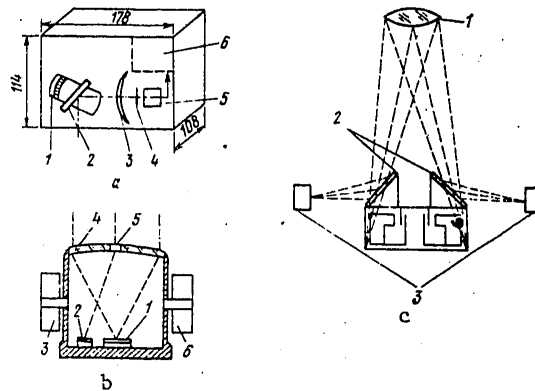
Figure 2.5. Schematic diagrams of horizon sensors:
a -- Lockheed Missile and Space Company (1 -- coding disc;
2 -- scanning mirror; 3 -- lens; 4 -- filter; 5 -- receiver;
6 -- electronics module); b -- Barnes Engineering Company
(1 -- mosaic of thermal elements; 2 -- silicon photoelements;
3 -- moment engine; 4 -- silicon lens; 5 -- prism directing
the solar radiation on the photoelement; 6 -- converter of the
angle of rotation to voltage); c -- horizon sensor of the
tracking type without rotating parts (1 -- objective; 2 --
mirrors; 3 -- radiation receiver).

The tracking horizon sensors usually combine several heads which track
the line of the earth's horizon directly. The angle between the optical
axes of the tracking heads and the reference axis is measured, and the
position of the pitch and bank axes is calculated. In some cases the
tracking heads are located at defined angular intervals azimuthally, for
example, every 120°, and they track any point of the horizon; in other
cases the heads realize scanning in the azimuthal direction and track the
line of the horizon.

The tracking system by one of the tracking horizon sensors [2.7] is shown
in Fig 2.3. The sensor has a head with a small field of view (usually
1x1°), which realizes nutation oscillations of the optical axis with
respect to the horizon within the limits of the angle of about 5° with a
frequency of about 20 hertz. In addition, slow rotation of the earth takes
place within the limits of the angle of 80 to 90° along the line of the
horizon. A sensor of this type has precision better than 0.15°, The sensor
weighs 6 kg, and the intake power is 8 watts.

25

One of the horizon sensors of the tracking type was developed by the
Barnes Engineering Company for automatic orientation of the Apollo space-
craft [2,9]. This orientation system has three sensors placed on a uni-
axial gimbal commiting search scanning by the field of view with respect
to the angle of ascent. The schematic of the position of the sensor
fields is shown in Fig 2.3, e. A silicon lens is used as the objective,
in the focal plane of which there are three thermal elements. By using an
electronic switching system the thermal elements are connected to the input
of the synchronous demodulator. The field of view of the thermal element A
touches the infrared horizon of the earth, and the fields B and C are
directed toward space. The sensor measures the level of radiant flux of
the earth with respect to space with successive connection of thermal ele-
ments A and B to the demodulator. In order to exclude interference from
the sun, silicon photoelements are used, the fields of which are super-
posed on the fields of view of the thermal elements A and B. In the case
where the image of the sun moves into the fields of view A or B by the
photoelement signal insensitive to the earth's radiation, the field of
view B is replaced by the field of view C located 1° lower. The angles of
rotation of the frame of the gimbal are reckoned by the electronic "angle-
voltage" converter, and they are sent in the form of electric signals to
the logical circuit for calculating the angular deflection of the axes of
the spacecraft.

In the modified tracking type instrument [2.10] there are three identical
sensors which are combined into a system for tracking the infrared horizon.
The sensors have a plane tracking mirror, a parabolic mirror objective,
an optical filter with pass band and a wave length of 14 to 16 microns
and a detector. The tracking mirror is fastened at the ends of two pairs
of bimetallic plates. The other ends of the plates are fastened on the
base. On variation of the plate temperature, the angle of inclination of
the mirror changes. The plates are heated when an electric current passes
through them. In order to lengthen the path of the electric current,
longitudinal slits are made in the plate. The ends of the plate are built
into fiberglass plugs.

In order to determine the position of the tracking mirror with respect to
the spacecraft, a high-current reading system is used which contains a
reading mirror connected with the tracking mirror by struts. The reading
system also has a system of lenses and masks. A neon tube is used to
light the masks. The light passing through the masks reaches four voltaic
photoelements.

The detector of the sensor is a system of three thermocouples on a single
base encompassing the zone at the horizon about 3° high. If one edge
thermocouple records the earth radiation at the horizon, the third edge
thermocouple is directed 3° above the horizon. The output signal is
equal to the sum of the signals of the edge thermocouples minus the signal
from the middle thermocouple. The width of the field of view of the middle
thermocouple is twice the width of the field of view of the edge ones.

26

The output signal is equal to zero when the middle thermocouple is directed toward the middle of the radiation gradient at the horizon. On shifting from this position, a signal occurs, the amplitude of which depends on the magnitude of the shift and the sign depends on the direction of the shift. The signal is also equal to zero when all of the thermocouples are directed only toward space or toward the earth. The direct current of the thermocouples is modulated by a chopper; then it is amplified, rectified and goes to a phase inverter which sends the signal to one pair or another of bimetal plates of the tracking mirror. The advantage of this device is considered to be high precision in the absence of constantly moving parts and bearings. The instrument has calibration and measuring modes.

In one of the tracking type sensors [2.11] without rotating parts for scanning, rocking of the mirrors under the effect of an electromagnet is used. The absence of rotating parts permits an increase in service life of the sensor and does away with the solution of the highly complex problem of maintaining lubrication in the bearings under conditions of almost absolute vacuum which arises in space. The laboratory model of the sensor weighs less than 230 grams. Insignificant consumption of electric power (10 milliwatts) permits a decrease in mass of the equipment and the volume occupied by it as a result of reducing the solar batteries and storage batteries needed to power it.

The oscillatory circuit is used to rock four small mirrors by means of which the earth is scanned in two mutually perpendicular directions. The mirrors are fastened to symmetrically installed flat springs connected on one end to a sound coil and on the other to the housing. Fig 2.5, c shows two mirrors permitting examination of space in one direction. The image of the earth is formed by the lens objective in the plane of the image shown in the figure. Small sections of the image of the edges of the earth are created using mirrors on the receiving platforms of the infrared detectors made of indium antimonide. On oscillation of the sound coil, the mirrors rock synchronously, by which the horizon of the earth is examined, at the diametrically opposite edges, and pulses are obtained at the output of the infrared detectors.

The functional diagram of the circuitry for comparing the pulses and obtaining control signals with respect to one direction is presented in Fig 2.6.

The pulse repetition frequency corresponds to the scanning speed. However, if the examined target (the earth) is not on the optical axis, then the pulse durations from the opposite detectors are not equal. At the output of the limiters the signals have a constant level independently of the brightness of the object, the sensitivity of the photoelements or the amplification of the different channels. Then rectification and filtration of the pulses takes place, and a constant voltage is obtained which is proportional to the pulse duration.
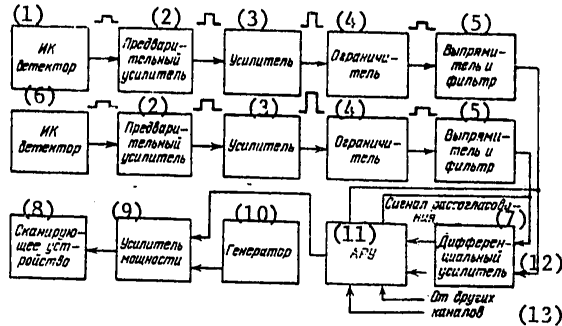
Figure 2.6. Functional diagram of obtaining the control signal
in the tracking type sensor without rotating parts

Key:
  1. Infrared detector
  2. Preamplifier
  3. Amplifier
  4. Limiter
  5. Rectifier and filter
  6. Infrared detector
  7. Mismatch signal
  8. Scanner
  9. Power amplifier
 10. Generator
 11. Automatic gain control
 12. Differential amplifier
 13. From the other channels

 A constant voltage is fed to the differential amplifier which generates
the mismatch signal which is equal to zero if the object is on the optical
axis. Otherwise, the signal is generated, the magnitude and sign of which
depend on the position of the object with respect to the optical axis.
The sound oscillator generates an AC voltage of defined fixed frequency
equal to the resonance frequency of the oscillations of the scanner, which
permits expenditure of a minimum quantity of energy to provide
scanning. The oscillator signals are fed to the power amplifier. The
automatic gain control permits insurance of the required amplitude of the
oscillations during scanning. Mismatch signals and rectified voltages
from all detectors are fed to the automatic amplification regulator. The
computer determines the optimal oscillation conditions of the mirrors. The
large scanning amplitude occurs with significant magnitude of the mismatch
signal with respect to one or both channels. The scanning with maximum
amplitude takes place if the mismatch signals and the rectified voltages
are equal to zero. This is possible if the earth is not in the field of
view, and large oscillation amplitude is required to find it.

28

For small mismatch signals the amplitude of the mirror oscillations decreases, which permits an increase in the accuracy of determining the direction toward the center of the earth when it is approximately on the optical axis of the system.

The radiation-balance sensors are used for direct determination of the local vertical as the direction of the center of the earth's disc. The image of the earth is projected on the system of stationary infrared detectors. The mismatch signal with respect to each axis is proportional to the signal difference in the corresponding pair of opposite detectors. For identical sensitivity of the detectors and uniform brightness of the disc of the planet, the orientation error is equal to zero for orientation on the center of the disc. The schematic of the arrangement of the field of view of the detectors is shown in Fig 2.3, g. With constant orbit altitude, for example, in a geostationary orbit, a system is used in which additional sections of the field of view below the line of the horizon are used (the radiation-compensation field of view), which permits the orientation error to be decreased for small mismatch angles.

The basic advantage of the radiation-balance sensors is considered to be absence of moving parts, low energy intake, small mass and high reliability. Usually thermocouples which generate a natural thermal current are used as the detector in the sensors of this type. One of the standard radiation balance sensors developed by the Barnes Engineering Company [2.7] uses bismuth antimonide thermocouples as the detector. The accuracy of orientation of the sensor is $\pm0.3°$. It weighs 1.5 kg, and the intake power is 3 watts. An accuracy of up to $\pm0.1°$ is planned for the developed sensors.

The correlation sensors are close to the radiation-balance sensors. In the correlation sensors it is not the signals themselves that are compared, but the correlation functions of the signals taken in each pair of detectors.

The accuracy of determining the infrared vertical depends on the error of the selected method of constructing the vertical (the procedural error), that is, the type of sensor and the instrument error which depend on the structural parameters of the specific developed model.

The procedural errors in constructing the vertical by the sensors of various types have been analyzed theoretically in advance [2. 12]. The influence of the following factors on the operation of the sensors was taken into account: the inaccuracy of insertion of the satellite into the given orbit (dispersion 25 km^2), nonsphericalness of the earth, instability of the altitude of the infrared horizon (dispersion 9 km^2), the incidence of cold clouds in the field of view of the instrument, broad nonuniformity of the radiation of the earth, and the radiation fluctuations. The calculations were performed for a field of view of the sensors of 3°. The relations obtained as a result of the calculations for the limiting angular error in angular minutes (with a fiducial probability of 95%) as a function of the flight altitude of the satellite are presented in Fig 2.7. In the figure the numbers indicate the curves pertaining to the following types
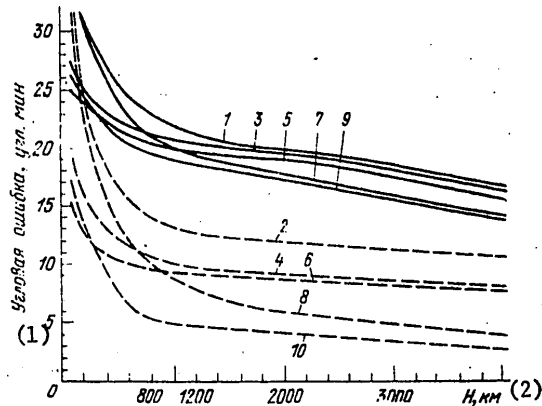
29

Figure 2.7. Dependence of the angular error of determination of
the local vertical on the flight altitude of the
artificial earth satellite.

Key:

1. Angular error, angular minutes
2. H, km

of sensors: 1, 2 -- radiation-balance; 3, 4 -- tracking; 5, 6 -- scanning;
7, 8 -- tracking the earth's horizon with respect to the entire circle;
9, 10 -- correlation. The solid lines indicate the curves for the
meridional plane, and the dashed lines, for the equatorial plane. By the
results of the calculations the conclusion is drawn that in the meridional
plane all of the investigated methods are in practice equivalent. In the
equatorial plane the most exact for altitudes of 100 to 900 km will be the
scanning and correlation sensors, and from 900 km up, the correlation
sensors and the sensors for circular tracking of the horizon.

In the United States [2.13] statistical processing of the flight data of
the scanning sensor of a satellite in low orbit has been carried out, and
joint tests have been run on the sensor model of the horizon and the
synthesized model of the horizon on computers. The sensor had two optical
heads realizing circular scanning by an instantaneous viewing angle of 40°.
On simulation of the horizon of the earth, radiation profiles of the horizon
were used for each month with intervals with respect to geographic latitude
of every 10°. The scanning configuration and optical characteristics of
the heads for simulating the signals of the bolometers were simulated for
various orbital parameters. The last signals went to the analog model of
the electronic part of the horizon sensor. The radiation profiles of the
horizon were calculated by integration over the spectrum in the range of
14-16 microns considering the transmission spectrum of the optical filter.
As a result of the simulation it was established that the largest errors
in determining the local vertical are characteristic of January. The mean
square deviations of the errors (in January) are 0.09° with respect to

30

pitch for orbital inclination of 60° and 0.08° for inclination of 114°; the maximum value is 0.26°. The maximum value of the error with respect to the yawing angle was 0.22°.

It is possible to use sensors of the infrared horizon also to solve other navigational problems, for example, sending instructions to switch on the engines of the second stage of a rocket when it reaches the calculated pitch angle. This method was used in designing a space missile launched from an aircraft providing for insertion of light weight satellites into orbit [2.14]. Two identical infrared horizon sensors are installed on the rocket, the optical axes of which make an angle of 12° with the longitudinal axis of the rocket. The infrared sensor has an objective, at the focal point of which the infrared radiation receiver is located.

When the rocket flying along a ballistic trajectory reaches an altitude of 85 km, the longitudinal axis of the rocket will be inclined +3° to the horizon. In this case the infrared radiation of the earth will fall into the field of view of the infrared sensors. As a result of rotation of the rocket at a rate of 5 rpm, the horizon sensors will generate voltage pulses which after amplification and integration create a controlling signal to switch on the engines of the second stage of the rocket. Integration prevents starting of the engine from random signals at the output of the sensors. For reliability, two independent channels are installed on the rocket for switching on the engines.

The infrared radiation of other planets, just as the radiation of the earth can be used to determine the local vertical of these planets during flights in direct proximity to them. The orientation with respect to the local vertical of the planets is required to guide the equipment designed to study the planets and also for landing the spacecraft on the planet. Proper orientation of the space object with respect to the selected planet and also the earth and the sun is important to transmit the observation data to the earth using directional radio antennas. The choice of the operating part of the spectrum of the orientation system sensors is determined by the radiation spectrum of the planets.

The surface of the cloud layer of the atmosphere of Venus [2.9] has a quite constant radiation temperature of 200-25°K. At the edges of the planet disc the temperature diminishes to 185-190°K (as a result of variation of the viewing angles and an increase in the proportion of the radiation of the colder, upper layers of the atmosphere). The latitudinal and diurnal variations in the radiation of the disc of Venus are almost unnoticeable. The brightness temperature of the atmosphere in the spectral range of 8 to 14 microns is within the limits of 215-240°K, and in the spectral bands of 3.5-4.0 microns and 17.5-22.0 microns it is about 240°K.

31

Stronger latitudinal and diurnal variations are observed in the radiation of the surface of Mars connected with its less dense atmosphere. By the measurement data from the Mariner 6 and 7 spacecraft, the radiation temperature in the spectral range of 8.5-12.5 microns fluctuates from 200°K on the dark side to 285°K on the light side, and in the spectral range of 18-25 microns, 150°K in the vicinity of the southern Polar cap (freezing point of CO_2) to 270°K in the middle latitudes. As a result of the low radiation temperatures of these planets the equipment for constructing the vertical must be sensitive to the long wave part of the infrared spectrum.

As a result of inaccuracy of the radiation parameters of the planets when using one parameter in the radiation profile of the infrared horizon, the errors in determining the altitude of the horizon (the mean square deviation) are 15 km for Mars and 20 km for Venus [2.15]. In order to increase the orientation precision to 10", it is propose that the data on the atmospheric parameters of the planets obtained in flight be processed on the ground and transmitted to the spacecraft to introduce corrections into the horizon sensors. The simulation of this technique on a computer demonstrated that it permits improvement of the accuracy of determining the infrared horizon for Mars and Venus to 5 km.

In order to determine the local vertical of the planets, sensors of the infrared horizon of the earth investigated above can be used. However, in cases where the orientation with respect to the planets begins at a larger distance, additional requirements are imposed on the sensors: the search for the planet and the operation in a wide range of variation of angular dimensions of the target.

The Barnes Engineering Company has developed an infrared system for orientation of the Mariner type spacecraft when flying near Mars or Venus beginning with a distance of about 160,000 km. After finding and detecting the planet, the orientation system switches to the automatic tracking mode. The object is oriented in this case so that the instruments designed to study the planet will be directed toward the center of its disc.

In order to find the planet, a scanning system is used which applies a pair of optical wedges rotating in opposite directions with different velocities (about 300 and 100 rpm). The instantaneous viewing angle of the system in this case is equal to 0.5x0.5° and describes a four-lobed pattern in space within the limits of the scanning angle of 70°. In the search mode the four-lobe sanning pattern formed as a result of rotation of the pair of optical wedges rotates as a unit whole at a velocity of about 5 rpm. By measuring the duration and distribution in time of the pulses from the target, the system generates mismatch signals with respect to each lobe of the scanning pattern. The equality of the mismatch signals achieved as a result of the corresponding change in position of the spacecraft means that the center of the disc of the target planet is on the axis of the system.

32

As the radiant energy receivers in the orientation systems with respect to Mars and Venus, an immersion thermistor bolometer is used which has high sensitivity and reacts to the radiation in a wide frequency range, including the long wave part of the spectrum in which these planets have maximum emission. The short wave radiation is clipped by the optical filter. Along with the determination of the local vertical, the horizon sensor can be used to determine the flight altitude by the angular dimensions of the planet disc.

If we consider the earth to be a sphere, the angular dimensions of the disc and the slight altitude of the satellites will be related by the following expression:

$$2\alpha = 2\text{arctg}\,\frac{R_3 + h_r}{\sqrt{2R_3(H - h_r) + (H^2 - h^2_r)}}, \qquad (2.1)$$

where 2α is the angular dimension of the observed disc of the earth; R_3 is the radius of the earth; H is the flight altitude of the satellite; h_Γ is the altitude of the infrared horizon.

As follows from formula (2.1), the angular dimensions of the earth's disc depend on the altitude of the infrared horizon and the flight altitude of the satellite. Table 2.1 gives the angular dimensions of the earth calculated by (2.1) for different flight altitudes. In the calculations the earth's radius is taken to be R_3=6371 km, and the altitude of the infrared horizon h_Γ=11 km. The derivative $d2\alpha/dH$, the maximum error in determining the angular dimensions $\Delta 2\alpha$ if the altitude of the horizon fluctuates from 6 to 16 km and the error connected with this in determining the flight altitude are also presented in the table.

Table 2.1

H, км	300	600	900	1200	1500
2α	145°52'	144°57'	143°10'	140°57'	138°10'
(1) $d2\alpha/dH$, угл.мин/км	0,22	0,28	0,38	0,50	0,64
(2) $\Delta 2\alpha$, угл. мин, при $\Delta h_r = 5$ км	18	17	16	15	15
(3) ΔH, км, при $\Delta h_r = 5$ км	82	63	42	30	22
(4) $\Delta H/H$, %, при $\Delta h_r = 5$ км	27,2	10,5	4,7	2,5	1,5

Key:
1. $d2\alpha/dH$, angular minutes/km
2. $\Delta 2\alpha$, angular minutes at Δh_Γ=5 km
3. ΔH, km, at Δh_Γ=5 km
4. $\Delta H/H$, %, at Δh_Γ=5 km

33

From Table 2.1 it is obvious that for low orbits the fluctuations of the altitude of the infrared horizon significantly influence the accuracy of determining the flight altitude. The accuracy of determining the flight altitude by the infrared horizon of the earth at low altitudes is low if there are no exact data on the altitude of the horizon. With an increase in orbital altitude the accuracy of determining the altitude increases.

2.3. Infrared Sensors Operating by the Radiation of the Sun, the Stars and Solar Radiation Reflected from the Planets

In order to determine the direction of the center of the disc of the planets (local vertical), sensors can also be used which operate by the solar radiation reflected from the planet. The advantage of these sensors is significantly lower cost (cheaper short wave radiation receivers and cheaper optical materials are used) and simplicity of structural design connected with easier tuning and adjustment of the instruments in the short wave part of the spectrum and simplicity of the structural design of the radiation receivers themselves. However, in this case they have appreciably lower accuracy ($\pm 0.5°$) as a result of less stability and determinacy of the characteristics of the solar radiation reflected from the planets. The albedo of the earth (the reflection coefficient of the solar radiation flux by the earth-atmosphere system) fluctuates within broad limits: from 2-3% (the average for the entire spectrum of the solar radiation) for certain ground surfaces to 23-26% for clouds [2.7]. In the visible part of the spectrum these fluctuations are still greater: from 3-6 to 55-78% for the same reflecting formations. In addition, the magnitude of the reflected solar radiation is influenced by a number of other factors, in particular, the optical thickness of the atmosphere, the sun height, and so on.

As the sensitive elements in the sensors operating by reflected radiation, usually silicon photovoltaic elements are used which are sensitive to radiation in the spectral range of 0.35 to 1.1 microns, that is, the visible and near infrared regions of the spectrum. The use of this spectral range permits us to decrease the range of oscillations of the initial signals by comparison with the visible radiation sensors. In addition, the silicon elements are distinguished by the highest stability of the characteristics under the conditions of inconstancy of the input signals and also the effect of the external environment (radiation, variable thermal conditions, and so on). The use of the reflected solar radiation sensors is limited, of course, only to the day side of the planet.

For angular dimensions of the earth of 0.2 to 12° usually sensors are used with shadow masks which insure the required field of view and also radiation and balance sensors analogous to the infrared horizon sensors.

The high signal level permits us to get along with a simpler optical system, in particular, a slit optical system. For rotation-stabilized satellites, sensors with slits and irises for limiting the field of view and the digital equipment for processing the signals are used. Thus, for the

34

FOR OFFICIAL USE ONLY

Neos artificial earth satellite stabilized by rotation the VAS Company
developed a sensor with two slit (fan) fields of view. One field of view
is meridional parallel to the axis of rotation of the satellite and the
other is inclined by 30° to the meridional target, Three cylindrical
lenses create an image of the earth illuminated by the sun on silicon
photoelements. The fields of view of the sensors are created jointly by
the slits and cylinders 120x1°. The sensor is capable of operating with
irradiation of no less than $0.6 \cdot 10^{-6}$ watts-cm^{-2} in the spectral range of
0.35 to 1.1 microns. The accuracy of orientation is $\pm 0.5°$. Shutters are
used which exclude the interference of the sun at an altitude to 15°. The
sun is the most powerful source of radiation for optical sensors in flight
within the limits of the solar system, and therefore it is used as one of
the basic navigational reference points. Its angular dimensions are about
32'.

The maximum in the radiation spectrum of the sun is in the middle of the
visible part of the spectrum (about 0.5 microns). However, in the visible
and the ultraviolet parts of the spectrum, the scattering of the solar
radiation by the earth's atmosphere is large; therefore the brightness of
the solar disc observed from the earth's surface depends to a significant
degree on its altitude and the meteorological conditions. As a result of
significant fluctuations of the output signals of the equipment on variation
of the observation conditions of the sun, the use of the visible part of
the spectrum for operation of solar sensors is inconvenient when tuning
the equipment under ground conditions. From this point of view it is more
efficient to use the short wave infrared part of the spectrum. Therefore
in the solar sensors basically silicon photoelements are used which are
sensitive to the spectral range of 0.35 to 1.1 micron and distinguished by
the best stability of the characteristics for high sensitivity. In addition,
cadmium selenide photoresistors are used which have a number of advantages
when operating under high illumination conditions. These advantages include
the following: a decrease in internal resistance leading to a decrease in
noise level, and a decrease in its periodicity with an increase in the light
flux incident on it. When using cadmium selenide photoresistors with red
optical filters, maximum spectral sensitivity of about 0.25 microns is
insured with a long wave boundary of about 1.1 microns.

The solar orientation systems usually have rough orientation sensors which
have a wide viewing angle and provide for the initial search and lockon of
the target (the sun) and precision orientation sensors having a narrow
viewing angle and permitting orientation of the spacecraft with respect to
the sun with the required accuracy. The rough orientation system is used
to stop the rotation of the spacecraft obtained as a result of the effect
of various disturbances and it insures that the sun will fall into the
field of view of the exact orientation system. In addition, the orientation
system has a sensor which generates the lock on signal for the precision
orientation system.

35

FOR OFFICIAL USE ONLY

There are several basic types [2.7] of solar sensors: analog sensors with
the application of shadow gratings and masks, analog sensors with a square
mosaic made up of four photoelements, sensors with slits and rasters and
also digital sensors.

In the analog sensors with the application of gratings and masks, the rela-
tion is used for the output signal of the detector (usually a silicon
photoelement) as a function of the magnitude of the incident radiation flux
which, in turn, is connected with the angle of incidence of the solar radia-
tion. The diagram of one of the analog sensors with the application of a
shadow mask is shown in Fig 2.8, a. In this sensor, with an increase in the
angle of inclination of the solar radiation α, the area of the illuminated
section of the photoelement decreases. For a quadratic photoelement with
a length of side L the operating signal will be

$$I = k_1 PA \cos \alpha = k_1 P (L - d \operatorname{tg} \alpha) \cos \alpha =$$
$$= k_2 \cos \alpha - k_3 \sin \alpha \approx k_2 \cos \alpha,$$

where P is the solar constant; A is the area of the illuminated section
of the photoelement; d is the distance from the masks to the photoelement;
k_1, k_2, k_3 are constants.

One of the deficiencies of the sensors with shadow gratings and masks is
their weak noise resistance to the radiation of the earth illuminated by the
sun. The investigated type of sensor is used on rockets and artificial
earth satellites. The typical sensor built by the Ball Brothers has a
heading accuracy of $\pm 5°$ with an angle of field of view of ± 90 and $\pm 0.02°$
with respect to the precision channel with a viewing angle of 15°.

One of the sensors of the same type which has come to be called the "multi-
slit shadow direction sensor" was used for exact orientation of the photo-
electric spectrometer for extraatmospheric studies of the sun [2.16]. The
sensor provided for aiming the spectrometer with a precision up to $\pm 7"$.
It uses a set of z-profile irises which are in the form of gratings behind
which two counter-included silicon photoelements are installed which
generate a mismatch signal with respect to one axis. On coincidence of the
optical axis of the sensor with the direction of the center of the solar
disc, both photoelements are in the shadow, and the signal is equal to zero.
On the appearance of the mismatch angle, one of the photoelements is lit,
and the level of its illumination depends on the size of the mismatch angle.
In order to obtain data on the orientation with respect to the second axis,
a second sensor of analogous structural design is used. Each sensor con-
tains 8 z-type plates 6 mm wide each. The height of the plates is 60 mm.
The sensor has a linear output characteristic within the limits of the
field of view of about $\pm 20°$. High requirements of identity of the counter-
included two photoelements are not imposed on these sensors inasmuch as
on coincidence of the optical axis of the sensor with the center of the
sun both photoelements are not illuminated. The mutual divergence in the
operating process of the parameters of the photoelements used in one sensor
by 10% leads to an angle error of a total of 0.54'.

36
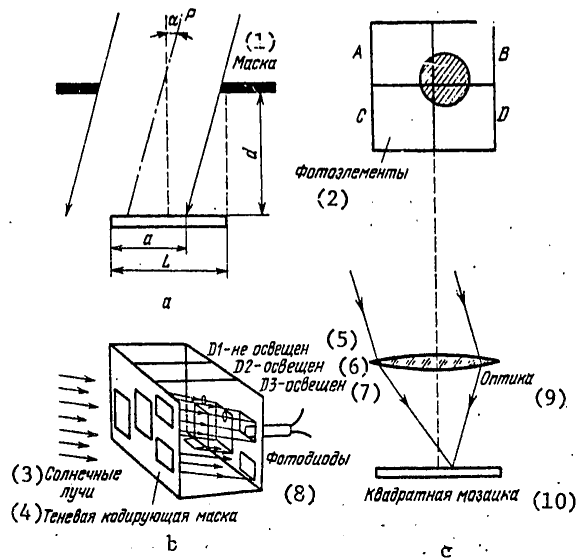
Figure 2.8. Optical systems of the sensors for orientation
by the sun:
a -- analog sensor with shadow mask; b -- analog sensor with
square mosaic of four photoelements; c -- digital pickup

Key:
1. Mask
2. Photoelements
3. Sunbeams
4. Shadow coding mask
5. D1-not illuminated
6. D2--illuminated
7. D3--illuminated
8. Photodiodes
9. Optical system
10. Quadratic mosaic

In the analog solar sensors with quadratic mosaic, the image of the sun or
the shadow from the mask is projected on the mosaic of four photoelements
forming a square. The schematic of one version of the sensor [2.7] is
shown in Fig 2.8, b. When the mismatch error is equal to zero, the image
is located in the center of the mosaic, and all of the photoelements are
illuminated identically. When a mismatch error appears, the photoelements
are illuminated differently, and the angular errors with respect to the
two axes can be defined in the following order with respect to magnitude
of the photoelement signals:

Pitch error equal to (A+B)-(C+D);

Error with respect to yawing angle equal to (A+C)-(B+D).

Linearity of the characteristic depends on the shape of the image of the sun. The greatest linearity is achieved for a rectangular shape which is created by using a mask. In order to provide for search for the sun usually additional peripheral elements are used.

The Bendix Corporation has developed several sensors with quadratic mosaic. One of the sensors searches for the sun within the angular limits of $\pm 90°$ using peripheral photoelements, and exact tracking within the limits of the angle of $\pm 10°$. In the other sensor of the same company, exact tracking is realized to 1" within the limits of a small viewing angle (40') which is insured using a long focal-length lens (50 cm). In the sensor made by RAE Company, an accuracy of ± 10" is achieved in the viewing angle of 20x10°. It is possible to include the sensors using photoelements having longitudinal photoeffect among the same type of sensors (these are the so-called coordinate photoelements) [2.17], in which the signal characterizing the position of the light spots on the sensitive layer of the photoelement is picked up from two pairs of contacts arranged with respect to two mutually perpendicular axes of the photoelements.

The sun sensors with slits or rasters are used to insure a specific shape of the field of view, usually narrow. Most frequently these sensors are used in rotating spacecraft to determine the speed of rotation and the angle between the axis of rotation and the direction of the sun. One of the simplest sensors of this type developed by the RAE Company has been installed on the Skylark research rocket [2.7]. In the sensor two narrow slits are used with an angular size of 1x180° intersecting at an angle θ. Each field of view is formed by a narrow slit notch in a hemisphere above a silicon photodiode. On rotation of the rocket, sunbeams hit the slit notches, and photocurrent pulses arise. The time between these pulses can be converted to the angle of rotation ψ. The angle Φ between the direction of the sun and the axis of rotation is determined from the expression $\operatorname{ctg}\Phi = \sin\psi \operatorname{ctg}\theta$. The accuracy of this sensor is no less than 0.25°.

The optical system of the 3-bit digital solar sensor [2.7] is illustrated in Fig 2.8, c. The sunbeams reach the three silicon photodiodes through the shadow coding mask. Between the photodiodes there are opaque baffles which insure that the sunlight will hit the photodiodes only through the holes located directly in front of them. Here defined combinations of illumination of the photodiodes are insured for different rising angles of the sun. The accuracy of orientation depends on the digital capacity of the sensor. The field of view is broken down into 2n-1 segments for a number of binary detectors (photodiodes) n. The code of the investigated 3-bit detector is presented in Table 2.2.

38

FOR OFFICIAL USE ONLY

Table 2.2.

(1)

Номер сегмента поля зрения	Номер диода (2)		
	1	2	3
0			
1			1
2		1	
3		1	1
4	1		
5	1		1
6	1	1	
7	1	1	1

Key:
1. No of the segment of the field of view
2. No of the diode

The digital sun sensors have the following advantages: the digital form of the signals permits direct transmission of the orientation data over the telemetric channel; the radiation reflected from the earth can be selected as a result of choosing the response threshold of the triggers at the photodiode output; the small energy consumption, mass and dimensions; they can be used both in rotating spacecraft and in vehicles with triaxial stabilization. A seven-bit digital solar sensor built by the Alcole Corporation with seven photodiodes is used in practice. Its field of view is $\pm 64°$, the angular resolution is $1°$. The dimensions of the device, including the optical system and the diodes are $3.2 \times 3.2 \times 1.4$ cm^3, and it weights 112 grams.

During interplanetary flights the stars are the most important reference points. They have different temperature and different spectral composition of their radiation--from ultraviolet to the near infrared. The radiation characteristics of some of the brightest stars beyond the Earth's atmosphere are presented in Table 2.3.

Table 2.3

Star	Maximum spectral density of irradiation, watts-cm^{-2}-micron^{-1}	Wave length corresponding to the spectral maximum of the irradiation, microns
Sirius	$4 \cdot 10^{-11}$	0.3
Canopus	$3 \cdot 10^{-12}$	0.6
Antares	$8 \cdot 10^{-13}$	1.3

39

FOR OFFICIAL USE ONLY

In the stellar orientation sensors, photomultipliers are used as the sensitive elements. When operating with respect to the stars having maximum radiation in the infrared part of the spectrum, usually photomultipliers are used with oxygen-cesium photocathode sensitive to the near infrared radiation (to wavelengths of about 1.4 microns). Several basic types of stellar sensors are distinguished [2.9]: static, sensors with optomechanical and electronic scanning.

The static sensors usually contain an objective, a light divider in the form of a two-sided prism and two photomultipliers. The angular position of the star is determined by the difference of the signals from two photomultipliers.

The sensors with mechanical scanning are made with different raster type rotating discs which realize amplitude, frequency or phase modulation of the radiation fluxes from the star.

The sensors with electronic scanning can be used as the radiation receivers of the photomultipliers or cathode-ray tube with an image dissector.

Thus, the infrared devices are used primarily in nagivation for the construction of the local vertical of the planets and also for orientation with respect to the sun and certain stars.

The generalized characteristics of the standard orientation sensors [2.7] using infrared radiation of the planets, the sun and the stars are presented in Table 2.4.

Table 2.4

Object used for orientation	Angular dimensions of the object	Used spectral range, microns	Operating level of irradiation, watts-cm^{-2}	Type of radiation detector	Typical accuracy of orientation of the sensor, °
Sun	0.53°	0.35-1.1	10^{-1}	Silicon photo-elements	± 0.03
Reflected radiation of the Earth	100-2° (depending on altitude)	0.35-1.1	10^{-2}-10^{-6}	The same	± 0.5
Infrared radiation of the Earth	150-10° (depending on altitude), 17.3° for geostationary satellites	Usually 14-16	10^{-3} for geostationary orbits	Thermistors, Bolometers, Thermocouples	± 0.2
Stars	0.04-0.005° (depending on the star)	0.15-1.4	10^{-11} to 10^{-14} (depending on the star)	Photo-multiplier	± 0.003

CHAPTER 3. ASTROPHYSICAL RESEARCH

3.1. Problems and Characteristics of Astrophysical Research, Conducted
     With the Help of Infrared Equipment

The problems and characteristics of astrophysical research performed
at the observatories throughout the world make it possible to obtain
various information about the stars and planets. When studying the
heavenly bodies astronomers usually use direct photography, photometry
and spectrography.

At first the majority of astrophysical measurements were performed using
photographic plates. In the last decades, in connection with the appearance
of highly sensitive infrared radiation receivers, these studies have begun
to be performed not only in the visible but also in the infrared parts of
the spectrum using highly sensitive photomultipliers (including with oxygen-
cesium photocathode) and various photoresistors having high sensitivity in
a wide band of the infrared spectrum. The spectral analysis of the emission
of the heavenly bodies is of the greatest interest in astrophysical research.
The spectral measurements permit, for example, determination of the tempera-
ture of the heavenly body, the chemical composition and structure of the
atmosphere, the direction of motion with respect to the observer, the
distance and even the age of stars. A significant part of these data are
obtained during spectral studies in the infrared part of the spectrum.

The overwhelming majority of astrophysical data available at the present
time were obtained during observations from the earth's surface. However,
the observation through the earth's atmosphere creates a number of diffi-
culties when performing astronomical measurements. Thus, the atmosphere is
not transparent for an entire series of sections of the infrared spectrum.
The absorption bands of water vapor and gases contained in the earth's
atmosphere are superposed on the absorption bands of the same gases and
vapor in the atmosphere of other planets, which complicates the spectroscopic
studies of the properties of their atmospheres.

The observation conditions from the earth change continuously depending on
the time of day and the state of the atmosphere (clouds, air humidity and
so on). The turbulence of the atmosphere does not permit realization of
the theoretical resolution of the telescopes, and the glow of the sky re-
strictsthe limits of resolution of the telescopes with respect to brightness.

The glow of the daytime sky in the spectral range to 4 microns is caused by scattering of the sunbeams in the atmosphere. In the range of $\lambda > 4$ microns, the thermal emission of the atmosphere predominates. The brightness of the daytime sky depends on the angular distance of the investigated point of the sky from the sun and its altitude. Fig 3.1 shows the spectral brightnesses of various points in the sky for infrared part of the spectrum [3.1]. The glow of the daytime sky is a serious obstacle for astrophysical studies in the short wave pawrt of the infrared spectrum. The glow of the night sky is caused by several things. About 7% of the light flux of the night sky is sunlight which is scattered in the lower layers of the atmosphere. The luminescent glow of the upper layers of the atmosphere is about 40%. The latter does not interfere with observations by telescopes at an altitude of more than 800 km. The zodiacal light is sunlight scattered by meteoritic dust and gases within the boundaries of the solar system. It amounts to about 20%. Approximately 20% falls to the lot of starlight -- the light from stars and galaxies which are not zoned as individual stars by the telescopes. The remaining 13% is light from the stars scattered by the interstellar (cosmic) dust and gases. The starlight and the glow of cosmic dust gases will limit the observation possibilities also at great distance from the surface of the earth.
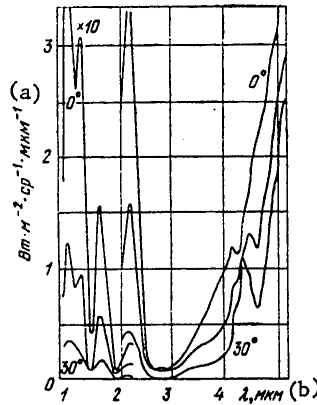
Figure 3.1. Spectral radiance of the daytime sky and the infrared part of the spectrum (for various angles of elevation above the horizon).

Key: (a) watts-m^{-2}-steradians^{-1}-micron^{-1}

(b) micron
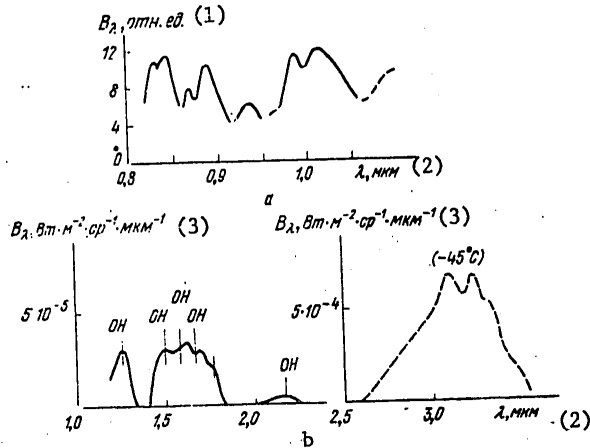
Figure 3.2. Spectral radiance of the night sky

Key:
1. Relative units
2. λ, microns
3. B_λ, watts-m^{-2}-steradians^{-1}-microns^{-1}

The total brightness of the night sky in the darkest sections during observation on large telescopes is approximately equal to the mean overall brightness of one magnitude 20 star* for the solid angle formed by a cone with the angle at the apex equal to one arc second. This glow limits the resolution with respect to brightness of the astronomical instruments. With a field of view of several arc seconds it is impossible to detect a magnitude 23 star.

In Fig 3.2, a, the spectral brightness of the night sky in the spectral region of 0.8-1.1 microns is presented in relative units [3.2]. The bands existing in the spectrum are caused basically by the radiation of molecular oxygen O_2.

The infrared part of the spectrum to 1.1 micron exceeds by 100-200 times the radiation of the green line of the night sky with the center at 0.5577 microns.

---

*By the stellar magnitude of a heavenly body we mean the value of $m=14.2-2.5$ lg E, where E is the illumination in lux created by the heavenly body at the observation point in the plane perpendicular to the beams. The illumination created by a magnitude 20 star on the ground surface is equal to $2.1 \cdot 10^{-14}$ lux.

In the 1.2-2.5 micron band there are intense radiation bands (Fig 3.2, b) caused by the presence of hydroxyl OH in the upper layers of the atmosphere [3.3]. In the $\lambda > 2.5$ micron region, the thermal radiation of the atmosphere is noticeable even in low air temperature (-45°C),

On wave lengths of more than 4 microns the radiation of both the day and night skies is caused by the natural emission of the atmosphere which basically depends on the air temperature in the lower layers and the water vapor content. The spectra of the thermal emission of the atmosphere are presented in Fig 3.3 [3.4].
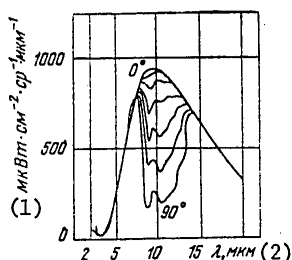
Figure 3.3. Thermal radiation of the atmosphere at various angles of elevation above the horizon

Key:
1. Microwatts-cm^{-2}-steradians^{-1}-microns^{-1}
2. λ, microns

3.2. Astrophysical Studies from the Earth's Surface

In the infrared region of the spectrum studies were made of the radiation of the sun, the moon, the planets and some of the stars.

In 1947 Koyper published a series of planetary spectra in the infrared band of 0.7-2.5 microns [3, 5]. The study of the planetary spectra made it possible to discover the composition of their atmospheres. Thus, Koyper detected very strong absorption bands of methane CH_4 and ammonia NH_3 in the spectra of the sun and Jupiter. A quantitative estimate is also made of the content of the various gases in the atmosphere of the planets. For example, according to Koyper's estimate, in the atmosphere of Saturn the methane content is equivalent to a layer 350 meters thick under normal conditions, that is, at a temperature of 0°C and a pressure of 760 mm Hg. The spectrum of the rings of Saturn investigated in the wave length band of 0.7-2.0 microns was identified with the reflection spectrum of frost. Koyper's hypothesis was confirmed by the measurements of V. I. Moroz [3.6], who compared the spectra of the rings of Saturn with the spectrum of frost and snow also in the 2.0-2.5 micron region and detected a diffuse maximum at 2.22 microns characteristic of the selective reflection of frost.

45

A large volume of research to study the spectra of the moon was performed when selecting the landing sites for the Apollo spacecraft.

The selection of the landing sites on the moon had to insure maximum safety. In addition, the samples of lunar rock picked up at the landing sites and delivered to the earth had to give the most complete information about the lunar surface. The California Institute of Technology [3.7] performed ground studies of the spectral reflectivity of the moon in the visible and near infrared part of the spectrum and the spectral emittance in the far infrared part of the spectrum of 5 of the first landing sites of the Apollo spacecraft. In addition, studies were made of photographs obtained by the Lunar Orbiter to estimate the comparative age of the surface layer.

In order to determine the difference in structure and composition of the surface layer of the first five proposed landing sites for Apollo the measurements of the spectral emittance of the surface of the moon were performed in the range of 0.4-1.1 microns. The measurements were performed during summer and fall of 1968 from Mt Wilson using the 61 and 152-cm telescopes and a special twin-beam photoelectric multichannel photometer with filters. The narrow band interchangeable interference filters used to separate the entire spectral range into section every 0.02 to 0.05 microns were installed behind the active iris. In the 61-cm telescope an iris was used which provided a field of view of 10" (18 km on the surface of the moon at the center of the observed disc), and on the 152-cm telescope, 6" (10 km). Cooled photomultipliers were used, and an analog synchronous and high-speed two-channel pulse counting system were used to record the signals. By using each filter, the intensity of the signal reflected from the surface of one section was measured with respect to the signal from the other section (usually the section in the Mare Serenitatis with the coordinates 21.4° east longitude, 18.7° north latitude). For each point 6 to 18 measurements were taken with each filter with an identical phase angle of the sun for all points. A large difference in the reflecting properties of points 1, 2 and 3 was noted. The properties of points 4 and 5 are close. No strict correlation was detected between the reflecting properties in the visible and near infrared regions of the spectrum. In addition to the effect of the phase angle of the sun, no other dependence of the reflecting properties on time, in particular, luminescence, was found. The results of the measurements with different fields of view agree well with the exception of some of the measurements and points 1 and 2.

The measurements of the spectral emissivity were performed in the range of 8.2-13.4 microns for nine sections of the lunar surface, including five landing sites for the Apollo spacecraft. The ratios of the difference in the radiation spectra of two different sites to the spectrum of one of them obtained in series were determined. The results were processed by the least squares method to exclude the effect of the surface temperature difference and the variations of the transparency of the atmosphere.

The measurements were performed using the Ebert-Fastie spectrometer with a mercury-alloyed germanium receiver. The average spectral resolution is 0.08 microns. The angle of the conical field of view was 27" (the size of the site on the surface of the moon was 40 km), The spectrometer output was digital. From June to October 1968, 12 to 24 spectra were obtained for each of nine sections of the moon. In addition to the five landing sites for Apollo, the emissivities of the cirques and craters were also measured: Plato, Copernicus, Aristirchus and the southern part of the crater Gassendi, As a result of the measurements, significant differences were detected in the spectra of five Apollo landing sites and other sections with the exception of the anomaly in the spectrum of Plato.

When analyzing the results, a study was made of several different hypotheses. The most probable explanation is that the differences in surface structure for small, the Si and O ratios in the surface layer are different, and the observed spectral difference is caused by the Christiansen vibration frequency. This hypothesis agrees with the particle distribution with respect to size obtained using the Surveyor spacecraft with investigation of the morphology by the Lunar Orbiter photographs.

In addition [3.8] measurements were made of the relative reflectivity of sections of the moon in the spectral range of 0.72–1.1 micron which are joined to the results of the preceding measurements of the same sections of the moon in the spectral range of 0.4–0.8 microns.

No less than 3 measurements of each part of the moon were taken in one night. The measurements were performed on several nights over the extent of several lunar months. A total of 22 sections of the lunar surface were examined. The spectra were normalized with respect to reflectivity on the wave length of 0.52 microns. In the visible range of the spectrum the color contrast decreases with a decrease in the phase angle of the moon. In the spectral range of 0.4–0.8 microns when changing the phase angle by 90° the maximum variation of the color contrast reaches 2 to 3%. This effect was not detected in the spectral range of 0.8–1.1 micron. The measurement errors basically do not exceed 1%. The spectra obtained are distinguished by great variety. In some spectra the maximum of about 1 micron, the rise and fall in the light blue part of them are noted. The amplitudes on different spectral sections are poorly correlated. The correlation is detected between the form of the spectrum and the morphology of the observed section, The spectra are grouped in the following groups: plateaus, seas and the bottoms of bright craters. Possible causes of the difference in spectra of the sections of the moon are the difference in physical characteristics of the surface (the particle sizes, density, and so on), physical or chemical effects, aging processes and also the difference in chemical composition. In accordance with the results of the laboratory studies the conclusion was drawn that the difference in reflectivities is connected with the mineralogical difference and difference in composition.

FOR OFFICIAL USE ONLY

3.3. Astrophysical Studies Using Equipment on Board Aircraft, Balloons and Rocket Probes

On rising above the atmosphere, the resolution of the equipment with respect to angle and brightness increases significantly. At an altitude of 25 km the atmospheric interference is already insignificant, and even the scattered solar emission at night does not disturb the astronomical research. The ascent to this altitude made it possible to reach the theoretical resolution of a 30-cm telescope. In order to perform studies from altitudes of more than 10 km, balloons are used which can make extended measurements without great material expenditures. The installation of the astronomical measuring equipment on balloons was the first step along the path of expanding the possibilities of radiation of the universe using infrared equipment. The measurements in the infrared range of the spectrum performed from the balloons made it possible to obtain some new data on planets. Thus, when analyzing the spectrum of the reflected radiation of Venus obtained in 1959 using the equipment installed on the balloon, the water vapor absorption bands were detected. On observing through the earth's atmosphere, which contains a large amount of moisture, it was not possible to detect these bands in the atmosphere of Venus. The discovery made permitted advancement of the proposition of the possibility of the existence of certain forms of life on this planet.

It is proposed that further use be made of inflated balloons to investigate the planets of the solar system. In 1983 it is planned to deliver inflated balloons to Venus on a Soviet automatic interplanetary station, the gondolas of which will contain Soviet and French instruments [3.25].

The research rockets are used for astrogeophysical, biological and ionospheric studies, for the development and testing of spacecraft equipment. These problems were solved by the B2A and B5V Soviet geophysical rockets in the interest of creating the first artificial earth satellites [1.1]. The complex studies of the solar emission were performed by the Vertikal' type rockets (1970-1977) by the program of cooperation of socialist countries in the field of the investigation and use of outer space for peaceful purposes [1.1].

The tests of some of the instruments for the Apollo and Skylab American spacecraft were performed on the Aerobee 150 rockets [3.27].

A great deal of attention has been given to the investigation of the nature of the emission of the sky in the far infrared part of the spectrum using equipment installed on research rockets. Thus, on the Black Brant VB rocket launched from the test area on Wallops Island (Virginia, USA) on 24 February 1971 [3.9], there was a liquid-helium cooled telescope constructed for astronomical studies in the far infrared and submillimeter parts of the spectrum. The photometer had two channels: with Ge:Ga receiver for measurements in the spectral band with the center at $\lambda=100$ microns and with the GaAs receiver at $\lambda-280$ microns. Helium cooling was realized for 216 seconds of flight. The data were obtained at altitudes of 130-275 km. The orientation of the rocket at the time of the

48
FOR OFFICIAL USE ONLY

measurements was with the help of a gyroplatform of the MIDAS system and an ordinary sidereal photometer. The calibration was done by a model of an absolutely black body at an ambient temperature of 4.2 K. The laboratory studies demonstrated that the sensitivity of the Ge:Ga receiver in practice does not change on variation of the temperature within the limits of 4.2-2.8 K, and the sensitivity of the GaAs receiver is cut in half. Equivalent power of the receiver noise is $6 \cdot 10^{-14}$ and $4 \cdot 10^{-12}$ watts·hertz$^{-1/2}$ respectively at a temperature of 4.2 K. The absolute calibration was made with no more than twofold error.

The measurements demonstrated that the energy brightness in the two spectral sections is constant at zenith distances of 0-20°, and it is equal to $1.4 \cdot 10^{-9}$ watts-cm^{-2}-steradians^{-1} on $\lambda=100$ microns and $2.5 \cdot 10^{-9}$ watts-cm^{-2}-steradians^{-1} on $\lambda=280$ microns. At large zenith distances the signals increase, which is explained by scattering of radiation reflected from the earth inside the instrument, especially in the spectral channel of 280 microns, inasmuch as in the given part of the spectrum the blackened surfaces inside the photometer have a large reflection coefficient. Insignificant variation of the energy brightness in time (at altitudes to 275 km) is noted. By the measurement results the conclusion is drawn that the radiation is not connected with the ionosphere.

On 29 May 1971, measurements were made of the infrared radiation of the night sky from on-board a rocket launched from the test area in the Hawaiian Islands. The measurement data were obtained [3.10] on two spectral channels: with center of $\lambda=100$ microns and in the range of 0.8-6 microns (maximum sensitivity about $\lambda=1.1$ micron). The radiometer had a conical optical system and germanium bolometers with optical filters. The size of the sensitive area was 4x4 mm^2, and the viewing angle was about 0.1 steradian. The bolometers and the entire optical systems were cooled by helium. A radiation calibration of the instrument was made periodically on board, which excluded the effect of the decrease in the amplification coefficient of the amplifiers observed during the flight on the accuracy of the measurements. At an altitude of 120 km, the nose cone was jettisoned, the axis of the instrument was directed at an angle of 11° to the zenith in an easterly direction, and scanning began in the north-south plane within the limits to 65° from the zenith. A total of two complete scans were made. The measurements were performed at altitudes of 185-340 km for 420 seconds.

The emission near the horizon in the range of 0.8-6 microns turned out to be somewhat higher than expected. The average radiation temperature is $3.1^{+0.5}_{-2.0}$ K. The upper radiance limit was $1.5 \cdot 10^{-10}$ watts-cm^{-2}-steradians^{-1}. The mean square value of the equivalent noise power of the instrument is $3 \cdot 10^{-11}$ watts-cm^{-2}-steradians^{-1}. Considering the instrument noise, the nonlinearity of the electronics and the telemetric system and also the calibration errors, the accuracy of the measurements of the radiation temperature (maximum error) is 40%. In the spectral channel with center near $\lambda=100$ microns, the maximum value of the energy brightness of the sky is $1.2 \cdot 10^{-10}$ watts-cm^{-2}-steradians^{-1}.

FOR OFFICIAL USE ONLY

3.4. Astrophysical Studies Using Spacecraft

The astrophysical studies on board artificial earth satellites and auto-
matic interplanetary stations have become the basis for a qualitative
discontinuity in the study of space targets and outer space. Space
astrophysics takes its origins from the launching of the second Soviet
satellite. The astronomical and astrophysical observations, the study of
interplanetary space constitute a component part of the research program
of the majority of artificial earth satellites that have been launched
and are to be launched. In the USSR such studies have been performed by
the satellites in the Prognoz series, which are solar observatories, the
Proton and Elektron series. Complex studies of the upper layers of the
atmosphere, radiation belts, the ionosphere and the radiation of the sun
are made by satellites of the Interkosmos and Kosmos series [1.1].

In the United States astrophysical studies are being performed by a series
of four orbital astronomical observatories (OAO). The studies of the sun
are realized using the OSO series satellites, and a broad program of
astrophysical studies is being performed by the Explorer series of satellites.

The scientific data on the moon and the planets of the solar system obtained
using automatic interplanetary stations in flight near planets and in
planetocentric orbits are of great value. The beginning of these studies
was the flights by the Soviet automatic interplanetary stations "Luna-1"
("Mechta") in 1959, Venera-1 in 1961, "Mars-1" in 1962 [1.1]. The studies
of the moon were made by the Soviet automatic interplanetary stations in
the "Luna" and "Zond" series, the American Luna Orbiter, and Surveyor series.
The American automatic interplanetary stations of the Mariner, Pioneer and
Viking type performed studies of the planets of the solar system. The
automatic interplanetary stations Mariner 4, 6, 7, 9 and Viking 1, 2
investigated Mars, Mariner 10 investigated Venus and Mercury, and Pioneer
10 and 11 investigated Jupiter and Saturn.

Table 3.1

Type of observations	Total volume of data obtained, bits	Maximum resolution on the surface, km	Total cost, dollars.10^8
All ground observations (telescopes)	$7 \cdot 10^7$	100	--
Mariner 4 (1965) -- fly-by	$3.5 \cdot 10^6$	3	1.25
Mariner 6 and 7 (1969) -- fly-by	$5 \cdot 10^8$	0.3	1.5
Mariner 9 (1971) -- orbital	$5 \cdot 10^{10}$	0.06	1.5

50
FOR OFFICIAL USE ONLY

The flights of the automatic interplanetary stations in planetary satellite orbits permit periodic examination of in practice the entire surface with high resolution, and they provide large volumes of information.

The comparative estimate of the informativeness and cost of the Mars observations from earth and using automatic interplanetary stations [3.11] is made in Table 3.1. The infrared equipment plays a significant role in obtaining information about the moon and planets of the solar system.

The first astrophysical investigations to study the infrared spectrum of the solar emission reflected from the surface of Mars were to be performed from on board the "Mars" and Mariner automatic space stations in 1962-1964 to check out the hypotheses of the presence of certain forms of vegetable life on Mars advanced by Soviet scientists headed by G. A. Tikhov and based on seasonal changes in color on its surface and the presence of absorption bands near 3.5 microns in the Martian spectrum analogous to the absorption band of terrestrial lichens and certain forms of desert vegetation.

In recent years the hopes to detect certain forms of life on Mars have diminished significantly, especially after the flights of Viking 1 and 2 (1976). Now some astronomers [3.12] explain the seasonal changes by fluctuations of the water content in the rock: the evaporation of moisture can influence the color of organic and inorganic materials. Another important cause is considered to be the change in structure and the particle size as a result of dust storms. Large particles settle on the high plateaus and fine ones in the lowlands.

In 1969 Mars was examined by the Mariner 6 and 7 space stations on flying past the planet.

Mariner 6 was designed to observe the equatorial region, and Mariner 7, the southern polar cap. The following equipment was installed on board: two television cameras, an IRS infrared spectrometer for detecting water vapor, carbon dioxide, methane, ethylene, acetylene and other organic gases; an IRR infrared radiometer for determining the surface temperature; a UVS ultraviolet spectrometer for identification of gases in the upper layers of the atmosphere and determination of the quantity of them.

In the IRS spectrometer [3.13] a monochromator was used with rotating interference filters with variable pass bands. In order to encompass the range of 1.9-14.4 microns, two optical channels are used with different radiation receivers. The Hg:Ge photoresistor cooled to a temperature of 22°K by using the two-stage (N_2 and H_2) Joule-Thomson cryostat is used in the first long wave channel (4.0-14.4 microns). In the second channel (1.9-6.0 microns), a PbFe photoresistor is used which operates at a temperature of 175°K as a result of radiation cooling.

In order to lower the level of internal interference and decrease the
sensitivity, the entire spectrometer was cooled to a temperature of 280°K
as a result of radiation cooling of the heat regulating surface 10x8.3 cm.
The input objective of the instrument was a two-component Dall-Kirkhal
mirror objective. The radiant flux at the output of the objective is
split into two parts using a light dividing prism. Part of the aperture
and shielding used for the long wave channel has a temperature of 175°K.
The focused radiant flux in each channel is modulated by a moving dipole
and passes through the corresponding variable interference and cutoff
filters. Then the radiant fluxes are incident on the ellipsoidal mirrors
and are focused on the detectors. The objective has a focal length of
49.8 cm and a relative aperture of 1:2. In the center of the second mirror
is an opening with a diameter of 2.86 cm behind which a conical mirror
reflector is placed (with apex angle of 90°) insuring viewing of the cosmic
background (effective radiation temperature 4°K). All $_0$of the mirrors are
aluminum with a surface layer of silicon monoxide 500 Å thick. The
reflection coefficient is 96% in the range of 1.9-14.4 microns. A special
system for attaching the mirrorsexcludes vibration of them.

The variable filters are in the form of two semicircular interference
filters joined with cutoff filters. The spectral resolution varies accord-
ing to the spectrum within the limits of 0.7-1.1%. The average trans-
mission coefficient of the filters is 45%. At the junction of the two
halves of the filters there is a slit through which the reference signal
passes (the long wave mark) through the cutoff filter. The total light
losses are 89%. The detectors have sensitive areas 1x5 mm in size.

The detecting capacities of the detectors of the Mariner 6 (Mariner 7)
detectors are as follows: PbFe -- 2.4 (2.6)$\cdot 10^{10}$ watts$^{-1}\cdot$cm$\cdot$hertz$^{1/2}$;
Hg:Ge -- 2.52 (2.73)$\cdot 10^{10}$ watts$^{-1}\cdot$cm$\cdot$hertz$^{1/2}$. In channels 1 and 2 the
flux modulation frequency is 500 hertz. The modulators are simultaneously
absolutely black supporting emitters (degree of blackness 96%). The mod-
ulator temperature is 175 and 238°K respectively. The detector signals
go to the amplifiers, the demodulators, logarithmic and digital converters
and then to the memory or telemetric system. The total mass of the instru-
ment is 70.4 kg, including the cooling system, 5.9 kg. The intake power
is 11 watts for measurements and 8.7 watts in flight. The monochromator
dimensions are 32x23x18 cm^3. The spectrometer of the Mariner 6 spacecraft
made it possible to obtain 108 spectra using channel 2. Channel 1 did not
operate as a result of failure of the cooling system. Two channels
operated correctly on the spectromer of the Mariner 7 spacecraft, and up
to 130 spectra were obtained in each. The on-board calibration of the
spectrometer with respect to the absorption spectrum of polystyrene was
performed in flight using a model of an absolutely black emitter. The
results of the calibration confirmed the operating reliability of the
spectrometer.

The spectra obtained were used to determine the composition of the Martian atmosphere [3,14]. Brightly expressed absorption bands of carbon dioxide (the basic component), carbon monoxide and water vapor were recorded in the spectra. The content of about 40 small components in the atmosphere was estimated.

The IRR infrared radiometer [3.15] developed by the Jet Propulsion Laboratory has two separate spectral channels: 8-12 and 18-25 microns. The diameter of the objectives is 254 cm, and the field of view is 0.7x0.7°. As the radiation receivers, thermocouples are used which were developed by the Santa Barbara Research Center. The thermocouples have five bismuth and antimony contacts applied to a thin layer of aluminum oxide film applied to a sapphire disc. The thermocouples are under a pressure of $133 \cdot 10^{-5}$ Pa. The size of the sensitive area is $0.25x0.25$ mm^2, the resistance is 10 kilohms, the time constant is 75 milliseconds, the sensitivity is 150 volts/watt, and the detecting capacity is $4.2x10^8$ cm-hertz$^{1/2}$-watts^{-1}.

In the 8-12 micron channel, a primary uncoated lens of Irtran 2 glass and a secondary germanium lens coated with a layer of zinc sulfide are used. In the 18-25 micron channel, both lenses are uncoated and are made of Irtran 6 glass. The instrument has a 3-position scanning mirror which provides for viewing the planet, space and a standard emitter. The mirror is made of beryllium electrolytically coated with nickel, polished and aluminum coated. The scanning mirror is placed at an angle of 45° to the optical axis. The mirror is rotated by a stepping motor. The mirror can be locked in one of three positions by an electromagnetic lock. The scanning cycle is 63 seconds. The viewing of space (the zero reference point) takes place in 4.2 seconds during which time the memory circuit returns to the initial position. The mirror turns toward the planet in 27.3 seconds. The mirror turns to the on-board calibration source in 2.1 seconds. In 29.4 seconds the mirror again returns to the planet. Pulses 60 milliseconds long are used for the mirror rotations. The average power of the rotating mechanism is 0.2 watts.

The signal from the thermocouple output is modulated with a frequency of 200 hertz, it is then intensified and demodulated by a synchronous demodulator. In order to decrease the effect of the dependence of the sensitivity of the thermocouple on the ambient temperature, a thermistor circuit is used which regulates the amplification coefficient of the amplifier. The use of a filter with a 0.68 hertz band insures that the mean square value of the noise level will be reduced to 0.1% of the dynamic range of output signals of the equipment. The electrical output is connected to the DC memory circuit. When viewing space the capacitors of the memory circuit are charged to a level corresponding to the signals as a result of thermal emission of the optical system and electrical mixing in the circuit which makes it possible to record the zero level of reckoning.

FOR OFFICIAL USE ONLY

The calibration of the equipment under ground conditions was performed in a vacuum chamber at a pressure of $<133.10^{-5}$ Pa using two models of an absolutely black body: with a temperature 77°K for simulation of space and with an adjustable temperature of 100-350°K for simulation of a planet. The linearity of the calibration curves is about 2%, and the recurrence rate of the data, greater than 0.5%.

In flight the radiometers function normally [3.16]. According to the data from the signal obtained from the calibration plate, the amplification varied no more than 10%. The dependence of the amplification coefficient on temperature by the results of the on-board calibration corresponded to the results of the ground calibration. When processing the measurement results, the sensitivity distribution function with respect to the viewing field was taken into account. The scans on the surface of Mars during flights of the two spacecraft were broken down into five bands, in each of which fixed viewing angles of the scanning platform with respect to the spacecraft were maintained. In the majority of measurements the temperature exceeded 200°K, and the accuracy of quantization was about 0.3°K (relative measurement error). It is proposed that the systematic measurement error does not exceed 5°K. The signals obtained from the Polar caps, even in the spectral range of 18-25 microns were about 5% of the signals in the equatorial regions, and accordingly, they had large systematic errors. The results of the space measurements in the 8-12 micron range agree well with the results of the ground measurements in the 7-13 micron range (the difference is 4-6°K).

The following basic conclusions were drawn from the measurements. The maximum value of the brightness temperature on a wave length of 10 microns measured in the thermal section (Merediani Sinus) corresponds to the results of the ground measurements. The temperatures of the localized sections are strongly correlated with light and dark parts. The observation of the thermal nonuniformities was limited by the spatial resolution of the radiometers. The dependence of the temperature on the local time on the light side gives the value of the thermal inertia coefficient of 0.025 joules-cm^{-2}-sec$^{1/2}$-K^{-1} for bolometric values of the albedo in the range of 0.2-0.4. The values of the night temperatures are systematically higher than the values of the temperatures for the uniform model constructed by the measurements on the day side. For the darkest section observed by the Mariner 6 spacecraft (Syrtis Major), a value of the thermal inertia coefficient of 0.038 joules-cm^{2}-sec$^{1/2}$-K^{-1} is acceptable for an albedo of 0.15. The thermal peculiarities of the surface of Mars can be explained by the presence of particles 0.2-1 mm in diameter. The temperature of the southern Polar ice cap according to the measurements from the Mariner 7 spacecraft is 148°K, which provides a basis for considering its frozen carbon dioxide a basic component.

FOR OFFICIAL USE ONLY

After successful completion of the study programs using the "Mars-2, 3" and Mariner 9 automatic interplanetary stations observing from Mars-centric orbits, an exceptionally large amount of information was obtained on the composition and physical characteristics of the Martian atmosphere (the peculiarities of the pressure and temperature distribution, clouds) and the nature of its surface relief. The studies were performed during a storm that began unexpectedly on Mars which lasted from September 1969 to January 1970.

The infrared equipment of the "Mars-2, 3" station for examining the atmospheric surface of Mars was on board the orbital compartments and included the following instruments [3.17]:

Infrared radiometer with sensitivity range of 8-40 microns to obtain a picture of the temperature distribution over the surface of Mars on the flight trajectory; field of view on the surface of the planet 30-40 km;

An infrared spectrometer with narrow-band optical filters to study the surface relief by measuring the degree of absorption of solar radiation reflected from the surface of Mars by the atmospheric carbon dioxide in the 2.06 micron band.

An infrared spectrometer for determining the water vapor content by the nature of absorption of solar radiation in the 1.38 micron band.

In addition, the following equipment was installed in the orbital compartments:

A visible band photometer for studying the reflectivity of the surface and the atmosphere in the spectral range of 0.4-0.7 microns in several spectral intervals;

An ultraviolet spectrometer for determining the density of the upper atmosphere of Mars, determining the atmospheric oxygen, hydrogen and argon content in the atmosphere;

An instrument for determining the radio brightness temperature of the surface in the wave length band of 3.4 cm, its dielectric permeability and the surface layer temperature at a depth to 30-50 cm;

Two phototelevision cameras with different focal lengths for photographing the surface of Mars.

The axes of the measuring instruments (in addition to the ultraviolet spectrometer) and the phototelevision cameras were installed parallel, which made it possible to perform a simultaneous investigation and photograph the selected sections of Mars.

In the spring of 1971, NASA prepared two Mariner spacecraft for insertion
into Martian orbit. The Mariner 8 launch was unsuccessful. Mariner 9
was inserted into the calculated trajectory on 30 May.

The scientific equipment of Mariner 9 includes the following instruments
which were placed on the standing platform, the axes of which are parallel
to each other: 1) two television cameras; 2) an ultraviolet spectrometer
for determining the presence and concentration of defined gases; 3) an
infrared radiometer for thermal mapping of the surface of Mars; 4) an
infrared interferometric spectrometer for studying the structure and
properties of the atmosphere and the emitting properties of the surface.
The spacecraft has the form of an octahedron 127 cm in size. The mass of
the spacecraft is 18 kg. The television system is made up of two cameras
(A and B) and an electronic circuit. Camera A is wide band, and the field
of view is 11x14° with low resolution. Eight filters installed on a
rotating disc permit isolation of eight spectral sections. Camera B with
high resolution and narrow field of view of 1.4x14° operates in a fixed
spectral band.

The infrared radiometer of the Mariner 9 spacecraft is analogous to the
radiometers of the Mariner 6 and 7 spacecraft. The field of view of
channel 1 (8-12 microns) is 0.53x0.53°, channel 2 (18-25 microns) 0.7x0.7°.
The mass of the radiometer is 3.6 kg, and the intake is 2.5 watts.

The infrared interference spectrometer was constructed by the Michelson
interferometer scheme. The field of view coincides with the field of
view of a narrow-band television camera (1.0x14°). The internal scanning
mirror is used for series viewing of the planet, space and a model of an
absolutely black body with a temperature of 290+2°C. During viewing of
the planet, the scanning mirror realizes compensation of the image shift
within the limits of the angle of 5°. The pencil of beams is split into
two approximately equal parts after the scanning mirror using a light-
dividing mirror. One part of the beams goes to the stationary mirror,
and the other, to the Michelson mirror which moves at a speed of 0.0233 cm/sec.
The beams from the two mirrors mix, and circular interference takes place.
The diffraction rings are focused on an infrared detector. The detector
dimensions provide for overlap of the maximum central ring in the investi-
gated band. The detector -- a crystalline dielectric triglycinesulfite --
is located between the electrodes. The capacitance of the dielectric
depends on the heating by the instrument radiation. In order to control
the speed of the Michelson mirror, the radiation of a gas-line neon tube
on a wave length of 692.9 nm is used. The light of the neon tube also
goes to the light dividing mirror, and interference of it takes place.
The interference rings of the neon tube are focused on the photomultiplier.
When the Michelson mirror moves at a speed of 0.0233 cm/sec the diffraction
rings will be formed with a frequency of 675 hertz. The signal at the
output of the photomultiplier will also have a frequency of 675 hertz.
The frequency obtained is compared with the divided frequency of the
control clock used to control the speed of the Michelson mirror. The

operating band of the spectrum is 6-50 microns, the circular field of view is 4.5°. The mass is 23 kg, and intake power, 24-28 watts.

The information from the measuring equipment passes through the DAS automatic control system to the DSS magnetic accumulator at a speed of 132.3 kbits/sec. The reproduction rate is 16.2, 8.1, 4.05, 2.25 or 1.0125 kbits/sec. The mass of the DAS system is 6.35 kg, and the power is 23 watts. The DSS device has an 8-track magnetic tape 12.7 mm wide and 174 m long. The memory is $1.8 \cdot 10^8$ bits. The error intensity is $1 \cdot 10^{-5}$ at speeds of 4.05-16.2 kbits/sec and $1 \cdot 10^{-4}$ at lower rates. The DSS mass is 11.3 kg, and the intake power, depending on the conditions is 13-22 watts. The telemetric system has the following transmission regimes: 1) current scientific data with the rate of 50 bytes/sec (on a subcarrier frequency of 34.286 kilohertz) and technical specifications about the systems (subcarrier 24 kilohertz); 2) technical and scientific data with a rate of 16.2 or 8.1 kbits/sec or recorded data with a rate of 16.2-1.0125 kbits/sec.

The infrared spectrometric measurements on board the Mariner 9 spacecraft [3.18] made it possible to determine the temperature of the vertical profile, the surface, pressure and composition of the atmosphere.

After ground processing in the computer, individual spectra of the interference spectrometer were printed out in the form of absolute energy values as a function of wave length. By comparison with the infrared spectra of the earth obtained using analog equipment from the meteorological satellites of the Nimbus type, the emission spectra of Mars are extremely nonuniform, especially the spectra near the southern polar cap. The examples of the spectra of the nonpolar and polar regions are presented in Fig 3.4. Curve A represents the emission spectrum of the nonpolar region (18° south latitude, 13° west longitude) at 1200 hours local time. Curve B is the emission spectrum of the southern polar cap. The smooth curves designate the emission spectra of an absolutely black body with the indicated temperatures. The sections of the spectrum 400-600 and 850-1250 cm^{-1} are characteristic of all of the spectra on which the absorption of the surface emission in the atmosphere in nonpolar regions and an increase in the surface emission of Mars in the polar region and also the molecular absorption by carbon dioxide in the 54-800 cm^{-1} range are noted. The difference in nature of the spectra is explained by the difference in temperature profiles in the lower layers and the amount of dust in the atmosphere.

In the nonpolar spectra the effect of the molecular bands of CO_2 reduces to attenuation of the surface radiation inasmuch as with an increase in the altitude, the temperature in the atmosphere drops rapidly. In the polar spectra in the ranges of 550-625 and 700-800 cm^{-1}, the increase in the surface emission is noticeable as a result of the fact that the lower layers of the atmosphere are warmer than the surface itself. The unclearly expressed valleys in the sections near 470 and 1075 cm^{-1} in
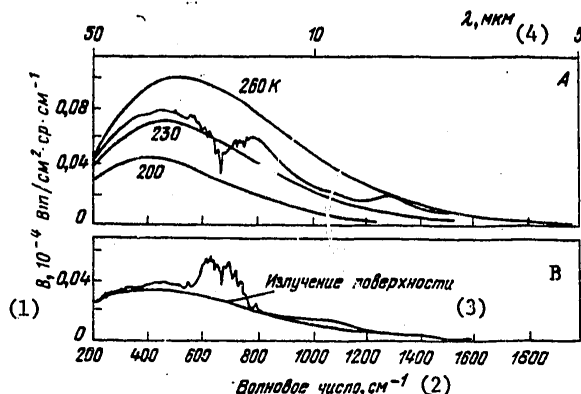
Figure 3.4. Examples of the emission spectra of Mars

Key:
1. B, 10^{-4} watts/cm^2·steradians-cm^{-1}
2. Wave number, cm^{-1}
3. Surface emission
4. λ, microns

the nonpolar spectra and the rises in the polar spectra are explained by the effect of the spectral bands belonging to the dust particles containing silicon. According to the preliminary data, 55-65% silicon is contained in the Martian dust.

The processing of the emission spectra in the absorption band of CO_2 at 667 cm^{-1} made it possible to estimate the vertical temperature profiles of the atmosphere of Mars. The processing was carried out by inversion of the integral transport equation of the radiant flux in the atmosphere analogously to how this is done when processing the emission spectrum of the earth received from the equipment on board the meteorological satellites (see Chapter 5). It was considered here that the atmosphere is made up wholly of carbon dioxide, and the effect of the dust was not taken into account. The initial data were the data on the atmospheric pressure at the surface of Mars obtained during ground radar measurements and also by the data from the ultraviolet spectrometers of the Mariner 6 and 7 spacecraft. The examples of the temperature profiles obtained for three regions on Mars are presented in Fig 3.5. A clearly expressed temperature inversion can be seen only on the profile above the southern polar cap, which explains the increase in emission in the spectral regions corresponding to the strong CO_2 absorption bands.
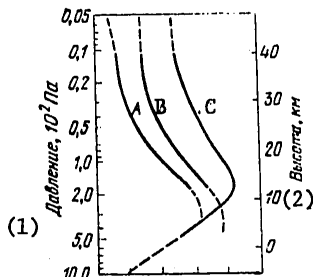
58

Figure 3.5. Temperature profile of the atmosphere of Mars with respect to altitude for the following regions: A -- 15.0° south latitude, 64.2° west longitude (Sinai), 1200 hours; B -- 38.0° south latitude, 3282.8° west longitude (Hellas), 1900 hours; C -- 86.6 south latitude, 342.2° west longitude (southern polar cap), 1300 hours.

Key:
  1. Pressure, 10^2 Pa
  2. Altitude, km

Atmospheric isotherms are presented in Fig 3.6 for a vertical cross section in the vicinity of the southern polar cap as the Mariner 9 spacecraft flew over it. The broad line along the x-axis indicates the position of the polar cap itself. As a result of indeterminacy connected with the effect of the dust and inaccuracy of the data on the atmospheric pressure at the surface in the lower part of the diagram the isotherms are depicted by dotted lines. In the area over the polar cap there is a clearly expressed region of warm air at altitudes of approximately 10-20 km. The possible causes of the given phenomenon are considered to be the constant illumination of this region during the summer by the sun, reflection of solar radiation from the surface of the cap and also the atmospheric dynamic effect.

As a result of analyzing the temperature data [3.14] at various altitudes, its diurnal variation was detected approximately to an altitude of 30 km. When there is a lot of dust in the atmosphere the maximum temperature is observed at 60° south latitude during the late afternoon hours. As the atmosphere clears, the maximum weakens, moving toward the equator, and it comes earlier in the day. The diurnal fluctuations of the atmospheric temperature are within the range of 15 to 30°K.

The infrared radiometers of the "Mars-2, 3" and Mariner 9 automatic inter-planetary stations made it possible to measure the surface temperature at different latitudes at different times of day. These data make it possible to determine the properties of the materials of the ground surface.
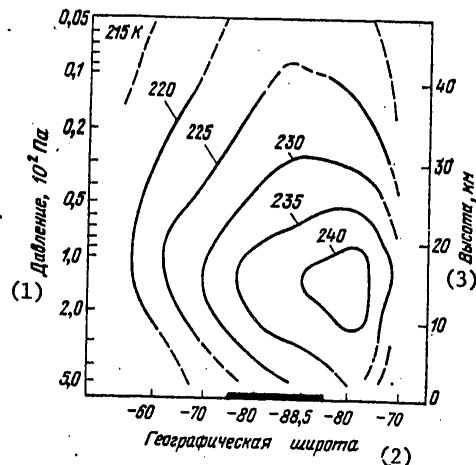
Figure 3.6. Isotherms in a vertical cross section of the Martian atmosphere in the vicinity of the southern polar cap

Key:
1. Pressure, 10^2 Pa
2. Geographic latitude
3. Altitude, km

The measurements on the Mariner 9 automatic interplanetary station were performed using a two-channel radiometer (on wave lengths of 10-20 microns) analogous to the radiometer of the Mariner 6, 7 automatic interplanetary station. The spatial resolution of the radiometer in the periapsis is about 20 km. The resolution with respect to temperature is about 0.5°K. The measurement results [3.19] in 1971 during a dust storm differ sharply from the measurement results of 1969 using the Mariner 6 automatic interplanetary station. Thus, whereas in 1969 in the vicinity of 30° south latitude the temperature fluctuated from 185 to 290°K, in 1971 this gradient was a total of 195-225°K. The maximum temperature (about 250°K) was recorded in the vicinity of 65° south latitude. On the surface of Mars at a temperature of 148°K, solid carbon dioxide is formed. This temperature was observed on the surface of Mars using the Mariner 7 automatic interplanetary station at the southern polar cap during the early Martian spring. During the observations of Mariner 9, the minimum temperature at the southern polar cap was 25°K above the freezing point of CO_2. However, according to the data from the television images obtained simultaneously with the radiometric measurements, at least 95% of the area of the cap has a high reflection coefficient. It is considered that the cap is formed of solid carbon dioxide, and the high values of the temperature are explained by the effect of the atmospheric dust emission.

60

In the vicinity of Tartis (11° north latitude, 119° west longitude) the radiometer recorded a zone of about 300 km, the temperature of which is 8°K above the temperature of the surrounding regions. On the television image this zone was observed in the form of a dark spot.

According to the measurement results of the "Mars-2, 3" automatic interplanetary station the surface temperature [3.14] (operating range of the radiometers 8-40 microns) varies as a function of time of day and latitude within signigicant limits: from 180°K (at 1900 hours local time by 19° north latitude) to 286°K (at 1400 hours local time by 11° south latitude). On the northern polar cap the temperature decreases to 163°K.

The fact that the diurnal behavior of the temperature turned out to be less than expected is explained by the effect of the dust, the density of which decreases toward the South Pole.

According to the data of the "Mars-2, 3" automatic interplanetary station, the low night temperatures indicate fast cooling of the Martian surface after the sun goes down and, consequently, very low thermal conductivity of the ground. As a result of a quantitative evaluation of these data it was established that this thermal conductivity corresponds to dry sand or dry dust in the rarefied atmosphere.

The temperature of the dark sections of the Martian surface (the "seas") is approximately 10°K above the temperature of the light sections ("continents"), which is explained by the lower reflection of the surface of the "seas."

According to the measurement results using the ultraviolet spectrometer of Mariner 9 [3.14] it was possible to construct a pressure map and a map of the relief of Mars in the latitude range of 50° south latitude to 20° north latitude. In the examined section of Mars, the altitude of the relief fluctuates from -2 to +10 km. According to the data of the infrared measurements of Mariner 9, the maximum altitude reaches +14 km. The results obtained using the infrared photometer of the "Mars-2, 3" automatic interplanetary station operating in the absorption band of carbon dioxide of about 2.06 microns and determining the degree of absorption of the solar emission by carbon dioxide demonstrated good coincidence with the measurement data of Mariner 9. The profile of the relief along the flight trajectory of the automatic interplanetary station was determined by the infrared measurements from the "Mars-2, 3." Altitude gradients to 12-14 km in significant sections are detected in the equatorial band. By the observations of [3.14] using an infrared spectrometer on board the "Mars-3" automatic interplanetary station taking measurements in the water vapor absorption band near $\lambda=1.38$ microns, it was established that the water vapor content did not exceed 5 microns of precipitated water during the entire measurement period, which is several thousand times less than in the earth's atmosphere.

FOR OFFICIAL USE ONLY

New missions with respect to the investigation of Mars were carried out by the Viking 1 and 2 stations launched on 21 August and 9 September 1975. The Viking automatic interplanetary stations studied Mars from an orbital module and a module which descended to the surface of Mars and performed the following basic experiment:

Measurements of the radiation temperature distribution on the surface of the planet, determination of the water vapor content in the atmosphere, obtaining a television image of the surface of Mars from the orbital module;

Radio transmissions from on board the orbital module to determine the vertical temperature profile in the troposphere;

Determination of the density and temperature of the atmosphere by the conditions of entry of the landing module into the atmosphere;

Studies of the composition of the atmosphere and the surface, the properties of Martian soil, the performance of biological experiments and television observations from the landing module.

The large volume of research from on board the orbital module provided for the use of a six-channel infrared radiometer of the so-called IRTM infrared thermal mapping instrument. The IRTM instrument [3.20] is designed to obtain thermal maps in various spectral bands to investigate the thermal nonuniformities of the surface, for determination of thermal inertia and the spectral emissivity of the soil, the cloud temperature and the temperature of the ice formations on the surface and also measurements of reflected short wave radiation.

The operating principle of this instrument is the same as that of the radiometers on board the Mariner 6, 7 and 9 stations. The optical system of the radiometer and its composition are illustrated in Fig 3.7. The objective of the instrument has a relative aperture of 1:3 and a diameter of 11.4 cm. The measurements are performed in six spectral channels. The sensitive elements are thermocouples with an operating temperature of about 0°C. In the 0.2-3.5, 9-13, 18-24 micron channels, mosaics are used which are made of eight thermal elements in the form of rules. In the 6-8, 8-9.5 and 24-35 micron channels, "rules" made up of four elements are used. The separation of the corresponding spectral bands is realized using interference light filters. The diagram of the fields of view of the thermal elements in the plane of the radiometer image is presented in Fig 3.8. The field of view of 5x5 millirads corresponding to each thermal element is isolated by the mirror light guides with quadratic input openings placed in the image plane. The overall size of the field of view of the entire radiometer in the direction perpendicular to the flight trajectory is 40 millirads, which corresponds to the television system of the orbital module.
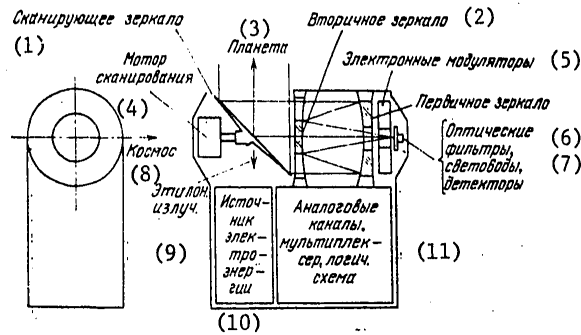
62

FOR OFFICIAL USE ONLY

FOR OFFICIAL USE ONLY

Figure 3.7. Optical system and composition of the infrared
radiometer of the IRTM device on the Viking
spacecraft

Key:
1. Scanning mirror
2. Secondary mirror
3. Planet
4. Scanning motor
5. Electronic modulators
6. Primary mirror
7. Optical filters, light guides,
   detectors
8. Space
9. Standard radiation
10. Electric power supply
11. Analog channels, multiplexer,
    logical circuitry

The interference light filters are placed above each light guide, and the
bimetal thermocouples are installed in the constricting end of the light
guides. The use of light guides permits increase in the effective relative
aperture of the entire optical system to 1:1, it facilitates separation
of the fields of view and the placement of the current conductors, and it
creates massive thermal barriers excluding the mutual effect of individual
channels.

By using a scanning mirror inclined at an angle of 45° to the optical
axis, successive sighting of the planet (rotation by 0°), space (rotation
by 90°) and the standard radiator (by 180°) is accomplished.

When viewing space the DC amplifiers in each channel are zeroed, and the
storage capacitor is charged to the voltage determined by the sum of the
electric and thermal signals in the given position. In the next position
the standard emitting surface is viewed, and its temperature is measured.
The total cycle is 50 seconds, of which the planet is viewed for 48 seconds,
Repeated viewing of the planet is realized with an accuracy better than
+0.8 millirads.
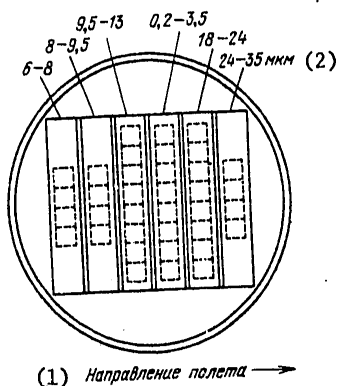
(1) *Направление полета* ⟶

Figure 3.8. Schematic of the arrangement of the fields of
view of the IRTM radiometer

Key:
    1. Flight direction
    2. Micron

The time constant of the detector-amplifier system is about 0.5 seconds.
The output signal of each detector is picked up twice during the time
corresponding to a frame of the on-board television camera, and it is
converted to digital form with a word length to 10 bits. During the
mirror rotations, data on the state of the radiometer are transmitted.
The total transmission rate of the radiometer data is 321 bits/second.
The data transmission is both in real time and from memory.

The temperature measurements of the surface of Mars are required to study
the dynamics of the planet atmosphere. In order to determine the true
surface temperature, a correction for the emissivity of the surface is
needed. For this purpose the spectral channels of the radiometer were
selected from the characteristic spectral emissivities of the materials
expected on the surface of Mars: 8-9.5 microns for acid silicates,
9-12 microns for basic silicates, 5.5-7.2 microns for carbonates.

The three channels isolating the spectral regions make it possible to
measure the spectral emissivities. The error in measuring the radiation
temperature in 5 spectral regions intended for measuring the natural thermal
emission is no more than 1°K with a temperature resolution on the order of
0.5°K. The true surface temperature can be found with an accuracy on the
order of several degrees (as a rule, 2°C) after introducing the correction
for the emissivity. The most important mission of the radiometer on board
the Viking station is measurement of the thermal inertia of the ground
surface with respect to the time behavior (during the day) of the surface
temperature. The data on the thermal parameters of the soil make it
possible to explain the nature of the seasonal variations observed from
the surface of Mars in the visible part of the spectrum.

FOR OFFICIAL USE ONLY

In order to study the heat balance of the planet and separate the factors determining the surface temperature (thermal conductivity, density, heat capacity), simultaneous measurements will be made of the albedo in the wave length range of 0.2-3.5 microns.

The thermal measurements will be used to detect the internal heat sources and determine the nature of the ice (CO_2 or H_2O) formations and also to determine the temperature and the altitude of the upper boundary of dense clouds.

The experiment with respect to water vapor detection in the atmosphere of Mars and compilation of its distribution maps has two goals. On approaching the planet and on the upper orbits the determination of the water vapor distribution is important for selecting the landing site of the landing stage, for the possibility of existence of life on the planet is connected with the presence of maximum amount of water. During orbital flights a study is made of the latitudinal and time (diurnal and seasonal) variations of the water vapor content in the atmosphere, which is important to understanding the processes occurring in the atmosphere of Mars and also for mutual exchange between atmospheric and surface moisture.

The instrument on board the Viking station designed to determine the water vapor distribution in the atmosphere of Mars [3,21] is a monochromator with stationary diffraction grating, in which the isolation of five spectral segments in the absorption band of water vapor with the center near 7300 cm^{-1} (1.4 microns) is realized by a 5-element PbS photoresistor with radiation cooling. The spectral resolution is 1 cm^{-1}. Using a small input mirror objective 2.5 cm in diameter with a relative aperture of 1:5 (Fig 3.9) the radiant flux is focused on the entrance pupil of the monochromator. A modulator is installed in front of the entrance slit. The instantaneous field of view of the instrument is 0.92x0.12°, which at an altitude of 1500 km provides for viewing of a section on the surface of the planet of 24x3 km in the periapsis.
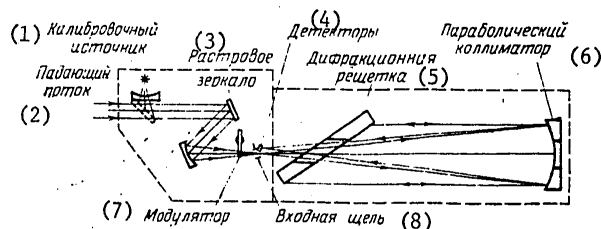

Figure 3.9. Optical system of the 5-channel spectrometer for determining the water vapor content in the atmosphere of Mars

Key:
1 -- Calibration source; 2 -- instant flux; 3 -- raster mirror;
4 -- detectors; 5 -- diffraction grating; 6 -- parabolic collimator;
7 -- modulator; 8 -- entrance pupil

65

FOR OFFICIAL USE ONLY

The radiation passing through the entrance pupil goes to the parabolic collimation mirror with a focal length of 50 cm. The dispersed radiation reflected from the diffraction grating having 12000 lines/mm returns to the collimation mirror and is focused by it on the sensitive elements located alongside the entrance pupil. Each element has its own amplifier. After amplification the signals are demodulated by synchronous demodulators, they are integrated and converted to digital form.

The instrument realizes spatial scanning by an instantaneous field of view across the trajectory as a result of stepped movements by the raster mirror. The instantaneous field of view is directed with its long side (24 km) along the velocity vector. A total of 15 scanning steps are realized, as a result of which the band 45 km wide is examined. During the return movement of the raster mirror, data are transmitted on the operating conditions of the instrument and its elevation by wave lengths.

In order to check the spectral operating stability of the monochromator during the return stroke of the raster mirror, radiation is directed on the optical system of the instrument from a monochromatic standard radiator which is incident on a system of silicon photoelements. In the case of a spectral shift (as a result of the effect of the thermal expansion or mechanical shifts) the photoelements generate a control signal which causes the necessary rotation of the diffraction grating.

In order to check the sensitivity of each channel, a plane mirror is periodically introduced in front of the raster mirror through which the radiation hits the instrument from the calibration sources (the set of tungsten tubes). The sensitivity calibration provides for absolute measurement precision to 10% and relative accuracy (of one channel with respect to the others) to 1%. For checking the absence of the effect of undesirable absorption lines, stepped scanning is periodically realized with respect to the spectrum by rotations of the diffraction grating during the return stroke of the raster mirror within the limits of 20% of the resolved element. In 100 such steps the diffraction grating turns from its central position to one edge, then to the other, and returns to the central position. Thus, spectral scanning is realized in the entire operating spectral band of the monochromator.

The minimum amount of water vapor which can be recorded by the instrument corresponds to a layer of precipitated water of 0.5 microns. The accuracy of determining the water vapor content is 5% with a total of more than 10 microns of precipitated water.

The studies of Mars, using the Viking 1 and 2 stations were completed in 1977, and their results have only been partially published.

The joint study of the data obtained by the "Mars," Mariner and Viking stations will permit sufficiently exact representation of the physical conditions on the surface of Mars [3.26]. The atmosphere of Mars is much

more rarefied and cold than the atmosphere of the earth. The average pressure at the surface is $6.1 \cdot 10^2$ Pa, and the average temperature is 220°K. The basic components of the atmosphere are as follows: 95% carbon dioxide, 2-3% nitrogen, 1-2% argon. In addition, the atmosphere contains small components: 0.035-0.3% molecular oxygen, 0.04-0.3% carbon monoxide. Ozone O_3 and the ozone layer at an altitude of about 40 km, molecular and atomic hydrogen and other small components are detected in the atmosphere. The water vapor content in the atmosphere varies with the seasons and latitude within the limits of approximately 5 to 50 microns of precipitated water (at least 3 orders less than the atmosphere of the earth); sometimes it drops to fractions of a micron over the polar caps, and in the lower latitudes sometimes it reaches 100 microns. The atmosphere contains a significant amount of aerosols, and the sky is from rose to dark orange in color.

The experiments performed by the landing modules of Viking 1 and 2 did not offer facts which could be considered as certain evidence of biological activity.

New outstanding progress has been made by Soviet science and engineering in the investigation of Venus [3,22]. On 22 and 24 October 1975, the landing modules of the Venera-9 and Venera-10 automatic interplanetary stations transmitted an image of the planet to the earth for the first time in the history of cosmonautics, and the stations themselves became the first artificial satellites of Venus.

By the results of narrow-band photometric probing of the brightness of the atmosphere in three wave lengths of bands of about 0.8 microns data were obtained on the landing modules regarding the cloud distribution with respect to altitude and the chemical composition of the atmosphere [3.23]. Three filters centered on the following wave lengths were used in the experiment: 0.8 microns -- continuous spectrum; 0.18 microns -- H_2O absorption bands; 0.87 microns -- CO_2 absorption bands. It was established that the basic layer of the clouds is above 50 km. A second cloud layer is possible at altitudes of 35-45 km with a small scattering coefficient. The ratio of the H_2O/CO_2 contents is about 10^{-3} in the altitude range of 25-45 km.

By the results of measuring the thermal emission of Venus using an infrared radiometer on board the orbital modules, the large asymmetry in the day-night direction was detected [3.24]. The brightness temperature of 244°K corresponds to the emission on the night side, and 233-243°K, on the day side.

The extent of the upper layer of clouds in which the thermal emission is formed is 4-6 km. The altitude of the emitting layer above the surface of the planet (64-67 km) was determined by the brightness temperature in the existing models of the atmosphere of Venus.

3.5. Astrophysical Studies on Manned Spacecraft

The flight programs of the manned spacecraft and orbital stations include, as a rule, astrophysical studies. An advantage of the investigations from the manned spacecraft is the possibility of combining them with visual observations, operative control and correction of the programs during the flight process, more complete use of the possibilities of the equipment and evaluation of its technical level.

A large volume of original astrophysical studies were performed on the Apollo spacecraft, on the joint Apollo-Soyuz flight and on the Skylab and "Salyut" orbital stations.

From the experiments performed during the Apollo spacecraft flights, it is necessary primarily to isolate the first astronomical observations performed by man on the lunar surface [3.27]. The first optical telescope was installed on the moon on 20 April 1972 by the Apollo 16 astronauts. This telescope was an electron-diffraction camera spectrograph for observations in the far ultraviolet of 50-160 nm. The camera was designed to obtain the spectra and direct images of the earth's atmosphere, the geocorona and magnetosphere, for observations of the stars, the Andromedids, and so on. The telescope was constructed on the basis of the Schmidt system with a diameter of the entrance pupil of T=75 mm, a relative aperture of A=1:1 and an angular field of view of 20°. The ultraviolet diffraction camera demonstrated the high possibilities of diffraction camera recording of images and the advantages of the lunar surface for future astronomical observatories, especially in the ultraviolet part of the spectrum. The hydrogen corona of the earth which extends to several terrestrial degrees interferes with observations in the far ultraviolet from orbital stations in low earth orbits.

The study of the moon and the space around the moon from a selenocentric orbit on the Apollo 15, 16 and 17 spacecraft was realized by a set of scientific equipment which, in particular, included a high-resolution panoramic camera, a medium resolution mapping camera which operated together with a sidereal camera and laser altimeter, scanning infrared radiometer and ultraviolet spectrometer. The panoramic camera was designed for stereo photography of the lunar surface with a resolution of 1-2 meters from an orbit of 110 km. The field of view of the camera in the orbital plane was 10x0.75°, and the rocking angle of the camera above the lunar surface was 108°.

The cartographic camera had an objective with a focal length f=766 mm, a relative aperture A=1:4.2 and a field of view of 74x74°. The camera resolution was about 18 meters. In front of the plane of the film there was a glass plate with engraved measuring crosshairs which were used as the reference points for photogrammetric processing. Each frame of the cartographic camera covered an area of 259 km^2. The exact gridding of the coordinates of the pictures was insured by the sidereal camera equipped

with an objective with f=76 mm and A=1:2,8. A laser altimeter for measuring the altitude of the spacecraft above the lunar surface with an accuracy of ±2 meters operated synchronously with the set of cartographic and sidereal cameras,

The thermal emission of the lunar surface was recorded by a scanning infrared radiometer, the system of which included a Cassegrainian telescope, an Hebert mirror and bolometer. In the temperature range of ‑213...+127°C a resolution with respect to temperature of 1°C was insured,

On the joint Apollo-Soyuz flight, out of 24 scientific experiments ten were performed in the field of astronomy and astrophysics, geodynamics, the investigation of natural resources and study of the atmosphere. Within the framework of these scientific experiments astronomical objects were mapped in the soft x radiation and far ultraviolet range, a determination was made of the intensity and spatial distribution of the glow of helium using a narrow band photometer, the concentrations of atomic oxygen and nitrogen in outer space were measured by the signal absorption in the ultraviolet range (297.2 nm for O_2 and 346.9 nm for N_2) with distances between the spacecraft from 150 meters to 1 km.

The experiments in photographing the earth to study natural resources which were performed in the following basic areas were significant in size:

Geological studies of large faults, vegetative cover and runoff;

Hydrologic studies of river basins and snow cover, in particular, the floods in India and snows in the Himalayas;

The study of uplifts of the ocean floor, their biology and role in current formations;

The observation of meteorological phenomena in the tropical zone such as tornadoes, frontal waves, storm formation and local atmospheric disturbances.

The equipment of the Apollo and Soyuz spacecraft included an infrared photometer for determining the concentration of aerosols in the stratosphere to discover their effect on the ozone layer. The sun was observed at the horizon by using this infrared photometer. The absorption of the solar radiation makes it possible to determine the vertical distribution of the aerosols in the atmosphere, The measurements began 3.5 minutes after sunrise or 3.5 minutes before sunset and lasted approximately 20 seconds. The altitude of the probed layer changed by 1500 meters every second,

The first American manned space laboratory Skylab was launched on 30 April 1973. Three crews of astronauts worked successively on board it, They completed the research program on 8 February 1974.

One of the main parts of the Skylab was the first manned solar observatory, the ATM (Apollo Telescope Mount). The accuracy of orientation and stabilization of the platform on which the ATM instruments were installed was about 2.5" during time periods of up to 15 minutes. The ATM instruments included the following: a visual coronograph for measuring brightness, form and polarization of the radiation of the solar corona; a chromospheric spectrograph for the 97-397 nm range; a slitless spectroheliograph for operation in the far ultraviolet range of the spectrum 15-65 nm; an x-ray telescope for photographing the sun in 6 spectral bands from 0.2 to 6 nm; a spectrometer-spectroheliometer for observing the evolution of solar flares in the range of 30 to 135 nm and two H_α telescopes for observing the sun in the 626.28+0.01 nm line. They were designed to observe the chromosphere of the sun and to a significant degree duplicated each other. One H_α telescope was designed to obtain a video image which the astronauts used to sight the other instruments on selective parts of the solar surface. The other telescope provided for photorecording of the selected targets. Both telescopes used a Cassegrainian system. The diameter of the optical system D=165 nm, and the relative aperture, A=1:28. The main telescope for photographic recording had a variable field of view from 7 to 35', an angular resolution of 1" and a spectral resolution of 0.06 nm. A telecentric corrector and the Fabry-Perot filter system were installed in front of the focal plane of the telescope. At the output of the Fabry-Perot filters the beam went to a light divider which directed 90% of the light through the objective with variable focal length on a vidicon, and the remaining radiation was sent through a stationary objective to a moving camera. The second telescope had a constant field of view of 35', and the movie camera was not used in it.

The set of astronomical and astrophysical instruments on the Skylab orbital space station included ten more instruments for studying the earth's atmosphere, particle detection near the spacecraft, investigation of the background flow, obtaining solar spectra, and investigation of the stars, nebulas and the galaxies. The experiments with respect to the program of investigation of the earth's resources from on board the Skylab orbital space station were performed using the EREP instruments which included two microwave radiometers, an infrared radiometer with Cassegrainian telescope (D=250 nm) for operation in the 0.4-2.4 and the 6.2-15.5 micron bands and a 13-channel scanning instrument for recording images of the earth's surface in narrow spectral bands in the visible and far infrared region from 0.41 to 2.35 microns with angular resolution of 38". The EREP equipment also included two photographic systems. One of them was a multispectral setup of six cameras with a resolution of about 30 meters operating in the band of 400-900 nm. The second photographic system had a resolution of 11.5 meters and provided detailed information about the sections which were recorded by the multispectral device.

The Soviet orbital scientific stations of the Salyut series launched in 1971 were designed for performing a broad program of scientific research and technical experiments: medical-biological, astrophysical (recording

the spectra of the stars, gamma quanta, primary cosmic radiation), a complex photographic experiment to study natural resources of the earth, studies of micrometeorites and charged particles in the space next to the earth [1.1].

The original astrophysical studies in the infrared range were performed by the crew of the "Salyut-4" station made up of A. A. Gubrev and G. M. Grechko using the ITS-K infrared telescope-spectrometer. The instrument was developed by the Physics Institute of the USSR Academy of Sciences, and is the first operator-controlled space infrared telescope-spectrometer in Soviet and foreign practice [3.28].

The operating range of the ITS-K spectrum is 1-8 microns. This range is of special interest, for the greater part of it is inadmissible for astronomical observations from the earth as a result of absorption by the atmosphere. From space in this band it is possible to investigate the bands characterizing the molecular components of the earth's atmosphere, planets and the galactic sources (for example, H_2O, CO_2, NO, CO, OH and so on).

The ITS-K is made up of three modules: the SKIS infrared scanning spectrometer, the observation and movie making module and the control module. The information is recorded by an on-board magnetic recorder. The SIS module is installed outside the sealed compartment. It is made up of several functionally connected assemblies (Fig 3.10).

The telescope assembly is made up of the main spherical mirror Z_1 0.3 m in diameter and with an effective area of 400 cm^2 and a system of rotating plane mirrors. The rotating mirrors Z_2 and Z_7 are fastened to the same bracket and are rotated around two axes by miniature stepping motors, insuring exact sighting and tracking of the observed astronomical target. The system of plane mirrors split the radiation flux. The mirror Z_2 sends the basic part of the flux to the collimating mirror Z_3 of the mono-chromator, and a small part is sent by the mirrors Z_7 and Z_8 from the telescope assembly to the viewer assembly. The angle of the field of view of the telescope with the monochromator (for a focal length of Z_1 of 450 mm and a monochromator slit 1x2 mm) is 8x16'. The angle of the field of view of the telescope with the exit part of the viewer is 3x3°.

The viewer is fastened to the frame of the telescope and is made up of a semitransparent mixing mirror Z_9, the scale M and two objectives O_2 and O_3. On rotating the rotary mirror Z_2, the image of the investigated target simultaneously is displaced with respect to the entrance pupil of the monochromator and with respect to the viewer scale. The objective O_2 is used to obtain a wide-band image on the scale of the viewer 35x35°. The narrow field of view 3x3° was used primarily for astronomical observations, and the wide field of view 35x35° is used for geophysical observations. By using the objective O_3, the scale and the image of the object are projected through the illuminator of the OK_2 field chamber on the

FOR OFFICIAL USE ONLY
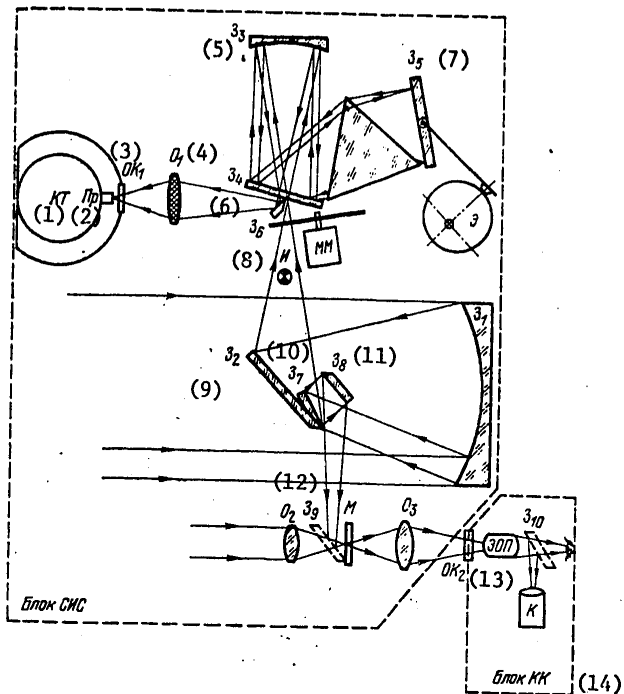
Figure 3.10. Structural diagram of the infrared ITS-K
telescope-spectrometer.

Key:
1. KT
2. Pr
3. OK_1
4. O_1
5. Z_3
6. Z_4
7. Z_5
8. Z_6
9. Z_2
10. Z_7
11. Z_8
12. Z_9
13. Image converter
14. KK module

photocathode of the image converter EOP of the KK module. The EOP
converts the infrared radiation of the target to $\lambda \lesssim 1.2$ microns to the
visible radiation, it intensifies the brightness and also permits observa-
tion and photography of the image by the camera K. The photographic
frames have gridding to the absolute coordinates of time and spectral
scanning.

The spectral part of the instrument includes the monochromator with the prism P made of fluorite assembled by the joint Littrov-Pfund system. At the input of the monochromator the radiation is clipped with a frequency of 600 hertz by the MM modulator which is a rotating disc with slits.

The scattered radiation is picked up from the monochromator by the mirror Z_6, and through the entrance opening OK_1 it goes to the radiation receiver Pr. A photoresistor made of germanium alloyed with gold is used as the radiation receiver. The photoresistor is placed in the vacuum cavity of the cryostat KT, and it is in thermal contact with solid nitrogen. The cryostat with solid coolant has a capacity of 19 liters and insures cooling for several months. The operating temperature of the photoresistor is 50°K. At this temperature the photoresistor reaches the background limitation conditions and maximum sensitivity. The operating conditions of the photoresistor are stabilized by a special system. The signals from the output of the photoresistor are amplified by selective amplifier with a 100 hertz band. The amplification coefficient remains in practice constant on variation of the instrument temperature within the limits of $\pm 60°C$. The amplifier has three channels which are distinguished for 10 times with respect to amplification, insuring a dynamic range of 10^4. The accuracy of the recording in each channel is 0.2%. The time constant of the entire electronic channel for the most sensitive channel is 10^{-1} sec; for the coarser ones, it is 10 times less. The noise level of the input circuit of the amplifier is appreciably below the noise level of the photoresistor.

On the average the ITS-K insures a spectral resolution of approximately 0.3microns with a recording time of the spectrum of 2.5 seconds. The sensitivity of the instrument is $(2-3)\times 10^{-12}$ watts/cm^2. The mass is about 10 kg with the cryogenic section. The power intake in the recording mode is 30 watts. The overall dimensions of the basic SIS module are 800x700x700 mm.

The ITS-K was used to study the upper atmosphere of the earth and the radiation sources in the Cassiopeia constellation. The extraatmospheric spectra of lunar emission in the 1-8 micron band were obtained for the first time using the ITS-K. They made it possible to determine the reflection coefficients of the lunar soild in its natural occurrence [3.29].

The observations of the moon were made on the 514-th orbit of the "Salyut-4" station on 27 January 1975 at full moon [3.29]. Before the beginning of the observations, the station was turned so that the telescope was directed at the moon. During the observations the image of the lunar disc traveled to the spectrometer slit 28-29, 333-358- 523-528 and 596-613 seconds after the beginning of the recording and opening of the telescope shutter. A total of about 20 lunar spectra were recorded. The image of

the moon on the viewer screen was photographed automatically with a period of 2.5 seconds. The photographs also show the position of the spectrometer
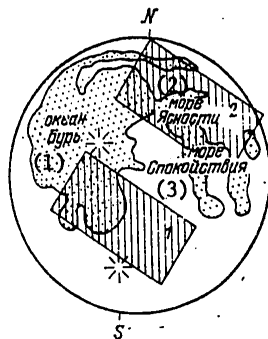

Figure 3.11. Position on the lunar disc of the sections investigated from the Salyut-4 spacecraft

Key:
   1. Oceanus Procellarum
   2. Mare Serenitatis
   3. Mare Tranquillitatis

slit with respect to the image of the moon. Thus, in practice it is possible to compare every received spectrum to a region on the surface of the moon, the emission from which was incident on the instrument. Fig 3.11 shows the position of the spectrometer slit on the disc of the moon for two times, after 335 and 356 seconds (2 and 1). Both positions correspond to mixed marine and continental regions (approximately in the ratio of the sea and continent areas of the entire visible disc of the moon), and they are distinguished by the distance from the center of the disc. The average temperatures are 405°K for region 1 and 387°K for region 2.

In the first phase the experimental data were processed in the range of 3.5-7 microns. The values of the signal in this range were reckoned at 12 points approximately 0.3 microns from each other.

Fig 3.12 shows the infrared emission spectra of the moon for the two indicated sections. Values are presented here for the spectral densities of the emission for an absolutely black body at temperatures corresponding to sections 1 and 2. The spectral reflection coefficient ρ_λ of the lunar surface was determined by calculation on the basis of the fact that the measured radiation flux I_λ is made up of the natural thermal emission of the surface and the reflected solar emission. The value of ρ_λ is determined by the ratio

$$\rho_\lambda = (I_{\lambda_{A\text{ЧT}(1)}} - I_n)/(I_{\lambda_{A\text{ЧT}}} - I_{\lambda_c}),$$

Key:
   1. ABB -- absolutely black body.

74
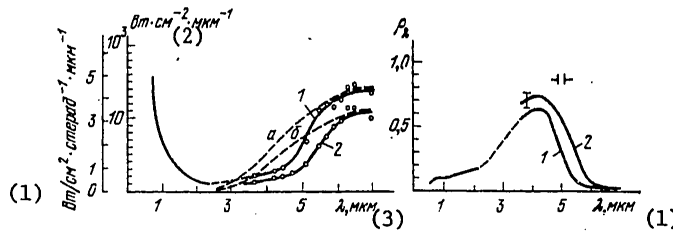
Figure 3.12. Infrared emission
spectra of the moon:
a -- emission of an absolutely
black body with T=405°K;
b -- with T=387°K
Key:
    1. watts/cm^2-steradians^{-1}-
       micron^{-1}
    2. watts-cm^2-micron^{-1}
    3. microns

Figure 3.13. Spectral reflection
coefficient of the lunar surface
Key:
    1. λ, microns

where $I_{\lambda_{ABB}}$ is the radiation intensity of an absolutely black body with
the surface temperature of the moon on the given wave length; I_{λ_c} is the
intensity of the solar emission on a wave length λ.

The spectral behavior of the reflection coefficient is illustrated in
Fig 3.13. By the experimental results the relations were constructed for
the 3.5-7 micron range. The known data of [3,30] were used in the
0.5-2.2 micron range, and the values were interpolated for the 2.2-3.5
micron range. The reflection coefficient reaches a maximum at λ~4 microns.
This qualitatively agrees both with the astronomical data and with the
data of the laboratory studies of the lunar soils, but the value of the
reflection coefficient at the maximum is close to the astronomical data.
The reflection spectra of the moon and the laboratory spectra of the
surface lunar soil (regolite) are similar with respect to spectral nature:
in both cases there is an intense reflection band in the 3-5 micron range.
The difference is that the reflection at the maximum for the moon is
somewhat higher, and the long wave edge of the band is steeper and is on
a shorter wave length than for the images delivered to the earth. It is
proposed that this difference is connected with the structural differences
of the laboratory soil subject to mechanical effects and the soil in its
natural occurrence.

FOR OFFICIAL USE ONLY

CHAPTER 4. INFRARED EQUIPMENT FOR TARGET OBSERVATION, TRACKING AND
RANGE MEASUREMENTS

4.1. Principles of Constructing Infrared Observation and Tracking
Instruments

Infrared equipment can be used to observe ground targets, the state of the
earth's atmosphere, monitor outer space, determine the location of and
to track artificial earth satellites, planets, cosmonauts or targets on
the surface of other planets, for detection and tracking of the nose cones
of intercontinental ballistic missiles in the middle and final segments
of the trajectory. The instruments of this group combined with other
equipment are used to solve scientific and practical problems such as the
investigation of the natural resources of the earth and world oceans,
they are used to monitor the environment, study the dynamics of the
continents, monitor and predict the trajectories of spacecraft and in
military engineering, for reconnaissance with respect to the natural
thermal emission of the equipment of missile bases and exercise areas,
launch pads and technical positions, ships, naval ports and other military
engineering targets for the creation of antimissile and antisatellite
defense systems. The interest in using infrared devices to solve the
problems of antimissile and antisatellite defense systems in recent years
has increased significantly in connection with the development of compact
mosaic photoreceivers executed in the form of an instrument with charged
coupling -- structures -- or forming a united whole with the charged
coupling instrument matrix.

The infrared observation and tracking instruments have a number of advan-
tages by comparison with radar; they have less mass and smaller dimensions,
and they have better resolution. In many cases they are less complicated.

The basic disadvantage of the infrared instruments is worsening of the
characteristics and even in practice impossibility of the operation under
unfavorable meteorological conditions (fogs, clouds), which limits the
application of infrared devices in the systems operating in the atmosphere
or through the atmosphere.

76

FOR OFFICIAL USE ONLY

FOR OFFICIAL USE ONLY

Depending on what factors the radiation from the observation target is caused by, passive and active systems are distinguished.

The group of passive systems includes three types of instruments in which the natural thermal emission, solar radiation reflected and scattered by the target or the emission of autonomous beacons -- pulsating light sources installed on the target -- are used to obtain information about the target.

The active systems include systems which have sources to "illuminate" the target -- transmitters. These include systems for tracking targets equipped with optical corner reflectors (cataphots), systems which receive the radiation reflected or scattered by the targets and systems which receive the luminescent re-emission of the targets.

The passive systems are goniometric systems, and the location of the target is determined by them primarily by the method of triangulation, that is, simultaneous measurement of the direction of the target from several points with known coordinates. The simultaneousness of the measurements is achieved by synchronizing the operation of the measuring means, for example, by the transmission of commands over radio channels to record measurements at the times t_1, t_2, ..., t_n. When installing an optical beacon on the target, it is switched on by a defined program. In order to distinguish the times of switching on the beacon t_1, t_2, ..., t_n, the emission can be modulated by programmed encoded sendings.

The passive observation and tracking instruments contain radiometric devices as the basic assembly recording the magnitude of the radiant flux from the elements of the field of view and, in addition, depending on the purpose either a device for making a thermal map or devices which analyze the scanning field and isolate information about the coordinates of the heat-emitting targets. In the majority of instruments developed at the present time, the field is scanned by a single or multiple element receiver in the form of a rule. Each independent element of the receiver receives radiation in the instantaneous angle of the field of view ω_{view}

determining the spatial resolution of the system.

The number of expansion elements N in the field of view is

$$N = \Omega / (k_{пр}^{(1)} \omega_{зр}^{(2)}), \qquad (4.1)$$

Key: 1. rec; 2. view

where Ω is the size of the field of view; k_{rec} is the number of independent elements of the receiver.

FOR OFFICIAL USE ONLY

The duration of the pulse from a point target will be

$$\tau_{и}=T_{обз}/N=\omega_{ap}k_{пр}T_{обз}/\Omega,$$
$$(1)\quad(2)\qquad(3)(4)(2)$$
(4.2)

Key: 1. pulse; 2. scan; 3. view; 4. rec

where T_{scan} is the scanning time for the scanning field.

The optimal pass band of the instrument channel Δf_{sig}, depending on the shape of the pulse and the type of filter, is within the limits from $0.25/\tau_{pulse}$ to $0.75/\tau_{pulse}$. For approximate calculations it is frequently assumed that

$$\Delta f_{с}\simeq 0,5/\tau_{и},$$
$$(1)\qquad(2)$$
(4.3)

Key: 1. sig; 2. pulse

The possibility of detecting a target is defined by the expression

$$\Phi_{об}-\Phi_{фон}\geqslant\Phi_{пор},$$
$$(1)\quad(2)\qquad(3)$$
(4.4)

Key: 1. target; 2. background; 3. threshold

where Φ_{target} is the radiant flux from the element of the image with the target; $\Phi_{background}$ is the background radiation flux; $\Phi_{threshold}$ is the threshold value which insures given magnitude of the detection probability with fixed magnitude of the false alarm:

$$\Phi_{пор}=(S/N)\sqrt{A_{пр}\Delta f_{c}}/D^{*}$$
$$(1)\qquad\quad(2)\ (3)$$

Key: 1. threshold; 2. rec; 3. sig

where S/N is the required signal/noise ratio; A_{rec} is the area of the independent element of the photoreceiver; D^{*} is the detecting capacity.

The condition of detection of the target (4.3) considering (4.2) and (4.3) assumes the form

$$\Phi_{об}-\Phi_{фон}\geqslant(S/N)\sqrt{0,5A_{пр}\Omega}/D^{*}\sqrt{\omega_{ap}k_{пр}T_{обз}},$$
$$(1)\quad(2)\qquad\qquad(3)\qquad\quad(4)(5)(6)$$
(4.5)

Key: 1. target; 2. background; 3. rec; 4. view; 5. rec; 6. scan.

From (4.5) it follows that increasing the number of independent elements of the solar receiver will permit detection of the targets with lower contrast of them with respect to the background.

For the prospective observation and detection systems planned for use in 1980's, mosaic photoreceivers are being developed which are made up of several thousands or even tens of thousands of photosensitive elements, the set of which encompasses the entire scanning field. These photoreceivers make it possible to create nonscanning systems. For nonscanning systems

78
FOR OFFICIAL USE ONLY

$$\omega_{3p}k_{\text{пр}} = \Omega, \qquad (4.6)$$
$$(1)\ (2)$$

Key: 1. view; 2. rec

and the effective integration time of the signal is T_{scan}.

In order to obtain heat maps, broad use is made of infrared devices with
linear scanning of the scanning field. When recording a heat map from a
flying vehicle (aircraft or spacecraft) the scanning is done in the
direction perpendicular to the line of path (see Fig 4.1).   Each of
the elements of the photoreceiver records a line of the image L_c. The
scanning in another direction is realized as a result of the translational
displacement of the equipment. The gauge on the receivers records k_{rec}
lines in a scanning cycle. the line scanning is synchronous with the
displacement rate of the equipment W. The receiver gauge encompasses a
section of the terrain $\ell_k = k_{\text{rec}} H \omega_{\text{view}}$ in the flight direction. A survey of
this section must be completed during the time spent flying over it, that
is,

$$T_{\text{pec}} = l_k / W = k_{\text{пр}} H \omega_{\text{вид}} / W,$$
$$(1) \qquad (2) \qquad (3)$$

Key: 1. scan; 2. rec; 3. view

where H is the flight altitude of the equipment.

In   nonscanning devices, a gauging line of the receivers is used which is
installed perpendicular to the flight line of the equipment and by means
of which the entire line is observed immediately. A heat map is similar
to a photograph. The difference is connected on the order of the difference
in physical parameters of the objects causing the contrast on the photograph
and the heat map. The contrast between the elements of the image of the
heat map depends on the radiation coefficient and the temperature of the
targets inscribed in these image elements, and in the photograph it is
determined by the difference in reflectivity and illumination of the scanning
field.

In active tracking and range measurement systems, predominantly pulsed
laser transmitters are used to "light" the targets. With small dimensions
of the optical antennas these transmitters make it possible to obtain high
directionalness of the radiation.

The lasers with continuous emission are used to obtain images of the
earth's surface. The collimated laser beam is deflected by a scanner in
the plane perpendicular to the flight direction, and subsequently it
illuminates the sections of the terrain, the direction from which is
recorded by the photoreceiver. The image is formed just as in the passive
devices with linear scanning [4.9].   Active devices of this type frequently
are called Laser Line Scanners.
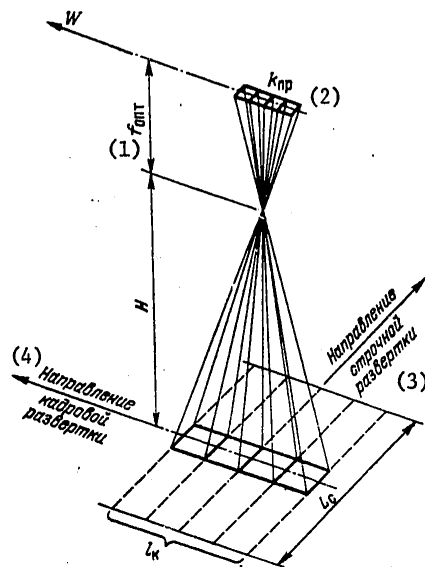
Figure 4.1. Scanning diagram of the terrain by a gauging line
of receivers

Key:
1. f_{opt}
2. k_{rec}
3. Direction of line scanning
4. Direction of frame scanning

Ruby lasers (λ=0.69 microns) and yttrium-aluminum-garnet (YAG) lasers with neodymium admixture are used in pulsed lasers. At the present time preference is being given to the YAG lasers operating on a fundamental frequency λ=1.76 microns or on the second harmonic λ=0.53 microns. Lasers usually operate in the modulated Q-factor mode, which makes it possible to obtain powers of up to several thousands of megawatts with short pulse duration (from tenths to 20-30 nanoseconds). Semiconductor gallium arsenide GaAs lasers are used for systems designed for short range.

The optical radar system for tracking and measuring coordinates is made up of four basic parts (see Fig 4.2):

The transmitter, including a laser, transmitting optical system, power supply and control systems;

80

FOR OFFICIAL USE ONLY

The receiver which includes the receiving optical system, the optical filter, photosensitive element and signal amplifier;

The homing and tracking systems by means of which homing on the target and tracking of it are accomplished;

The information processing system in which data are generated in the coordinates of the target, angular velocity, and so on.

The sounding pulse is formed in the laser. A small part of the radiation from the output of the laser is used to shape the pulse which starts the ranch measuring system. The practical divergence of the beam at the output of the laser is usually 1-10 millirads. In order to increase the directionalness, the radiation is collimated by a transmitting telescope.

The reflected radiation is gathered by the receiving optical system. In order to decrease the background illumination from external sources, an optical filter is used. The amplified signals from the output of the receiver are introduced into the processing system in which the range with respect to the propagation time of the signal to the target and back and the angular coordinates are recorded. The information about the coordinates usually is represented in digital form.

In order to aim the transmitting and receiving antenna, as a rule, additional information on the position of the target obtained using other means, for example, radar, or as a result of forecasting the trajectory of the spacecraft. is used.

The operating range of the system is determined by the operating conditions. Two basic versions are possible:

1. The useful signal is caused by optical emissions scattered by the surface of the target. In this case the operating range with equiprobable sighting errors within the limits of the width of the radiation pattern is defined by the relation

$$L = \sqrt[4]{\dfrac{1{,}82 P_{\text{л}} \tau_1 \rho_{\text{д}} S_{\text{д} \text{ об}} \tau_2 S_{\text{пр м}} \tau^2 L}{\pi^2 \theta^2_{\text{пер}} P_{\text{пр мин}}}}, \qquad (4.7)$$

Key: 1. trans; 2. rec min; 3. rec op; 4. d targ,

where P_ℓ is the laser power; τ_1 is the transmission coefficient of the transmitting optical system; ρ_d is the coefficient of diffuse reflection of the target; $S_{d \text{ targ}}$ is the effective area of diffuse scattering of the target; τ_2 is the transmission coefficient of the receiving optical system with optical filters; $S_{\text{rec op}}$ is the area of the entrance pupil of the receiving optical system; τ_L is the transmission coefficient of the medium; θ_{trans} is the width of the radiation pattern at the output, of the transmitting optical system; $P_{\text{rec min}}$ is the minimum signal power at the input of the photodetector.

81
FOR OFFICIAL USE ONLY

FOR OFFICIAL USE ONLY
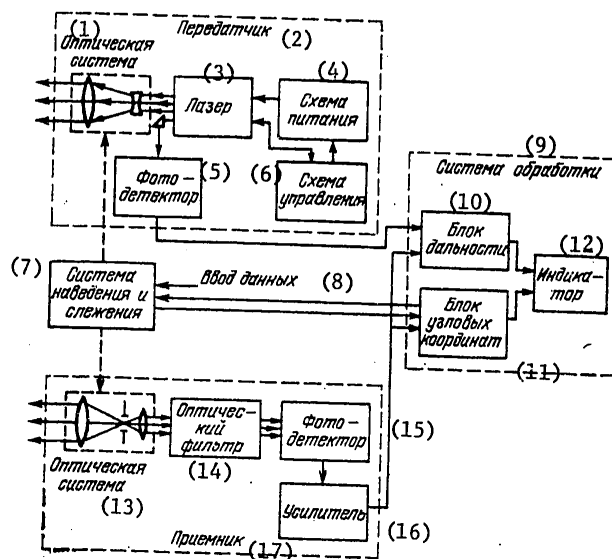
Figure 4.2. Structural diagram of the optical coordinate
tracking and measuring system

Key:

1.	Optical system	10.	Range unit
2.	Transmitter	11.	Angular coordinate unit
3.	Laser	12.	Display
4.	Power supply	13.	Optical system
5.	Photodetector	14.	Optical filter
6.	Control circuit	15.	Photodetector
7.	Homing and tracking system	16.	Amplifier
8.	Data input	17.	Receiver
9.	Processing system		

The value of the effective area of the diffuse scattering is determined by
the configuration of the target and, as a rule, is less than the midship
area of the spacecraft with respect to the viewing direction. For spheri-
cal targets with a radius R, $S_{d\ targ}=(2/3)\pi R^2$ [4.1]. The value of 2/3
can be used as the approximate value relating the effective area to the
midship area.

2. The useful signal is formed by the optical emission reflected by the
angular reflector (or set of reflectors) installed on the target. In
this case

82

FOR OFFICIAL USE ONLY

$$L = \sqrt[4]{\frac{7,28 P_{\pi}\tau_1\tau_2 \overset{(1)}{S}_{y\,o} \overset{(2)}{S}_{\text{np}_M}\tau^2 L \rho_{y\,o}}{\pi^2\theta^2_{\text{nep}}\theta^2_{y\,o} P_{\text{np min}}}},$$
$$(3) \qquad (4)$$

Key: 1. corner reflector; 2. rec op; 3. trans; 4. rec min

where $\rho_{\text{corner reflector}}$ is the reflection coefficient of the corner reflector; $S_{\text{corner reflector}}$ is the area of the corner reflector (or set); $\theta_{\text{corner reflector}}$ is the width of the radiation pattern reflected by the corner reflector.

The value of $\theta_{\text{corner reflector}}$ is defined by the diffraction of the reflected radiation and the imprecision of manufacturing the reflector

$$\overset{(1)}{\theta_{y\,q}} = \lambda/(d\cos\beta) + \theta',$$

Key: 1. corner reflector

where d is the diameter of the corner reflector; β is the angle of incidence of the radiation. The value of θ' for modern reflectors is 2-5", and $\theta_{\text{corner reflector}}$ does not usually exceed 10-20" or $(5-10)\cdot10^{-5}$ radians.

The minimum power of the signal $P_{\text{rec min}}$ is defined by the noise in the channel of the optical receiver and essentially depends on the type of photodetector used.

When using a photomultiplier, the basic noise sources are quantum fluctuations of the proton flux and the background illumination $P_{\text{background}}$.

For a photomultiplier $P_{\text{rec min}}$ is defined as

$$\overset{(1)}{P_{\text{np min}}} = \frac{2h\nu\Delta f_c F_{\text{m}}\,(S/N)}{\eta} \times \left\{1 + \left[1 + \frac{\eta P_{\phi}(4)}{h\nu\Delta f_c F_{\text{m}}\,(S/N)}\right]^{0.5}\right\},$$
$$-(2)(3)$$

Key: 1. rec min; 2. sig; 3. noise; 4. background

where $h\nu$ is the quantum energy of the radiation; F_{noise} is the noise coefficient of the photomultiplier; η is the quantum effectiveness of the photo cathode of the photomultiplier. In order to decrease the effect of the background illumination, it is expedient to decrease the duration of the sounding pulse, that is, expand the signal spectrum Δf_{sig}.

When using photodiode receivers, the thermal noise and the noise from the background illumination are predominant. For such receivers

FOR OFFICIAL USE ONLY

$$P_{\text{пр маш}} = \left[\left(\frac{S}{N} \right) \Delta f_c \frac{2eP_\phi S_i R_{\text{н}}^{(4)} + 4kTF_{\text{ш ус}}}{(3) \quad S_i^2 R_{\text{н}} \quad (5)} \right]^{\bullet,\bullet},$$

(1) (2)

Key: 1. rec min; 2.sig; 3. background; 4. load; 5. amplifier noise

where S_i is the current sensitivity of the photodiode, amps/watt;
R_H is the load resistance; $F_{\text{amplifier noise}}$ is the noise coefficient
of the amplifier; T is the load temperature; k is the Boltzmann constant.

The power of the background illumination $P_{\text{background}}$ depends on the
parameters of the receiving optical system and optical filter:

$$P_\phi = (\pi/4) \Delta\lambda \theta^2_{\text{прм}} S_{\text{прм}} \tau_{\text{прм}} b_{\lambda_\phi},$$

(1) (2) (3).

Key: 1. background; 2. rec op; 3. background

where $\Delta\lambda$ is the pass band of the optical filter, $\overset{\circ}{A}$; $\theta_{\text{rec op}}$ is the angle
of the field of view of the receiving optical system; b_{λ_ϕ} is the spectral
brightness of the background watts-cm^{-2}-steradians$^{-1}\overset{\circ}{A}^{-1}$.

The estimate of the operating range of the laser system by the presented
formulas indicates that for diffuse reflection, the tracking of such
targets as spacecraft and the nose cones of intercontinental ballistic
missiles can be carried out at distances   of several hundreds of
kilometers when using solid-state lasers with an output power on the order
of 100 megawatts and a photomultiplier in the receiving channel. The
installation of corner reflectors on the targets permits an increase in
the tracking range to several thousands of kilometers. The photodiodes
and photoresistors are significantly inferior to the photomultipliers with
respect to sensitivity. Their use in portable short-range devices gives
a decrease in the overall dimensions and mass first of all as a result of
excluding the high-voltage power supply.

4.2. Passive Infrared Observation and Tracking Means

The detection of the targets and the tracking of them can be realized by
passive instruments with respect to the solar radiation or natural thermal
emission reflected from their surfaces. The value of the reflected flux
recorded by the instrument depends on the size, shape, reflecting properties
of the surface of the target and the phase observation angle α, that is,
the angle between the directions of the sun and the target and the target
and the observer [4.1].

The illumination on the entrance pupil of the instrument E created by
the reflected emission beyond the limits of the atmosphere on diffuse
reflection from the target of spherical shape is

$$E = \frac{2}{3\pi^2 L^2} E_\odot S_{KA} \rho_{\text{д}} [\sin\alpha + (\pi - \alpha)\cos\alpha]. \qquad (4.8)$$

where $E_\odot$ is the solar constant, 0.14 watts-cm^{-2}; L is the range;
S_{KA} is the cross sectional area of the spacecraft turned in the direction
of the sun (midships); ρ_{d} is the diffuse reflection coefficient.

For mirror reflection

$$E = \frac{1}{4\pi L^2} E_\odot S_{KA} \rho_{\text{з}}, \qquad (4.9)$$

where ρ_3 is the mirror reflection coefficient. The spectral distribution
of the reflected emission corresponds approximately to the solar emission.

The radiation reflected by the spacecraft can be used for exact measure-
ment of its position against the background of the stellar sky. When
using an optical system with a diameter of the entrance pupil of 20 cm,
a relative aperture 1:3 and a field of view of 5x30°, we obtain a precision
of determining the angular coordinates of 3" with a range of several
thousands of kilometers [4.2]. The continuous tracking with the applica-
tion of coordinators can be used for the spacecraft to approach the part
of the orbit lighted by the sun [4.3].

For observation of the situation in space, it is planned that the network
of GEODSS stations be built which will record the solar radiation reflected
by the targets. The network must include five GEODSS stations and insure
higher operativeness of the information received than the SPACETRAC system
in which radar is used. The new GEODSS stations will make it possible to
record the targets at a distance from 5500 to 37000 km with an angle of
elevation above the horizon from 30 to 90° [4.5]. The stations provide
information about the range, the height of the perigee and apogee of the
orbit and even the shape of the targets. Several proposed technical ver-
sions of the GEODSS stations are similar to each other. The targets are
observed by means of a telescope which tracks the stars. The telescope
is connected with the television camera which, in turn, is connected with
the moving target display. The targets are detected by comparison of a
series of photographs obtained successively with an interval of about
10 seconds in a computer.

The natural thermal emission permits detection of the space targets in
any part of the trajectory.

For the spacecraft the orbital altitudes are usually selected no less than
180 to 200 km in order to insure a sufficiently prolonged time for the
spacecraft to be in orbit. At such altitudes the density of the environ-
ment is extremely low, and the heat removal from the spacecraft can take

place only by radiation from the surface. The heat balance equation of the spacecraft has the form

$$\sum_{i=1}^{n} m_i C_i dT_i = (Q_{\text{нар}} + Q_{\text{вн}})dt - Q_{\text{изл}}dt, \qquad (4.10)$$
$$\qquad\qquad\qquad (1)\qquad (2)\qquad\quad (3)$$

Key: 1. outside; 2. inside; 3. radiation

where m_i, C_i, T_i are the mass, the specific heat capacity and temperature of the spacecraft element; Q_{outside} is the heat flux reaching the surface of the spacecraft from the outside; Q_{inside} is the heat flux caused by the heat evolution inside the spacecraft; Q_{rad} is the heat flux of the natural radiation of the spacecraft into the surrounding space.

The basic outside sources of heat are the following: direct solar radiation Q_C, solar radiation reflected from the surface of the planet Q_{refl}; the thermal radiation of the planet Q_{pl}, the heat generation caused by collision of the spacecraft with molecules Q_{mol}. The amount of the heat flux supplied from the outside is

$$Q_{\text{нар}} = \alpha_C (q_0 S_{\text{м с}} + q_{\text{отр}} S_{\text{м отр}}) +$$
$$(1)\qquad\quad (2)\qquad\quad (3)\qquad (4)$$
$$+\, \varepsilon q_{\text{пл}} S_{\text{м пл}} + q_{\text{мол}} S_{\text{м мол}}, \qquad (4.11)$$
$$(5)\quad (6)\qquad (7)\quad (8)$$

Key: 1. outside; 2. m solar; 3. refl; 4. m refl; 5. pl; 6. m pl
     7. mol; 8. m mol

where α_C is the absorption coefficient of the solar radiation; ε is the degree of brightness of the outside surface of the spacecraft; q_C, q_{refl}, q_{pl}, q_{mol} are the specific heat fluxes (per unit area of the midship cross section); $S_{\text{m solar}}$, $S_{\text{m refl}}$, $S_{\text{m pl}}$, $S_{\text{m mol}}$ are the areas of the midship cross section of the spacecraft with respect to the direction of each flux. The value of Q_{rad} is determined by the total radiation of all elements of the spacecraft in all directions.

The general solution to the problem of determining the temperature of the spacecraft and its thermal emission is possible only with significant simplifications, for example, for the model of a spherical or cylindrical satellite having constant temperature, absorption coefficient α_C and degree of brightness ε over the entire surface without considering the heat capacity of the inside elements of the spacecraft. The ratio α_C/ε has basic influence on the temperature of the spacecraft, and the selection of this ratio insures defined thermal conditions [4.4]. Usually for near-earth orbits in order to insure $T \approx 300°K$ the value of α_s/ε can be within the limits of 0.2–0.8 [4.4]. For a cylindrical satellite made of sheet titanium 0.4 mm thick and moving in an elliptic orbit, the values of the outside surface temperature in the range of 160 to 450°K were calculated [4.6]. For spherical satellites of different types at an

orbital altitude of 480 km the calculated temperature range is 250-350°K [4.7].

For real satellites the temperature range is limited to more narrow limits. By selecting the parameters α_C and ε, using the active methods of temperature stabilization (the use of internal heating, variation in area of the cooling radiators) a spacecraft hull temperature of about 273°K is insured with deviation of 30-40°K in the direction of a decrease or increase. For example, for the hull of the Mariner 10 spacecraft, a heat protective coating made of elastomer organosilicon material 92-007 of Dow Corning Company was used with the parameters ε=0.84-0.90, α_C=0.14-0.20, which insured a hull temperature within the limits of 275-297°K. The maximum temperature of the radiators reached 311°K. The greatest temperature fluctuations of 244-383°K were observed for the panels of the solar cells. These temperature conditions occurred on variation of the intensity of the solar radiation by 5 times [4.8].

The nose cones of intercontinental ballistic missiles in the middle (transatmospheric) part of the trajectory have approximately the same temperature conditions as the spacecraft.

Thus, the space targets are low-temperature emitters (T=250-300°K). The spectra of their emission are distinguished insignificantly; a maximum is observed near 10 microns.

The radiation flux of the spacecraft can be approximately estimated by the total magnitude of the energy fluxes coming to the spacecraft from the outside and the internal heat generation. The value of $Q_{outside}$ is determined by the midship cross section of the spacecraft and its orbital altitude.

The specific direct solar radiation flux Q_C even at significant distances of the earth ($h \leqslant 10^6$ km) is in practice constant, and its value is approximately equal to 1400 watts/m^2.

The specific heat flux of the reflected solar radiation is determined by the altitude of the orbit and the angle ψ between the sun-earth and earth-spacecraft direction. For $\psi \leqslant 70°$, the diffuse reflection from the planet predominates

$$q_{\text{отр}1} = \frac{2}{3} a_{\text{пл}} q_C \left[b_0 (b_0 - \sqrt{1 - b_0^2}) + \frac{2}{b_0} (1 - \sqrt{1 - b_0^2}) \right] \cos \psi, \qquad (4.12)$$

Key: 1. refl; 2. pl

where a_{pl} is the albedo of the planet; $b_0 = R_{earth}/(R_{earth}+h)$; R_{earth} is the average radius of the earth.

APPROVED FOR RELEASE: 2007/02/08: CIA-RDP82-00850R000200010007-1

FOR OFFICIAL USE ONLY

For angles of $\psi > 70°$ it is necessary also to consider mirror reflections

$$q_{\text{отр}(1)} = \frac{a_{\text{пл}}q_C}{2\sin\psi} \cdot \frac{b^2_0 \sin 2\beta}{2\cos(2\beta-\psi) - b_0\cos\beta}, \quad (4.13)$$

Key: 1. refl 2; 2. pl

where β is determined from the equality

$$\sin\beta\,\text{cosec}(\psi-2\beta) = b_0/(1-b_0).$$

The dependence of q_{refl} on ψ and h is shown in Fig 4.3.

The specific heat flux of the radiation of the planet q_{pl} is

$$q_{\text{пл}} = 0,5(1-a_{\text{пл}})(1-\sqrt{1-b^2_0})q_C.$$

Key: 1. pl; 2. pl

The variation of q_{pl} with altitude of the orbit is illustrated in Fig 4.4. At orbital altitudes of h>1000 km the effect of the radiation of the earth can be neglected by comparison with the direct solar radiation.
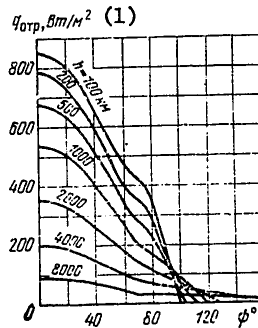

Figure 4.3. Variation of the specific heat flux of reflected solar radiation at different orbital altitudes of the spacecraft.

Key:
1. q_{refl}, watts/m^2

The specific molecular heat flux is determined by the density of the medium ρ at orbital altitude and speed of the spacecraft

$$q_{\text{мол}} = 0,5\alpha\rho v^3,$$

Key: 1. mol

where α is the accommodation factor (α=0,9-1.0). The value of q_{mol} quickly decreases with an increase in orbital altitude (Fig 4.5).

88
FOR OFFICIAL USE ONLY

APPROVED FOR RELEASE: 2007/02/08: CIA-RDP82-00850R000200010007-1

The internal heat flux Q_{int} can vary as a function of the purpose of the spacecraft within very broad limits from values of somewhat less than 100 watts for small satellites to units, and in the future to tens of kilowatts [4,9].

The approximate estimate of the flux emitted by the spacecraft by the sum $Q_{outside}+Q_{inside}$ for a midship cross sectional area of 1 m² gives a value of several hundreds of watts at orbital altitudes from 200 to 1000 km, which makes it possible to obtain irradiation on the surface within the limits from 10^{-12} to 10^{-14} watts/cm². For direct measurements of the infrared radiation of a number of satellites [4.10], radiation was recorded from $2 \cdot 10^{-12}$ to 10^{-14} watts/cm² in the range of 1-3 microns and $3 \cdot 10^{-12}$ watts/cm² in the range of 2-6 microns.
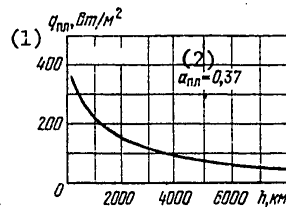

Figure 4.4. Variation of the specific heat flux of the earth's radiation as a function of the orbital altitude of the spacecraft
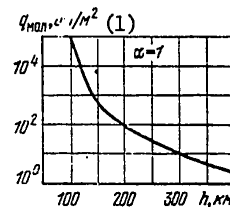Key:
1. q_{pl}, watts/m²
2. a_{pl}=0.37

Figure 4.5. Variation of the specific molecular heat flux as a function of the orbital altitude of the spacecraft
Key:
1. q_{mol}, watts/m²

The nose cones of the intercontinental ballistic missiles in the trans-atmospheric section of the trajectory are also characterized by a radiation flux of several hundreds of watts.

Although the space targets are not intensive sources of radiation, their detection by infrared devices is possible at ranges of about 100 km in a field of view of 10x10° for a diameter of the optical system D<0.5 meters and a number of receivers in the gauge k_{rec}<10 [4.11]. The application of mosaic photoreceivers with more than 1000 elements permits the detection range to be increased by an order. The modern infrared pickups are capable of detecting spacecraft and the nose cones of intercontinental ballistic missiles in space at a distance of more than 1600 km [4.12], which permits the infrared devices to compete successfully with the radar systems for monitoring outer space. In 1977-1978, in the United States it was proposed that developments be started on satellites for observing the space situation equipped with long-wave infrared detectors. Several satellites must

provide global scanning [4.13]. The experiments in building the P-80B satellite for detecting strategic bombers from space [4.14] from altitudes of about 185 km had an analogous nature.

The creation of observation satellites is also planned in France by 1982-1985 [4.15]. These satellites will be equipped with the MRVIR and the HVR radiometers. Their equipment will also include a refrigerator, on-board digital computer and transmitter.

The MRVIR radiometer (Moyenne Resolution Visible Et InfraRouge) is a scanning radiometer, and it is designed for operation in the visible and the infrared regions in four bands: 0.5-1.1, 1.5-1.7, 2.1-2.3, 10.5-12.5 microns. The scanning band width of the radiometer is 300 km, the resolution is 100 meters in the visible band and 200 m in the infrared region. In order to record radiation in the visible band, the plan calls for using photodiodes with fiber optics or instrument with charge coupling. For the infrared region use will be made of detectors based on the ternary compound Hg-Cd-Te cooled to 80°K using a passive radiator similar to the radiator on the Meteosat satellite. The MRVIR radiometer with radiator weighs about 100 kg.

The high resolution radiometer HVR (Haute Visible Resolution) is to be made nonscanning. About 3000 detectors will be used in it on instruments with charge coupling, forming a line gauge oriented perpendicular to the orbital motion of the satellite. The range of the HVR radiometer is 0.5-1.1 micron, its resolution is 10 meters, and the scanning band width is 30 km. The device weighs 40 to 45 kg.

It is proposed that an observation satellite be inserted into a circular solar-synchronous orbit with an altitude of 800 km and inclination of 98°.

The application of multielement, long-wave infrared detectors for anti-missile defense means is considered to be highly effective. In the United States the work in this area is provided for by the ATP [Advanced Technology Program] program, including a number of specialized programs in laser and infrared engineering. The ATP program provides for experiments connected with the study of the possibility of interception of the warheads of intercontinental ballistic missiles in the transatmospheric section and in the atmosphere. It is proposed that the intercept experiment be performed in 1980 [4.16]. The target is to be tracked by an optical system. The preliminary orientation of the optical sensor is realized according to the data from the early detection satellite and a special radar.

For the solution of the problem of detection and target recognition it is considered expedient to use jointly with the radar, infrared telescopes having high sensitivity and resolution when recording long-wave radiation of the fragments of the jettisoned last stage of the intercontinental ballistic missile, false targets and other means of penetrating the

UU ER

BY
29 OCTOBER 1979   YU. P. SAFRONOV AND YU. G. ANDRIANOV   2 OF 3

FOR OFFICIAL USE ONLY

antimissile defense system and also the warheads of the intercontinental
ballistic missiles themselves [4.12].

Significant attention is also being given to the complex problem of target
recognition, for the solution of which provision has been made for
experiments according to several specialized programs. Studies are being
made of the spectra and the intensity of radiation of the various targets,
their variation in time, the nature of the angular displacement of the
various targets.

The Lincoln Laboratory of Massachusetts Institute of Technology has
developed and built a 48-inch (121.8 cm) telescope-spectrograph. It is
included in the equipment on Kwajalein Atoll (Marshall Islands) and is
designed for collection of the spectral signatures of the nose cones of
intercontinental ballistic missiles and spacecraft on entry into the
atmosphere in accordance with the PRESS program (the investigation of
electromagnetic signatures in the Pacific Ocean Missile Range). The
program is being financed by the Scientific Research Planning Administra-
tion of the U.S. Department of Defense. The telescope-spectrograph makes
it possible to obtain high-quality radiometric and spectrographic data
on spacecraft entering the atmosphere in the visibility zone of the tele-
scope. The field of view of the telescope is 0.4°. The effective focal
length is 267 cm; the spatial resolution is 2", and the spectral resolu-
tion is less than 0.1 mm. The spectrographic system of the telescope is
made up of a diffraction grating, camera and mechanism for drawing the
film. The system includes two 35-mm cameras. One of them has a focal
length of 81 cm and takes pictures at a rate of 8 frames/sec. The field of
view of this camera is 1.6x1.1°. The second camera is an objective with
a focal length of 15 cm, and a field of view of 7.5x6°; the picture taking
rate is 24 frames/sec. In addition to the cameras, the system has a
superorthicon television camera. The field of view of this camera is
17x12°.

By the SOFT program studies are being made of the characteristic radiation
of the fragments of the last stage of the intercontinental ballistic missiles
[4.12]. Within the framework of this program in January 1975 a special
system including infrared sensors was launched from Kwajalein using the
high-altitude rocket built by the Boeing Company. Simultaneously the
Titan II intercontinental ballistic missile was launched from Vandenburg
Base in the direction of Kwajalein. The last stage of the Titan II was
blown off in such a way that the fragments would be of known size. The
fragments were also recorded by radar, The experiment demonstrated the
possibility of recognizing the fragments and the warhead. Two missiles
and another system with infrared sensors were built for the continuation
of the SKOFT research program in 1976.

The studies of the characteristic infrared radiation of the fragments of
the last stage, false targets and warheads are also being performed under
the FAIR program [4.12]. The Atlas rockets are being launched for this
purpose with a system including infrared sensors built by Rockwell

FOR OFFICIAL USE ONLY

International and Hughes Aircraft and also fragments, false targets and mockups of warheads. All of these targets are released from the Atlas missile. The system with the infrared sensors uses its own control system. The goal of the experiments includes, in particular, obtaining information about the influence of the background radiation of the earth, moonlight and starlight and also the jet after the rocket engine on the effectiveness of the sensors. Reports have appeared on the performance of four such experiments and their continuation in the future.

4.3. Plans for Building Antisatellites in the United States

One of the earliest designs for the American antisatellites was the interceptor satellite plan [1.3] in which it is proposed that a system be installed for exact determination of the orbits of the inspected satellites made up of radar, of a television set, the infrared sensors, instruments and equipment for counteraction of the reconnaissance and communications systems and combat charges for destroying military satellites. The infrared equipment on board the interceptor satellite can be used both for stabilization and for detection of the inspected satellites by the solar radiation reflected from them when the satellites are on the illuminated part of the trajectory or by the natural thermal emission of the satellites on the section of the trajectory in the shadow of the earth. In one of the articles [4.17], two possible types of antisatellites are characterized.

1. The antisatellite designed for the control of the reconnaissance satellites. It is inserted into orbit calculating that it will be near the reconnaissance satellite, flying information with it, creating interference for its on-board equipment. The jamming of the optical and infrared equipment is accomplished by special light and heat sources; the radio jamming is accomplished by radio interference generators. In order to create interference with the on-board reconnaissance information transmission units, the command modules and telemetric equipment, the simplest amplifiers can be used. The antisatellite can record information transmitted by the reconnaissance satellite to the ground and relay it to the control center. The necessity for considering the fact that the reconnaissance satellite can be equipped with means of maneuvering out of range of the interference is noted.

2. An antisatellite designed for recognition and, if necessary, destruction of unidentified (unlisted) satellites. For this purpose, the antisatellite is inserted through the orbit of the unidentified satellite, it rendezvous with it and docks with it to determine its functions and monitor the operation of the on-board equipment.

In general, artificial earth satellites must be classified as targets with comparatively low infrared radiation intensity. In spite of this fact, their detection by modern infrared equipment is an entirely realistic goal. For example, the Martin Company (United States) has built a search instrument for the nose cones of antimissiles. The mirror optical system of this

92
FOR OFFICIAL USE ONLY

instrument has a diameter of 40 cm. Highly sensitive cooled photoresistors made of zinc-alloyed germanium are used as the infrared radiation receivers in the scanning equipment. By the claims of the company, the satellites are detected by the system at distances exceeding the range of any other instruments known abroad. The focal length of the system is 300 mm, the viewing angle is 12°. When tracking a space target with a surface area of 1 m², a skin temperature of 250°K and an emission coefficient of 0.5, the device has a maximum range of about 200 km.

The U.S. Air Force proposes to announce competition among the companies to obtain contracts to study the problems connected with creating on-board antisatellite systems which will be designed to rendezvous with suspicious satellites, inspect them and if necessary destroy them [4.18]. The possibility is assumed that after completion of the work under these contracts the air force will conclude contracts to develop the on-board systems themselves for the antisatellite in order to make some demonstration flight tests. It is proposed that Lockheed Missiles and Space Company, LTV Aerospace, North American Rockwell, and Grumman Aerospace participate in the announced competition. The two last-mentioned companies were previously under contract to the Air Force to study the general problems of building antisatellites capable of rendezvousing with a suspicious satellite, flying in formation with it, making an inspection (and if necessary destruction), and then changing orbit.

It is reported that some on-board antisatellite systems are already in various stages of development. Thus, at the Special Weapons Center of the Curtland U.S. Air Force Base, a detector is being developed for remote detection of nuclear devices. LTV Aerospace has developed an infrared homing system under contract with the U.S. Air Force. It is to be used for direct (on the ascending arm of the trajectory) intercept of satellites [4.19]. The first launch under this program in 1971 from Cape Kennedy was unsuccessful. Studies have been made for a number of years to build a rocket with infrared foaming [4.20]. The McDonnel-Douglas Company is under contract with the U.S. Army to study the construction of an improved version of the Spartan antimissile in which provision is made for using an infrared sensor operating in the long wave part of the infrared spectrum for detection and homing on the warhead of intercontinental ballistic missiles of the enemy. The Spartan antirocket must in the improved version have the capacity to maneuver in the final segment of the trajectory.

Rockwell International Company is making ground tests of the HOST long-wave infrared detector of modular construction protected from the damaging factors of nuclear blasts and designed for the on-board target detection and tracking devices [4.21].

In 1975 it was reported that the Division of Space and Missile Systems proposes to begin the development of a small antisatellite designed for launch both from the earth's surface and from aircraft [4.22]. A long-wave infrared system is used for guidance. It is proposed that the enemy satellite

FOR OFFICIAL USE ONLY

will not have a warhead, and the target will be destroyed by force of
impact on collision. The projects were designed to last 3 years. The
successive reports [4.23, 4.24] show that the choice of the guidance
principle by infrared radiation probably is the final choice, but in order
to increase the effectiveness of the antisatellite it is proposed that
an explosive charge be placed on board it to destroy foreign satellites.
The work program for the creation of antisatellites provides for testing
them in 1980.

4.4. Tracking Targets Equipped with Optical Corner Reflectors

The optical corner reflectors installed on the tracking targets provide
for direct rereflection of the incident radiant flux in the direction of
the transceiving system just as in radar systems. These systems are used
for tracking of satellites, movement of astronauts over the surface of the
planet, and to measure distances to planets, in particular, the moon.

RCA has developed a pulsed infrared laser locator for NASA which is designed
to determine the location of astronauts on the surface of the moon [4.25].
The system provides for tracking the astronauts and determining the
distance to them up to 700 meters with a precision to +0.5 meters and an
angular accuracy of +0.5 millirads and also aiming of the television
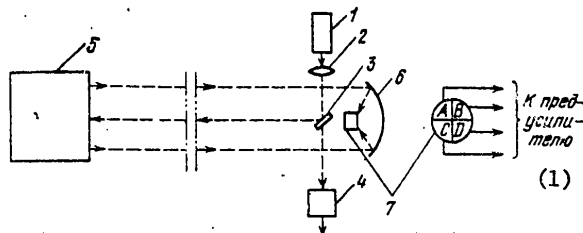camera at the astronauts.

Figure 4.6. Optical diagram of a locator for determining the
location of astronauts on the moon:
1 — semiconductor laser; 2 — objective lens; 3 — plane mirror;
4 — photodiode for starting the time reckoning system;
5 — optical corner reflector; 6 — mirror objective; 7 —
mosaic of photodiodes
Key:
1. to the preamplifier

The basic advantages of the infrared locator by comparison with radar are
considered to be the small dimensions of the corner reflector with which
the astronaut is equipped and also insurance of high tracking precision
with small dimensions, mass and energy consumption.

94
FOR OFFICIAL USE ONLY

FOR OFFICIAL USE ONLY

The optical system of the locator is shown in Fig 4.6. In the transmitting
part a flat GaAs laser diode 1 is used which has radiation power in
pulses on a wave length of 0.905 microns to 25 watts with a pulse duration
of 60 nanoseconds. The laser beam has a rectangular cross section. When
using the cylindrical lens objective 2 small defocusing of the beam to
dimensions of 1° with respect to azimuth and 3° with respect to the angle
of elevation is accomplished. The transmitting beam is directed in the
direction of the corner reflector using the plane mirror 3 which passes
a small part of the radiant flux to the photodiode 4, the time reckoning
starting system. The radiation reflected from the corner reflector 5 is
connected using a mirror objective 6 14 cm in diameter on the quadratic
mosaic of photodiodes 7. If the reflector is located on the optical axis
of the locator, then all four photodiodes have identical irradiation, and
their output signals are equal. Otherwise the signals are not equal, which
permits us to obtain information about the mismatch angle. The output
signals of the photodiode mosaic and the photodiode for starting the time
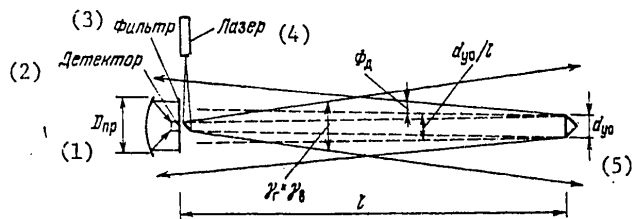reckoning system are fed to the electronic module for tracking and measur-
ing the range.

Figure 4.7. Diagram of the propagation of incident and
refracted beams

Key:
   1. D_{rec}
   2. Detector
   3. Filter
   4. Laser

   5. Corner reflector

In order to determine the required precision for measuring the range of
±0.5 meters, the required signal/noise ratio must be 460.

The radiant flux reflected from the corner reflector (Fig 4.7) is spread
as a result of diffraction by an angle $\Phi_d = 1.22\lambda/d_{corner\ reflector}$, and its
diameter in the plane of the receiver is

$$D_{отр} = 2(d_{уо} + l\Phi_д).$$

Key:
   1. reflected
   2. corner reflector

95

FOR OFFICIAL USE ONLY

At the maximum range, $D_{refl} > D_{rec}$. Taking this into consideration, the required radiation power was calculated as a function of the operating range for ground conditions (damping coefficients 0.18 km^{-1}) and for lunar conditions (vacuum). In Fig 4.8 we have the results of the calculation and the results obtained for ground testing of the locator model (the operating range of 1200 meters is achieved instead of the given 700 meters). In order to provide for reflection of the signal with arbitrary orientation of the astronaut, an 8-cell prism corner reflector was used. Safe distance from the laser emitter is 1.28 meters with radiation power of 25 watts and pulse duration of 60 nanoseconds (considering the maximum admissible irradiation level during the time of the pulse of the eyes of the astronauts equal to $0.1 \cdot 10^{-6}$ joules/cm^2).
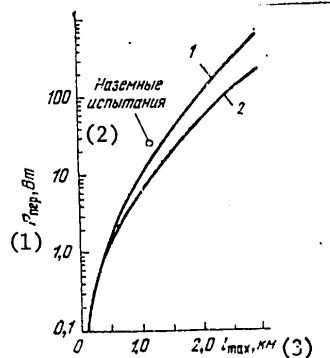

Figure 4.8. Required peak power of the transmitter as a function of the maximum operating range under ground conditions (1) and on the moon (2)

Key:
1. P_{trans}, watts
2. Ground tests
3. l_{max}, km

It is considered [4.26, 4.27] that laser location can more precisely determine the characteristics of the earth-moon system, explain some of the problems of celestial mechanics and space geodetics. The radar measurements will make it possible to introduce clarity into such complex problems as the drift of continents. The method of laser location will become basic in the study of the movement of the earth's poles. These studies were started with delivery of optical corner reflectors to the moon on the Soviet Lunokhods 1-2 and the crews of the American Apollo spacecraft.

The Lunokhod-1 [4.27] had French reflectors made up of 14 separate three-sided quartz prism reflectors with lateral dimensions of 105 mm. The effective transverse cross section of the reflectors $\sigma = 8 \cdot 10^{11}$ cm^2-steradians^{-1} (the grinding precision of the prisms is 0.07 microns).

FOR OFFICIAL USE ONLY

The measurements were performed from ground stations at the Crimean
Observatory and the French Pik-du-Midi Observatory. At the French
observatory a ruby laser was used with radiation energy of 3 joules per
pulse and an angle of divergence 0.7 millirads. In order to construct
the beam, the mirror telescope was used with a mirror diameter of 1 meter
and 60-fold angular diminishing. The size of the illuminated part of the
moon was 3.8 km (angular dimensions 2") at an intensity level of 0.5 of
the maximum. Here the irradiation was 0.02 joules/km^2 or $7 \cdot 10^{16}$ photons/km^2
(the total number of photons per pulse was 10^{19}). As a result of
scattered reflection from the moon surface on the ground it is possible to
expect irradiation of only up to 1 photon per 10 m^2. When using corner
reflectors the radiation flux received by the ground station is

$$P_{rec} = \sigma EAT \ell^{-2},$$

where E is the irradiance of the lunar surface; A is the area of the
receiving telescopes; T is the transmission coefficient of the atmosphere
(for a double path), the telescope and the interference filter in the
receiver; ℓ is the distance to the moon.

For measurements of $T \approx 0.15$; $E = 7 \cdot 10^{16}$ photons/km^2, and the telescope mirror
diameter is 106 cm. For such conditions reception of 6.5 photons in
each pulse is insured. The use of the interference filter with a band
$\Delta\lambda = 1$Å (or a transmission coefficient the laser signal of about 50%)
insures a background signal level (field of view 10x10°) considering the
effect of the glow of the earth's atmosphere of less than 10^{-1} photons
in a pulse time of 10 nanoseconds with the moon completely illuminated
by the sun.

In order to increase the receiving area of the optical system at the
Pik-du-Midi station, a receiving system was also used made up of 210 simple
lens objectives 25 cm in diameter with a focal length of 280 cm. The
light flux was gathered on the radiation receiver using glass fiber
light guide 200 microns in diameter bounding the field of view to 15".
The time of transmission of the signal, according to the measurements in
December 1970 at 1900 hours was 2.4354567 sec, and the distance to the
moon was 365065.8 km. The possible accuracy of matching the propagation
time of the laser signal (10^{-8}) is appreciably higher than the accuracy
of knowing the speed of light (about 10^{-6}) which determines the possible
accuracy of measuring the distances. In addition, the accuracy of the
measurements is influenced by the atmospheric refraction (to 15 nanoseconds).

Analogous measurements were made by the tracking of the earth's satellites
equipped with cataphots from the earth. Thus, the Japanese company Hitachi
developed a laser system for tracking artificial earth satellites equipped
with reflectors. The accuracy of the system is 10 times higher than for
ordinary radio engineering tracking systems. A ruby laser is used in the
transmitting part. The beam is focused by a telescopic optical system.

FOR OFFICIAL USE ONLY

In the receiving part of the system there is a mirror objective, photo-multiplier and interference filter. The peak power of the pulses was 5 megawatts, and the average pulse repetition frequency was 1 hertz; the maximum operating time was 1 minute. The angle of opening of the beam was 1 milligram. The mass of the entire system was 1 ton, height 3000 mm and width 1500 mm. The system permits us to track artificial earth satellites with an orbital altitude of 300-2000 km.

An experiment with respect to the geodetic observations using the PEOLE satellites with broad-scale international participation was developed in 1970 by the International COSPAR Committee program. The orbital altitude of the satellite in the perigee was 730 km, and the apogee, 860 km, and the orbital inclination was 15°. The experiment included laser ranging using the reflectors of the satellite and determination of the angular position using photographic cameras. The measurements were planned in the interests of geometric and dynamic geodesy and also geophysics. Simultaneous optical measurements provided for gridding the points at a distance of several thousand kilometers (with a precision of 10^{-6} for points 8000 km away). The measurements using several satellites permit more precise determination of the model of the earth, determination of the continental drift, variation in the rotation of the earth, and so on.

The Lageos passive geodetic satellite equipped with 426 corner reflectors was launched in the United States in 1976 to study the dynamics of the continents [4.28]. Two mobile ground stations for laser location are used to track a satellite. The transmitter at each station includes 5 YAG lasers operating in the frequency doubling mode (λ=532 nm). The pulse power is $1.5 \cdot 10^9$ watts, and the pulse duration is 0.2 nanoseconds. The repetition frequency is 1-3 pulses/sec [4.28, 4.29].

Independently of the satellite orientation, the incident radiation is reflected by approximately 7 corner reflectors. Laser location is carried out with an angle of elevation of the satellite above the horizon of no less than 20°. On passage of the satellite directly over the station, the session can continue up to 1 hour. It is considered that the accuracy of the measurements will be 5 cm, and then it will be improved to 2 cm. The laser locator with such characteristics installed in the Hawaiian Islands was used in 1975-1976 for laser location of the moon. The re-reflection of the radiation was insured by corner reflectors installed on the moon by the astronauts of the Apollo spacecraft. The accuracy of the measurements is estimated at 15 cm.

The development of laser location is provided for in the Interkosmos space research program. In the vicinity of the city of Santiago de Cuba a powerful laser rangefinder was put into operation at the satellite tracking station (Fig 4.9). Specialists from Cuba, the USSR, Czechoslovakia and other socialist countries [4.30] participated in the development of its structural design and installation. Corner reflectors were installed on the Interkosmos-17 satellite to perform laser experiments.
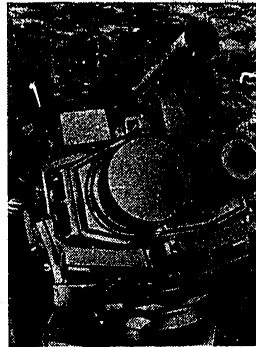
98
FOR OFFICIAL USE ONLY

Figure 4.9. Laser rangefinder of the satellite tracking station

4.5. Tracking Targets Equipped with Optical Beacons and also Having Scattered Reflection and Luminescent Re-radiation

A large volume of work is being done to track the satellites by recording the laser emissions scattered by the surface of the satellite and also the radiation of special on-board optical beacons. In the rangefinding system of the Goddard Space Flight Center [4.31] a laser transmitter and receiving system were used which were installed on the modified Nike-Ajax radar base. In order to provide for setting the laser transmitter and the receiving telescope, the elevation angle control channel was modified. A 17-bit "shaft-number" optical coder is used in the elevation angle control channel, and in the azimuthal channel, a sliding ring unit for installing the same coder and a rotating coaxial joint for supplying water to the cooling system of the laser transmitter. A special computer is used for tracking control.

The dynamic accuracy of the tracking is $\pm0.005°$. The laser transmitter operates on a pulsed ruby laser with a radiation power of 1-2 joules and with a pulse duration of 15 nanoseconds in the mode with adjustable Q-factor having a tenfold telescopic unit for decreasing the beam width approximately from 10 to 1.2 millirads. In the lasers xenon flash tubes and a ruby rod 0,95 cm in diameter and 14 cm long are used. The Q-factor is regulated by a prism with total internal reflection at 2400 rpm. The optical filter contains the solution of kryptocyanin and methanol. The diameter of the objective of the Cassegrainian receiving telescope is 40.6 cm, the focal length is 762 cm. In the detector there is a photo-multiplier EMI 955°C with an interference filter.

The least squares method is used to determine six orbital elements in a rectangular inertial coordinate system, the position of the station,

the systematic instrument error, the braking coefficient of the atmosphere, and the solar light pressure. The characteristics of the laser system are determined by comparing the tracking results when tracking the GEOS-1 satellite as the given and radar doppler systems. The mean square error in measuring the laser system is less than 2 m. The system operated successfully in the daytime. Further increase in measurement accuracy is proposed as a result of using the Amperex 56 TVP photomultiplier which has an electron transport time of 0.5 nanoseconds in contrast to 14 nanoseconds in the EMI 955A photomultiplier, which leads to an equivalent decrease in the range errors to 0.8 meters and also as a result of more exact measurement of the time intervals.

At the Ondrzheyovskaya Observatory (Czechoslovakia) experiments were run to measure the distance to the GEOS-B satellite [4.32] by a laser range-finder. The rangefinder uses the lasers from the Czechoslovakian University of Technology, the optical camera built by the Karl Zeiss Co. (Jena) and a special photometer developed by the observatory coworkers. The laser had a ruby rod 15 mm in diameter and 150 mm long with end faces at the Brewster angle. The rod was placed in the bielliptical reflector for pumping the energy of the xenon pulse tubes. The laser had water cooling and an adjustable Q-factor as a result of rotating the Brewster-Porro prism. A power of 200 megawatts was emitted by the laser for 20 nanoseconds within the limits of the 3 millirad angle. The width of angle was recorded using a Galileo telescope within the limits of 0.5-5 millirads. The recording camera used with modified photometer directed the collimated reflected signal through an interference filter ($\Delta\lambda=4$ mm; the transmission coefficient is ~45% for the laser radiation line) on a photocathode of the S-20 type of the EMI 955A photomultiplier. According to the measurement data on 9 October 1970 at 202829 hours Greenwich, the distance to the satellite was 1213.94 ± 0.35 km. In order to measure the delay time of the reflected signal, a twin-beam oscillograph and braked multivibrator were used. The comparatively low accuracy of the measurements is explained by the low accuracy of the measurements of the time intervals.

At the Rome Scientific Research Center of the U.S. Air Force experiments were performed [4.34] with respect to the location of artificial earth satellites on low and medium orbits using a CO_2 laser locator (wave length 10.6 microns) with an emission power of 2 kilowatts. At the ground station in Boston the GEOS-B satellites were tracked by the radiation of the on-board optical pulse beacon. The ground equipment included a telescope, photomultiplier, amplifier, recorder, power supply and clock. The telescope had a 300 cm reflector. The field of view was 8°. The lens system provided for incidence of the entire pencil of rays on the Amperax 150 AVP photomultiplier with spectral sensitivity of the S-11 type. The signals from the photomultiplier were fed after amplification to the recording oscillograph with rated frequency of 2.1 kilohertz. The maximum drive rate was 152 cm/sec, the process recording speed was up to 117,800 cm/sec. The reference time pulses are generated by a system synchronized with the Loran-C system, and they have deviation of no more than

FOR OFFICIAL USE ONLY

10 microseconds from the time of the U.S. Marine Laboratory. Four xenon beacons εG & G type LS-97 are used on the satellites. The flash output of one beacon is 1375 candles-sec where 90% of the energy is emitted in two milliseconds. The spectral composition of the radiation is close to the solar spectrum, 60% of the energy is emitted on wave lengths greater than 0.8 microns. After every minute 5 or 7 flashes are emitted which follow each other after 4 seconds+40 microseconds. The flashes are controlled using the on-board timer synchronized with an accuracy of +0.4 milliseconds with respect to the station time standard. The orbit of the satellite was circular with an altitude of 965 km and an inclination of 106°. The slant range to the satellite varied during the measurements from approximately 1100 to 2175 km. The light strength of the beacons increases on going away from the optical axis to approximately 50°, which insures in practice identical signals on the earth's surface with zenith angles of about 50°. At a distance of 1774 km with a zenith angle of 29° and using all of the tubes, the amount of illumination was $31 \cdot 10^{-10}$ lux-sec, and the maximum illumination was 16.5×10^{-7} lux. The possibilities of recording the signals are limited by the background of the sky. The anode current from the target was about 31 microamps, and the constant component from the background (under the conditions of illumination of the sky from the city of Boston) was 100-200 microamps, and the level of the fluctuation signals from the background was 4 microamps on amplification of the photomultiplier 10^7 and with a frequency band of the system of 50,000 hertz. Light signals and time pulse radio signals with a frequency of 100 hertz were recorded on the oscillograph. At the beginning of each second, there were reference signals -- 10 pulses lasting 100 microseconds every 10 milliseconds.

The experimental results demonstrated that the light signals from the satellite beacons can be detected by comparatively simple equipment. The accuracy of recording the flash time is +0.1 milliseconds. The data are obtained in real time and are easily processed. The given equipment can be used to determine the flash time for geodetic purposes and for rough determination of the distance to the satellite and also to investigate the transparency of the atmosphere.

Aircraft and satellite laser layer systems designed for remote measurements of atmospheric pollution by nitrous oxide, and compiling maps for the distribution of it are being developed [4,33]. The systems are based on NO fluorescence in the atmosphere on excitation by a laser beam. A laser is selected, the emission lines of which are strongly absorbed by nitrous oxide and poorly by other atmospheric gases. In particular, the CO laser has such emission lines. In contrast to the ground systems, the aircraft systems have mobility and exclude interference created by atmospheric dust.

It is considered expedient to use a two-position aircraft system (with separation of the receiving and transmitting parts by several meters).

FOR OFFICIAL USE ONLY

The application of the single-position pulse systems does not insure
the required resolution with respect to time. The basic interference of
the aircraft system is considered to be the thermal noise of the optical
system (a temperature of 250°K). The field of view of the system is 1 to
10 millirads. Here the equivalent power of the noise on the receiver is
10^{-14} watts with a pass band of 0.1 microns on a wave length of 5.2 microns,
an area of the optical system of $5 \cdot 10^2$ cm^2 and a transition coefficient
of 0.8. The calculations were performed for the radiation of the laser
on a wave length corresponding to a wave number of 1935.48 cm^{-1} and
NO emission on 1935.53 cm^{-1}. The radiation power of the laser is
25 watts, and 40% of it is emitted on the given wave length. Under these
conditions a signal/noise ratio of 14 is insured. The satellite observa-
tions permit periodic measurement on a global scale. The control of the
emission wave length as a result of the doppler effect is possible for
various angles of inclination of the laser beam to the vertical.

The basic interference of the satellite system is considered to be the
thermal noise of the earth. At a flight altitude of the satellite of
1100 cm, the altitude of the measured layer from the surface of the earth
is 20 km, and the layer thickness is 1.2 km. The field of view is 4×10^{-2}
millirads, and the area of the optical system is 0.5 m^2, and the trans-
mission coefficient is 0.5. The optical transmission band is 0.1 micron.
The resolution with respect to time is $8 \cdot 10^{-6}$ sec. For a nitrogen oxide
concentration of 10^{40} cm^{-3}, a pulse radiation power of 0.5 joules is
needed for a signal/noise ratio of one. The system permits measurements
at sea level with a nitrogen oxide concentration of 2×10^{11} cm^{-3}, and a
radiation energy of 5 joules and a signal/noise ratio of one.

CHAPTER 5. METEOROLOGICAL STUDIES USING SPACE INFRARED EQUIPMENT

5.1. General Problems of Meteorological Research from Space

Meteorology (from the Greek μετεωρχ -- atmospheric or heavenly phenomena and λογοc -- science) is the science of the earth's atmosphere, its structure, properties and the processes occurring in it. Inasmuch as the atmosphere is in constant interaction with the surface of the earth, meteorology also considers the thermal conditions of the soil and the upper layers of the bodies of water, the heat exchange between soil or water in the air, evaporation from the underlying surface, and so on. The atmosphere is connected with outer space; therefore meteorology also deals with certain problems which are close to astrophysics, in particular, the solar constant which determines the inflow of solar radiation to the earth which is the only, in practice significant source of energy for the atmosphere.

In order to study the atmospheric phenomena, meteorology applies general laws established in various areas of physics: hydromechanics, thermodynamics, the science of radiant energy and electricity, and so on. Inasmuch as the geographic situation is taken into account in which the atmospheric processes take place, meteorology is one of the geophysical sciences. It discovers the laws of the atmospheric process primarily by statistical analysis of the observation data.

In the modern procedure for compiling meteorological forecasts, the formal and statistical methods are used such as extrapolation, finding analogs, and so on. When forecasting the weather by such a procedure it is proposed that if the synoptic processes have similarity in one stage, then they continue to pursue some other development. However, inasmuch as it is difficult to select absolutely similar processes, the divergencies which are at first insignificant can lead to great differences after a prolonged period of time. The complexity of the weather forecasting by this procedure basically consists in the fact that for compiling synoptic maps which reflect the meteorological situation, until recently there was insufficient information about the actual state of the weather. Before the appearance of the first meteorological satellites in the 1960's, the network of ground meteorological stations encompassed a total of 20% of

the surface of the earth, Incomplete data on the state of the weather in
the various parts of our planet frequently have led to great errors in
the long-range weather forecasts,

Various meteorological data on all of the regions of the earth can be
obtained using artificial satellites equipped with special equipment.
An important role in the meteorological studies performed from satellites
belongs to the infrared equipment. The measurements from the satellites
in the infrared part of the spectrum will permit determination of the
distribution of the cloud cover over the surface of the Atlantic, study
of the radiation bounds of the system made up of the earth's surface and
atmosphere, realization of the temperature sounding of the atmosphere
and determination of its composition in practice at any point of the earth
with cyclicity unaccessible to other means,

The satellites of the Soviet Meteor space meteorological system insure
that complex meteorological information will be obtained: television,
infrared, and actinometric both from the lighted side of the earth and
from the shadow side [5.2]. The Soviet Meteor meteorological satellites
(for example, Kosmos-122, 144, 156, 184, 206, and so on) were inserted
into a circular near-polar orbit at an altitude of 625 to 630 km. The
solar cells of artificial earth satellites were oriented by an autonomous
system on the sun. The composition of the meteorological equipment
included the following: two television cameras, infrared equipment operating
in the 8-12 micron band, and actinometric nonscanning radiometers. The
lockon band width for television and infrared equipment in the field was
1000 km, and for actinometric equipment, 2500 km. The spatial resolution
in the nadir was 1.25x1.25, 15x15 and 50x50 km^2, respectively.

The first meteorological satellite of the United States Tiros series was
launched in 1960. Ten meteorological satellites of the Tiros series
launched before 1965 and having means for television and infrared reconnais-
sance of meteorological conditions on board made it possible to obtain
rich material offering the possibility in the first decoding phase of going
to operative use in the weather service of television and infrared images
of the cloud cover [5.1].

The artificial earth satellites are for meteorologists the means of obtain-
ing data which cannot be compared with any other with respect to spatial
and time informativeness, However, they have both theoretical and instru-
ment limitations determining the attainable resolutions and accuracy.
Today and in the expected future the contribution of satellite equipment
to meteorology is considered to have its accent on the operating
characteristics and limitations [5,37]. The discussed problems include
the following: 1) synoptic meteorology for which it is possible to use
satellite cloud observations to determine the wind characteristics,
cyclogenesis and the possible precipitation zone; 2) the profiles of the
atmospheric parameters, including the vertical temperature profiles,
moisture and concentration of a number of gas components; 3) the radiation

FOR OFFICIAL USE ONLY

balance or energy exchange between the earth and solar space; 4) the
characteristics of the underlying surface that are important to meteorology
are temperature, soil moisture and the ice cover of the seas.

Satellites will be widely used for gathering and transmitting data from
measurements performed by the instrument installed on buoys, balloons and
ground stations. However, the accuracy of such data and the degree to
which the earth surface is encompassed are not considered in the given
paper inasmuch as they will be determined in each specific case not by the
satellites, but by the sensors.

5.2. Some Peculiarities of Utilizing Meteorological Satellites [5.37]

At the present time the significance of remote sounding basically is
determined by the necessity for gathering meteorological data on such
broad scales that when using a means or direct measurement methods, this
operation will be unreasonably expensive or simply impossible. For example,
a satellite in polar orbit, examining the entire earth every 12 hours,
permits us to obtain a scan which was previously impossible when using
local sensors as a result of the absence of means for construction and
support of the operation of such an enormous network. The most successful
utilization of satellites designed to study the earth is noted in
meteorology, to a greater degree when studying the atmosphere than the
underlying surface. When recording radiation from a satellite, primarily
the atmosphere is observed, which is the object of investigation of
meteorologists. The satellites of the United States existing at the present
time to study the ocean and atmosphere for the (NOAA) can perform an
instantaneous effective scan of the earth's surface from an altitude of
1500 km within the limits of a circle of radius 1300 km, which is about
2% of the earth's surface. The orbits of these satellites are such that
the entire earth's surface is scanned in 12 hours (the entire earth is
examined in 24 hours during daylight).

For the images of various clouds, entirely defined peculiarities are
characteristic. The dense cumulus clouds near the earth's surface where
the temperature is approximately equal to the surface temperature are
hardly distinguishable on an infrared image; at the same time, these
clouds are clearly manifested in the visible range of the spectrum under
daylight. On the contrary, the thin cirrus clouds cannot appear in the
visible part of the spectrum, and they will be highly noticeable in the
infrared region as a result of the fact that they are very cold.

Primarily three types of orbits are used for meteorological satellites;
polar solar-synchronous; geostationary, inclined. A satellite in polar
(heliosynchronous) orbit rotates in a plane containing the axis of
rotation of the earth or inclined to it at a small angle. The ideal polar
orbit does not precess and, consequently, it is not heliosynchronous,
that is, intersecting the equator on each turn at the same local time.
In order to eliminate this deficiency inclined orbits are selected which
precess as a result of the fact that the earth has a gravitational field

105
FOR OFFICIAL USE ONLY

which differs from spherically symmetric. The angle required for the synchronous mode is a function of altitude. For example, from Table 5.1 it is obvious that for a satellite designed to investigate the earth's resources (ERTS) with an orbit at an altitude of 912 km, inclination of the orbit at 82 or 8° from the pole is required at the same time as for the ITOS satellite at an altitude of 1500 km, an inclination of 78° is required. In order to increase the contrast in the reflected light the angle of incidence of the beams is selected equal to 45°, Here the intersection of the equator with respect to local time will take place at 0900 or 1500 hours. In order to perform observations from satellites in the equatorial regions, a circular orbit is selected with a period of 115-120 minutes and an altitude on the order of 1500 km. It is impossible to use a polar orbit when studying fast processes.

The geostationary (synchronous with respect to the earth) orbit is circular with an altitude of the satellite equal to 35,600 km at which its rotation period is equal to the rotation period of the earth. The satellite with geostationary orbit always remain the same meridian. If the orbital plane coincides with the plane of the earth's equator, then the satellite will be above the same point of the equator. The great height of the geostationary satellites complicates the obtaining of high spatial resolution. However, this type of satellite is ideally suited to study fast processes inasmuch as it constantly observes the same part of the earth.

The inclined orbit is similar to a synchronous orbit, but its plane makes a much larger angle with the axis of rotation of the earth. The orbital plane precesses very rapidly. It is possible in practice to insure any displacement of the orbit. The polar zone is not examined with an inclined orbit.

The masses, the dimensions and powers of the spacecraft used for remote sounding are presented in Table 5.2. At the present time only nuclear sources can provide the required energy at large distances from the sun, and they have already been successfully used on the Pioneer spacecraft.

One of the means of obtaining the radiation characteristics of the earth from orbital stations simultaneously in several spectral bands is optical-mechanical scanners. In recent years a systems approach toward the design of electromechanical scanners has been noted. The characteristics of 15 electromechanical satellite scanners are presented in Table 5.1. From the table it is obvious that in the thermal band scanners (10-14 microns) constant and quite fast growth of the resolution is observed as a function of the launch time. The mass of these scanners recalculated for one channel has been reduced noticeably, which indicates the progress in the manufacturing process of the radiation receiver from the electronic equipment. The possibilities of the scanners are expanding significantly with an increase in their resolution.

FOR OFFICIAL USE ONLY

Table 5.1

Characteristics of the Equipment Installed on Artificial Earth Satellites

(1) Сканер и КА, на котором он установлен	(2) Дата первого запуска	H, км	(3) $\Delta\lambda_1$, мкм	(4) α_1, 10^{-3} рад	Δl_1, км	(5) $\Delta\lambda_2$, мкм	(6) α_2, 10^{-3} рад	Δl_2, км
High-resolution infrared radiometer of the Nimbus satellite (HRIR)	4/69	1 100	0,7—1,1	7,9	8,7	3,4—4,2	7,9	8,7
Scanning radiometer (SR) of the ITOS satellite	1/70	1 460	0,55—0,73	2,7	4,0	10,5—12,5	5,6	8,2
Temperature and humidity variation infrared radiometer (THIR) of the Nimbus satellite	4/70	1 100				6,7 10,5—12,5	21 7	23,2 7,7
Very high resolution radiometer (VHRR) of the ITOS-D satellite	9/72	1 460	0,55—0,73	0,6	0,88	10,5—12,5	0,6	0,88
Multispectral scanner (MSS) of the ERTS-1 satellite	7/72	920	0,5—0,6	0,086	0,079	(B) 10,4—12,6	0,258	0,237
Radiometer for mapping the earth's surface (SCMR) of the Nimbus satellite	11/72	1 100	0,6—0,7 0,7—0,8 0,8—1,1 0,8—1,1	0,6	0,66	8,3—9,3 10,2—11,2	0,6	0,66
Multispectral scanner (S-192) of the Skylab Space Laboratory	5/73	435	(9) 0,41—1,2	0,182	0,08	(3) 1,2—2,35	0,182	0,08
Very high resolution modified radiometer (AVHRR) of the Tiros-N satellite	4/75	1 475	0,5—0,7 0,75—1,0	0,55	0,81	(1) 10,2—12,5 6,5—7,0 10,5—12,5	2,65 0,55	3,9 0,81

Key:

1. Scanner and spacecraft on which it is installed
2. Data first launch
3. $\Delta\lambda_1$, microns
4. α_1, 10^{-3} radians
5. $\Delta\lambda_2$, microns
6. α_2, 10^{-3} radians

107

FOR OFFICIAL USE ONLY

FOR OFFICIAL USE ONLY

[Table 5.1 continued]

Description	Date	H	$\Delta\lambda_1$	α_1	$\Delta\ell_1$	$\Delta\lambda_2$	α_2	$\Delta\ell_2$
Cartographic scanner (TM) of the EOS satellite	1/79 ?	1 000	0,5—0,6 / 0,6—0,7 / 0,7—0,8 / 0,8—1,1	0,040	0,04	1,55—1,75 / 2,08—2,35	0,040 / 0,120	0,04 / 0,12
Camera for photographing the cloud cover with scanning by rotation of the satellite (SSC); of the ATS-1 satellite	12/66	35 870	0,47—0,6	0,1	3,6	10,4—12,6		
Camera for color photographing of cloud cover with scanning as a result of rotation of the satellite (MSSC); ATS-111 satellite	11/67	35 870	0,38—0,48 / 0,48—0,58 / 0,55—0,63	0,1	3,6			
Radiometer with scanning as a result of rotation of the satellite operating in the visible and infra-red bands of the spectrum (VISSR); SMS satellite	10/73	35 870	0,55—0,75	0,025	0,9	10,5—12,6	0,250	9,0
Very high resolution radiometer (VHRR) of the ATS-F satellite	1/74 ?	35 870	0,55—0,7 / 0,5—0,7	0,3	1,1 / 0,2	10,5—12,5 / 3,4—4,1	0,3 / 0,042	1,1 / 1,5
Very high resolution scanner of the SEOS satellite	1/81 ?	35 870	0,8—1,2 / 0,8—1,2	0,006 / 0,014	0,5	10,5—12,5 / 6,3—6,7	0,140	5,0
Multispectral aircraft scanner (MSS)	$V/h=0,02$—$0,18$		(10) 0,37—1,1	2,0		(14) 1,2—13,0	2,0	

Note. The following abbreviations have been adopted in the United States for the names of the spacecraft on which the scanners enumerated in this table have been installed (or are to be installed):

ATS — satellite for studying technological processes
SMA — synchronous meteorological satellite
EOS — earth orbital observatory
SEOS — synchronous earth orbital observatory
ITOS — modified Tiros meteorological satellite
ERTS — satellite for studying natural resources
H   — orbital altitude

$\Delta\lambda_1$ — spectral bands in the visible and near infrared regions
α_1 — instantaneous viewing angle in the visible and near infrared regions
$\Delta\ell_1$ — resolution in the nadir
$\Delta\lambda_2$ — spectral bands in the infrared region
α_2 — instantaneous viewing angle in the infrared region
$\Delta\ell_2$ — resolution in the nadir in the infrared region

FOR OFFICIAL USE ONLY

Table 5.2

Characteristics of Meteorological Satellites

Spacecraft	Orbit	Mass of the spacecraft, kg	Mass of payload, kg	Volume of satellite, m3	Usable power, watts	Output power of the solar cell, watts
Nimbus	Circular, almost polar (81°); heliosynchronous; intersection of the equator at noon; orbital altitude 1000 km	775	222	1.14	156	550
ITOS	Circular, almost polar (78°), heliosynchronous; intersection of the equator at 0900 hours; orbital altitude 1500 km	396	113	1.43	125	400
TIROS-N	Circular, almost polar (81°), heliosynchronous; intersection of the equator at 0800 or 1500 hours; orbital altitude 833 km	545	122	1.71	125	400
ERTS	Circular, almost polar (82°), heliosynchronous; intersection of the equator at 0930 hours; orbital altitude 930 km	940	200	1.48	271	550
Skylab	Circular, inclination 50°	90600	3940	2565	500	22000
ATS	Geostationary	1340	236	1.37	400	600

In Table 5.3 values are presented for the numbers of the parallel-included detectors n in each channel and the diameter of the entrance pupil of the objective D for the existing MSS and VISSR scanners and also the values of the parameters α and D which would be selected for increasing the resolution of these scanners by two and ten times while keeping the remaining parameters constant. When selecting these values it is necessary to give preference to an increase in the parameter n, and not D, inasmuch as this is connected with a smaller increase in mass, cost, scanning rate and speed of the receivers. From the table it is obvious that a twofold increase in resolution can be achieved basically as a result of the increase in n, and in order to increase the resolution by tenfold it is necessary significantly to increase both parameters. Increasing the aperture diameter and number

109
FOR OFFICIAL USE ONLY

FOR OFFICIAL USE ONLY

Table 5.3

Values of n and D for the existing MSS and VISSR scanners
and values of these parameters required to increase the
resolution by 2 and 10 times

(1) Сканер	(2) Тип приемника	(3) Существующие значения параметров			(4) Значения параметров, необходимые для увеличения разрешающей способности					
					в 2 раза (5)			в 10 раз (6)		
		α, 10^{-3} рад	D, см	n	α, 10^{-3} рад	D, см	n	α, 10^{-3} рад	D, см	n
MSS	ФЭУ(8)	0,086	22,86	6	0,043	23	100	0,0086	125	2 000
VISSR	ФЭУ (9)	0,025	40,60	8	0,0125	75	40	0,0025	250	1 000
MSS	Фотодиод	0,086	22,86	6	0,043	23	200	0,0086	175	2 000
MSS	Фотосопротивление (10)	0,258	22,86	2	0,129	40	10	0,0258	240	200

Key:
1. Scanner
2. Type of receiver
3. Existing values of the parameters
4. Values of the parameters required to increase the resolution
5. by twofold
6. by tenfold
7. α, 10^{-3} radians
8. Photomultiplier
9. Photodiode
10. Photoresistance

of detectors in order to increase the resolution of the instrument leads
to an increase of the scanner.

Structurally the electromechanical scanners are divided into two groups:
with surface (plane) scanning of the survey target and with scanning of
the image plane.

For systems in which it is necessary to have a large number of resolution
elements with respect to width of the image (for example, in the MSS
scanner of the ERTS satellite), the only acceptable method is the survey
with scanning in the plane of the target. This procedure makes it possible
to reduce the requirements on the development of the optical systems by
almost an order, that is, it actually makes practical execution of them
possible. The existing process for manufacturing optical systems will
permit an increase in resolution near the optical axis from 2 to 10 times.
The increase in aberrations on deviation from the main axis is the limiting
factor and requires the use of scanning in the plane of the objective in
the wide-angle optical scanning systems.

110
FOR OFFICIAL USE ONLY

FOR OFFICIAL USE ONLY

5.3. Synoptic Meteorology and Satellites

Synoptic meteorology, which studies the physical processes in the atmosphere determining the weather conditions and changes in the weather is based on the physical laws determining the variation in properties of the air and its movement. The operating method of synoptic meteorology is simultaneous spatial analysis of the weather conditons using synoptic maps. The state of the atmosphere at various altitudes in synoptic meteorology is basically characterized by the data on the pressure distribution, temperature and humidity of the air and also the wind. The meteorological satellites make it possible in a comparatively short time to obtain all of the necessary data for synoptic forecasting over an enormous territory.

The wind data can be obtained from the satellite using direct measurements by several techniques, but in practice most frequently one is used, successive   cloud images. Here it is proposed that the cloud moves jointly with the air surrounding it. The velocity vector of the clouds is with an error of 2 to 3 knots (1 knot=1.852 km/hr). The magnitude of the error depends on the resolution of the image, the gridding errors of the successive images and the change in shape of the cloud. The principal source of the error in determining the wind velocity consists in the difficulty in gridding the altitude corresponding to the wind vector that is found. After launching the SNS satellite which was inserted in orbit on 17 May 1974, images in the visible and infrared parts of the spectrum can be used to find the altitude of the upper cloud boundary. The altitude of the upper cloud boundary is determined by the radiationtemperature and local temperature profile as the altitude at which the radiation temperature is equal to the air temperature. In practice the determination of the wind velocity by the observation data from the SNS satellite is made using a semiautomatic device in which the successive images of the clouds are stored on discs with output to vidicons, which permits automatic tracking of certain peculiarities of the clouds and obtaining of the corresponding velocity vector.

Another method of determining the wind velocity from the satellite is based on observing the reflection of the sun on the ocean surface. The sun is reflected in the form of a disc 0.5° in diameter from entirely smooth water; on a wavy surface a large diffuse spot is formed, the dimensions and the brightness distribution in which are determined by the wind velocity at the surface. This method is interesting, but the limited nature of the surface on which it is possible to observe the sun significantly decreases its value. The difficulty in working with this method consists in consider-ing the effect of clouds which can both increase the brightness as a result of reflection and decrease it as a result of absorption. On the images from operative NOAA satellites the path of the sun looks entirely different. These images are line recorded by a scanning radiometer as the satellite moves, and the view of the sun is elongated along its path located on the sunny (eastern) side of the nadir line.

111
FOR OFFICIAL USE ONLY

FOR OFFICIAL USE ONLY

At the present time satellites are finding application in the solution of the problems of cyclogenesis (that is, the processes of the birth and development of cyclones) also in synoptic analysis. But the images of tropical cyclones are fast-changing elements of the photographs received from satellites; therefore tropical cyclones have immediately attracted the attention of the meteorologists. There is a procedure for classifying cyclones based on satellite images, including daily forecasting of the variation of their intensity. This procedure is used for operative estimation of the maximum wind velocity, especially for storms that are not very severe. The greatest accuracy is insure for wind velocity to 50 knots; medium accuracy in the case of severe storms (wind velocity more than 100 knots), and least accuracy for medium storms.

For a more than 14-day period the meteorologists primarily used observations from satellites with an orbit at low altitude and passing over the same area twice a day -- once in the daytime and once at night. Therefore the satellites having a system for obtaining images only in the visible part of the spectrum could make observations of the given region only once a day, whereas the satellites of infrared sensors could observe the same region twice a day. Therefore the satellites appear to be valuable primarily for studying phenomena not changing significantly in 12 or 24 hours.

The first operative SNS-1 geostationary satellite was developed by NASA and inserted into orbit on 17 May 1974. A two-channel scanning radiometer was installed on it which operated in the visible and infrared parts of the spectrum (VISSR). The possibility of continuous observation and tracking of the mesoscale phenomena (small scale phenomena) was checked out in accordance with the new experimental program for "operative" forecasting in July 1974, in the vicinity of Chesapeake Bay in the northwestern part of the Atlantic Ocean off the coast of the United States. On that day a cold front passed through the bay approximately from east to west. The images received from the satellite made it possible to discover the convective cells before they reached thunderstorm dimensions and began to rain. The possibility of observing a frontal break even in the absence of clouds was proved.

The observations of the cloud cover received from artificial earth satellites have been used many times to estimate the mean diurnal precipitation in the tropical and subtropical regions with spatial resolution, intermediate between mesoscale and synoptic. By the existing procedure provision is made for determining the proportion of the surface of the planet covered with clouds in one of three nimbus forms: cumulonimbus, nimbostratus and cumulus congestus, and the use of the empirical coefficient to predict the possible amount of precipitation. The experiments performed in the territory of Zambia (Africa) indicate quite good coincidence of the data on precipitation obtained by the images of the cloud cover from satellites in the tropical and subtropical regions with axial observation data for January 1970.

5.4. Thermal Sounding of the Atmosphere

The thermal emission of the atmosphere contains information in the vertical temperature distribution and concentration of the radiating components which are both optically active gases and other components (aerosol, clouds, precipitation). Measuring the thermal emission of the atmosphere by using a receiver installed on the satellite, it is possible to determine the temperature of various layers of the atmosphere. The infrared absorption spectrum of the atmosphere has sharply expressed selectivity. In accordance with this, the intensity of the thermal emission of the atmosphere essentially depends on the wave length.

In the regions of the spectrum where the absorption of the infrared radiation is intense (the absorption bands of different atmospheric gases), only the emission of the uppermost layers of the atmosphere will reach the infrared space instruments.

One of the most characteristic features of the atmosphere is its vertical nonuniformity, the presence of which is expressed in the existence of a defined vertical zonalness, and it permits us to talk about separation of the atmosphere into a number of layers having specific properties. This separation depends on the difference in the defining properties used as the basis for it. The most obvious difference in the properties of the layers is manifested in the temperature distribution with respect to altitude. The names of the basic and the transitional layers of the atmosphere corresponding to the generally accepted classification are presented in Table 5.4.

Table 5.4

Layer (sphere)	Average altitudes of the upper and lower boundaries, km	Transitional layer
Troposphere	0-13	Tropopause
Stratosphere	13-25	Stratopause
Mesosphere	25-80	Mesopause
Thermosphere	80-800	Thermopause
Exosphere	Above 800	—

The basic atmospheric components using radiation are water vapor, carbon dioxide and ozone. The concentration of all of these gases beyond the limits of the stratosphere and mesosphere is negligibly small. Thus, in the region of strong radiation absorption the radiating layers can be various layers located in the stratosphere and the mesosphere, In the weak absorption region (windows of transparency) of the atmosphere, the radiation will reach a satellite infrared unit in the form of a mixture of the radiation of the earth's surface and the great body of the atmosphere. In this case the infrared radiation of the earth is a complex function of the temperature of the earth's surface and the stratification of the atmosphere.

113

The intensity of the monochromatic thermal emission with a wave length λ passing in the direction of the zenith angle θ through the upper boundary of the atmosphere is defined by the expression

$$B_\lambda(\mu) = \int_0^\infty B_\lambda(\tau) e^{-\tau/\mu} \frac{d\tau}{\mu}. \qquad (5.1)$$

Here τ is the optical thickness of the atmosphere reckoned from the upper boundary of it; $\mu = \cos\theta$; $B_\lambda(\tau)$ is the intensity of the monochromatic radiation of an absolutely black body at the τ level, being a function of temperature on this level (Planck function). The expression (5.1) clearly reflects the fact that the intensity of the thermal radiation measured using radiometers installed on the spacecraft is a function of the stratification of the atmosphere. From the mathematical point of view the problem of determining the temperature distribution with respect to altitude of the atmosphere reduces to the necessity for inversion of the integral (5.1), that is, solution of the first type Fredholm integral integration. The procedure for temperature sounding of the atmosphere was developed by L. Kaplan, who proposed determination of the temperature distribution in the atmosphere by the result of simultaneous satellite measurement of the infrared radiation in the vicinity of the absorption band of carbon dioxide $\lambda = 15$ microns in 10 defined narrow spectral intervals about 5 cm^{-1} wide.

In the given section of the spectrum the spectral interval of 5 cm^{-1} corresponds to resolution 0.1 microns. Ten measurements permit calculation of the temperature in nine layers of the atmosphere. L. Kaplan [5.9–5.11] proposed measurements in the 15 micron range of the absorption band of carbon dioxide in connection with the fact that in the given case it presents no difficulty to give the concentration of the component of the atmosphere absorbing and emitting radiation, which is necessary to solve the integral equation (5.1). A significant advantage of measurements in the absorption band of carbon dioxide consists in the fact that the specific concentration in the atmosphere changes little with altitude and is on the average 0.03%. In determining the temperature stratification by the data on the outgoing radiation in the carbon dioxide band it is possible to extend the results of analogous measurements in the vicinity of the absorption of radiation by water vapor to the solution of the problem of the vertical distribution of water vapor in the atmosphere. The procedure of L. Kaplan is based on the fact that the spectral brightness in the atmosphere in the given part of the spectrum depends on the concentration of the carbon dioxide in various layers of the atmosphere, and its absorbing properties and dsitribution with respect to altitude of the temperature.

It is obvious that in the given case the transmission function and also the distribution with respect to the vertical of the concentration of absorbing and emitting materials must be known [5.3].
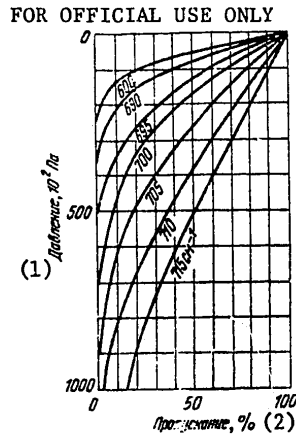
FOR OFFICIAL USE ONLY

Figure 5.1. Transmission coefficients along the vertical
of the layer of the atmosphere in the vicinity
of the carbon dioxide absorption band at
667.4 cm^{-1} (14.98 microns)

Key:
1. Pressure, 10^2 Pa
2. Transmission, %

In Fig 5.1 the relation is presented for the transmission coefficient of
carbon dioxide for layers of the atmosphere above the indicated pressure
selected from one side as a function of the absorption band with the
center at 667.4 cm^{-1} (14.98 microns). The pressure at the surface of the
earth is 10^5 Pa. Satisfactory results of the use of the discussed
procedure were obtained by Work [5.12] when calculating the temperatures
of three spectral intervals. He determined the temperature distributions
for three different cases of stratification of the atmosphere. During
the calculation, the spectral intervals were used with centers at 680
(14.70 microns), 690 (14.49 microns) and 695 cm^{-1} (14.39 microns). In
the calculations the atmosphere was broken down into layers with pressure
along the boundary layers of $1.1 \cdot 10^2$, $4 \cdot 10^4$ Pa. In Fig 5.2 the solid lines
indicate the calculated temperature distributions, and the dotted lines,
the given (true) temperature distributions. The fractions indicate the
temperatures in the following layers: in the numerator, for the calculated
distributions; in the denominator, for the true distribution. As is
obvious from the figure, the divergence between the true and calculated
values of the temperatures is low. With an increase in the number of layers,
and, consequently, the number of spectral bands in which the emission of
the "earth-atmosphere" system is measured, the temperature distribution
can be determined with even greater accuracy.
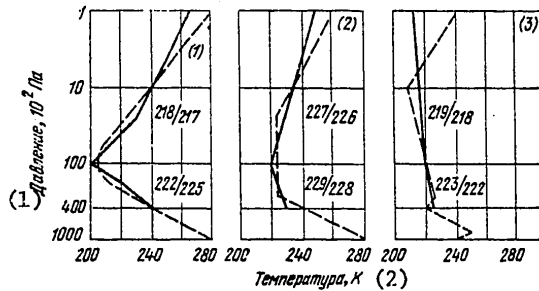
115

FOR OFFICIAL USE ONLY

Figure 5.2. True temperature distribution (- - -) and calculated temperature distribution (———) by the brightness values in three spectral intervals of 680 and 695 cm^{-1}

Key:
1. Pressure, 10^2 Pa
2. Temperature, °K

In the presence of solid clouds it is possible to consider the upper boundary of the cloudy layer to be opaque. It is obvious that in this case the measurements can give information about the temperature and altitude of the upper cloud boundary. However, under actual conditions of partial cloudiness and the absence of sharp transitions from the cloudy to the uncloudy part of the atmosphere, the interpretation of the measurement data of the out-going radiation is possible only for simultaneous television tracking of the clouds.

The estimates made by Kaplan show that a significant source of measurement errors can be the noise of radioengineering devices. Even with a signal/ noise ratio of 30:1, the errors in measuring the temperature caused by the noise can reach a value of 3-4°. The primary difficulty in solving the problem of thermal sounding of the atmosphere from a satellite consists in sharply expressed selectivity of the thermal emission of the atmosphere. The halfwidth of the absorption lines (and radiation respectively) near the earth's surface is less than 0.1 cm^{-1}, and it decreases with an increase in altitude proportionally to the pressure. Therefore the effect of the selectivity can be low only along the extent of the limitingly narrow sections of the spectrum having a width on the order of 10^{-2} to 10^{-3} cm^{-1}.

The idea of the interferometric method of filtration of radiation was stated by J. Houghton [5.13]. At the present time interferometers of various types are widely used for thermal sounding of the atmosphere from satellites (see §5.4). The interferometers are devices, the effect of which is based on the phenomenon of light interference. According to the wave theory of light when two light oscillations are imposed on each other having equal intensity I_1 and phase difference ϕ, the intensity of the resultant oscillation is

$$I = 4I_1 \cos^2\phi/2.$$

116

FOR OFFICIAL USE ONLY

Here $\phi=2\pi\gamma/\lambda$, where δ is the difference in path of the interfering beams; λ is the wave length of the light oscillations. Depending on the values of ϕ, the intensity of the resultant oscillations can assume various values from 0 to $4I_1$. Here, of course, there is no disturbance of the law of conservation of energy, for the decrease in energy in certain sections of space is completely compensated for by an increase in energy in other sections. In many cases interferometers give significantly higher accuracy than other instruments, and sometimes they permit the solution of the problems which cannot be solved in general by means of other instruments.
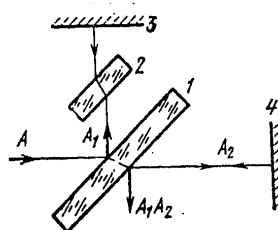
Figure 5.3. Schematic diagram of a Michelson interferometer

Fig 5.3 shows the schematic diagram of a Michelson interferometer. The pencil of beams A coming from the radiation source is split by the semi-transparent plate 1 into two beams: reflected A_1 and refracted A_2. After reflection from mirrors 3 and 4, both beams again are combined by the plate 1 and interfere. The plate 2 is used to compensate for the thickness of the glass of plate 1 and permits observation of the interference in white light. On displacement of one of the mirrors along the optical axis the interference bands shift: measuring the shift of the bands with an accuracy to 0.1 of the width of the band (the higher accuracy is possible), the magnitude of the displacement of the mirror is determined with an accuracy to 0.05 of the length of the light wave or with an accuracy approximately to 0.03 microns.

The results of the work of R. Wexler [5.14] indicate that the geographic distribution of the outgoing radiation obtained by observations from satellites in different regions of the spectrum can be a source of very important information about the horizontal nonuniformity of the temperature field. A comparison of the ground synoptic maps with satellite measurements makes it possible to draw the conclusion of high effectiveness of this method. Especially clear results are obtained when analyzing the geographic distribution of the outgoing radiation in the vicinity of the atmospheric window of 8-13 microns. Inasmuch as the regions of heat and cold are nevertheless zones of ascending and descending movements, the analysis of the geographic distribution of the effective temperatures can be useful also from the point of view of global tracking of the large-scale fields of vertical movements. The data on the temperature sounding from the satellite can be used directly for determining the vertical distribution of the water vapor in the atmosphere.

117

FOR OFFICIAL USE ONLY

5.5. Infrared Equipment Used on Meteorological Earth Satellites

One of the first spectrometers designed for thermal sounding of the atmosphere of the earth was built in the United States by the Barnes Engineering Company [1.2]. The instantaneous solid viewing angle of the instrument is 0.04 steradians. Here the near resolution of the instrument at the earth's surface is equal to approximately 220 km at a flight altitude of 1100 km.

The spectrometer determines the spectral composition of the radiation of this area, and the values of the spectral brightness in five narrow spectral intervals 698.8, 694.5, 688.5, 677.5 and 776.5 cm^{-1} (12.31, 14.40, 14.52, 14.76, 14.98 microns) are recorded simultaneously by five recording channels. The requirement of providing for the measurement of the spectral brightness is within the limits of $25 \cdot 10^{-7}$ watts-cm^{-2}-steradians^{-1}-cm^{-1} to $180 \cdot 10^{7}$ watts-cm^{2}-steradians^{-1}-cm^{-1}, which corresponds to the brightness of an absolutely black body with a temperature from -70 to +60°C, in the section of the spectrum in the vicinity of 15 microns, that is, in the vicinity of the carbon dioxide absorption band, was imposed on the spectrometer. In this case the accuracy of the measurements must be no worse than $25 \cdot 10^{-5}$ cm^{2}-steradians^{-1}-cm^{-1}. This value is equivalent to the variation in brightness of an absolutely black body having a temperature of -70°C for a change in its temperature by 0.5°C. The monochromator has a spherical mirror with a diameter of about 41 cm and a focal length of about 64 cm. The expansion with respect to the spectrum is realized by a diffraction grating about 30 cm^{2} in area. About 490 lines/cm are applied to the grating.

The radiation from the earth and its atmosphere is directed on the spectrometer by a plane mirror and is modulated using a two-section disc rotating at a speed of 450 rpm. The surface of the disc has a mirror coating. The axis of rotation of the disc makes an angle of 45° with the axis of the spectrometer. At the same time when the disc overlaps the pencil of beams from the earth, the radiation from space reflected from the mirror surface of the disc is incident on the spectrometer. Thus, the radiation fluxes of the earth and outer space fall alternately on the input slit of the monochromator. Inasmuch as the radiation of outer space in the investigated wave length range of the infrared part of the spectrum is close to zero, it is possible to consider that on rotation of the disc in practice complete modulation of the radiation of the earth is realized. The control of the calibration of the spectrometer sensitivity is by periodic rotation of a plane mirror insuring that the radiation from the calibrated absolutely black body hits the spectrometer. The temperature of the absolutely black body is not stabilized and is equal to the temperature of the spectrometer which can vary from 0 to +60°C. The temperature of the absolutely black body is measured continuously to introduce the required corrections by calculation.

FOR OFFICIAL USE ONLY

The radiation of the earth incident on the input slit of the monochromator is collected by a spherical mirror and is directed on the diffraction grating. The diffraction grating reflects the radiation which is expanded with respect to the spectrum again on the mirror which focuses the beams on the exit slits. Each exit slit isolates a defined narrow section of the infrared spectrum. The thermistor bolometers are placed directly behind the output slits. The calibration of the monochromator with respect to wave lengths is checked during the viewing by the instrument of an absolutely black body using a narrow-band interference filter installted in front of the exit slits. The spectral transmission of the filter is highly stable and in practice does not depend on the temperature gradient which can occur on the satellite. The checking of the correctness of the spectral calibration of the monochromator is realized by comparing the radiation from the black body in four narrow spectral ranges. As the receivers of infrared energy in the spectrograph, immersion thermistor bolometers are used. The sensitivity of the bolometer is increased significantly as a result of the fact that the application of the germanium collecting immersion lens with which the plates have optical contact (are glued), permitted the dimensions of the sensitive area to be kept to a minimum. The instrument tests demonstrated that by using the instruments the temperature gradients on the order of 0.2°C can be detected at room temperature.

The measuring infrared equipment of the meteorological satellites has been continuously improved and developed. The class of problems which are solved with the help of these satellites is growing. Thus, on the Nimbus F meteorological satellite an infrared scanning radiometer was installed for measuring the energy brightness of the edge of the observed earth's disc in four spectral ranges of 8.5 to 30 microns. These measurements make it possible to determine not only the vertical temperature profile in the atmosphere but also the vertical distribution of the ozone and water vapor from the lower stratosphere to the lower mesosphere, that is, approximately in the altitude range of 15-60 km on a global scale.

The radiometer has been called the LRIM (Limb Radiance Inversion Radiometer) inasmuch as the scanning is done through a limb or the edge zone of the planet earth with intersection of the horizon along the vertical, and the vertical distributions are obtained using a special algorithm of inverse conversion of the measured values of the energy brightness. The measurements are made in two regions of absorption of carbon dioxide near the wave length of 15 microns in one (about 9.6 microns) absorption band of ozone and in another encompassing the rotational band of water vapor. Vertical scanning through the horizon of the earth is done by scanning mirror which displaces the fields of view of the four radiation receivers of the radiometer correspondingly.

The radiometer is made up of an optical-mechanical part with two-stage cryostat using solid ammonia and methane, the electronics module with systems for preliminary processing of the signal of the scanning mirror

119
FOR OFFICIAL USE ONLY

FOR OFFICIAL USE ONLY

drive, the electronic coupling module which contains systems for processing and quantizing the signal, the converter of the feed voltage and the coupling circuit with the telemetric system of the meteorological satellite. The optical-mechanical part of the radiometer includes a specially designed shutter, a scanning mirror, an extraaxial parabolic mirror and other optical elements. The multielement radiation receiver, each element of which has its own spectral filter and the lens of the receiver are placed in a cryogenic compartment and are there at a temperature of 65°K.

In the radiometer of the Nimbus F meteorological satellite, the structural design of the shutter, the optical system with cryostat using solid cooling agents and the drive of the scanning mirror are of great interest (see Fig 5.4). Inasmuch as the optical axis of the radiometer can pass at a distance a total of 10° from the sun, to avoid direct illumination and to decrease the incidence of the scattered radiation of the lens of the receiver the radiometer is equipped with a shutter made of two segments. In the first segment there are ring depressions, formed by sharp projections and used to absorb the solar energy incident on the exit opening of the radiometer at large angles with respect to its optical axis. The sharp edges of the V-type annular projections are located at different distances, and the slope of the generatrices varies as a function of distance to the input opening (Fig 5.4). The front surfaces of the annular projections are at an angle such that the direct sunbeams will be incident on them, and the rear surfaces are inclined so that they will reflect the beams incident on the instrument at large angles. These beams must be reflected on the inside walls of the shutter of go back into outer space as a result of multiple reflection. The second segment of the shutter has the usual structural design which has already been widely used in space equipment. Here there are a number of annular baffles located perpendicular to the optical axis with intervals increasing as they go away from the input opening. These intervals are selected so that the beams passing from the edge of the input opening to the edge of the baffle will be incident on the wall of the shutter and on the next baffle. This arrangement of the baffles greatly weakens both the diffusely reflected light and the mirror reflected light. The housing of the shutter and its internal baffles are made of aluminum by milling with subsequent pickling to obtain maximum sharp edges which is highly important to prevent diffuse reflection on the edges. All of the internal surface of the shutter is colored black so that it absorbs infrared rays well. The calculations show that this design of the shutter insures a decrease by several orders of magnitude of the radiation scattered inside the instrument and penetrating to the receiver.

120

FOR OFFICIAL USE ONLY
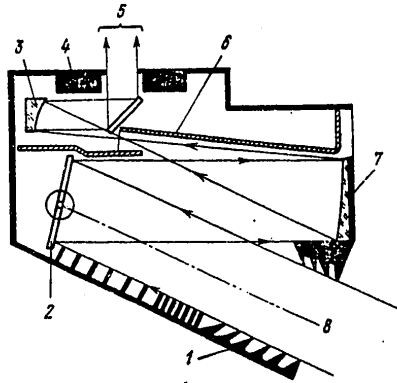
Figure 5.4. Optical-mechanical part of the infrared spectro-
             radiometer of the Nimbus F satellite: 1--Shutter;
             2--Scanning mirror; 3--Primary optical systems;
             4--Preamplifier; 5--Parallel pencil of beams reaching
             the receiver; 6--Stop aperture; 7--Parabolic mirror
             15 cm in diameter; 8--Dial.

The optical system provides angular resolution of $0.5 \cdot 10^{-3}$ radians
(approximately 1.5') in the entire field of view 2° wide. It is an afocal
system with tenfold diminishing. The objective of the receiver is irradiated
by a collimated beam of infrared radiation; therefore the focusing of the
instrument is noncritical. In addition, the optical diminishing of the
system improves the effect of angular deviation. The objective of the
receiver encompasses the field of view of about 6° and has a speed of 1:1.
It is made of the material Irtran-VI which transmits radiation in the
infrared band well, and it is at a temperature of 3n0°K. The objective
focusses the beam on the stop aperature which is cooled by the cryostat
to 152°K. Directly after the stop aper ture there is a window made of
Irtran-VI which forms a relatively small entrance into the cryostat with
respect to diameter. Then comes the system of parabolic mirrors which also
operate at a temperature of 152°K and, finally, the last correcting lens
in front of the receiver which together with the radiation receiver is
in the solid cryostat chamber with a temperature of 65°K. The sensitive
elements of the radiation receiver are made of HgCdTe inasmuch as they
do require cooling that is too deep, and the operating temperature of 65°K
is selected considering ensurance of the minimum variability of the de-
tecting capacity on the different wavelengths. The stop aperture de-
termining the field of view of the receiver is located at a distance of
50 microns above the mosaic of sensitive elements, and the spectral filter
for each of them is superposed on the aperture plate which overlaps the
field of view.

The radiation receiver in the form of a mosaic of sensitive elements, the
stop aperture, the aperture plate and lens are placed inside the
cryostat, which is a ternary Dewar cryogenic system with solid cooling

121

agents. The cryostat is made of a cylindrical tank with solid methane with a temperature of 65°K surrounded by a heat shield which is in close thermal contact with another tank containing solid ammonia with a temperature of 152°K. Both tanks are included in a common Dewar flask. Each of them has its own multilayered thermal insulation. The multielement receiver is fastened to the upper end of the tank with the methane. The radiation in the form of a collimated beam is incident on it through an opening in the shell of the Dewar flask and the thermal insulation. Each tank for methane and ammonia has one outlet tube each which serves simultaneously for filling with the cooling agents and the release of gas. Inside each tank there are coils for hardening of the cooling agents added in liquid form. The tanks of the cryostat are fastened by four concentric tubes of fiberglass passing through the central opening of the tank with ammonia and the central well of the tank with methane. A capsule with radiation receiver is in contact with the cryogenic tanks by special structural elements operating by shrinkage as the temperature is lowered. They ensure reliable thermal and mechanical connections.
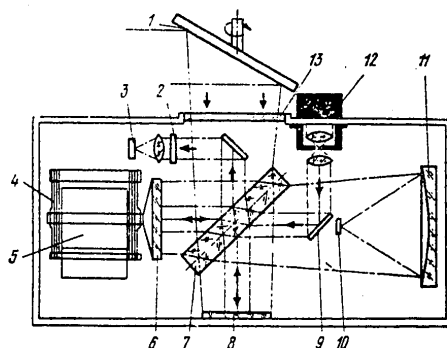

Figure 5.5.   Simplified diagram of a Michelson interferometer
              installed on the Nimbus 3 and 4 meteorological
              satellites: 1--Rotating mirror of the interferometer
              compensating for the displacement of the image as
              a result of rotation of the satellite; 2--Interference
              filter; 3--Radiation receiver; 4--System of parallel
              spring suspensions; 5--Linear displacement drive;
              6--Moving mirror; 7--Beam-refracting plane-parallel
              plate; 8--Stationary mirror; 9--Mirror; 10--Thermistor
              bolometer; 11--Objective that focuses the infrared
              radiation; 12--Source of infrared radiation with
              wavelength of 5852 Å;   13--Input opening--filter.

On the meteorological satellites of the Nimbus series, infrared radiometers and other types were used by means of which the data on the thermal sounding of the earth's atmosphere, relative humidity with respect to altitude and

and ozone content at different altitudes were obtained from outer space.
Thus, for example, on the artificial earth satellites the Nimbus 3 and
4 performed spectroscopic measurements of the thermal emission of the earth
in the wave number range of 400 to 1600 cm^{-1}, which corresponds to the
wavelength of the infrared band of approximately 25-6.25 microns. The
spectral band used in these measurements encompassed numerous absorption
and emission bands of the atmospheric gases. The resolution with respect
to wavelengths inside the indicated range was 5-2.8 cm^{-1} for these in-
struments.
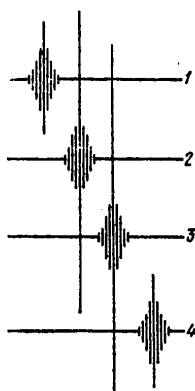
Figure 5.6. Standard interferograms recorded in orbit,
1, 2, and 4 obtained during observation of
the earth; 3--On observation of a heated black
body; 1 and 4--On observation of Arctic region;
2--On observation of a hot desert.

The radiation of the infrared band of the spectrum measured by the spectro-
radiometer was caused by several factors: the vertical distribution
profiles of the temperature in the atmosphere, the distribution of the
relative humidity and ozone with respect to altitude. The accuracy of
the measurements was $0.5 \cdot 10^{-7}$ to 10^{-7} watts/steradians^{-1}-cm^{-1} for weak
signals. The interferometer of the meteorological earth satellite,
Nimbus 3, operated continuously for 3.5 months and measured more than 1
million spectra in orbit. The spectrometer was called the IRIS (infrared
spectroscopy experiment).

Figure 5.5 shows a simplified diagram of a Michelson interferometer used on
the Nimbus 3 and 4 American meteorological satellites. The rotating mirror
of the interferometer compensates for displacement of the image occurring
as a result of the satellite. This plane mirror can be directed at the
earth, space or an emitter built into the instrument with known character-
istics (an absolutely black body) for calibration during operation. The

FOR OFFICIAL USE ONLY

temperature inside the instrument is maintained on the level of 250°K
with sufficient accuracy for practice. The telemetry data indicate that
the spectral sensitivity and equivalent power density of the interferometer
noise remained in practice unchanged for the year of operation in orbit,
which is quite good result. The operating principle of the Michelson
interferometer was investigated in §5.3. The standard interferograms are
shown in Figure 5.6. In the upper graph of 5.7 we have the radiation
spectrum obtained from the Nimbus 3 meteorological satellite as a function
of wave numbers in the 400-2000 cm^{-1} band (25-5 microns) without phase cor-
rection. In the lower graph we have the phase-correction. In the lower
graph we have the phase-corrected emission spectrum before calibration
in absolute units. The rotation by 180° of the initial spectogram
(the upper graph) in the wave number range of 600-800 cm^{-1} is easily seen.
Analogous rotations of the initial spectrograph were carried out also for
the remaining wave numbers in accordance with the recorded phase. These
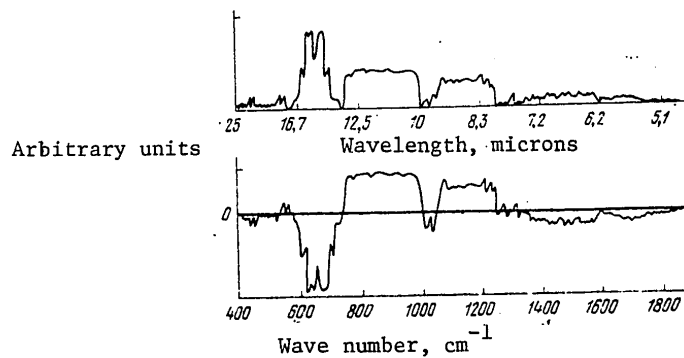corrections can be noted in the lower graph.

Arbitrary units   Wavelength, microns

Wave number, cm^{-1}

Figure 5.7. Radiation spectrum obtained from the Nimbus 3
Meteorological satellite.
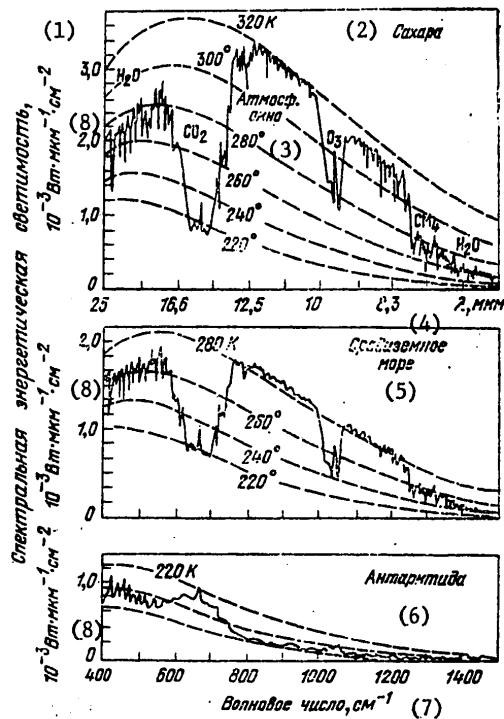
124

FOR OFFICIAL USE ONLY

Figure 5.8. Radiation spectra obtained from the meteorological satellite Nimbus 4. Spectral resolution 2.7-3 cm^{-1}

Key: 1. Spectral energy transmission
2. Sahara
3. Atmospheric window
4. λ, microns
5. Mediterranean Sea
6. Antarctica
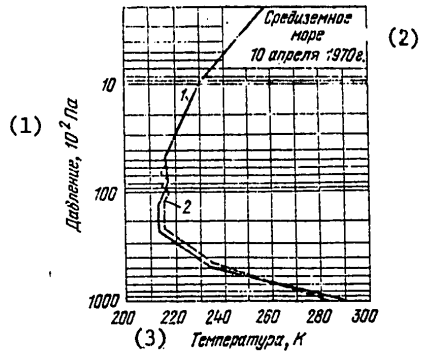7. Wave number, cm^{-1}
8. 10^{-3} watts-microns^{-1}-cm^{-1}

Figure 5.9. Vertical temperature profile in the earth's atmosphere obtained by the data from the Nimbus 4 meteorological satellite (curve 1) and by the radiosonde data (curve 2).

Key: 1. Pressure, 10^2 Pa
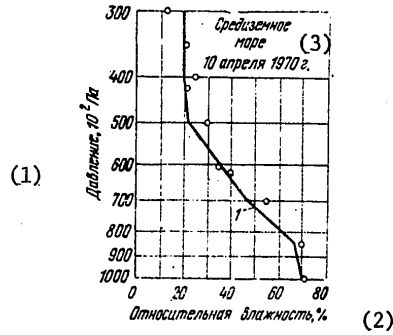2. Mediterranean Sea, 10 April 1970
3. Temperature, K

Figure 5.10. Distribution of the relative humidity of the air with respect to altitude according to the data of the Nimbus 4 meteorological satellite (curve 1) and according to the radiosonde data (ooo).

Key: 1. Pressure, 10^2 Pa
2. Relative humidity, %
3. Mediterranean Sea, 10 April 1970.

The radiation spectra in the wavelength band of 25-66 microns (400-1500 cm^{-1}) are presented in Figure 5.8 which were obtained when the Nimbus 4 meteorological satellite flew over the Sahara desert, the Mediterranean Sea and

126

FOR OFFICIAL USE ONLY

Antarctica. In all three graphs a grid of dotted curves is plotted corresponding to the radiation in this spectral range of an absolutely black body at various temperatures with a step size of 20°K. In the upper graph the chemical components of the atmosphere H_2O, CO_2, O_3, and CH_4 are presented giving the rise to the presence of brightly expressed absorption bands in defined spectral ranges. The wavelength scale on the upper graph is converted from wave numbers to microns. It is obvious that in the presence of the most heated underlying surface (the Sahara Desert) the maximum radiation falls to the window of transparency of the atmosphere of 700-1100 cm^{-2} and corresponds to the radiation of an absolutely black body with a temperature of 320°K. The picture changes if the underlying surface is cold, as when observing the surface of Antarctica from a satellite. In the lower graph it is noticeable that above Antarctica the maximum radiation corresponds not to the windows of transparency of the atmosphere through which the cold surface of this continent is observed, but to the CO_2 absorption bands between the wavelengths of 600-800^{-1} and atmospheric ozone O_3. The atmosphere above Antarctica turns out to be warmer than the continent itself, which explains this radiation distribution with respect to the spectrum. By using the data presented in Figure 5.8, by the algorithm for inverse conversion of the radiation, the vertical temperature profile of the atmosphere above the Mediterranean Sea and also the profile of relative humidity of the atmosphere in the ozone distribution with respect to altitude were found (see Figure 5.9-5.11). The data obtained using the IRIS interferometer correspond well to the results of the direct measurements of the values using radiosondes launched from the northern part of the Straits of Gibraltar at 1200 hours Greenwich time.

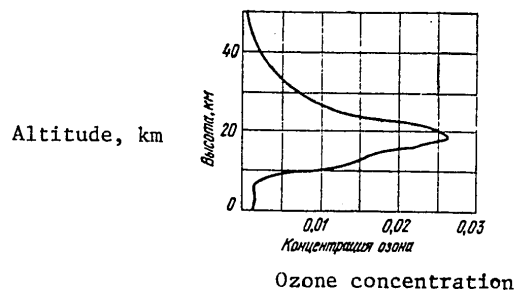
Altitude, km

Ozone concentration

Figure 5.11. Vertical concentration distribution of ozone with respect to altitude obtained using the Nimbus 4 meteorological satellite.

The results of the studies from the meteorological satellites completely confirmed the expediency of using infrared measuring equipment on them, which determined its stormy development in recent years. A brief description and the basic characteristics of some models of infrared instruments designed

for measurements of meteorological data from rockets and satellites are
presented below.

The high resolution two-channel radiometer built by the French CNES company
for the Meteosat satellite is designed for studying the cloud cover in the
visible (0.5-1.0 micron) band of the spectrum. The satellite is stabilized
by rotation around the axis perpendicular to the orbital plane, as a result
of which one of the two mutually perpendicular scanning movements required
for complete encompassing of the earth's surface is ensured. The second
movement is achieved by discrete displacement of the housing of the radiometer
by $\pm 9°$ in the plane passing through the axis of rotation of the satellite.
The complete scanning cycle lasts 25 minutes. The objective of the radiometer
is constructed by the Ritchi-Kret'yen system (a version of the Cassse-
grainian system with two hyperbolic surfaces). The diameter of the entrance
pupil of the target is 400 mm and the dispersion circle is 4" within the
limits of the field of view of 30'. Two photodiodes are placed in the
focal plane to investigate the emission in the visible part of the spectrum
and two receivers for investigating the infrared radiation based on cadmium
mercury teluride. The infrared   receiver assembly is cooled to an
operating temperature 77°K by radiation removal of the heat into outer
space. The system of shields protects the radiating cooling cavity from
direct illumination by the sun and the earth. The radiometer is calibrated
in flight by a built-in absolutely black body or the sun. The total mass
of the equipment does not exceed 50 kg, and the useful service life is 2
years.

An estimate of the effect of the radiometric errors in measuring the infrared
radiation of the underlying surface from a satellite on the accuracy of
measuring the temperature profile of the earth and the other planets by the
method of spectral scanning using absorption-emission pyrometry is presented
in [5.19]. There is a reference there to the development of a spectral
radiometer with high spatial resolution for indirect sounding of the
atmosphere [5.20]. The limits of accuracy of measuring the surface temperature
of the sea from a satellite by the results of measuring the infrared ra-
diation are analyzed [5.21]. The structural design and the operating
principle of the radiometer for remote sounding of the upper atmosphere are
presented in [5.20]. The use of diamond elements in the optical systems
of the Nimbus earth meteorological satellites is described in [5.23] and
the use of the onboard instruments of the meteorological satellites and
analysis of the results obtained by using them are presented in [5.28-
5.34].

The onboard equipment of the ITOS-D meteorological satellite launched in the
United States in the fourth quarter of 1972 includes an eight-channel VTPR
radiometer designed to obtain a vertical temperature profile of the atmosphere
in the altitude range of 0 to 30,000 meters above the earth's surface on
6 different levels. Every second this radiometer makes 16 measurements,
that is, 1,382,400 measurements a day, which makes it possible to estimate
the meteorological situation on a global scale and to compile more detailed
and accurate 5-day weather forecasts, and makes it possible to investigate

the factors influencing the weather conditions more completely. A pyro-
electric radiation receiver combined with eight optical filters is used
in the radiometer. Six of them provide for recording the radiation of
the carbon dioxide in the atmosphere, a seventh filter makes it possible
to determine the temperature of the earth's surface, and an eighth filter,
the water vapor content in the atmosphere. On the basis of this information,
the vertical temperature distribution in the atmosphere is calculated.
The information obtained using the radiometer is recorded on magnetic
tape for subsequent transmission to ground stations. The radiometer realizes
scanning in the latitudinal direction within the limits of the angle of
$\pm 30°$ with respect to the local vertical. Each scanning cycle gives in-
formation for 23 vertical temperature profiles, and each orbit around the
earth, information for 12,600 profiles. The accuracy of the radiometer
is no less than 0.5 percent. The instrument is calibrated to ensure this
accuracy of measuring the radiation in flight every 5 to 10 minutes [5.2].

5.6. Space Infrared Radiometers for Thermal Sounding of the Upper
Atmosphere

The best of the modern space spectroradiometers have spectral resolution of
5 cm^{-1}, and Michelson interferometers, suitable for use in satellite
equipment, give a resolution of 1 cm^{-1} in the best case. The instrument for
obtaining the temperature profile of the upper layers of the atmosphere
must have spectral resolution which significantly exceeds the possibilities
of any modern spectrometer or interferometer. This is explained by the fact
that the width of an spectral emission line generated by gas in the at-
mosphere at an altitude of 60 km is less than 0.001 cm^{-1}. Therefore, the
resolution of a space infrared radiometer for investigating the radiation
of the upper layers of the atmosphere must be just as high--less than 0.001
cm^{-1}. The creation of this type of infrared space instrument is a highly
complex scientific and engineering problem.

In the United States the plan calls for equipping the Nimbus F meteorological
satellite with such a radiometer in 1974. The radiometer is designed to
obtain a temperature profile in the layer of 40-80 km. Up to now the
temperatures of these altitudes have been measured only by rocket probing
at individual points on the earth. Even such separate observations have
made it possible to detect large temperature fluctuations in the stratosphere
and the intense movements of air masses connected with them. It is assumed
that by using temperature sounding of the high layers of the atmosphere
from onboard the meteorological satellite it will be possible to make new,
important discoveries with respect to the thermodynamics and stratification
of the atmosphere. For the Nimbus F meteorological satellite the Clarendon
laboratory of Oxford University (Great Britain) has developed the PMR radio-
meter with selective radiation modulation by changing the pressure in the
gas couvette. The cost of developing this radiometer by contract was
defined at 442,000 pounds sterling [5.30, 5.31]. All of the difficulties of
matching the elements of the optical channels characteristic of the pre-
ceding designs of radiometers have been eliminated in this new type instrument,
and possibilities are provided for using the method of selective modulation
to its theoretical limit which will permit thermal sounding of the atmosphere
to levels approaching the mesopause (on the order of 80 km).

Figure 5.12 shows the structural diagram of a radiometer with selective radiation modulation by varying the pressure in a glass couvette. The infrared radiation from the earth's atmosphere goes to the infrared radiation receiver equipped with the corresponding optical system through a couvette containing a small amount of CO_2 under low pressure. This pressure is varied by using a special modulator with frequency ω according to a sinusoidal law. As a result, the transmission of the carbon dioxide in the couvette on all frequencies corresponding to the lines of the rotational-oscillational absorption spectrum of CO_2 changes. The system includes an interference filter which transmits all of the 15-micron absorption band of CO_2, but excludes all other bands. Thus, the signal at the output of the receiver contains a component with modulation frequency ω. The amplitude of this component depends on the radiation intensity of the atmospheric CO_2 on a 15-micron wave which, in turn, depends on the temperature. The synchronous detection of the output signal of the receiver using an electronic circuit tuned to a frequency ω makes it possible effectively to supress any signal caused by radiation beyond the limits of the CO_2 band for $\lambda = 15$ microns. The calculations show that this type of instrument ensures discrimination by temperature inasmuch as the modulation of the radiation with a small amount of gas in the couvette takes place near the centers of the absorption lines.
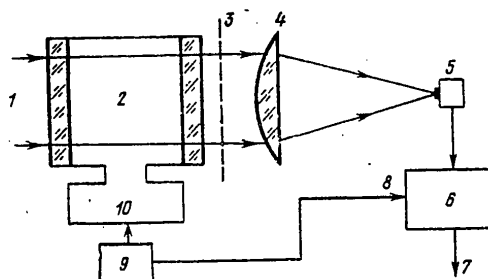

Figure 5.12. The structural diagram of a radiometer with selective modulation of the infrared radiation by pressure variation in a gas couvette: 1—Investigated radiation; 2—Couvette with CO_2; 3—Filter; 4—Collecting optical system; 5—Receivers; 6—Electron detector; 7—Output signal; 8—Reference signal; 9—Electronic modulator; 10—Pressure modulator.

The basic structural element of the radiometer is the pressure modulator with duralumin piston, the pushrod of which is suspended on two flat beryllium bronze springs. The pushrod of the piston contains a permanent magnet in the form of a rod. Both ends of this magnetic rod are surrounded by coils connected across by the Helmholtz pendulum system. An exciting voltage is fed to the coils from a special electronic circuit placed inside the modulator itself. The mass of the piston with the pushrod and the structure of

130

FOR OFFICIAL USE ONLY

the flat springs are selected so that the resonance oscillations will take place on a frequency of about 15 hertz. The structural design of the springs ensures a double amplitude of the piston oscillations to 1 cm with a gap between the piston skirt and the cylinder wall of the modulator of 0.5 mm. This gap with a length of the piston skirt of 1 cm ensures negligibly small leakage during oscillations of the piston and sufficient modulation of the pressure inside the gas couvette.

In the first models of the radiometer, a thermister bolometer was used as the radiation receiver, and in subsequent models, a pyroelectric receiver made of triglycine sulfate. The receiver was installed at the top of the goldplated conical light tube, the wide end of which is covered with a planoconvex germanium length with focal length of 5.5 cm. The interference filter is made directly on the flat side of this lens. The field of view of the entire system is 5 degrees. The output signal goes to the three-stage low-noise amplifier with amplification coefficient of $2.5 \cdot 10^4$ and then through a synchronous filter to a phase-sensitive detector. Then comes integration using the system with time constant of 5 seconds and the resultant signal is fed to a pen recorder, and in the satellite version of the radiometer, to the telemetry.

The method of ground testing of the radiometer consists in measuring the radiation passing through a large reservoir with a mixture of nitrogen and carbon dioxide, the ratio of which is calculated so that the transmission of the gases in the reservoir and the equivalent values of the line width are the same as on passage through the entire thickness of the atmosphere from the earth to its upper boundary. The pressures in the reservoir, the ratio of the components of the mixture and the path length are equal to $73 \cdot 10^2$ Pa, 0.2544 and 998 cm, respectively. The pressure of the gas mixture in the reservoir is reduced in stages so as to obtain correspondence to the lengths of the optical path between various levels and the upper boundary of the atmosphere.

In addition to the ground tests, the operation of the radiometer is checked out in flight on an aerostat with ascent to an altitude of up to 38 km. The radiometer is also equipped with a mirror system for standardizing the measurements every two minutes. The standardization is realized by receiving radiation successively from the blackened copper cone cooled by liquid air and then from the heated cone, the temperature of which is continuously controlled. The results of the measurements are reduced to a single-channel eight-bit digital telemetric unit and are transmitted to the ground by an FM transmitter operating in the ordinary radiosonde frequency band of about 28 megahertz.

131
FOR OFFICIAL USE ONLY

CHAPTER 6. APPLICATION OF INFRARED DEVICES DEVELOPED FOR USE IN OUTER SPACE TO INVESTIGATE NATURAL RESOURCES, IN GEOLOGY AND FOR FOREST FIRE DETECTION

6.1. Use of Pattern Recognition Methods as Applied to Multichannel Infrared Systems Developed for Use in Outer Space

In pattern recognition theory, the term "object" is a component part of the broader term "pattern," including such terms as "phenomenon" and "situation." Farm crops and forest fires, thermal maps of the terrain and weather forecasting, space objects and marine currents, volcanic eruptions and outcrops of geological rocks, and so on can constitute patterns [6.1]. In recent years infrared recognition devices have come to be used in space engineering which utilize spectral brightness, radiance (of the objects of recognition in the various spectral ranges are used as attributes. Hereafter, we shall stipulate that the term "attribute" means any characteristic of an object subject to quantitative description [6.2].

Inasmuch as in the final analysis an attribute is a defined number, it is possible to apply mathematical methods to the analysis of attributes and recognition of objects. In the general case it is possible to use N attributes for the recognition of objects. Then the object can be represented by a geometric point in an N-dimensional space of attributes. The objects (patterns) having similar attributes are combined into classes. It is possible to recognize an object by comparing its attributes with the attributes of several standards of the classes and classifying the object in one class or another on the basis of this comparison. The classes do not actually exist in the sense of the objects making them up. In the world of things, for example, there is no "satellite in general" as a special object, but there are only individual satellites which have common attributes by which they can be combined into a class. Usually the number of classes subject to recognition makes up a finite set which is called the "alphabet of classes." When using statistical recognition techniques, every class is assumed to be characterized by a differential distribution law of attributes.

In the graphical representation of classes, the differential laws are bounded by a line equal to the probability density which for the normal law in a two-dimensional space, is an ellipse. The boundary probability density is selected from the condition that a defined, usually previously given

132

percentage of all possible random combinations of primary attributes charac-
terizing a given class will fall inside the ellipse of the given class.
Thus, for example, in the two-dimensional space of primary attributes, the
probability of falling in the ellipse, the half-axis ratio of which to the
principal probable deviations is equal to k is defined by the formula [6.3]

$$P((x_1, x_2) \subset A) = 1 - \exp[-(k\rho)^2], \qquad (6.1)$$

where $\rho = 0.477$; A is the class of the object. The probabilities that a random
point will fall in ellipses with different values of k for the two dimensional
space are presented in Table 6.1

Table 6.1.

k	1	$\bar{2}$	3	4	5
$P((x_1, x_2) \subset A)$	0,203	0,598	0,871	· 0,974	0,995

k	6	7	8	9	10
$1 - P(x_1, x_2)$	$2,77 \cdot 10^{-4}$	$1,44 \cdot 10^{-5}$	$4,7 \cdot 10^{-7}$	$9,9 \cdot 10^{-9}$	$1,3 \cdot 10^{-11}$.

Values are presented in this table for the probability that a random point
will go beyond the limits of the ellipse at k > 5. It is obvious that for
k = 5 in practice all of the random points of the given class fall inside
the ellipse. With an increase in the dimensions of the half-axis of the
ellipse to k = 10 the probability that a random point of the given class
will go beyond the boundary of the ellipse becomes negligibly small. From
Table 6.1 it is obvious that even a small increase in the dimensions of the
half-axes of the ellipse will lead to a sharp decrease in the probability
that a random point of the given class will go beyond its limits.

When using three attributes simultaneously for pattern recognition, a three-
dimensional space is formed. For a normal distribution law the random
points belonging to the given class are grouped into a spatial configuration
--an ellipsoid, the probability of incidence within which is determined by
the known relation

$$P((x_1, x_2, x_3) \subset A) =$$
$$= \hat{\Phi}(k) - (2k\rho/\sqrt{\pi}) \exp[-(k\rho)^2], \qquad (6.2)$$

where $\hat{\Phi}$ (k) is the reduced Laplace function. Table 6.2 gives the probabilities
that a random point of the given class will fall inside an ellipsoid of
equal probability density, the half-axes of which are equal to k principal
probable deviations for comparison with the two-dimensional case.

FOR OFFICIAL USE ONLY

Table 6.2.

Probability	k				
	1	2	3	4	5
$P(x_1, x_2, x_3)$	0.0715	0.389	0.828	±0.937	0.989

If the boundaries of the classes of objects do not intersect in the attri-
bute space, then any point appearing in the space of the primary attributes
can in practice reliably be classified in one of the classes. If the classes
forming the alphabet intersect, then the point presented for recognition
can simultaneously fall into the regions of several classes. In this case
recognition can be accomplished, for example, by the probability method.
It is obvious that recognition must be accomplished considering some criterion
which is used as the basis for this process and ensures the required re-
cognition reliability. In a number of cases the recognition criterion is
identified with the so-called separating function, the problem of which in-
cludes the classification of the presented point in one of the classes of the
alphabet to which it is similar. In the final analysis, the boundary is
drawn in the attribute space which optimally (from the point of view of the
selective criterion) separates all of the points of the given space into the
classes.

Let two classes A_1 and A_2 exist in the attribute space, the random points of
which are distributed according to a normal law. The a priori probability
of the appearance of both classes and their value are identical. It is
necessary to draw the optimal decision boundary between them. The most
general form of writing then normal distribution law in a plane has the
form

$$f(x_1, x_2) = (2\pi\sigma_{x_1}\sigma_{x_2}\sqrt{1-r^2})^{-1} \times$$

$$\times \exp\left\{-\frac{1}{2(1-r^2)}\left[\frac{(x_1-\bar{x}_1)^2}{\sigma^2_{x_1}} + \right.\right.$$

$$\left.\left. +\frac{(x_2-\bar{x}_2)^2}{\sigma^2_{x_2}} - \frac{2r(x_1-\bar{x}_1)(x_2-\bar{x}_2)}{\sigma_{x_1}\sigma_{x_2}}\right]\right\}.$$

The distribution depends on five parameters: $\bar{x}_1$, $\bar{x}_2$, σ_{x_1}, σ_{x_2}, r, which,
as is known, are the mathematical expectations of the values of x1 and x2,
their mean square deviations, and the correlation coefficient.

Let the random points in the plane of two attributes X_1, X_2 be classified
in the classes A_1 or A_2 by comparing the probability densities. If an
inequality of the type $f_{A_1}(x_1, x_2) > f_{A_2}(x_1, x_2)$ is observed for a specific
point of the coordinate plane, then the point belongs to the class A_1. Other-
wise the point belongs to the class A_2. It is obvious that in this case
the equation of the optimal decision boundary separating the two classes
A_1 and A_2 can be obtained from the equation of the normal law in a plane
under the contiion $f_{A_1}(x_1, x_2) = f_{A_2}(x_1, x_2)$.

134
FOR OFFICIAL USE ONLY

It is easy to show that in the given case the optimal decision boundary
equation can be represented in a plane in the form of the second-order line
equation:

$$AX^2_1 + BX^2_2 + CX_1X_2 + DX_1 + EX_2 + F = 0 \qquad (6.3)$$

where A, B, C, D, E, and F are constant coefficients defined by the formulas:

$$A = \frac{1}{2\,[1-r^2(A_2)]\,\sigma^2_1\,(A_2)} - \frac{1}{2\,[1-r^2(A_1)]\,\sigma^2_1\,(A_1)};$$

$$B = \frac{1}{2\,[1-r^2(A_2)]\,\sigma^2_2\,(A_2)} - \frac{1}{2\,[1-r^2(A_1)]\,\sigma^2_2\,(A_1)};$$

$$C = \frac{r(A_1)}{[1-r^2(A_1)]\,\sigma_1(A_1)\,\sigma_2(A_1)} - \frac{r(A_2)}{[1-r^2(A_2)]\,\sigma_1(A_2)\,\sigma_2(A_2)};$$

$$D = \frac{\overline{X}_1(A_1)}{[1-r^2(A_1)]\,\sigma^2_1(A_1)} - \frac{r(A_1)\,\overline{X}_2(A_1)}{\sigma_1(A_1)\,\sigma_2(A_1)\,[1-r^2(A_1)]} -$$
$$- \frac{\overline{X}_1(A_2)}{\sigma^2_1(A_2)\,[1-r^2(A_2)]} + \frac{r(A_2)\,\overline{X}_2(A_2)}{\sigma_1(A_2)\,\sigma_2(A_2)\,[1-r^2(A_2)]};$$

$$E = \frac{\overline{X}_2(A_1)}{\sigma^2_2(A_1)\,[1-r^2(A_1)]} - \frac{r(A_1)\,\overline{X}_1(A_1)}{\sigma_1(A_1)\,\sigma_2(A_1)\,[1-r^2(A_1)]} -$$
$$- \frac{\overline{X}_2(A_2)}{\sigma^2_2(A_2)\,[1-r^2(A_2)]} + \frac{r(A_2)\,\overline{X}_1(A_2)}{\sigma_1(A_2)\,\sigma_2(A_2)\,[1-r^2(A_2)]};$$

$$F = \frac{r(A_1)\,\overline{X}_1(A_1)\,\overline{X}_2(A_1)}{\sigma_1(A_1)\,\sigma_2(A_1)\,[1-r^2(A_1)]} - \frac{r(A_2)\,\overline{X}_1(A_2)\,\overline{X}_2(A_2)}{\sigma_1(A_2)\,\sigma_2(A_2)\,[1-r^2(A_2)]} -$$
$$- \frac{\overline{X}^2_1(A_1)}{2\sigma^2_1(A_1)\,[1-r^2(A_1)]} + \frac{\overline{X}^2_1(A_2)}{2\sigma^2_1(A_2)\,[1-r^2(A_2)]} -$$
$$- \frac{\overline{X}^2_2(A_1)}{2\sigma^2_2(A_1)\,[1-r^2(A_1)]} + \frac{\overline{X}^2_2(A_2)}{2\sigma^2_2(A_2)\,[1-r^2(A_2)]} +$$
$$+ \ln\left(\frac{C_1}{2\pi\sigma_1(A_1)\,\sigma_2(A_1)\,\sqrt{1-r^2(A_1)}}\right) -$$
$$- \ln\left(\frac{C_2}{2\pi\sigma_1(A_2)\,\sigma_2(A_2)\,\sqrt{1-r^2(A_2)}}\right),$$

where r_{A_j}, σ_{x_i,A_j}, $\overline{x}_{i,A_j}$ are the corresponding numerical characteristics of the
primary attributes of one of the classes. From analytical geometry it is
known that the equation (6.3) defines the second-order curves in general
form in a plane: a circle, ellipse, parabola, and hyperbola. The form of
each specific curve depends on the ratio of the numerical characteristics
of the distribution laws of each of the classes subject to recognition.
In particular, the decision boundary can be a straight line in a plane.
This decision rule is the most convenient for practical realization. Figure
6.1 shows the decision boundaries optimally separating the class F from the
classes A_1, A_2, A_3 and A_4 under the condition that the point belongs to
class A or F according to rule (6.3), which corresponds to making the deci-
sion by the criterion of the minimum average risk. The distribution laws
are normal. The solid ellipses were constructed for all classes with iden-
tical two-dimensional distribution probability densities equal to

FOR OFFICIAL USE ONLY

$$f(x_1, x_2) = 10^{-i}.$$

The optimal decision boundaries are plotted by dashed lines and are denoted
for each pair of separating classes

$$R(A_1, F), R(A_2, F), \ldots, R(A_i, F).$$

For clarity, the values of the decimal logarithm of the two-dimensional
distribution density are plotted on the optimal decision boundaries:
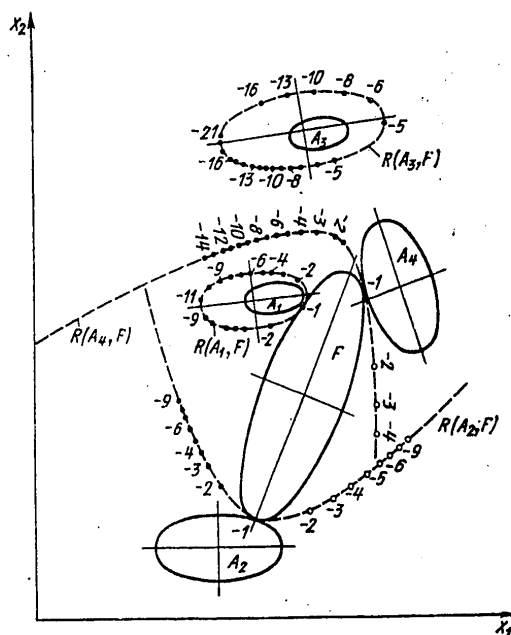
$$n = \lg 10^n = \lg f(x_1, x_2).$$

Figure 6.1. Decision boundaries $R(A_i, F)$ which separate the classes
A_1, A_2, A_3, A_4 from the class F in the space of the
primary attributes x_1, x_2. The boundary probability
density for all classes is assumed equal to $\lg f(x_1, x_2)$.

FOR OFFICIAL USE ONLY
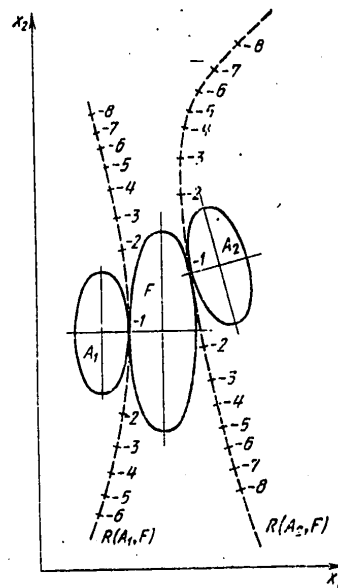
Figure 6.2. Optimal open decision boundaries for near values
of the mean square deviations for different classes.

The decision boundaries pass through the points of equal probability densities
of the two classes A_j and F. From the figure it is obvious that for classes
the mean square deviations of which differ by two or three times, open
optimal boundaries are characteristic: parabolas or hyperbolas R (A_2, F)
and R (A_4, F). For the classes the mean square deviations of which differ
by four or more times, closed decision boundaries are characteristic:
circles and ellipses R (A_1, F), R (A_3, F). The direction of the principal
axes of the optimal decision boundaries does not coincide with the direction
of the principle axes of the separated classes.

In certain places near the points of tangency of the ellipses R (A_1, F),
R (A_2, F) the optimal decision boundaries are close to straight lines
(see Figure 6.2). This approximation is more exact, the smaller the angle
between the principal axes of the contact ellipses and the closer the
values of their mean square deviations. Here the optimal decision boundaries
can exist considering replacement by straight lines of the simplest from
the point of view of practical realization.

A characteristic feature of infrared devices made for use in outer space
designed for the detection of geological resources, forest fires, the
investigation of the flora of the planet and other ground objects consists
in remote use of them. For infrared recognition devices made for use from
space, the primary attributes can only be the characteristics of the

137

FOR OFFICIAL USE ONLY

FOR OFFICIAL USE ONLY

electromagnetic field of the object. These include the field intensity, the degree of polarization of the emission, the spectral composition, the direction of propagation and variation of these characteristics in time. The majority of modern infrared devices for use from outer space are scanning systems. A given segment of the terrain is examined in a narrow instantaneous zone viewing angle. The primary attribute in any infrared space system is the magnitude of the average (with respect to the instantaneous field of view) effective energy brightness of the radiation sources which are located outside the field of view at a given point in time:

$$x_i(t) = \frac{1}{\omega} \int\limits_{(\Delta\lambda_i)} \int\limits_{(\omega)} b_\lambda(\omega)\,\varphi_\lambda(\omega)\,\tau_{i\lambda}(\omega)\,d\lambda\,d\omega, \qquad (6.4)$$

where $x_i(t)$ is the average effective brightness of the radiation sources with respect to the instantaneous field of view of the instrument, watts-cm^{-2}·steradians^{-1}; $b_\lambda(\omega)$ is the spectral energy brightness of an arbitrary point inside the instantaneous field of view of the system, watts-cm^{-1}-micron^{-1}-steradian^{-1}; $\phi_\lambda(\omega)$ is the spectral sensitivity of the infrared radiation receiver, relative units; $\tau_{i\lambda}(\omega)$ is the spectral transmission coefficient of the infrared optical system of the device in the ith spectral range, relative units; λ is the wavelength, microns; ω is the solid instantaneous angle of the field of view of the instrument, steradians.

The processing of the primary attributes of the objects permits us to establish the secondary attributes: the shape of the objects, their mutual range, the interrelation, and variation in time. The secondary attributes of the objects are also widely used for recognition. In the infrared recognition system for use from outer space, there can be several receptors operating simultaneously. Then it is considered to be a multichannel device. The spectral range in each channel is separated by means of optical filters, diffraction gratings or prism systems so that in the space of the primary attributes that is formed, optimal recognition of a given alphabet of classes will be ensured. The general principles of the construction of recognition systems discussed above can be applied fully to the multichannel infrared recognition systems. The primary goal of the receptors of the infrared devices to be used from outer space consist in measuring the values of the primary attributes with given accuracy, speed, resolution and conversion of them to electric signals which are also used to solve recognition problems. The relation between the primary attributes and the electric signals at the output of the radiation receiver is described by the expression

$$U_i(t) = k_i X_i(t) S_0 \omega + U_{noise}(t), \qquad (6.5)$$

where k_1 is the proportionality coefficient between the effective radiant flux, reaching the radiation receiver and the useful signal at the output of the radiation receiver; in general form this coefficient can depend on the magnitude of the radiant flux when making the transition from the space of the primary attributes to the space of the signals nonlinear transformations can be observed; S_0 is the area of the entrance pupil of the objective of the infrared system; $U_{noise}(t)$ is the signal caused by the internal noise of the radiant energy receiver and the amplifier.

138

FOR OFFICIAL USE ONLY

FOR OFFICIAL USE ONLY

It is obvious that the expression for the signal which is processed by the decision-making system includes two components: the useful component caused by the measured primary attribute and the component which distorts the investigated picture caused by the internal noise of the receiver and the amplifiers. An effort is made to reduce the second component to a minimum by the corresponding projection and manufacture of the amplifying systems. In order to reduce their relative contribution to the distortion of the observed picture on making the transition from the space of the primary attributes to the space of the signals, either the sensitivity of the radiation receiver or the area of the objective or the magnitude of the instantaneous solid viewing angle of the system is increased. From equation (6.5) it follows that as a result of increasing one of the parameters k_1, S_o, ω (or several simultaneously) the former can be increased so much that the latter can be neglected. If for any reason this increase in the indicated system parameters turns out to be impossible, then the separation of classes in the space of the signals is carried out considering the distortion of the boundaries of the classes by the internal noise of the amplifying and receiving channel of the instrument. Here, as a rule, the reliability of the recognition of the classes is reduced.

In spite of the variety of modern infrared systems for use from outer space both with respect to purpose and with respect to structural design, it is possible, nevertheless, to represent the structural diagram of the recognition system in the most general form (see Figure 6.3). On exiting from the receiving device, the electric signals go to a comparison circuit where the value of the presented realization is automatically compared at each point in time with the description of all classes--standards. The comparison circuit outputs quantitative indexes which characterize the closeness of the presented realization to all of the classes--standards. The realization, that is, the point in space of the signals is shifted continuously as a result of scanning in the general case. At each subsequent point in time, its closeness to one standard class or another is different. The comparison circuit must continuously provide for quantitative estimation of all of the information coming from the receiving module. The description of the standard classes is stored in the memory module. A comparison of the probability characteristics found with respect to the given criterion and classification of the object in one of the classes are accomplished in the decision-making device. In addition to the primary attributes, the recognition systems can include modules which use the secondary attributes of the objects for decision making such as the angular coordinates and their derivatives, the distance to the object and other parameters. In this case the recognition system can contain goniometric and range finding units.
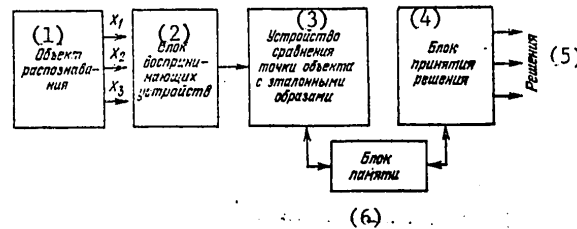
139

FOR OFFICIAL USE ONLY

Figure 6.3. Structural diagram of the infrared recognition
system.

Key: 1. Object of recognition   4. Decision making module
2. Receiving module   5. Decisions
3. Device for comparing   6. Memory module
the point of the
object with the
standard patterns

6.2. Geological Resource Exploration and Investigation Using Infrared
Systems in Space

The remote study of geological resources using the infrared systems made
for use from outer space is based on the fact that various natural formations
have different spectral reflection curves both in the visible and in the
infrared ranges of the spectrum. This difference will permit the detection
and recognition of natural resources with respect to the reflected solar
or natural thermal radiation. The spectral characteristics of the radiation
of the same natural formation, for example, a forest, fields, soil, and so
on, do not remain constant in time. In a number of cases they depend
highly significantly on the seasonal conditions, the relative position of
the sun and the observation instrument, the soil moisture and many other
causes. Therefore such specific natural formations as, for example, a
"green meadow," can be represented in the primary attribute space not as a
single point, but as a set of points grouped in some region.

This situation can be clearly illustrated in the example of analyzing the
spectral brightness coefficients for numerous natural background formations
presented in [6.4]. By the brightness coefficient we mean the value of

$$r = B_\Phi / B$$

where B_Φ is the true brightness of the natural background formation under
defined conditions of illumination and observation; B is the brightness of
an absolutely white plate reflecting the radiant flux according to Lambert's
Law under the same illumination conditions. As the primary attributes in
Figure 6.4, the spectral brightness coefficients are selected on the wave-
lengths of 0.56 microns, which corresponds to the characteristic reflection
band of vegetation explained by the presence of chlorophyll and 0.8 microns
where the Wood effect is sufficiently well manifested for a number of back-
ground formations.

It is obvious that the background formations of the investigated classes are grouped into clearly expressed regions: "soil," "vegetation," "sand," "snow," "water." For defined values of the attributes, the "soil," "water," "vegetation," and "sand" classes partially intersect each other, as a result of which for given values of the primary attributes the solution of the problem of whether a random point belongs to one of the enumerated classes is not entirely defined. In order to draw the optimal decision boundary in intersecting sections of these classes, statistical methods discussed previously in this chapter can be used. In Figure 6.4 each point which enters into one class or another is numbered. These numbers correspond to the following natural formations: 1--bark of a birch tree, 2--spruce, 3--juniper, 4--alder, 5-8--aspen in various seasons, 9-10--saxaul, 11-13--pine in different seasons, 14--weeds, 15-16--alpine meadow, 17--pasture in the chernozem region, 18-20--meadow with profusely flowering crowfoot, 21-26--dry valley meadow with sun height of 25 degrees, 27-30--grass, 31-37--barhan [sand dune] sand without shadows, 38-50--barhan sand with shadows across the crests, 51-59--wet sandy loam, 60--grey soil, 61--leached chernozem soil, 62-65--chernozem, 66--wet clayey loam, 67,78--cobblestone roads, 69-70--water, 71--freshly fallen snow, 72-74--dry snow with frozen crust.

The mutual arrangement of the classes presented in the figure is characteristic only for the given combination of primary attributes. On variation of the spectral bands, which can be achieved, for example, by replacement of the optical filters in each of the channels of the infrared system, the mutual arrangement of the classes changes. The distance between some of them increases, as a result of which their recognition becomes more reliable, and between others, on the contrary, it decreases. Consequently, the problem of selecting the optimal combination of primary attributes is closely connected with the specific problem of recognition of a defined alphabet of classes. Each alphabet of classes can have its own optimal combination of primary attributes. This is well illustrated by the following example. In [6.5, 6.6] data are presented on the reflectivity of clouds, snow covers and inversion trails of jet aircraft lit by the sun in the infrared range of the spectrum. In Figure 6.5, the position of the random points of some objects are plotted according to data of [6.5, 6.6] in the x_1, x_2 coordinate system representing the spectral background radiances on wavelengths of 1.7 and 2.1 microns (milliwatts-cm^{-2}-microns^{-1}).
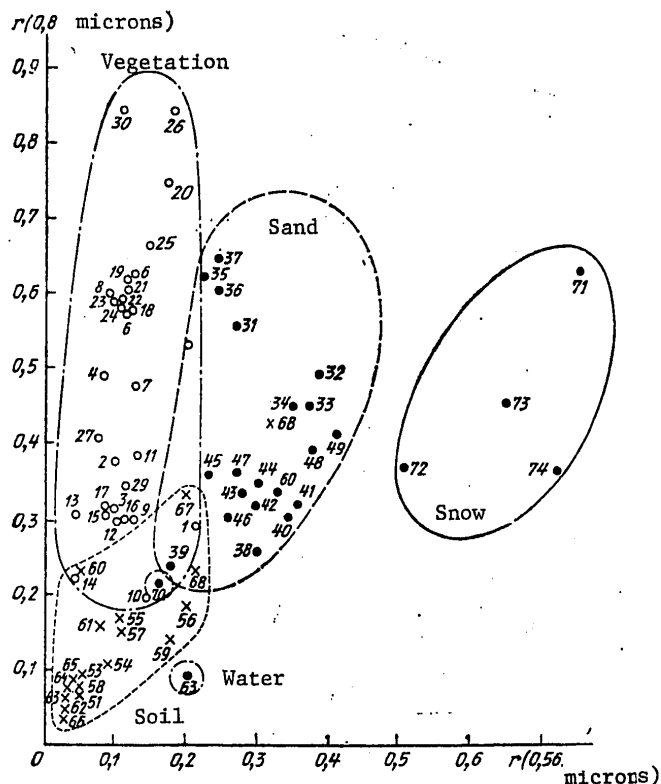
FOR OFFICIAL USE ONLY

Figure 6.4. Arrangement of the spectral brightness coefficients of random points of various natural formations in two-dimensional space.
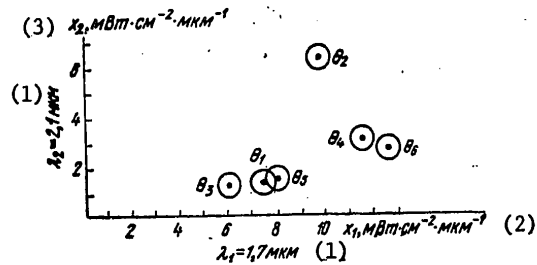
142

Figure 6.5. Position of the points of various objects in a two-dimensional space of primary attributes x_1 91.7 microns), x (2.1 microns): θ_1--cirrus (H = 11.89 km); θ_2--stratiformis (water); θ_3--cirrus; θ_4--cirrostratus (H = 7.62 km); θ_5--snow on the surface of the earth; θ_6--inversion trail of a jet aircraft. All of the measurements were taken in the daytime from an aircraft at an altitude of 13.1 km.

Key: 1. Microns
2. x_1, milliwatts-cm^{-2}-micron^{-1}
3. x_2, milliwatts-cm^{-2}-micron^{-1}
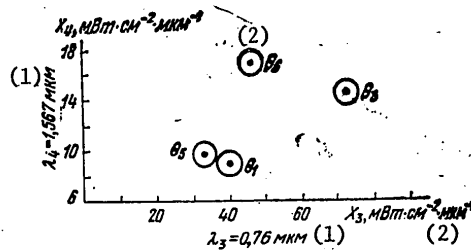
Figure 6.6. Measurement of the position of random points of objects with different classes on variation of the primary attributes (λ_4 = 567 microns, λ_3 = 0.76 microns.

Key: 1. Micron
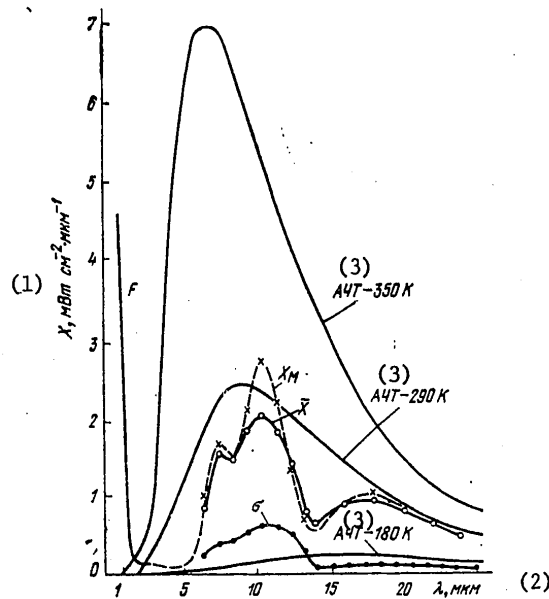2. Milliwatts-cm^{-2}-micron^{-1}.

143

Figure 6.7. Spectral distribution of the radiance (the
energy brightness) of terrestrial backgrounds
and an absolute black body with a temperature of
180, 290, and 350° K: the $\bar{x}$ curve corresponds to
the mathematical expectation of the spectral
radiance of the background; x_M corresponds to
the mode; σ corresponds to the mean square
deviation.

Key: 1. X, milliwatts-cm^{-2}-micron^{-1}
     2. λ, microns
     3. Absolutely black body

144

FOR OFFICIAL USE ONLY

With this combination of primary attributes the distance between the points of different objects is entirely defined, which offers the possibility of stating the problem of the recognition of these classes of objects with specific probability. The position of the points of different objects in the coordinate plane of the primary attributes changes significantly if the primary attributes change--the spectral ranges in which the reception of the radiant energy takes place. In Figure 6.6 (in contrast to Figure 6.5), the spectral radiances on a wavelength of 0.76 microns (x_3) corresponding to the oxygen absorption band, and 1.567 microns (x_4) corresponding to the window of transparency of atmospheric gases are selected as the primary attributes. The designations of the points on the figures by classes of objects are identical. The fact that the points θ_3 and θ_6 have changed their relative position along the x-axis by comparison with their position in Figure 6.5 attracts attention; the points θ_1 and θ_6 have changed their relative position both with respect to the x-axis and with respect to the y-axis. The spacing between these points has increased noticeably. Thus, the spacing between θ_1 and θ_5 and the x_1, x_2 coordinate systems equal to 0.5 milliwatts-cm^{-2}·microns^{-1}, and in the x_3, x_4 coordinate system, 6.7 milliwatts-cm^{-2}-micron^{-1}, that is, 13.4 times more. Thus, proper selection of the attributes plays the primary role in the recognition of objects by multichannel infrared systems. Thus, for recognition of certain classes forming the alphabet, one combination of primary attributes can be favorable, and for the recognition of other classes, another combination. The use of multichannel systems instead of two-channel systems and the transition from the two-dimensional space of primary attributes to the multidimensional space will in a number of cases permit the distance between classes to be increased and, consequently, the probability of their proper recognition to be increased.

The recognition of various classes of objects using infrared multichannel systems can be carried out not only in the short wave part of the spectrum, but also in the long wave part of the spectrum. Figure 6.7 shows the spectral distribution of the radiance (energy brightness of the terrestrial backgrounds constructed by the data of [2.5, 6.5 and 6.62 and an absolutely black body with temperatures of 180, 290, and 350° K in the infrared range of 1-25 microns. It is obvious that at certain temperatures the spectral density curves of the radiation of an aboslutely black body and the ter-restrial backgrounds intersect. The mutual arrangement of the region of national background formations on the surface of the earth and an absolutely black body with different temperatures in two-dimensional space of the primary attributes is presented in Figure 6.8. Two pairs of spectral radiances, x_1, x_2 on wavelength of 12 and 15 microns respectively and x_1, x_3 on wavelength of 12 and 21 microns respectively were used as the primary attributes. In order to construct the region of natural background forma-tions, data were used on the correlation coefficients of the radiances of the background on different wavelengths presented in [2.5]. When construc-ting Figure 6.8, the correlation coefficients were taken equal to 0.47 for the combination of λ = 12 and 15 microns and 0.82 for the combination of λ = 12 and 21 microns respectively.
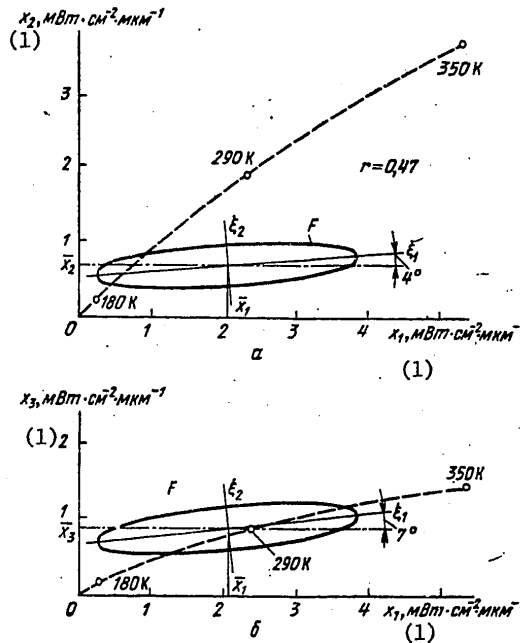
145
FOR OFFICIAL USE ONLY

Figure 6.8. Mutual arrangement of the region of terrestrial backgrounds and F and points corresponding to an absolutely black body with different temperatures (180, 290, 350° K), for two combinations of primary attributes: a) x_1--12 microns, x_2--15 microns; b) x_1--12 microns, x_3--21 microns.

Key: 1. x_2, milliwatts-cm^{-2}-$micron^{-1}$

For the known mean square deviations and correlation coefficients, the angles of inclination of the primary axis of the background region are determined by the known formula of mathematical statistics

$$\operatorname{tg} 2\gamma = 2r\sigma_{x_i}\sigma_{x_j}/(\sigma^2_{x_i} - \sigma^2_{x_j}),$$

and the mean square deviations with respect to the principal axes of the region of background formations, by the formulas

$$\sigma^2_{\xi_1} = \sigma^2_{x_1} \cos^2\gamma + \sigma_{x_2} \sin^2\gamma + r\sigma_{x_1}\sigma_{x_2} \sin 2\gamma;$$
$$\sigma^2_{\xi_2} = \sigma^2_{x_1} \sin^2\gamma + \sigma^2_{x_2} \cos^2\gamma - r\sigma_{x_1}\sigma_{x_2} \sin 2\gamma.$$

Considering Figure 6.8, let us draw the conclusion that in the long-wave part of the infrared spectrum, just as in the short-wave part, the variation

146

of combinations of primary attributes can noticeably change the relat.ve
position of the various objects in the space of the primary attributes.
Thus, in Figure 6.8, a the curve corresponding to the absolutely black
body with different temperatures intersects with the region of natural
background formations in a significantly smaller section than Figure 6.8, b.
The region of natural background formations in these figures is outlined
by the boundary at the level of three mean square deviations.

An important condition of using the multichannel infrared systems to in-
vestigate the geological resources and farm crops is simultaneousness of
obtaining the information from the same section of the terrain in all of the
spectral regions. After special computer processing the information is
output in the form of tables or charts in which very simple classifications
can be used such as green vegetation, soil, surface of water or more complex
classification, for example, areas where corn, soy beans, wheat, oats, or
alfalfa is grown and also data from geological surveys. At the present time
data are available on the spectral densities of the energy brightness of
real farm areas taken up by various plantings, although they are not so
numerous as the data on individual types of plants and types of soil. Refer-
ences [6.7, 6.8] include a quite complete bibliography of publications in
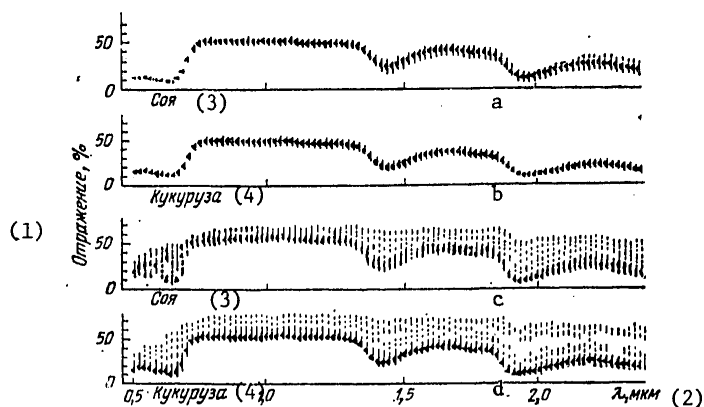this field.

Figure 6.9. Statistical composition of the results of
measuring reflection within the limits of
a hemisphere for the following: a) 108 soy
leaves; b) 184 corn leaves on 25-30 July 1966;
c) 97 corn leaves on 11-15 September 1966.

Key: 1. Reflection, %   4. Corn
2. λ, microns   5. Soy
3. Soy   6. Corn

147

Figure 6.9 shows the reflection spectra for normally developed fields of soy beans and corn. Each curve is a statistical composition of more than 100 discrete measurements. The significant absorption of chlorophyll on a wavelenght of 0.66 microns is obvious from the two upper curves. After a wavelength of 0.72 microns, an increase in the reflection coefficient to approximately 50 percent is observed. In the fall the spectral reflection coefficient of these fields changes as a result of loss of chlorophyll. The typical reflection curves for the visible and infrared radiation from the soil in the range of 0.5-2.6 microns are presented in Figure 6.10. The reflection curves for natural soil with undisturbed structure are similar to those depicted in 6.10, but, depending on the surface roughness, the values of the reflection coefficient can vary within broad limits [6.9].
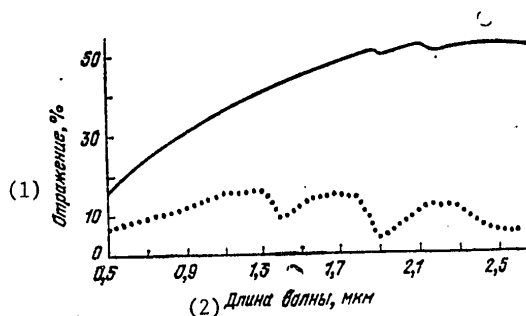

Figure 6.10. Results of measuring reflection within the limits
of a hemisphere using laboratory samples of soil:
_____sandy soil containing 5-12 percent moisture;
.....sandy soil containing 22-32 percent moisture.

Key: 1. Reflection, %   2. Wavelength, microns

Under actual conditions it is not the individual leaves of individual plants oriented in a defined way that fall into the instantaneous infrared field of view of the recognition device, but the set of these leaves both illuminated by the sun and in shadow and also the soil elements seen in the middles. The spectral energy brightness of such a section averaged over the instantaneous field of view of the instrument is of interest also for remote measurement. Figure 6.11 shows some results of similarly taken measurements of the spectral energy brightness of agricultural areas using the SG-4 high-speed scanning spectrometer built by the Perkin-Elmer Company. The gently sloping hump of the curves in the green part of the spectrum corresponding to the vegetation, the depression in the red region corresponding to the spectral density of energy brightness of chlorophyll and the high peak in the near infrared region play a significant role in many problems of recognizing farm crops. For each type of field different measurements will unavoidably be character-ized under the same conditions by statistical scattering caused by variation of the slope of the leaves, the number of plants inside the instantaneous

148

FOR OFFICIAL USE ONLY

field of view of the instrument, the specific value of the soil moisture
in each specific measurement, and so on, as a result of which groups of
points characterizing certain objects are formed in the space of the
primary attributes.

The investigated experimental diagrams pertain to the conditions of il-
luminating the plants by direct sun rays. In the case where the fields
are in the shadows of clouds (which can occur for a defined sun altitude
and in the presence of variable cloudiness as experiments showed) the
radiation spectrum changes mildly, which only leads to a portional decrease
in the vectors, and their direction remains in practice unchanged, which
is highly important for pattern recognition. It is proposed that the radiation
variation during the day caused by variation of the position of the sun
leads to an analogous effect. Thus, the parameters of the separating sur-
faces in the recognition technique can be corrected by a simple change in
scale. This is the first hypothesis within the limits of the working re-
flection region of 0.35-2.5 microns. Several families of spectral
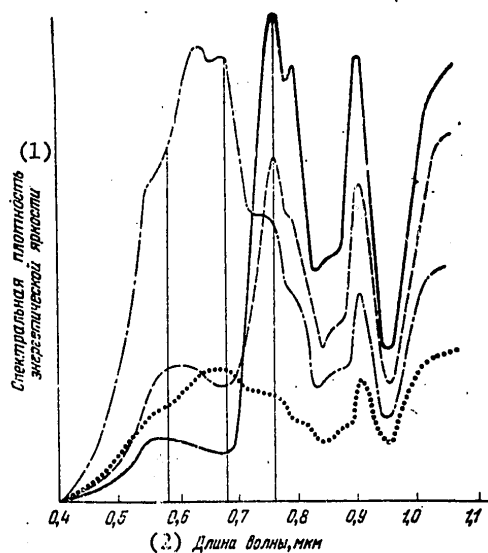radiation curves of different formations are presented in Figures 6.12-6.15.

Figure 6.11. Relative spectral densities of the energy brightness
(S) of different agrotechnical areas in the range of 0.4 to 1.05
micron; ———— green maturing soy beans; —————— mixture of brown
and green grass; -·-·-·- packed sandy road; .... powdery loam.

Key: (1) spectral density of energy brightness
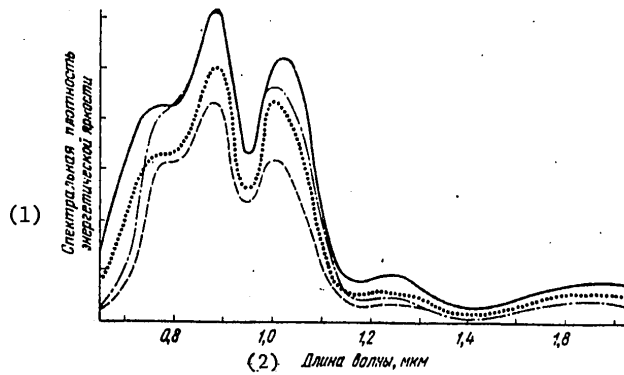   (2) wavelength, microns

149
FOR OFFICIAL USE ONLY

Figure 6.12. Relative spectral densities of the energy brightness (S) for four fields measured in range of 0.7 to 1.9 microns: _____ -- yellow mature wheat; ---- --corn; -.-.-.- --oats; ......--green maturing wheat. The data were obtained on 30 June 1966.

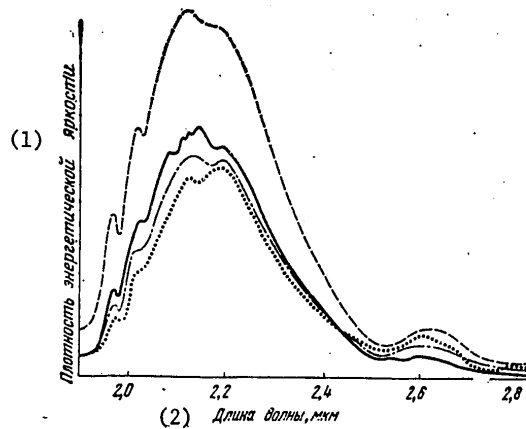Key: 1. Spectral density of brightness
     2. Wavelength, microns

Figure 6.13. Relative spectral densities of energy brightness (S): _____ wet soil; ------ green alfalfa; -.-.-.- yellow alfalfa; ...... wasteland severely overgrown with weeds. The data were obtained 11 August 1966.

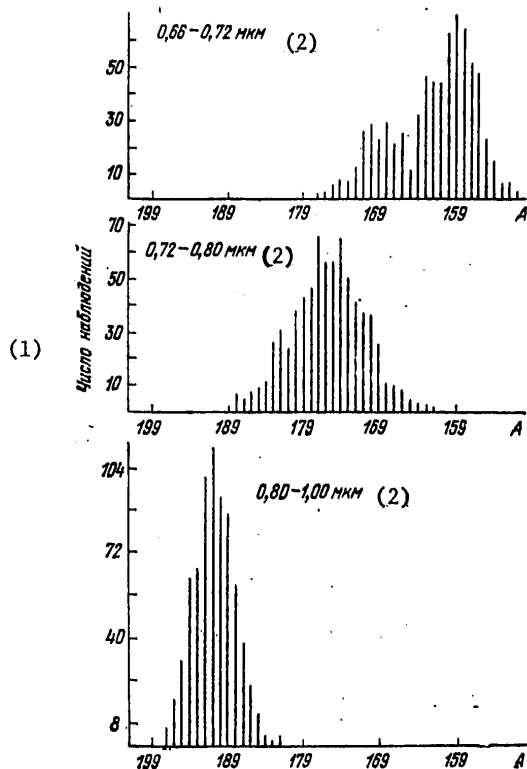Key: 1. Energy brightness density   2. Wavelength, microns

Figure 6.14. Standard histograms of the data obtained from
a soy bean field in three spectral bands as
a function of the signal amplitude in provisional
units (A).

Key: 1. Number of observations
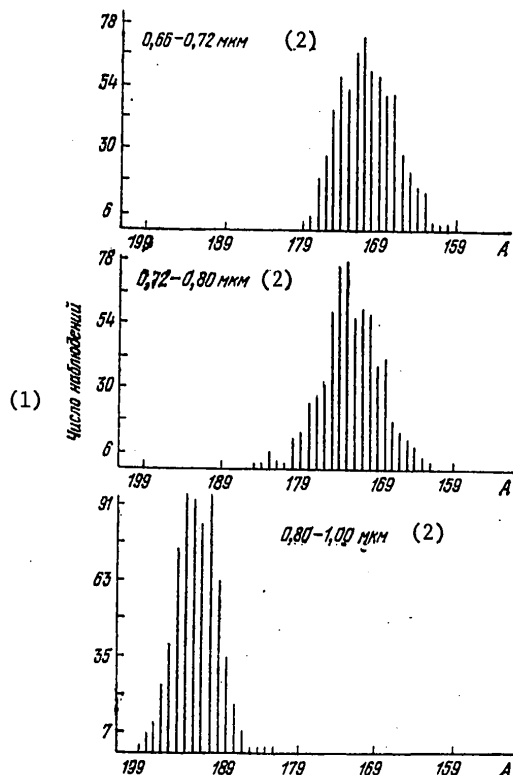2. Microns

FOR OFFICIAL USE ONLY

Figure 6.15. Standard histograms of data obtained from a
wheat field in three spectral bands as a function
of the signal amplitude in provisional units (A).

Key: 1. Number of observations
     2. Microns

When recognizing farm crops the calibration of the infrared equipment has
primary significance. Usually standard radiation sources are used for this
purpose which overlap the field of view of the system after defined time
intervals.

When using computers for pattern recognition the initial data on the radiation
value in each channel are subjected to preliminary statistical processing
[6.11], which can be illustrated in the example of a 12-channel system
operating in the following visible and infrared bands.

152

FOR OFFICIAL USE ONLY

FOR OFFICIAL USE ONLY

Band Number	Band, microns	Band number	Band, microns
1	0.40—0.44	7	0.55—0.58
2	0.44—0.46	8	0.58—0.62
3	0.46—0.48	9	0.62—0.66
4	0.48—0.50	10	0.66—0.72
5	0.50—0.52	11	0.72—0.88
6	0.52—0.55	12	0.80—1.00

The preliminary data processing consists in digitalization of the signals
in all 12 channels with respect to amplitude and   accumulation in the
corresponding memories. In order to estimate the statistical character-
istics of each class, objects from a training sequence were used the
classification of which was precisely known. For each class a uniform
histogram was constructed which was in the majority of cases unimodal. The
provisional (for each class) distribution functions were approximated by
multidimensional normal distribution functions. The vectors of the average
and covariation matrices for each class were estimated by selective mean
and covariation matrices which were determined by training sequences.

Figure 6.14 and 6.15 depict the standard histograms of three spectral bands
respectively for soy bean and wheat fields. Beginning with the proposition
of normalness of the distributions, the vector of the values of the at-
tribures X of each class has a multidimensional normal distribution, that
is,

$$P(X/\omega_i) = (2\pi)^{-N/2} |K_i|^{-1/2} \exp[-(X - M_i)^T \times$$
$$\times K_i^{-1}(X - M_i)], \quad i = 1, 2, \ldots, m,$$

where N - 12; M_i and K_i are the vectors of the average and the covariation
matrices of the ith class ω_i, respectively. As the criterion for selecting
the attributes for normally distributed classes the Kuhlbach divergence
was used [6.12]. In the presence of many classes, the criterion was used
which maximizes the miniumum of the pairwise divergences and expected
divergence. As applied to the problem of classification of farm crops it
is very difficult to determine the number of possible classes of the
patterns in advance. Some of the observed ground objects can be classified
in none of the previously defined classes (for example, roads, structures,
and so on). In this case the approach based on the formation of a special
"class of patterns" which includes the objects not belonging to any of the
previously selected classes is the most practical. This is done when the
magnitude of the discriminate function calculated for each object does not
exceed some threshold the magnitude of which depends on the criterion that
is used. The studies with respect to separation of fields into eight classes
(oats, soy beans, corn, alfalfa, red clover, rye, wheat and bare ground)
gave the following results (6.3).

Table 6.4

Class number	Class	Rejected with regard to threshold	Percentage correct classification	Number of objects classified in a class number							
				1	2	3	4	5	.6	7	8
1	Soy beans	131	95,7	6 860	126	0	35	10	1	7	1
2	Corn	12	91,4	126	2 535	0	24	0	73	5	0
3	Wheat	4	99,2	0	0	2 645	12	6	0	0	0
4	Oats	3	91,7	12	7	18	1 463	3	69	20	0
5	Rye	0	97,4	0	0	14	2	605	0	0	0
6	Red clover	14	91,0	21	26	3	23	0	2 120	0	0
7	Alfalfa	10	87,9	0	5	0	47	0	47	802	0
8	Bare ground	0	98,8	4	0	0	0	0	0	0	328

Two classes of wheat were combined into one in the table inasmuch as it was not required that they be separated in the given experiments. Thus, from the presented examples it is possible to draw the conclusion that the recognition of the fields of different crops is at least for defined times of year an entirely realizable goal.

Table 6.4

Channel	Spectral band, microns	Channel	Spectral band, microns
1	0,41—0,46	7	0,78—0,88
2	0,46—0,51	8	0,98—1,08
3	0,52—0,56	9	1,09—1,19
4	0,56—0,61	10	1,20—1,30
5	0,62—0,67	11	1,55—1,75
6	0,68—0,76	12	2,10—2,35
		13	10,20—12,50

For further improvement of the methods of remote recognition of farm crops in the field, additional studies are needed over broad areas during the entire growth period of the plants in order to discover what factors connected with agricultural practice and variability of the agricultural targets will significantly influence the radiation curves and, consequently, the recognition of the various classes.

Hopeful data on the possibility of remote recognition of a number of objects using an optical-electronic space unit have also been obtained from the skylab space station. The spectral bands of the MSS equipment on board the skylab are presented Table 6.4 [5.37].

The results of classifying objects of defined classes have demonstrated (see Table 6.5) that the color infrared photographs presented in digital form for the characteristics are found to be better everywhere than the digitalized black and white photographs taken in individual spectral bands. The four best channels for distinguishing the classes were selected in this experiment. The set of four channels was selected with respect to the largest value of the minimum transformed divergence for all possible combinations of pairs of elements of the image.

Table 6.5

№	(a) Класс	MSS станции (b) Skylab		MSS ERTS (c)	Цветные ИК снимки (d)	Черно-белые снимки (e)
		3, 7, 8, 11	3, 5, 6, 8			
1	Жилые массивы	97	81	97	91	84
2	Торгово-промышленные объекты	73	33	61	76	46
3	Районы горнодобывающей промышленности	51	59	61	32	34
4	Почва	87	78	83	67	78
5	Травяной покров	95	86	93	82	69
6	Рощи—лиственные леса	81	80	86	84	77
7	Хвойные леса	99	68	95	85	43
8	Реки	87	27	77	16	64
9	Озера	89	86	86	98	93
10	Общая характеристика	87	80	88	83	76
11	Среднее в классе	84	66	82	70	65

Key: a. Class
  b. MSS of the skylab
     station
  c. MSS ERTS
  d. Color infrared
     photographs
  e. Black and white
     photographs
  1. Populated areas
  2. Commercial-industrial
     sites
  3. Mining regions
  4. Soil
  5. Grass cover
  6. Woods--desiduous
     forests
  7. Coniferous forests
  8. Rivers
  9. Lakes
  10. General characteristics
  11. Average in the class

In Table 6.5, the general characteristics (item 10) means the ratio of the
number of all correctly classified elements of an image to the total number
of them in the control section of the terrain, and the term "average in the
class" means the arithmetic mean of the results of classifying all nine
classes. In the headings to Table 6.5 the channel numbers are presented
by means of which the indicated data are obtained. In the multispectral
scanner of the skylab station 256 equals 2^8 brightness quantization levels
were used. The performed experiments made it possible to draw the conclusion
that it is necessary to exercise great caution when giving preference to one
spectral band over another when describing the various classes of objects,
inasmuch as the choice of a solution regarding classification can be signi-
ficantly different depending on the magnitude of the noise in the channel
which depends on the structural design of the optical and electronic systems
of the scanner.

When processing the obtained data the results of reducing the effectiveness
of the multispectral devices as a result of the impossibility of exact

spatial matching of the photographs in all four spectral bands were discussed. When comparing the results pertaining to each individual class of objects, there is a case where the addition of one spectral channel in the middle infrared region greatly improves the classification characteristics, helping to distinguish rivers from commercial-industrial areas and heavy soil. If a channel belonging to the middle of the infrared spectrum is not used, then the distinguishing of such objects as rivers, commercial-industrial areas and heavy soils becomes much more difficult. When performing the investigation on skylab, in the opinion of the American specialists, optimal results of classifying the objects were not obtained. When analyzing each set of data and not using the same training patterns for all of the combined data, it is expected that better classification results will be obtained for some or even for all sets of multispectral data [5.37].

The described methods do not differ with respect to their theorectical basis when conducting a remote search for natural resources, for oceanological and glaciological studies, the study of the condition of the soil and the discovery of regions prospective for finding minerals, when analyzing soil moisture and river conditions, and so on. By using a multispectral device on board a satellite, it is possible more precisely to establish the time when the runoff of the water begins after the spring floods, which permits the yield of some farm crops to be increased by 25-50 percent without increasing the planted ground area. By increasing the accuracy of the prediction of how the seasonal changes take place in the water regime of the rivers, it is possible to increase the power of hydroelectric power plants without equipping them with additional generators.

The multichannel thermal infrared scanners operating in the 8-14 micron range have important significance for remote geological studies inasmuch as this region of the spectrum has minimum ratios of the radiation intensity of the rock material to the radiation intensity of a black body at the same temperature, that is, the minima of the so-called emittance which for polished surfaces coincides with the relative radiated power. At the minimum emittances the various spectral positions primarily depend on the mineral composition. Information about the composition which is based on interatomic vibrations cannot be obtained in others parts of the spectrum, for in this case the reflective properties of silicate rock will be explained by a physical phenomenon of another type, the intra-atomic electron transitions of the metal ions of the transition group.

The data obtained by a multichannel scanner [5.37] showed that the two-channel images obtained on the basis of the ratio of the radiation intensities in the range of 8.2-12.1 microns emphasize the variations in the emittance in open denudations of silicate rock with simultaneous elimination of the the temperature variations. The spectrometric studies on various aircraft and spacecraft also demonstrated that important information about the condition of the emitting surfaces can be obtained using remote infrared pickups and several channels. In the opinion of the American specialists, the

multichannel infrared scanning systems, for example, with 11 channels in the 8-14 micron range, will permit us to obtain images which can be used to determine the type of silicate rock. In remote geological studies the basic limiting factor is still the infrared pickups themselves. It is considered possible that on a transport spaceship an 11-channel spectrometer will be installed with spatial resolution of 100 meters. The application of the multichannel infrared scanner for geological mapping is the best illustration of the possibilities of remote studies during regional-scale mapping.

The main goal of the satellite equipment is not direct detection of the deposits deep in the earth which theoretically is impossible using infrared equipment, but discovery of the composition of the rock in the explored region, its tectonic structure, the presence of oil-producing rock and the nature of its occurrence. It is natural that the satellite method of exploring natural resources must be used in combination with well-developed ground methods.

The satellite infrared equipment can also be used in oceanological studies. Photosynthesis which takes place in the surface layer of the ocean is the key process of the marine ecologic system. The "health" of the ocean can be adequately established by the spectral composition of its emission. In the visible part of the spectrum the blue color of the ocean indicates the absence of chlorophyll and, consequently, the low nutrient value of the given part of the ocean for zooplankton. The greater part of the plants making up the plankton are diatomic algae; the zooplankton are predominately Copepoda. In the tropics over the course of an entire year the composition and quantity of plankton are approximately constant. In temperate lattidues, seasonal variations of the composition and quantity of plankton are observed. Rising in layers abundantly populated with phytoplankton, the Copepoda absorb an enormous quantity of food as a result of which the quantity of phytoplankton changes significantly during the day. For example, in the Black Sea at night the quantity of phytoplankton decreases on the average by two times, and in the daytime it recovers again. Phytoplankton is the basic food of the greater part of the animate population of bodies of water, including the most important commercial fish. In a region with abundant plankton mass accumulations of fish are observed migrating after them. Therefore the territorial accumulation of commercial fish by years and the quantity of them are subject to serious variations. Chlorophyll has a number of characteristic bands in the infrared region of the spectrum. The measurement of the spectral composition of the radiation of the ocean combined with the possibility of remote measurement of the ocean water temperature permits us to obtain important information for the fishing industry about the possible presence of commercial varieties of fish in a given part of the ocean at in practice any point in time--an operativeness unavailable through any other means.

The advantage of the satellite infrared equipment is fast surveying of large areas in the world ocean which is especially important in connection with variation in the chlorophyll concentration sometimes over the course of several days.

6.3. Satellites with Infrared Equipment for Investigating Geological Resources

On 21 July 1972 the specialized ERTS-1 satellite [Earth Resources Technology Satellite] designed for remote exploration of the earth's resources [6.22] was inserted into a circular near-polar orbit by a Delta rocket from the test grounds in the western United States on 21 July 1972. The altitude of the orbit was 920 km, and the mass was 820 kg. The primary goal of the launch was demonstration of the usefulness of multiple remote surveying of the earth's surface on a global scale. The goals established for the first satellite designed for exploration of geological resources reduced to the following: discovery of the composition of the natural and crop resources and also the environmental characteristics which can be best studied from on board a space vehicle with remote measurements; testing and demonstration of the procedures for gathering and processing data and also interpretation of the data as applied to agriculture, forestry, geography, geology, hydrology, oceanography and aerology; determination of what economic or social value multiple synoptic obervations have in many bands of the spectrum for commercial, scientific and governmental organizations.

Before the beginning of satellite studies, spectrozonal aerial photographic surveying in several spectral bands simultaneously was in second place after seismic methods in the study of mineral resources. For example, in Canada the combination of the method of aerial photographic surveying with electromagnetic and magnetic surveys and also the gravometric method made it possible to conduct fruitful studies of the raw material reserves and in particular, led to the discovery of large deposits of nickel and other metal ores. These methods also were the basis for the optical instruments used on board satellites to search for geological resources.

The basic instrument on board the ERTS-1 satellite was the multispectral scanner developed by Hughes Aircraft Company, which weighed 54 kg; it made simultaneous measurements of reflected solar radiation from the earth's surface in four spectral bands: 0.7-0.8; 0.8-1.1; 0.5-0.6; 0.6-0.7 microns. The instrument scans a strip on the ground 185 km wide [6.29]. The complete survey of the entire surface of the earth is realized with great overlap in 18 days. The satellite appears over various parts of the earth approximately at the same local time of about 0930 hours. This type of orbit is called heliosynchronous. The instrument scans mechanically. (A plane mirror 23x33 cm in size oriented at an angle of 45 degrees.) The radiant energy coming from the objective is transmitted through a fiber optical system to the radiant energy receivers. In the equipment a calibration tube is provided to provide for measuring the radiant energy in absolute units. The spectral bands are separated by optical filters installed in front the radiant energy receivers.

American specialists consider that every dollar invested in the ERTS-1 satellite brings in five dollars of net profit as a result of studies in the agricultural area alone. At the present time an inventory of areas and

crops is made in America on numerous small farms once every five years. The use of this type of satellite will make it possible to obtain such information annually and to trace the development of various farm crops in various seasons. Such crops as wheat, sugar beets or alfalfa, sago, beans, soy beans, potatoes, cotton, and so on should be identified from on board the ERTS-1 satellite. It is proposed that multispectral observation be used both to estimate the sizes of the areas and for early detection of diseased plants, determination of seasonal changes in their development, germination of crops and the general condition of one crop or another to predict its harvest not only in the United States but on a world scale.

Statistical studies of the cloud characteristics in a given region are of indirect value to agriculture in order to determine the illumination during various periods and the selection of the most appropriate crops for the fields in the given region. The use of the ERTS satellite will make it possible to analyze the possibility of studying structures and the productivity of forested regions. The ERTS satellite also has the following goals: the performance of studies in oceanology, geology, hydrology, and cartography, evaluation of the degree and nature of environmental pollution, the structure and dynamics of clouds and also the dynamics of the freezing of lakes in the central United States.

Plans have been made to investigate natural resources of the earth by the data obtained from the Skylab Orbital Station using the EREP equipment (Earth Resources Experiment Package) [6.24, 5.25] which includes the following: a six-spectral camera; a camera for photographing the earth's surface with a telescopic lens; an infrared spectrometer; a 13-channel multispectral scanning radiometer; a microwave radiometer-scatterometer with altimeter (K-band); and a passive microwave radiometer (L-band).

The data obtained with the help of the above-enumerated set of instruments can be used in the areas of ecology, geology, geography, meteorology and oceanography for compiling snow-cover maps, studying the nature of environmental pollution and determining the composition of the pollutants.

The Skylab space laboratory with the indicated equipment was put into orbit with a declination of 50 degrees and an altitude of 435 km with a crew ship of three people. The photographic film and magnetic sensors were returned to the earth [6.33]. The S-192 multispectral scanner used to investigate the earth's natural resources from on board the American Skylab orbital station was developed in accordance with the NASA specifications. The device contains a primary spherical mirror 61 cm in diameter, two scanning mirrors and a system of dispersing elements which splits the radiant flux, forming 12 spectral channels in the visible and near infrared band corresponding to reflected solar radiation, and one longer wave infrared channel corresponding to the natural radiation of the earth's surface. The photoreceiver module is made up of 13 cooled sensitive elements based on a ternary compound (mercury-cadmium-tellurium), the output signals of which are recorded on magnetic tape delivered to the ground when the Skylab crew

changed. The ground equipment which contains a computer converts the magnetic recordings to color photographs which are transmitted for analysis.

At orbital velocity of the station equal to 444 km/min and a transverse scanning speed of 6,000 rpm, information from approximately 30,000 km^3 of the earth's surface is recorded every minute of operation of the device. The data obtained are used to determine water and air pollution, to observe the maturing of farm crops and for geological research and many other purposes.

6.4. Detection of Forest Fires by Space Infrared Systems

The detection of forest fires and the control of them constitute an important national economic problem. The development of modern infrared equipment will permit us to detect forest fires from aircraft and spacecraft in the most initial stage of their occurrence. Infrared systems have been built and operated in a number of countries [6.16-6.19]. In the opinion of the American specialists, the economic gain from using space systems to monitor forest fires, for determining the harvest and losses, to study the migration of animals and for ecologic problems can result in an annual gain for the world on the whole in the amount of $11 \cdot 10^9$ dollars [6.17].

A forest is a global formation on the surface of the planet. The higher above it the observation point is located, the greater the area that can be inspected. Thus, from the orbital altitude of an artificial earth satellite of 250 km it is possible to inspect about 2 percent of the surface of our planet which corresponds to approximately $10^7 \cdot 10^6$ km^2. For comparison let us remember that the area of the Arctic Ocean is a little more than $13 \cdot 10^6$ km^2. Thus, for example, forest fires can be detected over an enormous territory from satellites. Unconditionally, not all of the planet's surface observed from a satellite is equivalent from the point of view of accuracy of determining the coordinates of the forest fire. A simple geometric analysis indicates that with an identical error in measuring the angular coordinates of the forest fire, the location of its center directly under the satellit, that is, in the nadir, is determined with appreciably greater accuracy than on the horizon. The linear error in locating the center of the forest fire on the earth's surface $\Delta \ell$ is connected with its position and error in determining the angular coordinates $\Delta \alpha$ by the expression

$$\Delta l = \left[(H + R_3) \frac{R_3 \cos \alpha}{\sqrt{R^2_3 - (H + R_3)^2 \sin^2 \alpha}} - R_3 \right] \Delta \alpha,$$

where H is the orbital altitude of the satellite, km; R_3 is the average radius of the earth equal to 6,371 km; α is the angular coordinate of the forest fire. Thus, with an error in measuring the angular coordinates of the forest fire equal to $1/4°$, its location directly under the satellite, that is, in the nadir, can be determined with a linear error on the order of 1 km,, and for the edge of the field of view at an angle of 70° to vertical, the linear error in determining the coordinates of the forest fire increased to 18 km. With a decrease in the orbital altitude of the

161

satellite under other equal conditions the accuracy in determining the coordinates increases.

The length of the scanning line from the satellite (from horizon to horizon) at an orbital altitude of 250 km on the earth's surface is about 3,500 km. The satellite makes one turn around the earth in approximately 1.5 hours. During this time a forest fire occurring at a lattitude of 55° is displaced as a result of the diurnal rotation of the earth from west to east by a distance of over 1,450 km. Consequently, a satellite circling the earth in a polar orbit will detect the same forest fire twice in a time interval of 1.5 hours. Then an approximately 12-hour break takes place (the forest fire is beyond the scanning area of the satellite during this time). Then the fire again is detected with an interval of 1.5 hours and again a 12-hour break comes. This is the cyclogram for the detection of a forest fire from one satellite in a polar orbit. During the day the coordinates and characteristics of the forest fire radiation can be measured four times independently of where it is located. It is impossible to achieve such operativeness by any other modern means.

The periodic measurement of the readition characteristics of a forest fire will permit determination of its scale, the phases of development and effectiveness of the measures to control the fire. Half of the forest fires arise from thunderstorms. In Yakutia this number reaches 70 percent [6.20]. Statistics indicate that the majority of forest fires can occur also from other "point " sources of fire--sparks from a steam engine, a campfire that has not been put out, matches, and so on. The area of a forest fire arising from a point source of fire grows with time a geometric progression and after several days can reach hundreds and thousands of hectares [6.19].

From the light engineering point of view such elemental phenomena as the forest fires are very powerful, complex sources of radiation, the exact calculation of the intensity of the spectral composition of which is a highly complex theoretical problem. In the majority of cases, in the initial stage forest fires are of a low nature--the dry grass, the forest litter made up of fallen leaves, branches, and twigs, small trees and brush burn first. The flame height in these cases reaches 2 to 3 meters with a width of the burning edge of 0.5 to 1.5 meters. The flame temperature fluctuates from 600 to 1200°C at the edge of the fire encompassing the burned out area with a temperature of 80-120°C around the perimeter. In a forest fire it is possible to isolate at least four radiating components having different spectral composition of the radiation: The incandescent solid surface of the burning wood, coal, flame and smoke. They all make their contribution to the total spectral composition of the radiation of the forest fire, but the contribution of each component is different. The incandescent surface of the burning wood (1400-1500°K) and coal having different temperature are sources with continuous energy distribtion of the radiation with respect to the spectrum, that is, by wavelengths. The flame of a forest fire is a highly complex source of emission having a band structure of the energy distribution by wavelengths. The energy emitted by the flame belongs

FOR OFFICIAL USE ONLY

primarily to wavelengths corresponding to the absorption bands of the materials contained in the flame. The products generated on burning wood (basically these are water vapor and carbon dioxide) have several characteristic absorption bands in the near infrared part of the spectrum with centers on wavelengths on the order of 1.3, 1.87, 2.7, 3.6 and 6.3 microns for H_2O and 2.7 and 4.3 microns for CO_2. The intensity of each spectral band varies as function of the flame temperature. In addition, inside the flame there are unburned particles which in addition to the band structure give off a continuous component of the radiation both in the visible and in the infrared regions of the spectrum. The total band composition of the emission of the flame is highly complex and varies continuously with time inasmuch as various parts of it are observed as a result of turbulence of the medium in the fire zone. Thus, a random band component of the flame radiation is superposed on the continuous component of the emission of the incandescent wood and charcoal. Finely, the last radiating component is the smoke (the remaining small particles suspended in the heated air). It is also an emitter with a continuous spectrum. The temperature of the smoke is appreciably above the flame temperature. Therefore the natural emission of this component is in the infrared part of the spectrum. Smoke scatters and absorbs the shorter wave emission of the flame, charcoal and burning wood. As a result of the presence of smoke, the intensity of the emission and spectral composition of the radiation of a forest fire vary randomly in time. Thus, the overall characteristics of the forest fire emission are complex random functions which vary with time and depend on a number of factors. The investigation of the characteristics of infrared radiation of a forest fire and its individual elements is the initial link in the process of creating equipment for remote detection of forest fires.

The results are presented in [6.27] from measuring the characteristics of the infrared emission of two models of a forest fire (burning moss and charcoal) obtained using a multichannel infrared unit. As the measuring equipment a four-channel spectroradiometer was sued. The investigated center of the forest fire was located at a distance of about 17 meters from the spectroradiometer. The radiation was focused using four objectives based on sensitive elements made of lead sulfide photoresistances. The radiant flux was chopped by a disc modulator with a frequency equal to the resonance frequency of the amplifiers. The signal from each channel was recorded on a separate loop oscillograph.

The characteristics of the spectral transparency of the filters and the spectral sensitivity of the photoresistances used in each channel are presented in Figure 6.16. By the experimental data obtained, some of the basic characteristics of the infrared emission of a forest fire are defined. These include the following: the maximum radiation density (energy emittance) in each of the investigated spectral bands, the mutual time relation (mutual correlation function) between the radiation intensity and the individual spectral bands, the correlation between the radiation in the different bands with respect to the set of investigated variables, the time characteristics of the development of the combustion process of an elementary section of the forest fire and so on.
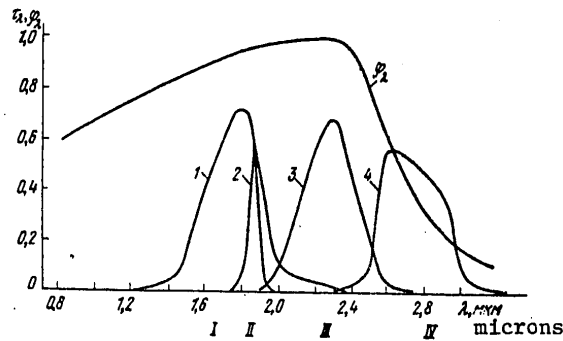
163
FOR OFFICIAL USE ONLY

Figure 6.16. Spectral transmission coefficients τ_λ of a four-channel spectroradiometer: ϕ_λ--spectral sensitivity of an uncooled lead sulfite photoresistance; 1-4--spectral transmission characteristics of optical filters

Table 6.6

Channel number	Correlation coefficients			
1	1,00	0,93	0,71	0,90
2	0,93	1,00	0,86	0,83
3	0,71	0,86	1,00	0,52
4	0,90	0,83	0,52	1,00

Figure 6.17 shows the time characteristics of the variation of the radiation density (energy emittance) of the center of the fire in the ignition and for powerful fire stages. The mathematical analysis of the characteristics of the infrared radiation of the forest fire model (burning moss) demonstrated that the nature of variation of the radiation in the various spectral bands of the forest fire model in time is identical in practice, which causes large values of the correlation coefficients presented in Table 6.6.

The normalized autocorrelations functions characterizing, as is known, the relation between the preceding and subsequent values of the brightness in the combustion process have quite long duration of the correlation, which indicates the small width of the spectrum of the process power (see Figure 6.18). The presence of low-frequency components in the variation of brightness of burning moss, which obviously is a characteristic feature of the variation in intensity of the infrared emission of a forest fire, attracts attention.
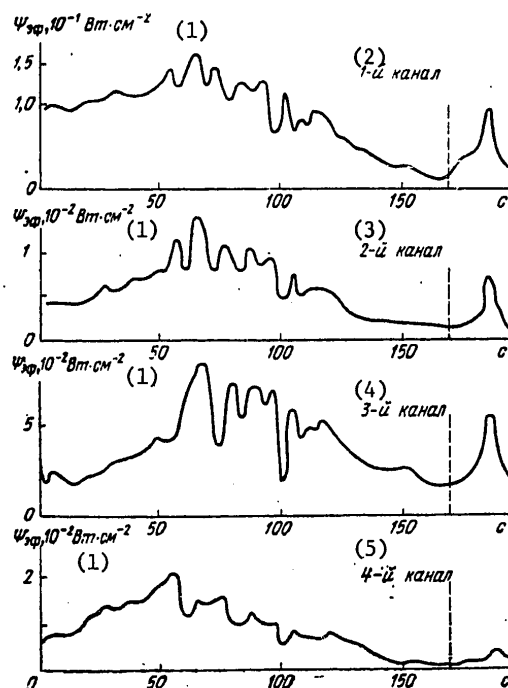
Figure 6.17. Variation of the radiation density (Ψ) of the center of a forest fire in time in the ignition and power fire phases.

Key: 1. Ψ_{ef}, 10^{-1} W-cm^{-2}
2. First channel
3. Second channel
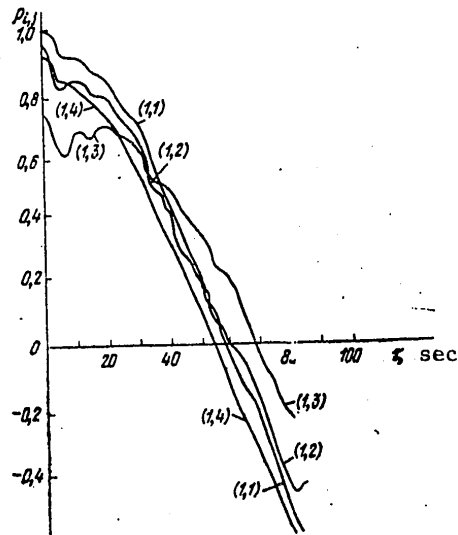4. Third channel
5. Fourth channel

Figure 6.18. Normalized mutual and autocorrelation functions of
the radiation intensity of a model of forest fires
(burning moss). The channel numbers are indicated
in parentheses.

The emission of a forest fire was picked up from artificial satellites by
infrared equipment only on the wavelength for which the entire body of the
earth's atmosphere was transparent. Figure 6.19 gives the graphs of the
spectral energy emittance of radiation sources with a temperature of 1500°K
(burning wood) and 700°K (charcoal) when observing then in the nadir from
a satellite. It is obvious that the forest fire emission received on the
satellite has a clearly expressed band composition. The radiation intensity
in each spectral band is different. Attention is attracted by the relation
between the power of the forest fire emission in the visible and infrared
bands of the spectrum. The visible part includes only an insignificant
proportion of the overall energy emitted by the forest fire. Figure 6.19
shows the part of the spectrum a with wavelength less 0.77 microns completely
blacked out. The remaining part b emitted by the forest fire is in the
invisible infrared part of the spectrum. The energy of the infrared part
of the spectrum exceeds by hundreds of times the energy emitted by forest
fire in the visible part of the spectrum. Thus, the incandescent surface
of the wood in the visible band of the spectrum emits a total of 0.1 percent,
and 99.9 percent is in the infrared part of the spectrum. The cooling coals
emit approximately 0.002 percent of the energy in the visible part of the
spectrum, and 99.98 percent in the infrared part, that is, in practice all
of the energy. The emission of the smoke is entirely in the infrared part
of the spectrum; therefore infrared equipment is used for detection of
forest fires from artificial satellites [6.17, 6.18, 6.22].
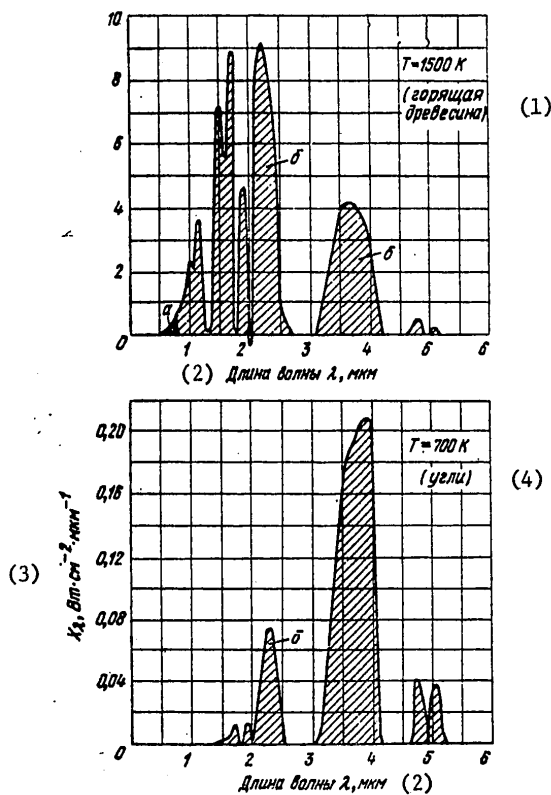
166

FOR OFFICIAL USE ONLY

Figure 6.19. Spectral distribution of the radiation energy
from an absolutely black body passing through the
entire thickness of the atmosphere vertically:
small black section (a)--energy in the visible
part of the spectrum; cross-hatched part (b)--
energy in the infrared part of the spectrum.

Key: 1. (Burning wood)
2. Wavelength, λ, microns
3. X_λ, W-cm^{-2}-micron^{-1}
4. Coals

167

FOR OFFICIAL USE ONLY

FOR OFFICIAL USE ONLY

Table 6.7.

(1)	(2)	(3)	(4)	(5)	(6)	(7)	(8)	(9)
Высота орбиты, км	Температура кромки пожара, °C	Температура внутри кольца, °C	Температура фона, °C	Ширина кромки, м	Линейное разрешение на земле, м	Пороговая чувствительность аппаратуры, Вт·см⁻¹× ×Гц⁻¹/²	Вероятность ложных тревог	Диаметр объектива, мм
200	600	80	40	2	400	10^{-9}	10^{-5}	300
200	1 200	120	10	2	400	10^{-9}	10^{-5}	300
200	1 200	120	10	1	400	10^{-12}	10^{-5}	300
400	600	80	40	2	800	10^{-9}	10^{-4}	300
400	600	80	40	1	800	10^{-12}	10^{-4}	300
400	1 200	120	10	1	800	10^{-12}	10^{-4}	300

Key: 1. Orbital altitude, km
2. Temperature of the edge of the fire, °C
3. Temperature inside the ring, °C
4. Background temperature, ° C
5. Width of edge, meters
6. Linear resolution on the ground, meters
7. Threshold sensitivity of the equipment, $W\text{-}cm^{-1}$ x $Hertz^{-1/2}$
8. False alarm probability
9. Lens diameter, mm

An evaluation of the noiseproofness of space-type infrared equipment designed for forest fire detection is presented in [6.19] for the simplest amplitude selection. Some results of these estimates are presented in Table 6.7.

During the calculations the degrees of blackness were assumed to be equal to the following: 0.3-0.4 for the edge of the forest fire; 0.9-0.95 inside the ring; 0.8 background. The outside diameter of the fire of 100 meters was considered constant. The safety margin was 4. The calculations showed that using infrared equipment with multielement radiant energy receivers with 30 areas for a threshold flux of 10^{-11} $W\text{-}cm^{-1}\text{-}Hertz^{-1/2}$ will permit us to ensure a high value of probability of proper detection of weak and intense forest fires from space altitudes.

In recent years the methods of controlling forest fires by artificially induced rain have been successfully used. The development of convective clouds is quite frequently observed over the taiga over the hot period of the year. During forest fires sometimes there are hundreds of thousands of tons of water hovering over the taiga which can be used to control the fire. Successful experiments have been conducted in extinguishing fires by artificially induced rain from cumulus clouds in the vicinity of the fire [6.20]. Artificial rain which begins approximately 11 minutes after the introductin of a special reagent into the cloud reaches a maximum after 30 to 40 minutes. Consequently, for successful application of this method it is necessary that powerful cumulus clouds be present in the vicinity of teh fire and that their distance from the center be in a defined combination

168

FOR OFFICIAL USE ONLY

FOR OFFICIAL USE ONLY

with the wind direction and velocity. It must be noted that the combination
of such conditions is not a rare occurrence over the taiga. In 1969 aircraft
probes extinguished forest fires covering an area of about $60 \cdot 10^3$ hectares
in Yakutia alone by this method. In 1974 experimental production groups
extinguished 76 fires in the forests of the Krasnoyarsk and Khabarovsk krays,
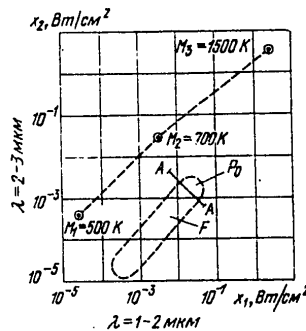Irkutsk Oblast and Yakutia.

Figure 6.20. Location in two-dimensional space of the primary
attributes of the regions of values of the
energy emittance of the natural background
formations under the day conditions F and at
the points M_1, M_2 and M_3 corresponding to
emittance of the forest fire in various
stages.

Key: 1. Watts/cm^2
2. λ = 2-3 microns
3. λ = 1-2 microns

The infrared satellite equipment can be of assistance when introducing this
method of controlling forest fires. As has already been noted, in the
vicinity of the fire it is necessary to select an approaching cloud from
which it is possible to extract rain. This search can be conducted from
the satellite. In particular, multichannel infrared equipment investgated
previously can be used here (see §6.1, 6.2). As an illustration of this
method Figure 6.20 shows the location in three-dimensional space of the
primary attributes fo the region of natural background formations F at
points M_1, M_2, and M_3 corresponding to different phases of forest fire:
M_1 (500°K) and M_2 (700°K)--coals with a different temperature; M_3 (1500°K)
--burning wood. The region P_0 of possible values of the energy emittance
of natural backgrouns illuminated by sunlight in the absence of forest fires
is constructed in the same system of coordinates. In the selected system of
coordinates of the primary attributes, the points of the values of the
energy emittance of a forest fire in different phases lie outside the
background region. This means that the multichannel infrared equipment is
on the basis of the analysis of the spectral composition of the emission
capable not only of detecting the fact of the forest fire itself, but also

169
FOR OFFICIAL USE ONLY

to some degree recognition of its phase (ignition, if for the previous coordinates at the given point of the earth's surface no forest fire was detected, or extinguishing). If the signals are grouped in the vicinity of the point M^3, this indicates a continuing forest fire. When the signals from the point M^3 are shifted at the point M_2 or M_1 on repeated measurements, this is a sign of extinguishing of the forest fire.

By using the same infrared equipment detection and recognition of not only the forest fires, but also the clouds needed for control of them is possible. Prospective cloudiness for extinguishing forest fires is considered to be the cloudiness, the upper edge of which is located at an altitude of 2 km and more above the earth's surface. This includes clouds with great vertical extent. It is these clouds which on observation from space are the brightest background formations, for the solar energy reflected from them passes through the thinnest layer of the earth's atmosphere by comparison with the energy reflected from the earth's surface. This means that the clouds that are "useful" for extinguishing forest firest will be grouped with respect to their light engineering characteristics in the investigated two dimensional space of primary attributes in the upper right hand part of the background region. This part of the background region is indicated in Figure 6.20 as P_0 and it is separated from the rest by the provisional linear boundary A-A. The aircraft probes can be directed by the signal from the satellite to the regions where favorable conditions exist for forest fire control.

The occurrence of a forest fire in different regions can be predicted before its appearance with defined probability. It was mentioned above that many forest fires occur from thunderstorms. Consequently, when observing the global development and displacement of thunderstorms over the earth from satellites, it is possible with defined probability to depict the appearance of forest fires in the dry regions.

The problem of the control of forest fires must be solved complexly. The space system equipped with infrared equipment must be considered as a component part of this large complex already actually used. The performed space experiments have made it possible to obtain images of forest fires that have started by using infrared equipment and in time to determine their coordinates on the earth's surface [6.21]. Thus, for example, by using the artificial earth's satellite inserted into synchronous polar orbit by the US Air Force, forest fires were photographed in the northwestern part of the United States. The observations from the satellite were performed in the visible and the infrared bands with wavelengths of 0.4-1.1 and 8-13 microns. The resolution on the earth was about 3.6 km in the nadir.

CHAPTER 7. SPACE COMMUNICATIONS

7.1. Characteristics of Laser Communications Systems

The creation of reliable and economical lasers, the development of effective methods of modulation and reception of optical signals have made the application of optical communications systems operating in the visible and infrared bands a realistic possibility in space.

By comparison with the radio engineering systems, the laser systems have high directionalness of emission achieved by using comparatively small optical devices and large width of the spectrum which can be used for information transmission [7.1, 7.2]. As a result, they are highly secret, they have insignificant mutual interference, broad possibilities for creating multichannel systems, small mass and low energy intake.

The gain of the transmitting antenna G equals $4\pi A_{trans}/\lambda^2$ in the visible and infrared bands (0.5-10 microns) can reach 100-110 decibels with an apperature of no more than 5 cm. The achievement of such a gain in the millimeter and centimeter bands would require the creation of enormous antennas with a diameter of 1000 to 10,000 meters. As a result of the high directionalness of the optical antennas, it is possible to decrease the energy consumption in the laser communication lines by comparison with radio engineering lines in spite of the lower sensitivity of the optical receivers.
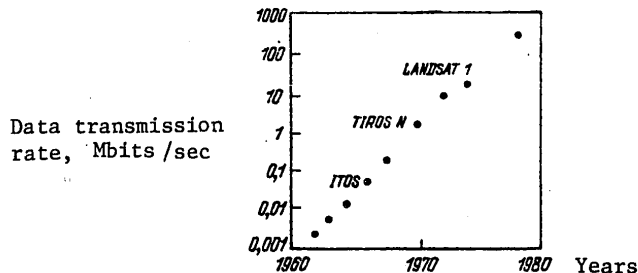

Figure 7.1. Requirements on the data transmission rate over space lines.

171

With high directionalness of the transmitting and receiving antennas in the laser transmission lines exact aiming of them is necessary, and when the target moves, continuous tracking with high angular accuracy is required. The possibility of solving the aiming and tracking problem has been demonstrated experimentally when working with active models under laboratory conditions and in space on board the orbital astronomical observatories (OAO).

The aiming and tracking system usually is made as a two-step system. It includes a mirror system for rought sighting with mechanical drive placed after the primary optical system and providing for sighting within a given angular field of view, and the precision sighting mirror system located in front of the primary optical system and sighting within the limits of a small angle with required precision. For the precision sighting mirrors a piezoelectric drive is widely used which permits tracking with high accuracy and speed.

The expediency of creating space laser communication systems arises from the increased volume of information and increased requirements on the data transmission rate. This trend is especially clearly manifested for the earth studies satellites (see Figure 7.1). For the prospective satellite of the 1980's, the volume of received information, primarily images, will reach 10^{11} bits/day, and the required data transmission rate, 300-500 Mbits /sec. For transmission rates of more than 100 Mbits /sec radio engineering systems probably cannot compete with laser systems with respect to dimensions, mass and energy intake which are rigidly limited for on board spacecraft equipment.

The development of space laser communications systems basically is proceeding along two primary lines: 1) pulse systems with photodetector reception with the application of YAG lasers operating in the visible (0.53 microns) or near infrared (1.06 microns) bands; 2) heterodyne systems on a wavelength of λ = 10.6 microns with the application of CO_2 lasers. For these two types of laser communication systems almost all of the elements suitable for use under space conditions have been built at the present time.

Theoretically heterodyne optical signal receivers have higher sensitivity, which exceeds by three decibels the limiting sensitivity of photodetector receivers. However, for photoheterodyning, high accuracy of the spatial matching of the heterodyne and received optical beams is required so that the phase difference of these beams will not exceed one rad within the limits of the photosensitive surface [7.3].

In heterodyne systems, optical systems of the focusing type are used in the receiving channel, for which the angular field of view θ_{rac} is

$$\theta_{rec} = 2.44 \, \lambda d_{ph}/(d)_d D_{rec}),$$

where d_{ph} is the diameter of the photosensitive surface; d_d is the diameter of the spot bounded by the diffraction limit; D_{rec} is the diameter of the receiver antenna.

172

On optimal selection of the photosensitive element D_{ph} = 0.74-1.0)d_d
[7.5] the angular field of view of the receiving antenna and the accuracy
of sighting it are determined D_{rec}. The possibilities of increasing the
area of the receiving antenna to increase the signal are limited in this
case. The necessity for matching the phases of the signal and heterodyne
beam are imposing high requirements on the quality of the optical system.
These requirements can in practice be satisfied for λ = 10.6 microns;
serious difficulties arise in the visible and near infrared bands [7.5].

For the photodetector receivers the phase of the optical signal plays no
role; these receivers react to the intensity of the optical signal. The
angle of the field of view of the receiver in this case is not connected
with D_{rec}, but is determined by the dimensions of the field-stop aperature.
In order to increase the signal level this permits antennas to be used with
large area without increasing the sighting accuracy requirements. In order
to suppress the background in the photodetector receivers, narrow band,
spectral filtration and time selection are used.

7.2. Designs of Space Laser Communication Systems

Space laser systems are planned for use to provide communications during
flights of interplanetary stations at distances exceeding hundreds of
thousands of kilometers (deep space) and for communications with space-
craft in earth orbits (near space).
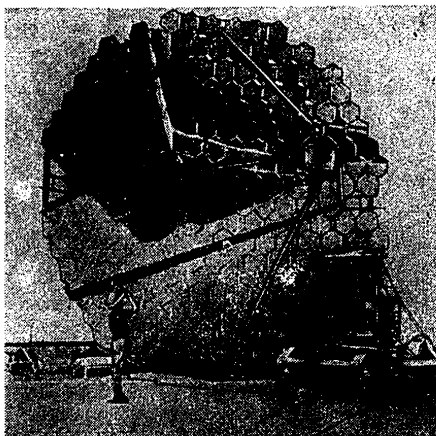

Figure 7.2. Ten-meter optical collector for direct detection of
             pulse signals from space.

Rigid restrictions on the dimensions and mass of onboard equipment and its
energy intake are characteristic of deep space. As analysis of the problem
indicates, these requirements are more easily satisfied if a system is used
which operates in the photodetector reception regime in the visible or near

173

infrared region [7.2, 7.4, 7.7]. In the visible range. in order to obtain
given beam divergence for the onboard equipment, an optical system is
needed with a diameter which is 10 to 20 times less than for $\lambda = 10.6$
microns. For photodetector reception in ground equipment it is possible
to use optical devices with large effective area (collectors) made from
segmented mirrors or a set of individual optical systems (Figure 7.2).
For the modern level of equipment, the diameter of the optical collectors
can exceed 10 meters. The direct detection conditions will permit practical
exclusion of the effect of the phase distortions in the atmosphere on the
operation of the system.

For the deep space communication systems it is expedient for the laser spot
to cover the entire earth. This greatly simplifies the aiming problem, for
there is no longer any problem with respect to orientation of the trans-
mitter beam relative to the ground stations or transfer of it from one
station to another as the meteorological conditions vary. The set of
separate ground stations will in this case permit certain reception of the
signals to be ensured. The directionalness of the emission of the onboard
laser transmitter when communicating from Jupiter, Saturn, Uranus and Neptune
orbit must be about 10 microrads [7.2, 7.6]. The problem of sighting and
tracking with this type of directionalness turns out to be highly complica-
ted as a result of the large transmission time of the signal and the
large (by comparison with the beam divergence) required angular leads.
Significant duration of the communications sessions (to 12 hours) and slow
changes in the angular position and radial velocity of the targets favor
the solution of the sighting problem.

In near space the laser communications systems are proposed for use in
data transmission from low-orbital artificial earth satellites to ground
receiving stations in real time [7.4, 7.5]. An effective means of operative
transmission of a large volume of data and information about emergencies
(fires, floods, storms, and so on] is utilization of a system of stationary
(geosynchronous) radio relay satellites (see Figure 7.3). Information
from the low-orbital artificial earth satellites is transmitted to one of
the stationary radio relay satellites; if necessary it is relayed to the
main stationary satellite and from it to the ground station. The transmission
rate in the lines of this sytem must be no less than 10^8 bytes/sec [7.9].
It is considered that the application of lasers will be preferable for
transmitting data from low-orbital satellites to stationary ones and between
stationary satellites. The problem of using lasers to transmit information
from a stationary radio relay satellite to ground stations has not been
finally solved. In the case of unfavorable meteorological conditions it
is proposed that aircraft stations be used to receive information from the
stationary earth satellites in the optical band and that it be transmitted
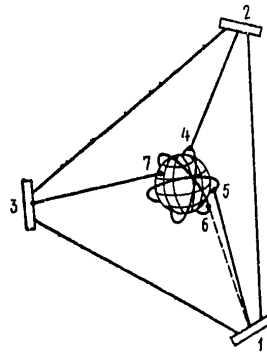to the earth by radio [7.1].

Figure 7.3. Satellite data radio relay system: 1, 2, 3--
stationary earth satellite; 4, 5, 6--Low-
orbital satellite; 7--Ground station.

The analysis of the operating conditions of the system with the application
of stationary radio relay satellites permits determination of the basic
technical requirements on the communications equipment [7.5]. The maximum
range between the low-orbital and stationary satellites can be 43,000 to
47,000 km, and between stationary satellites, 83,400 km. On the stationary
satellite the angular field of view within the limits of which sighting
and tracking must be realized must encompass the highest of the orbits of
the low-orbital satellite. The circular cone with apex angle of 22.5 degrees
encompasses circular orbits with altitudes to 1,852 km (Figure 7.4, a).
The angular field of view of the low-orbital satellite station must in the
general case encompass a hemisphere (Figure 7.4, b) so that the laser beam
can be directed to the stationary satellite station from any point of the
low orbit. Angular velocities are also different which must be traced by
two of the indicated stations: on the stationary satellite within the limits
from 0 to 220 microrads/sec, and the low-orbital satellite, from 0 to 1460
microrads/sec. The maximum values of the angular velocities decrease some-
what with an increase in altitude of the low orbit.

For development of the sighting and tracking system the lead angle which is
determined by the relative angular velocity of the communications stations
is important. The important role of the lead angles in the laser space
communications systems is explained by the fact that their values are
comparable to the angles of divergence of the radiation as the output of
the transmitter. The lead angle in the line between the two stationary
earth satellites can reach 40 microrads; between the ground station and
the stationary artificial earth satellite it will vary from 15 to 20 micro-
rads depending on the position of the ground station. For communication
between the low-orbital and stationary satellites the lead angle can reach
70 microrads.

FOR OFFICIAL USE ONLY
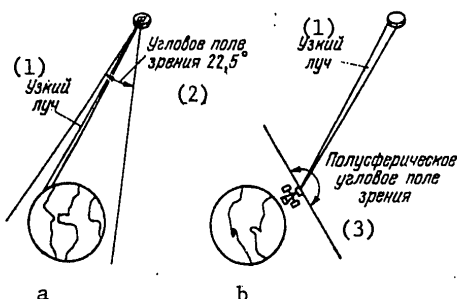

Figure 7.4. Angular fields of view of laser stations:
a—On the stationary earth satellite; b—
On the low-orbital satellite.

Key: 1. Narrow beam
2. Angular field of view 22.5 degrees
3. Atmospherical angular field of view

The sighting and tracking system of the laser station must also compensate
for imprecision in the stabilization of the spacecraft (within the limits
from 0.1 degrees) and its angular velocity (to 0.01 degrees/sec). The rigid
operating conditions of the sighting and tracking systems in the laser lines
require establishment of two-way communications in which both stations
actively tract each other. In the communications system depicted in Figure
7.3, the wide-band data from the low-orbital satellites are transmitted only
in one direction (to the ground station). A narrow band laser beacon line
operates in the opposite direction, ensuring mutual tracking of the stations.
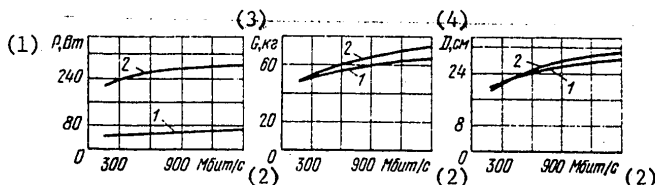
Figure 7.5. Optimal characteristics of receiving (1) and
transmitting (2) space communications stations
using CO_2 laser (range 46,72- km).
Key: 1. P, watts
2. Mbits /sec
3. G, kg
4. D, cm

The basic parameters of the laser equipment--the transmitter power, the
transmitting and receiving antenna equipment-- are selected by solving the
optimization problem [7.3, 7.5], in which the minimum mass or cost of
the equipment providing for the given information band and the signal/noise

176
FOR OFFICIAL USE ONLY

ratio is determined. Figure 7.5 shows the dependence of the aperature diameter D, the intake power P and the mass G of the optimal equipment with a CO_2 laser designed for a space communications line with 46,720 km range as a function of the data transmission rate.

7.3. Space Laser Communications Systems Equipment

The structural diagram of the laser equipment, the methods of signal modulation and reception are determined by the purpose of the communication line and to a significant degree depend on the type of laser. In the designs for the space laser systems provision is made for the use of two types of lasers: the YAG lasers which emit on the basic wavelength of λ = 1.06 microns and on the second harmonic of λ = 0.53 microns and the CO_2 lasers operating in the λ = 10.6 micron band. The selection of these types of lasers is explained by comparatively high efficiency and the possibility of creating highly sensitive receivers on the indicated wavelength. For an average radiation power of several watts the YAG laser have an efficiency from 0.62 to 1.0 percent, and the CO_2 lasers develop specially for reception have an efficiency of up to 9 percent [7.1, 7.5].

Direct detection is used for reception of the YAG laser emission. In this case the receiver includes an optical system, the elements of which determine the angle of the field of view, the narrow-band filter for spectral selection of the background and the photodetector, from the output of which the signal goes to the electronic amplification and processing system. On reception of the laser radiation, the value of the output signal of the photodetector does not depend on frequency, phase or polarization of the carrier, and it is theoretically determined by the intensity of the input optical signal. This fact permits significant simplification of the receiver. The necessity drops out for tracking the Doppler frequency shift occurring as a result of displacement of the receiving and transmitting stations. Reception can be realized through a nonuniform turbulent medium (in particular, the atmosphere) causing significant phase fluctuations. The requirements on the frequency stability of the transmitter are reduced. On wavelength of 0.53 and 1.06 microns these advantages of direct detection are decisive.

As the photodetectors in the visible and near infrared bands predominately photomultipliers are used. The sensitivity of the photomultipliers is determined by quantum noise and background illumination. The thermal noise of the load and the electronic circuitry have no noticeable effect as a result of the high internal gain of the photomultiplier. For analog data transmission the maximum signal power recorded at the output of the photomultiplier is

$$P_{c\,\text{мин}} = \frac{2h\nu\Delta f_c F_m^* (S/N)}{\eta m} \times$$
$$\times \left\{ 1 + \left[1 + \frac{\eta P_{\phi} m^2}{h\nu \Delta f_c F_m (S/N)} \right]^{0.5} \right\}, \qquad (7.1)$$

*sig min
**noise
***background
****signal

177

where $h\nu$ is the quantum energy; F_{noise} is the noise coefficient of the photomultiplier; Δf_{signal} is the information band; η is the efficiency of the photocathode; S/N is the required signal/noise ratio (for data transmission usually S/N > 10); $P_{background}$ is the background illumination power; m is the modulation coefficient.

The magnitude of the background illumination is defined by the formula

$$P_{\phi} = (\pi/4)\, \Delta\lambda\theta^2_{\text{прм}} S_{\text{прм}} b_{\lambda_\phi} \tau_{\text{прм}}, \qquad\qquad (7.2)$$

*receiver
**background

where $\Delta\lambda$ is the transmission band of the filter; $S_{receiver}$ and $\theta_{receiver}$ are the error and the viewing angle of the receiving optical system; $b_{\lambda_{background}}$ is the spectral brightness of the background, watts-cm^{-2}-steradians^{-1}Å^{-1}.

For a receiver on a stationary satellite recording information from a low-orbital satellite, $b_{\lambda_{background}}$ is determined by the solar emission reflected from the earth and its cloud cover, and it is within the limits of (10^{-6} to 10^{-5}) watts-cm^{-2}-steradians^{-1}Å^{-1}. The effect of the background emission can be reduced significantly, by selecting the narrow band filter ($\Delta\lambda$) and the viewing angle (θ_{rec}). Thus, in many cases the limiting sensitivity can be achieved

$$P_{c\,\text{прд}} = \frac{4h\nu F_{\text{ш}}(S/N)\,\Delta f_c}{\eta m}. \qquad\qquad (7.3)$$

*sig lim
**noise
***signal

The intake power at the output of the transmitter is

$$P_{\text{изл}} = \frac{\pi L^2 \theta^2_{\text{прд}} \tau_L}{4 S_{\text{прм}} \tau_{\text{прм}}} P_{c\,\text{мин}}, \qquad\qquad (7.4)$$

*emission, **transmitting
***receiving, ****sig min

where L is the range; $\theta_{transmitting}$ is the angle of divergence of the beam at the exit of the transmitting telescope; τ_L is the damping enroute.

For the pulse methods of data transmission the magnitude of the received signal is determined by the number of photoelectrons E_{sig} formed in the photodetector receiver in the symbol duration time τ_{sig} for a given probability of erroneous reception of the signal P_{err} (transmission and false alarm)

FOR OFFICIAL USE ONLY

$$P_{\text{sig min}} = h\nu N_c/\eta\tau_0 = h\nu N_c M_c/\eta,\qquad\qquad(7.5)$$

*sig min
**signal

where M_{signal} is the number of transmitted signals per second (data transmission rate).

For data transmission usually $P_{\text{err}} \leqslant 10^{-3}$. For this value of P_{err} the number of photoelectrons per symbol must be 5-10 for the most economical types of pulse-code modulation [7.3, 7.8]. The value of $P_{\text{sig min}}$ increases by no more than 20 percent for an average number of background photoelectrons per symbol within the limits of -.1-0.3:

$$N_\phi = \eta P_\phi \tau_c/h\nu = \eta P_\phi/(h\nu M_c) \leqslant 0,1{-}0,3.\qquad\qquad(7.6)$$

Using formulas (7.2), (7.4)-(7.6) it is possible to determine the output power of the transmitter and the required angle of the field of view of the receiving optical system.

The pulse-code methods of modulation are effective modulation methods for YAG lasers. In particular, for deep space the M-value position-pulse modulation is highly prospective (M-PCM-PPM), for which one pulse can be used to transmit several information bits. The use in this case of very short pulses will permit additional weakening of the effect of the background elimination as a result of time selection of the signals.

The parameters of the Neptune-Earth deep space communications line using the YAG laser and M-PCM-PPM modulation are presented in Table 7.1.

Table 7.1

Parameters of the Nepgune-Earth Deep Space Communications line	Value of the Parameters
Range, km	$4.5 \cdot 10^9$
Data transmission rate, bits/sec	10,000
Diameter of the transmitting antenna, cm	10
Diameter of the ground receiving antenna, m	16
Laser pulse duration, nanoseconds	1
Peak power of the laser emission, megawatts	1.2
Pulse repetition rate, pulses/sec	500
Average power of the signal, milliwatts	600
Angular field of view of the receiver, angular minutes	1
Band width of the optical filter in the receiving channel, nm	0.1

179

FOR OFFICIAL USE ONLY

FOR OFFICIAL USE ONLY

The short-pulse laser systems in deep space ensure high transition rates for large volumes of transmitted data per unit masss of equipment.

In the satellite data radio relay system operating in near space both digital and analog methods of data transmission can be used. For analog transmission the microwave subcarriers are modulated by the information signals. Then the subcarriers are combined and fed to an external opto-electronic modulator which simulates continuous emission of the YAG laser. Polarization modulation (PM) of the carrier is considered prospective. On the receiving side the changes in polarization are converted to changes in intensity by using a polarizer.

For digital data transmission methods it is proposed that a YAG laser be used operating in the mode synchronization regime. In this regime the laser emits super short pulses with a duration of about 30 picoseconds and a repretition rate of 200-500 megahertz. In the case of polarization modulation (PCM-PM) a data transmission rate of 200-500 Mbytes/sec is ensured. Multichannel transmission is realized using time multiplexing of the channels.

For laser lines in a satellite data radio relay system a YAG laser with a power of 1-2 watts is required; the intake power of the transmitter will be about 200 watts (Table 7.2).

Table 7.2.

Parameters of the Communication line of data radio relay satellite system with YAG laser	Values of the parameters
Stationary satellite to stationary satellite	
Range, km	80,000
Data transmission rate, Mbits /sec	100
Angular divergence of the transmitter beam, microrads	50
Receiving antenna diameter, cm	61
Transmitter radiation power, watts	2
Stationary satellites-stationary satellite	
Range, km	80,000
Data transmission rate, Mbits /sec	10
Transmitter with tracking system:	
Mass, kg	18.1
Intake power, watts	250
Receiver and optical beacon	
Mass, kg	36.2
Intake power, watts	100
Low-orbital satellite--stationary satellite	
Range, km	40,000
Data transmission rate, Mbits	10
Transmitter and tracking system on the low-orbital earth satellite	

[Continued on following page]

180

FOR OFFICIAL USE ONLY

[Continued from preceding page]

Angular beam width, microrads	50
Radiation power, watts	1
Mass, kg	18.1
Intake power, watts	100
10-channel receiving system on a stationary artificial earth satellite:	
Antenna diameter of each channel, cm	10
Mass, kg	56.6
Intake power, watts	200
Stationary Earth Satellite to ground station	
Range, km	40,000
Data transmission rate, Mbytes/sec	100
Diameter of the receiving antenna, cm	46
Transmitter emission power, watts	1

For near space systems lines are also being developed intensely with CO_2 lasers and heterodyne reception [7.5]. It is inexpedient to use direct detection conditions for recording CO_2 laser emission because the cooled photoresistors and the photovoltaic detectors sensitive to radiation in the 10.6 micron range have no internal gain, and the level of generation-recombination noise of the photosensitive element and the thermal noise of the load exceed by 5 to 6 orders the quantum noise level. The application of an optical heterodyne of sufficiently high power will permit supression of the generation-recombination and thermal noise and sharp attenuation of the effect of the background illumination. The minimum power of $P_{sig\ lim}$ required to record the signal in the heterodyne receiver in practice is determined by the quantum limit, and it is

$$P_{sig\ lim} = \frac{h\nu\Delta f_{intermediate\ frequency} F_{noise}(S/N)}{\eta},$$ (7.7)

*sig lim
**intermediate frequency
***noise

where $\Delta f_{intermediate\ frequency}$ is the passband with respect to the intermediate frequency.

By comparing the formulas (7.3) and (7.7) considering that in the case of two-band modulation $\Delta f_{intermediate\ frequency} = 2\ \Delta f_{sig}$, it is possible to note the heterodyne receiver is potentially twice as sensitive as the photodetector. In the real heterodyne receiver $P_{sig\ min}$ exceeds $P_{sig\ lim}$ by 3-10 decibels; the natural noise of the heterodyne plays a significant role in this.

In heterodyne systems high requirements are imposed on the frequency stability of the laser heterodyne and transmitter the temperature stability and rigidity of the structural elements ensuring matching of the signal and heterodyne beams on the photosensitive element. In addition, tracking of the Doppler frequency shifts is required.

181

(1) $f_д,МГц$

(3)

Угол
наклонения
$γ=90°$

85
75

45
0

−120 −60   0   60 120

Угол места $Ω,град$ (2)

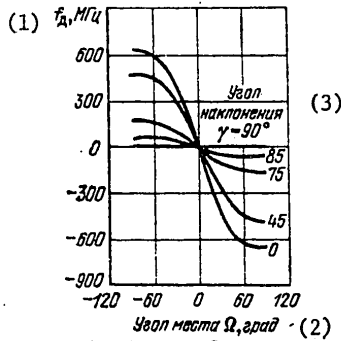Figure 7.6. Doppler shifts in the line between the low-
orbital and stationary artificial earth
satellites ($λ$ = 10.6 microns).

Key: 1. f_d, megahertz
2. Angle of elevation $Ω$, deg
3. Angle of inclination

The value of the Doppler frequency shift f_d in the line from the low-orbital
satellite to the stationary earth satellite depends on the angle of inclina-
tion $λ$ of the orbital plane of the low-orbital satellite with respect to the
plane passing through the stationary satellite and the earth's axis, the
angle of elevation $Ω$ of the satellite with respect to the plane of the earth's
equator (Figure 7.6) and it varies weakly on variation of the orbital
altitude. In practice in this system it is necessary to realize frequency
tracking within the limits of $\pm$700 megahertz. Two methods of tracking
f_d are known: by the optical frequency with the application of an adjustable
laser heterodyne and by the intermediate frequency with the application of
a second (radio engineering) mixer and a tunable   radio engineering
oscillator (GUN). In both cases technical difficulties arise in connection
with the great range of variation of f_d. In the laser receiver developed
specially for the satellite data radio relay system, both methods of tracking
f_d are used [7.5]. The structural diagram of this receiver is presented in
Figure 7.7. By using an AFC system, the frequency of the laser heterodyne
is tuned within the limits of $\pm$400 megahertz, that is, partial tracking of
f_d takes place. Then the second frequency conversion is realized in the
radio frequency mixer to which the voltage is fed from the voltage-controlled
(GUN). The tracking system ensures constancy of the second intermediate
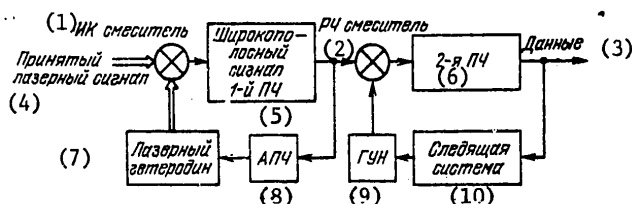frequency.

182

FOR OFFICIAL USE ONLY

Figure 7.7. Structural diagram of a laser heterodyne receiver
with double frequency conversion and tracking of
the Doppler shifts.

Key: 1. Infrared mixer
2. Radio frequency mixer
3. Data
4. Received laser signal
5. Wide-band signal of first intermediate frequency
6. Second intermediary frequency
7. Laser heterodyne
8. ANC
9. GUN tunable radio oscillator
10. Tracking system

It is proposed that a waveguide CO_2 laser be used as the optical hetero-
dyne (see Figure 7.8). A laser tube with a channel diameter of 1.25 mm
is made of beryllium oxide (BeO) having high thermal conductivity, and
it is filled with gas mixture at a pressure of 20 kPa. The higher pressure
by comparison with the ordinary CO_2 lasers ensures broadening of the frequency
tuning band. A grating (echelette) is used as the output mirror, which
simultaneously performs the functions of a polarizer and a coupling element
taking 0.5 percent circulating in the resonator. The generation wavelength
is set within the range 10.467 to 10.788 microns by selecting the grating
angle. The frequency tuning with respect to the initial frequency is
accomplished by a reflecting mirror attached to a PZT circular piezoelectric
bender.

A Stark cell is used for frequency stabilization and tuning of the laser
heterodyne. A part of the radiation is transmitted through the Stark cell
willed with a mixture of ND_3 and NH_3, and synchronization of the laser
frequency takes place over the NH_2D absorption line formed in the gas mixture.
On deviation of the laser frequency from the absorbtion line frequency an
error signal is generated in stabilization system which on the PZT piezo-
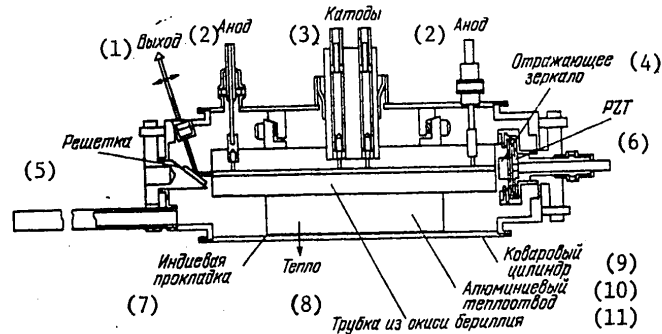electric unit, as a result of which this deviation is compensated for.

Figure 7.8. Tunable laser heterodyne.

Key: 1. Output
2. Anod
3. Cathodes
4. Reflecting mirror
5. Grating
6. PZT
7. Indium liner
8. Heat
9. Covar cylinder
10. Aluminum heat transfer element
11. Berylium oxide tube

On variation of a constant electric voltage applied to a Stark cell, the frequency of the absorption line changes, and the heterodyne frequency tuning is provided through the stabilization frequency.

The long-term and short-term frequency stability is 100 kilohertz (relative, $3.5 \cdot 10^{-9}$).

The frequency of the laser transmitter will be stabilized analogously.

The modulation of the radiation in the CO_2 lasers is realized by optoelectronic modulators, the operating principle of which is analogous to the modulators for YAG lasers. The use of external modulators in the long wave infrared band is connected with significant energy expenditures to 0.5 watts/megahertz by comparison with 0.04 watts/megahertz for modulation of YAG lasers. In order to decrease the expenditures of power in the CO_2 lasers, preference is given to internal modulators placed in the laser resonator. Figure 7.9 shows the structural design of the internal modulator. The modulator is a unit whole with the second mirror of the resonator, and it is attached directly to the end of the discharge tube of the laser of the transmitter. Modulation is realized by a cadmium telluride CdTe long with a transverse cross-section of 1.5 x 1.5 mm placed in a symmetric strip transmission line to which the information signal voltage is feed through a coaxial plug. The modulator band is 500 megahertz, and the intake power in the modulation channel is about 90 watts.
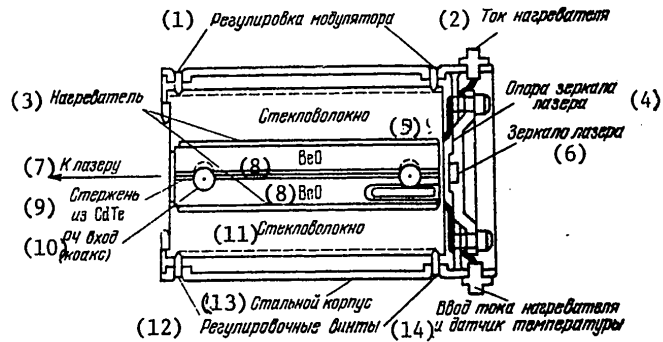
184

Figure 7.9. Structure of the internal modulator of a CO_2 laser.

Key:
1. Modulator adjustment
2. Heater current
3. Heater
4. Laser mirror
5. Fiber glass
6. Laser mirror
7. To the laser
8. BeO
9. CdTe rod
10. Operating frequency input (coaxial)
11. Fiberglass
12. Adjustment screw
13. Steel housing
14. Heater current input and temperature gage

The development of a heterodyne receiver and transmitter with CO_2 laser has made it possible to perform a sufficiently complete estimate of the receiving and transmitting stations of the low-orbital satellite to stationary satellite line with data transmission rate of 1,000 Mbits/sec (see Table 7.3).

Table 7.3

Equipment parameters for a satellite data radio relay system with CO_2 laser	Values of the Parameters
Transmitter of a low-orbital earth satellite:	
Range, km	47,000
Data transmission rate, Mbits /sec	1,000
Antenna diameter, cm	28
Output power of the transmitter, watts	1.21
Mass of the transmitting station with optical beacon, kg	67.3
Mass of the primary power supplies, kg	55.2
Intake power, watts	272.2
Receiving station on a stationary satellite:	
Antenna diameter, cm	26
Mass with guidance module and beacon, kg	59.6
Mass of primary power supplies, kg	17.3
Intake power, watts	65.2

On the basis of models of the receiver and transmitter, a heterodyne trans-
ceiver has been developed for the communication line between stationary
satellites. The simplified structural diagram of this transceiver is
presented in Figure 7.10. The general Gregory system telescope 28 cm in
diameter is used for transmission and reception. The primary mirror is
parabolic, and the secondary, almost confocal ellipsoidal. Exact aiming
of the beam is realized by an image motion compensator (KDI), and the
decoupling of the receiver and the transmitter, by a diplexer. In order
to track the radiation source, the system includes a nutator which realizes
conical scanning of the field of view of the receiver. As a result of
using a general telescope and sighting system the mass of the mass of the
transceiver is less than the sum of the masses of the receiving and trans-
mitting stations of the low-orbital satellite to stationary satellite line.
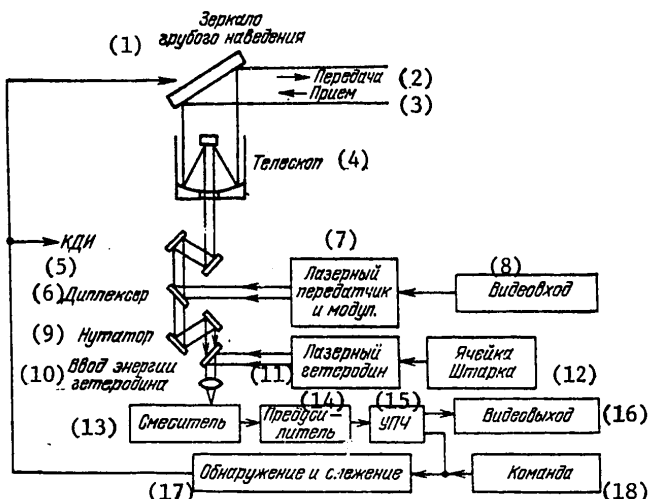
Figure 7.10. Simplified structural diagram of a laser heterodyne
transceiver

Key: 1. Deep sighting mirror
2. Transmission
3. Reception
4. Telescope
5. KDI [image motion compensator]
6. Diplexer
7. Laser transmitter and modulator
8. Video input
9. Nutator
10. Heterodyne power input
11. Laser heterodyne
12. Start cell
13. Mixer
14. Preamplifier
15. Intermediate frequency amplifier
16. Video output
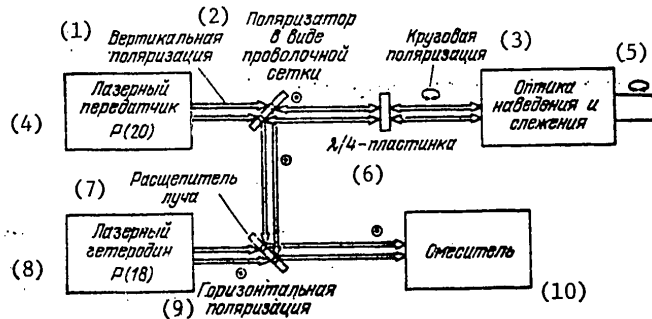17. Detection and tracking
18. Command

187

FOR OFFICIAL USE ONLY

Figure 7.11. Optical decoupling of receiving and transmitting channels.

Key: 1. Vertical polarization
2. Polarizer in the form of a wire grid
3. Circular polarization
4. Laser transmitter R(20)
5. Sighting and tracking optical system
6. $\lambda/4$--plate
7. Beam splitter
8. Laser heterodyne R(18)
9. Horizontal polarization
10. Mixer

The decoupling of the receiving and transmitting channels is realized as a result of different polarization of the waves (see Figure 7.11). The polarizer in the form of a wire grid transmits the vertical-polarized emission of the transmitter. After the $\lambda/4$-plate the radiation will be circularly polarized. As a result of circular polarization, the effect of the revolutions of the station on the signal reception is eliminated. The received radiation is converted by the same $\lambda/4$-plate to horizontally polarized, which is directed completely to the beam splitter ensuring matching of the signal and heterodyne beams in the photomixer. The photosensitive element of the mixer is the HgCdTe photodiode with dimensions of 200 x 200 microns cooled to T = 100-120°K. The sensitivity of the receiver at this temperature is about $1.5 \cdot 10^{-19}$ watts/hertz which is more than the quantum limit by formula (7.7) by approximately three times.

7.4. Search and Tracking Systems of the Laser Communications Systems

Let us consider the possibilities of search and tracking in the example of the communication line from the low-orbital artificial earth satellite to the synchronous satellite on which more rigid requirements are imposed (less time for search, tracking within the limits of a broader field of view) than on the search and tracking systems of the communication lines from the synchronous earth satellite to synchronous earth satellite or the synchronous earth satellite to a ground station. The operation of the search and tracking system is realized by the following procedure [7.1]:

188

FOR OFFICIAL USE ONLY

29 OCTOBERR 1979   YU. P. SAFRONOV AND YU. G. ANDRIANOV   3 OF 3

BY

FOR OFFICIAL USE ONLY

1. The search beacon beam with an angular width of ±0.2° corresponding to the indeterminacy of the angular orientation is switched on aboard a synchronous earth satellite, and it is directed at the earth satellite on the low orbit. At a range of 40,000 km the light spot has a diameter of 280 km. Since according to the orbit forecasting data the position of the satellite on the low orbit is known with an accuracy to 1 km, the satellite on the low orbit falls into the beacon beam (see Figure 7.12a).
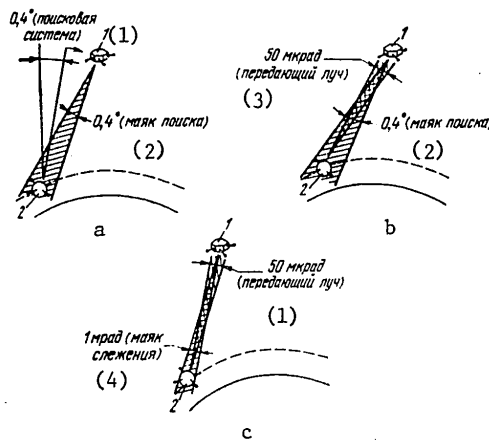

Figure 7.12. Search, sighting and data transmission sequence to the geosynchronous artificial earth satellite (1) from the low-orbital satellite (2).

Key: 1. Search system
2. Search beacon
3. 50 microrads (transmitting beacon)
4. 1 millirad (tracking beacon

2. A search system with electronic deflection searching within the angular limits of ±0.2 degrees (7 millirads) corresponding to the indeterminacy of the angular orientation of the earth satellite in low orbit is switched on on board the low-orbital satellite. After finding the synchronous satellite the system goes into the tracking mode for tracking the synchronous satellite and sends the laser beam of the communications system to it. From this time it provides for automatic aiming of the laser beam at the synchronous satellite (Figure 7.12, b).

3. The synchronous satellite searches for the transmitting beam and sends the tracking beacon beam 1 millirad wide to the low-orbital satellite (see Figure 7.12, c).

4. The low-orbital satellite is oriented on the tracking beam and begins data transmission. The total time required for search, aiming and the conversion to the transmission mode is less than 10 seconds.

189
FOR OFFICIAL USE ONLY

The individual search and tracking beacons ensures better flexibility and
less energy intake than for combined beacons. The emission power of the
search beacon laser (beam with 7 millirads) must be approximately 40 times
greater than the emission power of the tracking beacon laser (beam width
1 millirad). Inasmuch as the search time is less than 10 seconds, the
search beacon can be used successively for the search and aiming of the
systems of all artificial earth satellites on low orbits services by one
synchronous satellite.

The number of photons in the time of one emission pulse of the search beacon
received by the equipment onboard the low-orbit artificial earth satellite
is determined from the expression

$$n = \eta \lambda P_M D^2_{\text{受信}} T_0 / (hcM\Theta^2 R^2), \tag{7.8}$$

*receiving beacon

where P_M is the average emission power of the serach beacon; M is the pulse
repetition rate of the search beacon; $D_{\text{receiving beacon}}$ is the diameter of
the optical system of the beacon receiving the radiation (on the low-orbital
satellite); Θ is the beam width of the search beacon (7 millirads).

For $P_M = 1$ watt, $M = 100$ pulses/sec and $D_{\text{receiving beacon}} = 7.6$ cm, from
formula (7.4) it follows that n = 30 photons/pulse.

Usually two-stage search systems are used for the beacon search. If the
initial width of the field of view of the search system (in the first stage)
receiving the beacon emission is 500 microrads, the total number of possible
positions of the search system with indeterminacy of the angular orientation
of 7 millirads is 196. With an overlap coefficient of 0.7 (in order to
exclude skips) and two pulses for each scanning position the maximum time
for the initial search is 5.6 seconds.

However in order to direct the transmitting laser beam 50 microrads wide
from the low-orbital satellite to the synchronous satellite, the initial
search scanning field of 500 microrads must be reduced to 50 microrads.
The tracking within the limits of 1/10 of the field of view can be realized
using different scanning procedures. Assuming, just as in the preceding case
that the overlap coefficient is 0.7, and that there are two pulses for
each scanning position, we find that the time for orientation of the search
beacon with precision to 50 microrads is 2.9 seconds. The maximum time for
two search stages will be 8.5 seconds.

The two-stage search requires significantly less time than the one-stage
search. The maximum time for the single-stage beam search with a viewing
angle of 50 microrads within the limits of the field of view of 7 millirads
is 560 seconds.

The operation of the search beacon in the pulse mode permits us to use low-
power power supplies in the energy accumulation mode. For an average ra-
diation power of 1 watt and a pulse repetition frequency of 100 pulese/sec

190

FOR OFFICIAL USE ONLY

the radiation energy in each pulse is 10^{-2} joules. The beacon pulse duration usually is within the limits of 100-200 microseconds, which permits us to use a detection system in the beacon radiation reception system with matched filters with comparatively narrow transmission bands.

Increasing the pulse repetition frequency decreases the search time, but at the same time it leads to an increase in the intake power and mass.

In the tracking mode the power intake by the beacon can be appreciably reduced as a result of a decrease in its beam width. In accordance with (7.8) for 20 photons for 10^{-2} seconds, a tracking beacon beam width of 1 millirad (A_{trans} = 0.014 cm^2) and a diameter of the receiving optical system of 7.6 cm (A_{rec} = 46 cm^2) the radiation power of P_M = 0.013 watts is required. At this power it is possible to divide the beam into several channels to use one laser onboard the synchronous satellite to ensure communications with several satellites in low orbits.

The investigated search and tracking systems provide for operation of lines between satellites not having precision angular stabilization systems.

7.5. Practical Operations in the Creation of Space Infrared Laser Communications Systems

The scientific research laboratory of Lockheed Missiles and Space Company has performed tests confirming the possibility of creating a wide-band laser communications system for transmission of analogous data from artificial earth satellites in low orbits to remote ground stations using radio relays on one or several stationary earth satellites. Initially the tests of the real data transmission system of the Nimbus E satellites were planned for 1975, but they were postponed to 1978. In the initial plans the data were to be transmitted from the Nimbus E satellite over a wide-band laser channel (to 1000 megahertz) to the radio relays of the ATS-F and ATS-G satellites.

A passband of 720 megahertz provides for transmission of infrared images with resolution on the ground of about 1.5 meters which is equivalent to the transmission of television images with 6,000-line scanning at a frame frequency of 30 hertz.

If there is no necessity for using a wide-band channel, the laser beam can be frequency multiplexed by several narrow-band channels. During the tests of teh prototype of this system, the possibility of data transmission in the frequency band of 400 megahertz with a single/noise ratio of more than 30 decibels was demonstrated. The plan also calls for creating a system with a frequency band of 1 gigahertz with a single/noise ratio of 30-50 decibels.

In the developed communications system the transmitted data frequency-modulates the microwave subcarrier frequency generator, the voltage of which is fed to an optoelectronic modulator located between the laser emitter and

191
FOR OFFICIAL USE ONLY

transmitting telescope. The modulator converts the laser beam polarization in accordance with the amplitude of the subcarrier oscillations. On transmission of several signals, each of them has its own subcarrier frequency. The subcarrier frequencies are combined and fed to the input of the modulator.

In a receiver the polarization modulation is converted to the modulation of the intensity of the radiant flux incident on the radiation receiver. In the laboratory device the electric signal from the output of the radiation receiver was amplified, demodulated, analyzed and reproduced on a screen. On the radio relay satellites the signal is amplified and relayed to the ground stations over a laser or microwave channel.

The largest acceptable laser emitter in the given development is considered to be a neodymium laser with double frequency (λ = 0.53 microns) with pumping from sodium gas-discharge tubes.

It is considered that a transmitting system based on such a laser will use 10 times less energy than a system with single-frequency argon laser. On transmission in the 1 gigahertz frequency band with a single/noise ratio of 30 decibels a power of about 100 watts is required when using the YAG laser.

The system uses an optical modulator based on a lithium niobate crystal placed in the radio frequency field of a wide band microwave filter. The modulator is designed for operation in the 1 gigahertz band with respect to the central frequency of 1.5 gigahertz, and it requires about 5 watts for control.

A telescope with abberations close to the diffraction limit is used as the transmitting optical system. The diameter of the objective is 203 mm.

The halfwidth of the angle of divergence of the laser beam is 3 microrads. The precision of the telescope siting system is 1 microrad. A mirror objective is used in the receiver. The radiation receive is an avalanche silicon photodiode. The signal after the radiation receiver is amplified by a microwave amplifier and goes to the frequency detector.

The Perkin-Elmer Company has developed and tested a prototype of the optical laser communications system permitting transmission of five television channels a distance of more than $160 \cdot 10^6$ km (the distance between Mars and the Earth). During the tests, the operating conditions of the equipment on board a spacecraft were simulated.

The optical transceiving system is made up of a platform with a four-axial suspension, a 460-mm telescope and the optical equipment itself installed at the focal point of the telescope. The two internal axes of the suspension provide for rotation of the telescope with respect to the pitch and yawing axes required for ordinary aiming of the telescope. The two external

192

FOR OFFICIAL USE ONLY

FOR OFFICIAL USE ONLY

axes of the suspension are used to create mechanical disturbances to simulate the rotations of the spacecraft with respect to azimuth and heeling angle.

The optical system of the onboard equipment is depicted in Figure 7.13. The system provides for search, aiming and tracking of a ground station by the laser beam and transmission of information by the laser beam to the ground. The beam diameter on the earth is about 320 km for a range of 160×10^6 km. The accuracy of sighting the beam at one of the ground stations is better than ± 40 km.

In order to simulate space conditions the equipment was tested on a 30-ton pneumatic platform excluding seismic disturbances. The attentuation conditions of the optical signal at a distance of 160 million km, the effect of the scattered light of the earth, background noise and mechanical disturbances caused by movement of the spacecraft were simulated on the device. With angular oscillations of the spacecraft of up to ± 2 degrees at a speed of 13 degrees/sec, an accuracy of sighting the transmitted beam of better than 0.1 "was ensured."
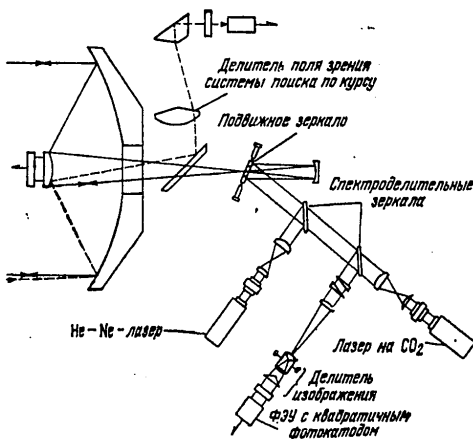

Figure 7.13. Optical system of the onboard laser system of the Perkin-Elmer Company for transmitting five television channels a distance of more than $161 \cdot 10^6$ km.
Key: 1. Divider of the field of view of search system with respect to heading
2. Moving mirrors; 3. HeNe laser; 4. CO_2 laser; 5. Image divider; 6. Photomultiplier with square photocathode.

193
FOR OFFICIAL USE ONLY

FOR OFFICIAL USE ONLY

Work is proceeding on the construction of more efficient and reliable lasers for space communication systems. The Honeywell Company [7, 12] is working on a CO_2 laser with a service life of 20,000 hours (2.5 years). The laser has operated for 7,000 hours in tests.

At the present time the studies and developments with respect to space laser communication systems are being conducted within the framework of the 405 Z program. According to this program in 1979-1980 a satellite will be inserted into a close to stationary orbit to perform an experiment in laser communications [7.10]. The final goal of the program is to build a laser communications system between a low-orbital satellite and a stationary satellite with an informativeness of 10^9 bytes/sec. Experiments are simultaneously planned for communications sessions with a ground station to estimate the effect of atmospheric conditions.

A YAG laser operating in the pulse mode will be used in the onboard transmitter. The diameter of the transmitting telescope is 19 cm, the beam divergence is 9.4 microrads. A distinguishing feature of the onboard laser is pumping by solar energy. The analysis that has been made [7.1] indicates that the mass of the solar condenser and the mechanism for aiming it is approximately equal to the mass of the panels of the solar elements and voltage converters. At the same time the use of solar energy for pumping greatly increases the service life of YAG lasers. In the United States the development of lasers with solar pumping for application in space is headed by the avionics laboratory of the U.S. Air Force.

As a result of the experimental design developments by a number of American companies with the participation of NASA specialists, models of transmitting and receiving stations with CO_2 lasers and heterodyne reception had been built which have high technical characteristics and are designed for use in a satellite data radio relay system [7.5]. The receiving station of the stationary satellite and the model of the transmitter provides for data transmission rates of 300 Mbits/sec, tracking of Doppler shift of ± 700 megahertz, spatial tracking in the range of 20 x 20 degrees. The signal detection and capture time is less than one minute with initial sighting of ± 0.1 degrees. It is considered that on the basis of the model a final version of the receiving station will be built for relaying data with intake of less than 100 watts from the onboard network (together with the laser beacon) and a mass of 50 kg.

The tracking characteristic has demonstrated that it is possible to use a beam with a divergence of 82 microrads. The statistical tracking error is 7 microrads, the dynamic error with an angular velocity of the target of 0.03 degrees/sec reached a total of 3.5 microrads. The maximum angular velocity of the target for which detection and capture of the signal are possible is 0.3 degrees/sec, and the detection field of view is 0.26 degrees. The indicated parameters more than ensure operation of the system for all the expected disturbances in the motion of the spacecraft.

Increasing the service life of the CO_2 laser to 50,000 hours instead of 5,000 hours at the present time has been stated as one of the most important problems of the future.

FOR OFFICIAL USE ONLY

CHAPTER 8. INFRARED SPACE SYSTEMS FOR MONITORING NUCLEAR BLASTS, DETECTION OF THE LAUNCHING OF BALLISTIC MISSILES AND SPACECRAFT

8.1. Some Characteristics of Nuclear Blast Radiation

The external picture of a nuclear blast is determined to a significant degree by the light emission and its interaction with the environment [8.1]. At the blast point, a blindingly bright flash is observed after which a bright fireball appears made up of incandescent vapor of the fission products of the materials in the atomic charge, the part of the charge material not entering into the reaction, the jacket and other parts and also incandescent air. As a result of the high excess pressure the fireball expands at a rate significantly exceeding the speed of sound.

In the case of air blasts approximately 1/3 of the energy is released in the form of radiation, and the rest is expended on the formation of a shock wave, radioactive and x-radiation [8.2]. The optico-electronic instruments detect nuclear blasts by the light emission. Consideration of the emission characteristics of the fireball has primary significance for the creation of space detection devices.

For a nuclear blast of $21 \cdot 10^3$ tons after 10^{-4} seconds the radius of the fireball reaches approximately 15 meters, and the temperature reaches 300,000°K. This ball is said to be isothermal inasmuch as the temperature at all points of it is the same [8.3]. The increase in size of the ball is accompanied by a drop in its temperature as a result of entrainment of new air masses in the ball. The fireball rises. The rate of ascent reaches 75-100 m/sec at the initial point in time. In the first phase of development of the blast lasting about 0.01 seconds the surface temperature of the fireball drops sharply, reaching a minimum 1,800°C. In the second phase again begins to rise and after 0.2-0.3 seconds reaches a maximum of 8,000°C. Then as a result of loss of energy to radiation and cooling of the incandescent gases, the surface temperature of the fireball gradually decreases and, finally, it stops producing light (see Figure 8.1).
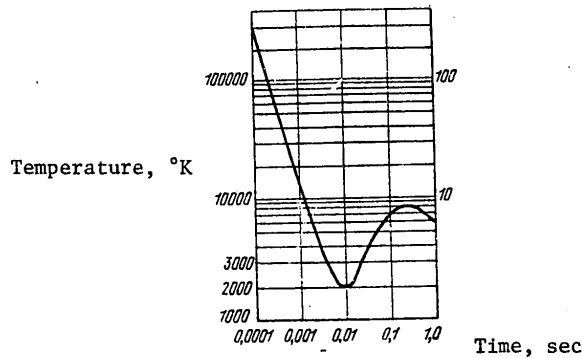
Temperature, °K

Time, sec

Figure 8.1. Variation of the surface temperature of the fireball
as a function of time for a 20,000 ton nuclear blast.

For high-power blasts the nature of the temperature variation of the out-
side surface of the fireball is the same as for a $20 \cdot 10^3$ ton blast, except
the temperature minima and maxima are shifted in time in the high direction.
The absolute values of the minima and maxima temperatures of the outside
surface of the fireball remain 1,800 and 8,000°C, that is, they do not depend
on the power of the blast. The dimensions of the fireball and its glow time
increase with an increase in power of the blast (see Table 8.1) [8.3].

Table 8.1

Characteristics of the fireball	TNT equivalent, tons				
	10^3	$20 \cdot 10^3$	10^6	$5 \cdot 10^6$	10^7
Maximum diameter, meters	140	470	220	4 100	5 400
Glow time, seconds	1	3	10	19	24

In the case of a ground nuclear blast, a glowing hemisphere is formed,
the radius of which is approximately 1.3 times greater than the radius of
the fireball of the air blast of the same power.

The high altitude nuclear blasts differ significantly from air and ground
blasts. In the summer of 1958, two nuclear blasts were produced in the
United States at an altitude of 43 and 77 km [8.2]. In one of them with a
power of several megatons at an altitude of 77 km the diameter of the fireball
0.3 seconds after the blast was already 17.6 km, and it increased to 29 km
after 3.5 seconds. In this case the fireball rose at high velocity. Its
initial rate of ascent was about 1.6 km/sec. Approximately a minute after
the blast the fireball was at an altitude of 145 km. The rate of its ascent
was at this time about 1 km/sec. The ball grew in the horizontal direction
at a rate of approximately 0.3 km/sec.

196

Photon energy

1МэВ 0,1МэВ 10кэВ 1кэВ 0,1кэВ 10кэВ 1эВ

Magnitude of
of the light
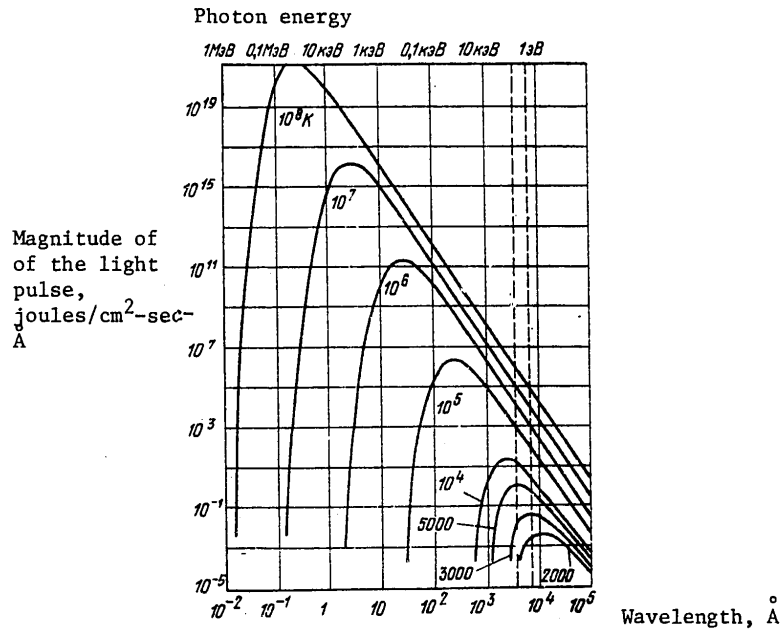pulse,
joules/cm^2-sec-
Å

Wavelength, Å

Figure 8.2. Intensity of the emission of an absolutely black
body as a result of the wavelength at different
temperatures.

At altitudes of 60-110 km, the light emission of nuclear blast exceeds 50
percent of all of the energy released during the explosion. A characteristic
feature of a high-altitude nuclear blast is the presence of a red glowing
spherical wave of very large size surrounding the fireball. This sphere
was observed for several minutes; 6 minutes after the explosion its diameter
was about 960 km. The spectroscopic investigation performed during the
tests demonstrated that the fireball behaves not exactly like an absolutely
body [8.2], but when calculating the light emission this difference can be
neglected. The spectral energy distribution of the radition of a nuclear
blast as a function of temperature calculated with Planc formula is presented
in Figure 8.2. From the figure it is obvious that the total magnitude of
pulse proportional to the area under each curve increases significantly
with a decrease in temperature [8.2]. With a change in temperature, the
spectrum of the radiant energy changes. At high temperatures, the short-
wave radiation predominates, and at low temperatures, the long-wave
radiation. For example, for a nuclear blast before the formation of the
fireball the temperature is several tens of millions of degrees and the
radiation during this period basically takes place in the range of 0.01 to
10 nm corresponding approximately to the spectrum of soft x-radiation. This

197

FOR OFFICIAL USE ONLY

radiation is absorbed by the surrounding mass of air, as a result of which
the fireball is created. Later (t > 0.01 seconds) the surface temperature
of the fireball usually is below 10,000°K, the radiation predominantly takes
place in the ultraviolet, visible and infrared bands of the spectrum. The
total radiation energy for all wavelengths from the entire of the surface
of the fireball can be found by the Stefan-Boltzman law. The magnitude of
the light pulses with a nuclear blast is a time function. The maximum
magnitude of the light pulse P_{max} corresponding to the maximum temperature
in the second phase and the time t_{max} during which this maximum is reached
are related to the power of the blast by the simple expression [8.2].

$$P_{макс} \approx 4 W^{1/2}, \; [кт/c]; \text{**} \qquad \text{*max}$$
$$t_{макс} \approx 3{,}2 \cdot 10^{-2} \; W^{1/2}, \; c, \qquad \text{**[kilotons/sec]}$$

where W is the power of the blast in kilotons (1 kiloton = 10^{12} cal).

For blasts in the megaton range the value of t_{max} can be somewhat less the
calculated value. For a ground (above-water blast) the fireball is formed
approximately the same as during an air blast of twice the power inasmuch
as the energy of the shockwave is reflected from the surface and is again
directed to the fireball. Hence, t_{max} for a ground blast can be somewhat
greater than for an air blast of the same power.

For calculating the light pulse on the limits of the atmosphere it is
necessary to consider the spectral transparency of the atmosphere.

8.2. Infrared Radiation of the Jets of Ballistic Missiles

The jets issuing from the engines of ballistic missiles are powerful sources
of infrared radiation. This radiation is used to detect missile launches
from satellites and for early warning about launches (see §8.3). The jet
behind a rocket is made up of the gases formed during combustion of the
rocket propellant and solid particles heated to high temperatures (about
2000°K). The gaseous composition of the jet depends on the type of fuel
used. In the majority of cases, the jet includes water vapor and carbon
dioxide [8.4]. Thus, for example, the J-2 engine installed on the Saturn
5 space rocket operates on liquid oxygen and liquid hydrogen fuel; therefore
its jet is basically made up of water vapor. The S-1 engine operates on
oxygen-kerosene fuel, and its jet includes a mixture of carbon dioxide and
water vapor. The solid fuel engines have a jet basically made up of carbon
dioxide, water, carbon monoxide and solid particles of aluminum and carbon
heated to high temperatures. In the spectrogram of the rocket jet it is
possible to observe a set of different emission lines of water vapor, carbon
dioxide and carbon monoxide and also the condinuous radiation of the heated
partices. The jet is a complex gas dynamic structure which has thermo-
dynamic parameters that vary from point to point: pressure, temperature
and density. In order to calculate the radiation of the jet they are
needed on the temperature distribution, the density distribution, pressure
and other characteristics of the gases in the entire jet region. As an
example, in Figure 8.3 the temperature field of the jet of one of the rocket

engines is presented in two operating modes. The solid lines--the isotherms--
belong to mode A, and the dotted lines, to mode B. The combustile component
of the propellant is RP-1 kerosene rocket fuel, and the oxidizing agent is
liquid oxygen. In mode A the thrust was 68 tons, and in mode B, 90.7 tons,
and the pressure in the combustion chamber is 39.3 and 51.4 kg/cm^2, repsective-
ly. The density of the combustion products in mode B is 30 percent higher
than in mode A. The pressure at the tip of the nozzle is 0.727 kg/cm^2 in mode
A and 0.917 kg/cm^2 in mode B. From the figure it is obvious that the jet
zone with a temperature to 540°C reaches 60 meters in length and about 4
meters in width. Consequently, the glowing area of the jet of the given
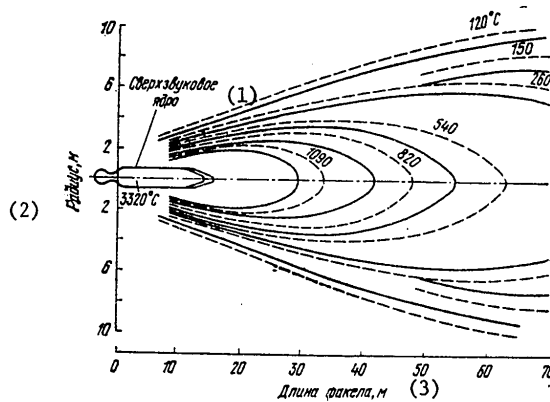engine will be 200-250 m^2, respectively [8.4].

Figure 8.3. Temperature field of the jet of a rocket engine

Key: 1. Supersonic nucleus
     2. Radius, meters
     3. Length of jet, meters

As numerous studies of the structure of the jets behind rocket engines in
the Uinted States have demonstrated, their radiation can be theoretically
calculated only approximately by breaking down the jet into a number of
isothermal zones with constant thermodynamic parameters. The intensity of
the radiation in each zone can be calculated quite precisely. Accordingly,
the problem of the theoretical calculation is broken down into two steps:
determination of the spectral intensity of the radiation in the zone with
defined values of the thermodynamic parameters and calculation of the
radiation of the jets presented in the form of a number of isothermal zones,
with the use of values obtained for the spectral density of the radiation
intensity for each zone. In the case of a jet that is uniform in composition
and uniform with respect to its invariant thermodynamic parameters in the
frequency band $\Delta\nu$, the magnitude of the radiation intensity will be [8.4].

$$I = \int_{(\Delta \nu)} I_\nu d\nu = \int_{(\Delta \nu)} I_{b\nu}(1 - e^{-k_\nu U}) d\nu, \tag{8.1}$$

where I_ν is the spectral radiation intensity of the spectral line at a frequency ν; k_ν is the absorption index of the gas; U is the mass of the absorbing gas; $I_{b\nu}$ is the spectral intensity of the radiation of an absolutely black body at a frequency ν.

When calculating the spectral intensity of the radiation of the jet, a model of the Alsasser bands with subsequent good modification [8.4] is of the greatest interest. In this model it is assumed that the position and the intensity of the lines with identical halfwidth of them are subject to probability laws. Accordingly, the spectral intensity of the radiation in some frequency range can be considered as the statistical mean. If the probability of the line distribution with mean intensity S_0 in some frequency range $\Delta \nu$ is described by the expression

$$P(S) = S_0^{-1} \exp(-S/S_o),$$

then for the dispersion loop the absorption index will be expressed as

$$k_\nu = \frac{S_0}{\pi} \frac{\nu}{(\nu - \nu_0)^2 + \gamma^2},$$

where γ is the halfwidth; ν_0 is the position of the center of the line. The application of the dispersion loop to calculate the lines in practical cases turns out to be highly valid. Considering the above-presented expressions it is possible to obtain the formula for the mean value of the spectral intensity

$$I = I_b \left\{ 1 - \exp\left[1 - \frac{S_0 U}{d\sqrt{1 + US_0/d}} \right] \right\}. \tag{8.2}$$

where di is the distance between lines, I is the total radiation of an absolutely black body in the investigated frequency range.

If the jet is sufficiently fine, that is, the condition $US_0/2\pi\gamma \gg 1$ is satisfied (the weak line), the magnitude of the spectral radiation intensity turns out to be

$$I = I_b US_0/d. \tag{8.3}$$

If the jet satisfies the condition $US_0/2\pi\gamma \gg 1$ with respect to thickness (strong line), then

$$I = I_b \Phi(\sqrt{U\gamma S_o/d}), \tag{8.4}$$

where $\Phi(x)$ is the probability integral.

For a nonuniform jet, that is, a jet which is a mixture of gases with variable thermodynamic parameters, the spectral intensity of the emission is calculated, as was pointed out above, by breakdown into n isothermal zones.

In this case the total spectral intensity of the emission of the entire jet with respect to all zones in the given direction turns out to be

$$I = \int_{\Delta\lambda} \left\{ \sum_{i=1}^{n} I_{b\lambda T_i} [1 - \tau_{i\lambda}] \prod_{h=0}^{i-1} \tau_{h\lambda} \right\} d\lambda, \tag{8.5}$$

where $I_{b\lambda T_i}$ is the spectral intensity of the radiation of the absolutely black body for the given wavelength λ and temperature T_i in the ith zone. $\tau_{i\lambda}$ is the spectral transmission coefficient of the gases for a wavelength λ in the given ith zone. The total amount of transmission with respect to all zones in the given direction is defined by the expression

$$\tau = \exp \left\{ \frac{\sum_{i=1}^{n} x_i \left[\frac{-\ln \tau_i}{f(x_i)} \right]^2}{\sum_{i=1}^{n} x_i \frac{-\ln \tau_i}{f(x_i)}} \right\} f \left\{ \frac{\left[\sum_{i=1}^{n} x_i \frac{-\ln \tau_i}{f(x_i)} \right]^2}{\sum_{i=1}^{n} x_i \left[\frac{-\ln \tau_i}{f(x_i)} \right]^2} \right\}, \tag{8.6}$$

where $f(x)$ is the Ladenburg-Reich function.

In the special case where $x_i < 0.2$; $f(x) \approx x = US/2\pi\gamma$, then

$$-\ln \tau \approx \left\{ \sum_{i=1}^{n} (-\ln \tau_i)^2 \right\}^{1/2} \tag{8.7}$$

and for all $x > 2$ the function $f(x)$ is approximately equal to $\sqrt{2x/\pi}$ and the equation (8.6) also assumes the form

$$-\ln \tau \approx \left\{ \sum_{i=1}^{n} (-\ln \tau_i)^2 \right\}^{1/2}. \tag{8.8}$$

The above-presented equations (8.5-8.8) permit sufficiently accurate calculation of the radiation of the jet if the pressure and temperature fields of the jet are known and also the spectral absorption or transmission coefficients.
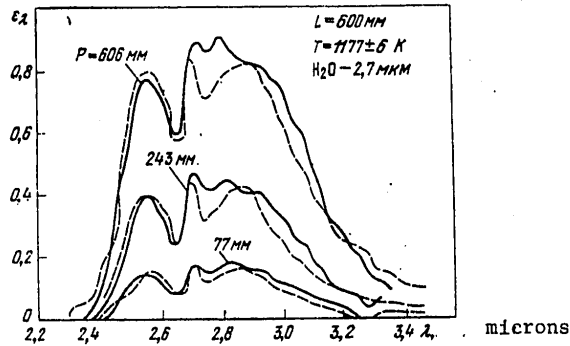
Figure 8.4. Spectral absorption capacity of water vapor in the
2.7 micron band as a function of wavelength.

The values of the absorption coefficients obtained in the special experi-
ments on the models of the J-2 engine agree well with the theoretical
values. In Table 8.2 the calculated and experimental values τ are presented
for water vapor (λ = 2.7 microns). The calculations are performed for the
two-zone model at different pressures in each zone and at a temperature of
1273°K. The optical thickness of each zone was 610 mm, X = 3.49, τ is the
mean value of the transmission coefficient with respect to two zones..

The relation is presented in Figure 8.4 for the spectral absorption capacity
ε_1 as function of wavelength in the range of λ = 2.7 microns. The dotted
line indicates the curves obtained by the calculations.

Table 8.2

Pressure, Pa		Measured spectral transmission coefficients			Calculated values of the equations	
P_1	P_2	τ_1	τ_2	$\overline{\tau}$	(8.6)	(8.8)
7 049	7 049	0,720	0,729	0,621	0,628	0,634
13 566	13 965	0,571	0,566	0,425	0,443	0,450
19 950	20 349	0,438	0,443	0,289	0,306	0,314
20 083	13 832	0,743	0,571	0,515	0,524	0,530
7 448	19 418	0,724	0,454	0,419	0,428	0,435

As a result of the laboratory experiments it was established that at high
temperatures the absorption coefficient of the water vapor is higher than
at room temperature. Thus, at 2,750°K the adsorption index k_λ is 40 percent
higher than room temperature for the 6.3 micron band and 15 percent higher
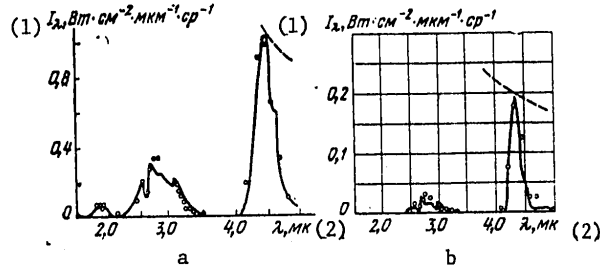for the 2.7 micron band.

202

Figure 8.5. Radiation spectra of the jet behind the F-1 model engine:
a--distance 15.2 mm; b--distance 250 mm; --measurement;
_____calculation; - - - curve for a black body (900°K).
Key: 1. I_λ, watts-cm^{-2}-micron^{-1}-steradians^{-1}
2. Microns

The theoretical calculation of the radiation spectra made for jets of the
F-1 and J-2 model engines using zone theory gives good agreement with the
experimentally obtained spectra of the corresponding jets. In Figure 8.5
the radiation spectra are presented for the jet behind the F-1 model
engine on the axis of the nozzle for two different distances from the
nozzle tip. The pressure when testing the model corresponded to an altitude
of 40 km. From comparing graphs a and b it is easy to see a decrease in the
emission peak by 2.7 microns on going away from the tip of the nozzle.
Analogous data are presented in [8.4] for the J-2 model engine.

When burning hydrocarbon fuels the main radiating components of the jet
behind the rocket are carbon dioxide, water and solid carbon particles.
The amount of carbon depends on the structural design of the chamber and
the composition of the mixture (the oxidizer-fuel consumption ratio). In
[8.4] relations are presented for the total emissivity as a function of
wavelength. In these calculations the gravimetric concentration of the
carbon was used which was determined from measuring the spectral emission
of the jet of the Atlas sustainer engine. For large optical thickness
characteristic of rockets of the Saturn class, the mission of the carbon
particles is more than half the radiation energy.

For the calculations, the emissivity of the carbon particles in the gas jet
of the rocket engine models operating on oxygen-kerosene RP-1 was measured.
By the measured spectral intensities and temperature, the spectral emissivity
of ε_λ of the mixture of gas with solid particles was determined. The pre-
sented values of the spectral absorption index k_λ multiplied by the gravi-
metric concentration of carbon particles in the flow ρ_c were found from
the expression

$$k_\lambda \rho_c = l^{-1}[-\ln(1-\varepsilon_\lambda) - k_{H_2O}U_{H_2O} - k_{CO_2}U_{CO_2}],$$

203

where U is the length of the optical path in the measured sample at normal temperatures considering pressure; ℓ is the path length, cm. In order to calculate the H_2O contribution, a statistical model of the band was used

$$k_{H_2O} U_{H_2O} = Uk(1 - Uk/4a)^{-1/2},$$

where k is the local absorption index averaged with respect to wavelengths, a is the term caused by averaging with respect to the fine structure of the band. The molar concentration of H_2O and CO_2 varies within the limits of 0.10-0.05 on variation of the ratio of the fuel compositions χ from 1.2 to 0.09, and $\chi = 2$, it was 0.3. The particle sizes were taken equal to 40 nm. In [8.4] relations are presented for $k_\lambda p_c$ a function of wavelengths for various temperatures with a geometric expansion of the nozzle equal to three.

The difficulties of the experimental investigation of the radiation of the rocket jets consists in the fact that the radiation characteristics of the jets vary with altitude. This leads to the necessity for using barochambers to simulate altitude. In the barochambers, as a result of the limited nature of their size, it is impossible to study rocket systems with large thrusts. Accordingly, in the United States broad use is made of the method of investigating the models of engines which are copies of real rocket engines which have been decreased to a fine field. However, in the closed volume of a barochamber, the pressure rises during the short period of the tests. In order to eliminate errors connected with this, spectrometers with high-speed scanning have been developed in the United States and are being successively used. An experimental study was jade of the jets of the F-1 and J-2 model engines fo the Saturn V booster rocket. Some characteristics of the models are presented in Table 8.3.

Table 8.3.

Component ratio	Engine	Gas temperature at the nozzel tip, °K	Diameter of the model, nozzle, mn	Scale of the model
2.25	F = 1	16 00	79	1:45
5.50	J = 2	1300	76	1:25

The measurements were performed through a saphire window transparent approximately to a wavelength of 7 microns in order to eliminate the distorting effect of the atmosphere, nitrogen filling of spectroradiometer was used. The pressure in the baro chamber corresponded to an altitude about 73 km for the J-2 engine and 10-67 km for the F-1 comparison with the measurements at the corresponding points of the het indicates that the remission of the H_2O bands with wavelentghs of 1.9 and 2.7 microns is more intense for the F-1 engine operating at higher temperatures. For the F-1 engine in the CO_2 emission band of 1.6-5 microns, the band with a wave length of 4.3 microns is the strongest.

FOR OFFICIAL USE ONLY

An experimental study was made of the variation of the spectral radiation
density with respect to length of the jet on a fixed wavelength of 4.3
microns on interaction of the hets of two closely arranged nozzles. The
spacing between the axes of the nozzles was approximately equal to one
and a half nozzle diameters. The spectral density of the radiation on the
axis of interaction of the two jets is appreciably greater (by approximately
three times) than the emission of each of the nozzles individually on the
same axis [8.4]. In the absence of interaction, the emission of the
carbon dioxide on the axis of the engine attenuates more sharply on going
away from the nozzle tip and on the axis of interaction of the jet. For
the zone of interaction of the jets the calculated data with respect to
spectral density of the radiation of the jet agree well with the ex-
perimental data is we assume that for an average of carbon particle radius
of 200 Å and a proportion of solid particles of 2 percent, the degree of
blackness on a wavelength of 2.2 microns is approximately 0.10.
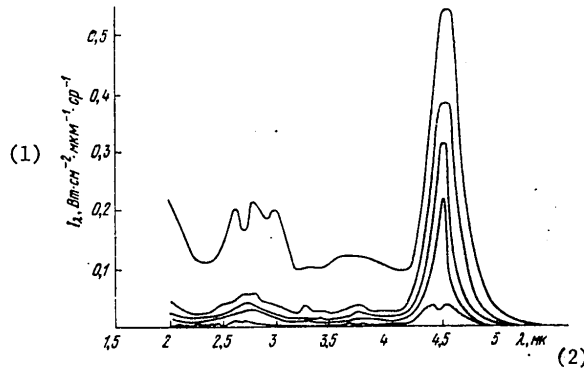

Figure 8.6. Spectral intensity of the radiation of a jet as a
function of wavelength for five types of solid-
propellent jet engines of the Saturn booster
rocket.

Key: 1. I_λ, watts-cm^{-2}-microns^{-1}-steradians^{-1}
2. λ, microns

Experimental studies were also performed in the United States with respect
to the radiation of the jets of the solid-propellent rocket engines [8.4]
In particular, the results have been published from measuring the spectral
radiation density of the jets of five auxiliary solid-propellent jet engines
of the Saturn booster rocket in the wavelength range of 1.6-5 microns. From
Figure 8.6 it is obvious that in the jet behind the solid-fuel engines, in
addition to the already investigated radiation bands of water vapor at 2.7
microns and carbon dioxide at 4.3 microns, there is a radiation band of
hydrogen chloride on a wavelength of 3.37 microns. As a result of

205
FOR OFFICIAL USE ONLY

FOR OFFICIAL USE ONLY

insufficient resolution of the spectrograph, the bands of carbon monoxide CO on a wavelength of 4.7 microns and carbon dioxide CO_2 on a wavelength of 4.3 microns did not differ. In addition to the emission bands caused by the gas components of the jet, in the spectrum of the jets a continuous radiation component of the solid particles is well noticeable. For the solid-propellent jet engine for the system of separating the first stage there is a high level of continuous radiation well-approximated by the radiation of a grey body with a degree of blackness of 0.03 at 1800°K.

Studies are also being made of the spectral composition of the radiation of the jets in the visible part of the spectrum of liquid and solid propellent engines. Some measurements were taken of the characteristics of the jets on the trajectory when ballistic missiles are launched from Cape Kennedy. During the measurements a spectral television camera was used with a spectral resolution of 1-2 nm operating in the waveband of 400-650 nm. The spectrum was photographed from the kinescope screen on 35-nm film. The intensity of the radiation of the spectral bands was determined by the degree of blackening of the photographic film. In this part of the spectrum, the continuous component of the radiation is well noted, on which the spectral bands of comparatively low intensity are superposed. The spectrum was obtained from the jet behind a rocket operating on oxygen and kerosene. The continuous component of the radiation of this jet is determined by the radiation of a black body with a temperature of about 2,000°K.
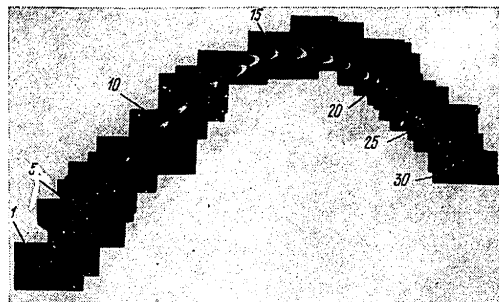
Figure 8.7. Variation of brightness and configuration of the jet during flight of a rocket.

By the movie films recording the flight of the rocket, it was possible to trace the dynamics of the development of the jet with an increase in altitude. Several interesting phenomena were noted. One of them includes the increase in brightness of the visible part of the jet when the rocket passes through the ozone layer at an altitude of 35-40 km. With a further increase flight altitude of the rocket, the brightness of the jet first decreases and then again increases somewhat. The variation of the observed brightness of the jet as a function of altitude is illustrated in Figure 8.7. The rocket

206
FOR OFFICIAL USE ONLY

jet was photographed from the Great Bahamas Islands during night launches
when the rocket trajectory was below the solar horizon. With an increase
in flight altitude, the shape of the visible part of the jet changes
sharply. Beginning with some altitude, the jet assumes a clearly expressed
crescent shape. A long radiating trail forms behind the jet. With a
further increase in flight altitude, the crescent-shaped jet again becomes
an ordinary glowing region.

The characteristics of the jet behind rocket engines in the United States
have also been investigated to determine the contamination of the optical
surfaces by the combustion products of jet fuels. A great deal of attention
has been given to the study of the angular distribution of the thermal
emission from the particles in the jet of a rocket engine in order to de-
termine their spectral emittance and also the scattering of the radiant
energy by them.

The investigation of the radiation characteristics of the jet behind the
rocket engine at high altitudes was performed in the United States not only
in the infrared part of the spectrum but also in the ultraviolet part. During
the course of the study of the ultraviolet radiation of artificial targets
in space in the United States, the OAO-2 orbital astronomical observatory
found application which was designed to observe heavenly bodies in the
vacuum ultraviolet region (100-400 nm) and has a platform with high orienta-
tion precision. Photometric measurements were made in bands near 298,
238, 192 and 150 nm. In the shortest wave band (150 nm), the signal from
the jet after the booster rocket did not exceed the noise level of the
system.

The creation in the United States of a three-stage, multipurpose Titan-3
C rocket required the solution of a number of complex problems, one of
which was the determination of the thermal emission of the jet of the zero
stage solid-propellent jet engine and the heating of the bottom part of
the stage. The development of rocket engines in accordance with the new
technical specifications for higher initial temperature at lauch has led
to a significant program with respect to volume and expense in firing testing
of liquid-propellent jet engines [8.5]. For a sufficiently accurate evalua-
tion of the effects of the jets and the subsequent development of the
corresponding means of heat protection of the liquid-propellent jet engines,
studies have been started with respect to estimating the radiant and
convective heating of the bottom part of the first stage of the rocket.
The tests run a barrow chamber demonstrated a significant decrease in
thermal emission of the jet behind the solid-propellent jet engines at
high altitudes. The average values of the incident heat flux determined
during firing tests were within the limits of 20.38 to 35.58 watts-cm^{-2}.
On injection of liquid into the engine nozzle, the average density of the
incident radiation flux increased by 61 percent. Taking this coefficient
as the criterion when designing the heat shielding of the bottom part of
the booster rocket, a value of the radiation flux density of the jet of
46 watts^{-2} was taken.

8.3. Satellites with Infrared Equipment for Detecting Rocket Launches and Nuclear Blasts

The problem of early detection of the launching of intercontinental ballastic missiles by the infrared emission of their engine jets from artificial earth satellites has been at the center of attention of the American military specialists in practice since the beginning of space engineering [1.3]. By using the MIDAS-IV satellite in October 1961, a specially launched TITAN rocket was dected at an altitude of 60 km 90 seconds after launching by the radiation of the engine jet. In 1965 the satellite development program for early detection of launches of ballastic missiles was reexamined, and the decision was made to create a multipurpose synchronous satellite which was to provide for [8.7] early detection of the launches of ballastic missiles and, in particular, missiles launched from submarines; it was to provide for the recording of nuclear blasts, the evaluation of the damage to targets from nuclear rocket weapons, the monitoring of the agreement to forbid nuclear tests, the observation of the entry of the nosecones of rockets into the atmosphere, the observation of the rocket stages in the passive part of the trajectory by the infrared radiation, and constant observation of the cloud cover.

The first multipurose satellite IMEWS (using the first letters of the English words "Intercontinental Multipurpose Early Warning Earth Satellite" program 647) was launched in the United on 6 November 1970 [8.8].

At the present time [8.11], three of the 647 satellites are in orbit near the earth carrying out the mission of early warning of the launching of intercontinental ballastic missiles. One of them was inserted at a point located above the Indian Ocean over the equator at approximately 65° east longitude. The other two are in the Western Hemisphere and record launches of ballastic missiles from submarines.

The overall length of a 647 satellite is 6.45 meters, and it is 2.7 meters in diameter and weighs about 1,130 kg. The basic equipment for detecting ballastic missile launches is infrared. On the satellite there is an infrared telescope of the Schmidt system with a diameter of the entrance opening of 0.9 meters. The axis of the telescope is directed at the earth's surface. In the Schmidt telescopes, the image is formed using a concave spherical mirror and a correcting aspherical lens at a distance of the radius of curvature in front it, one of the surfaces of which is flat, and the other is a complex surface of rotation. The Schmidt optical system is in practice free of all aberations, which permits creation of a camera with high speed and large field of view. The primary focal surface is in the middle between the correcting lens and the mirror and is a sphere which is concentric with the surface of the mirror. Its radius of curvature is equal to half the radius of curvature of the spherical mirror.

The infrared radiation from the engine jet passes through the correcting lens and is focused by the spherical mirror on a two-dimensional mosaic

of infrared receivers which has spherical shape, repeating the shape of the principal focal surface. Each of the receivers of this mosaic made of lead sulfide is covered with a narrow-band filter with maximum transmission on a wavelength of about 2.7 microns (according to other reports the infrared receivers are made up of 2,000 sensitive elements operating in the wavelength band of 3-5 microns with maximum spectral sensitivity on a wavelength on the order of 3.5 microns) [8.8]. Each elementary receiver of the mosaic corresponds on the surface of the earth to a section of the terrain with linear dimensions and a size of approximately 3.5 x 3.5 km, which for the standard orbit is approximately 10^{-3} x 10^{-3} radians or 3.5 x 3.5'.

It is stated [8.11], that the selection of the lead sulfide receivers having sufficient sensitivity with comparatively high temperature equal to 193°K made it possible to do away with the activity cooling system and use a passive radiatinon system which ensures high reliability of the infrared satellite system for an operating time measured in years. The optical axis of the telescope is shifted with respect to the longitudinal axis of the satellite around which the satellite turns slowly with an angular velocity on the order of 5-7 rpm. This provides for scanning of the mosaic of infrared receivers and increases the field of view of the telescope. The electronic equipment on board the satellite sees to the formation, amplification and quantization of the signal from each infrared receiver of the matrix and also multiplexing of the resultant signal in digital form for transmission over the telemetric channel simultaneously with the information from various other satellite systems. The threshold level of the detectors can be regulated by command from the earth.

The signals are received from the satellites by two ground stations. One of them is on Guam which is part of the system of American military bases, and the other in the central part of Australia near the city of Alice Springs. Information received from the 647 satellites is transmitted directly by these stations via the military communications satellites to the Joint Command Headquarters of the North American continent near Colorado Springs. The reception of the signals from the military communications satellites is accomplished by two American ground stations located near Denver [8.8-8.10].

The data coming to the ground station contains information for identification of each infrared receiver and the voltage of the output signal in digital form corresponding to the intensity of the infrared radiation. The information is processed at the ground stations almost in real time. The launch detection signal arrives no more than 90 seconds after the actual launching of a missile. The arrangement of the equipment on a satellite is presented in Figure 8.8 [8.9].

American specialists confirm [8.11] that on launching the first satellite in this series in 1971 more than 1,000 launches of intercontinental ballistic missiles and ballistic missiles from submarines by the United States, USSR, China and France were detected. In order to reduce the probability of

false alarms caused, for example, by such natural sources as forest fires, reflections for the upper edges of clouds, and so on, the onboard satellite system is equipped with logical circuits which provide for confirmation that the detected signal is an intercontinental ballistic missile launch based on analyzing the sequence of signals when scanning the mosaic. The analysis of the signal sequence in time also permits determination of the flight trajectory of the intercontinental ballistic missile and the proposed target area.
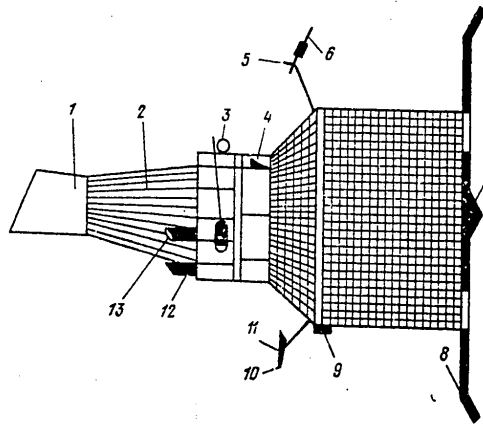

Figure 8.8. IMEWS satellite. 1--Solar shielding of the infrared detector; 2--Infrared detector telescope; 3--Stellar sensors of the orientation system; 4--Electronic equipment compartment; 5--Antenna used for transmission of data from the infrared detector to the earth; 6--Additional detectors for detecting nuclear blasts; 7--Basic detectors for detecting nuclear blasts; 8--Additional panels with solar elements (the basic ones are mounted on the side surface of the hull); 9--Engine module of the triaxial orientation system; 10--Antenna of the command system; 11--Antenna for transmitting data to the ground from the VLS television camera; 12--VLS television camera; 13--Solar tensor of the orientation system.

In the early articles devoted to the description of the series 647 satellites it was reported that in addition to the infrared receivers which are sensitive in the short infrared range, infrared detectors were installed on the satellite which operated in the 8-12 micron band (according to other reports 8-14 microns). These detectors were intended for tracking the slightly heated objects against the background of "cold" outer space. Primarily the warheads of ballistic missiles after separation of the last stage of the booster rocket are in the category of such targets [8.8-8.10]. However, in later papers [8.11] it is noted that the effort to use the longer wave

infrared receivers (8-14 microns) which would make it possible to track the intercontinental ballistic missile in the central part of the trajectory encountered difficulties connected with the necessity for using a system for cryogenic cooling of the sensitive elements of these receivers on the satellite which, in turn, is connected with the reliability of the equipment.

In the given phase the U.S. Air Force has ordered a total of 13 of the series 647 satellites. A large amount of work is being done to ensure noiseproofness of the equipment on board the satellite. In particular, on the new satellites of these series it is proposed that silicon receivers be installed which can detect a laser beam aimed at the satellite and provide timely response of a shutter to protect its optical system.

In addition to the infrared equipment, proton and x-radiation sensors have been installed on the satellite which will make it possible to record nuclear blasts [8.11].

In 1976 the U.S. Air Force had at its disposal six satellites for subsequent launches. At the present time the possibility of improving the characteristics of the manufactured, but as yet unlaunched satellites is being considered. During the modification process it is proposed that the satellites will be provided with protection against antisatellite defense means, the effects of laser radiation and a decrease in detection time. In particular, the possibility of replacing the infrared detectors made of lead sulfide by detectors made of cadmium telluride alloys of mercury and also replacement of the electronic system for processing the signals from the infrared detectors by an improved one is being considered.

In addition to the modification of the already manufactured satellites, a study is being made of the possibility of creating improved satellites which could in the next decade replace the IMEWS satellites [8.12].

On the improved satellites it is proposed that "monolithic" detectors of mosaic structure be installed. The use of the new mosaic photoreceiver will permit elimination of scanning, continuous observation of the entire controlled zone, recording of the variation and intensity of the radiation sources, more exact prediction of the flight trajectory of intercontinental ballastic missiles. In the nonscanning instruments it is possible significantly to attenuate the effect of the background by selecting invariant and stationary radiation sources, to ensure recording of brief phenomena which can be missed by a scanning instrument, to improve the recognizability of the targets by analyzing the variation in intensity of the radiation with time. For the improved satellite it is proposed that significant redundancy of the onboard systems be used along with the possibility of transmitting the information through radio relay satellites. In addition, effective measures must be provided to defend the improved satellites against antisatellite defense systems.

FOR OFFICIAL USE ONLY

BIBLIOGRAPHY

1.1. Glushko, V. P. RAZVITIYE RAKETOSTROYENIYA I KOSMONAVTIKI V SSSR
(Development of Rocket Construction and Cosmonautics in the USSR),
Moscow, Mir, 1973.

1.2. Hudson, R. INFRAKRASNYYE SISTEMY (Infrared Systems), Moscow, Mir,
1972.

1.3. Safronov, Yu. P., Andrianov, Yu. G., and Iyevlev, D. S. INFRAKRASNAYA
TEKHNIKA V KOSMOSE (Infrared Engineering in Space), Moscow,
Voyenizdat, 1963.

1.4. Kats, Ya. G., Ryabukhin, A. G., and Trofimov, D. M. KOSMICHESKIYE METODY
V GEOLOGII (Space Methods in Geology), Moscow, MGY, 1976.

1.5. Andronov, I. "V otlichiye ot prezhnikh" (In Contrast to the Past),
PRAVDA, 11 September 1977.

1.6. "Ispol'zovaniye kosmicheskoy tekhniki v prikladnykh tselyakh (Use of
Space Engineering for Applied Purposes," ITOGI HAUKI I TEKHNIKI SER.
RAKETOSTROYENYYE (Results of Science and Engineering. Rocke Building
Series), VINITI, Moscow, Vol 4, 1974.

1.7. AVIATION WEEK, Vol 105, No 7, 1976, pp 50-52.

1.8. AVIATION WEEK, Vol 103, No 23, 1975, pp 44-47.

1.9. JOURN. OF SPACECRAFT AND ROCKETS, Vol 12, No 7, 1975, pp 402-403.

1.10. Avduyevskiy V., Kondratyev, K., Bol'shakov, V. "Salyut-5--Results
of Work in Orbit," PRAVDA, 19 October 1977.

1.11 AVIATION WEEK, Vol 102, No 23, 1975, pp 47-49, Vol 103, No 10, 1976,
pp 38-42; Vol 105, No 4, 1976, p 16.

1.12 "Transport Space Ssytem," ITOGI NAUKI I TEKHNIKI SER. RAKETOSTRONIYE
VINITI, Moscwo, 1976, p 7.

1.13. Witteborn F. C., Young L. S. A cooled infrared telescope for space
shuttle--the Spacelab infrared telescope facility (SIRTF). AIAA
Paper, No 174, 1976, p 11.

1.14. Kruger, R. "A contamination experiment investigating the failure of
the Nimbus 4 filert wedge spectrometer," SPACE SIMUL. PROC. SYMP.,
New York, 1972.

1.15. Clancy, H. M. "Vacuum stability testing of Apollo 15 Scientific In-
strument Module (SIM) nonmetallic materials and revision of silicon
rubber in motor switch," SPACE SIMUL. PROC. SYMP. New York, 1972.

FOR OFFICIAL USE ONLY

1.17. Slemp, W. S., Hankincon, T. W. E. "Environmental studies of thermal control coating for lunar orbiting," AIAA PAPER, No 792, 1968.

1.18. Heaney, J. B., "Results from the ATS-3 reflectometer experiment," THERMPHYS.: APPL. THERM. DES. SPACECRAFT, New York-London, 1970, pp 249-274.

1.19. Crow, R. B., "Lamp and photoresistor adjust loop bandwidth automatically," ELECTRON. DESIGN., Vol 16, No 23, 1968.

1.20. Lankes, L. R., "The role of optics in the Apollo," OPT. SPECTRA, Vol 3, No 5, 1969.

2.1. "Third Soviet Space Rocket," PRAVDA, 27 October 1959.

2.2. "First Flight to Venus," PRAVDA, 26 February 1961.

2.3. "First Manned Flight in Space," PRAVDA, 15 April 1961.

2.4. "First Flight to Mars, PRAVDA, 15 December 1962.

2.5. Andrianov, Yu. G., Karavayev, I. I., Safronov, Yu. P., Tulupov, V. I., INFRAKRASNYYE SPEKTRY IZLUCHENIYA ZEMLI V KOSMOS (Infrared Radiation Spectra of the Earth in Space), Moscow Sov. radio, 1973.

2.6. Lebedinskiy, A. I., et al, "Meteorological Interpretation of the Spectra of Outgoing Radiation Recorded from the Kosmos Satellites," GEOMAGNITIZM I AERONOMIYA (Geomagnetism and Aeronomy), Vol 8, No 1, 1968.

2.7. Coldric, J. R. "Optical sensors for spacecraft attitude determination," OPTICAL AND LASER TECHNOLOGY, Vol 4, No 3, 1972.

2.8. Anderson, R. N., "An advanced horizon sensor for synchronous altitude 3-axis stabilized satellites," COMMUNS. SATELLITE 70'S TECHNOLOGY, Cambridge, 1971.

2.9. RABOVSKIY, A. Ye., "Physical Parameters of the Radiation of Heavenly Bodies and the Opticoelectronic Devices for Determining the Orientation of Spacecraft," ITOGI NAUKI I TEKHNIKI. SER. ISSLEDOVANIYE KOS-MICHESKOGO PROSTRANSTVA, VINITI, Moscow, 1973 p 3.

2.10. US Patent No 3360638, Knight, S. A., "Apparatus for tracking an infra-red radiation gradient and readout means therefor" (S. A. Knight, kl. 235-150).

2.11. Stanley, C. V., Dixon, T. P., "Horizon scanner has no rotating members," ELECTRONICS, 1961, No 2, Vol 34.

FOR OFFICIAL USE ONLY

2.12. Pavlov, A. V., Permyakov, Y. D., "Estimating the Accuracy of the
Methods of Constructing the Local Vertical Based on Using the
Infrared Radiation of the Earth," KOSMICHESKIYE ISLEDOVANIYA
(Space Research), Vol 10, No 4, 1972.

2.13. Weiss, R., "Conical scan CO_2 horizon sensing orbit accuracy and
horizontal noise model," AIAA PAPER, No 1021, 1970.

2.14. PLANET AND SPACE, No 3, 1961, pp 249-261.

2.15. Flander, I. H., Frasser, D. C., Lawston, L. R., "Technology for
guidance and navigation of unmanned deep space mission in the
1970's," AIAA 5TH ANNUAL MEETING AND TECH. DISPLAY, AIAA PAPER,
No 1104, 1968.

2.16. BRUNS, A. V., "Multislip Shadow Sensor of the Direction of a Luminous
Target," APPARATURA DLYA KOSMICHESKIKH ISSLEDOVANIY (Some Space
Research Equipment), Moscow, Nauka, 1972.

2.17. Andrianov, Yu. G., "Some Characteristic Features of Photoelements
Having Longitudinal Photoeffect," SVETOTEKHNIKA (Light Engineering),
No 7, 1968.

3.1. Ely, E. B., "Spectral radiance of sky and terrain at wavelength between
1 and 20 microns. II Sky measurements," J. OPT. SOC. AM., Vol 50,
No 12, 1960.

3.2. Krasovskiy V. I., "Study of the Infrared Radiation of the Night
Sky," UFN (Progress of the Physical Sciences), Vol 47, No 4, 1952.

3.3. Moroz, V. I., "Infrared Spectrum of the Night Sky 3.4 Microns,"
ASTRONOMICHESKIY ZHURNAL (Astronomy Journal), Vol 37, No 1, 1960.

3.4. Ginsourg, N., "Measurements with a spectral roadiometer," J. OPT.
SOC. AM., Vol 50, No 12, 1960.

3.5. ATMOSFERIY ZEMLI I DRUGIKH PLANET (Atmospheres of the Earth and
Other Planets), a collection of articles edited by D. P. Koyper,
Moscow, IL, 1951.

3.6. Moroz, V. I., "Infrared Spectra of Jupiter and Saturn," ASTRONOMICHESKIY
ZHURNAL, Vol 38, No 6, 1961.

3.7. "Differences between proposed Apollo sites," J. GEOPHYS. RES., Vol 74,
No 17, pt. 1/V. C. Murray.

3.8. "Differences between proposed Apollo sites," J. GEOPHYS. RES.,
Vol 74, No 17, 1969, pt. 2/T. B. McCord.

FOR OFFICIAL USE ONLY

3.9. McNutt, D. P., Shianandan, K., Feldman, P. D., "Rocket messurement of the far infrared sky background," NATUR PHYS. SCI., Vol 234, No 45, 1971.

3.10. Blair, A. G., "Measurement of the far infrared background radiation in the night sky," PHYS. REV. LETT., Vol 27, No 17, 1971.

3.11. Davies, M. E., Murray, B. C., VIEW FROM SPACE, New York-London, 1971.

3.12. "Discovering the Secrets of the Universe," PRAVDA, 17 December 1971.

3.13. Herr, K. C., Forney, P. B., Pimentel, G. C., "Mariner Mars 1969 Infrared Spectrometer," APPL. OPT., Vol 11, No 3, 1972.

3.14. Kondrat'yev, K. Ya., Bunakova, A. M., METEOROLOGIYA MARSA (Meteorology of Mars), Leningrad Gidrometeoizdat, 1973.

3.15. Chase, S. C., "Infrared radiometer for the 1969 Mariner mission to Mars," APPL. OPT., Vol 8, No 3, 1969.

3.16. Neugebauer, G., "Mariner 1969 infrared radiometer and thermal properties of the martian surface," ASTRON. J., Vol 76, No 8, 1971.

3.17. "Mars: Complex Research," PRAVDA, 19 December 1971.

3.18. "Infrared spectroscope experiment on the Mariner 9 mission: preliminary results," SCIENCE, Vol 175, No 4019, 1972.

3.19. "Infrared radiometry experiment on Mariner (," SCIENCE, Vol 175, No. 4019, 1972.

3.20. Kieffer, H. K., "Infrared thermal mapping experiment: The Viking Mars orbiter," ICARUS, Vol 16, 1972.

3.21. Farmer, C. B., La Porte D. D., "The detection and mapping of water vapor in the martian atmosphere," ICARUS, Vol 16, 1972.

3.22. Avduevskiy, V., et al, "Outstanding progress in Soviet cosmonautics," PRAVDA, 21 February 1976.

3.23 Markov, M. N., et al, INFRAKRASNAYA SPEKTROSKOPIYA LYNY S ORBITAL'NOY STANTSII "SALYUT-4" (Infrared Spectroscopy of the Moon from the Salyut-4 Orbital Station) Moscow, Fiz. in-t AN SSSR, 1976.

3.24. Ksanfomaliti, L. V., et al, INFRAKRASNOYE IZLUCHENIYE OBLAKOV VENERY (Infrared Radiation of the Clouds of Venus), In-t kosm. issled. AN SSSR, Moscow, 1976.

FOR OFFICIAL USE ONLY

3.25. AVIATION WEEK, Vol 105, No 15, 1976, p 26.

3.26. Izakov, M. N., Krasitskiy, O. P., "Model of the Composition of the Martian Atmosphere," KOSMICHESKIYE ISSLEDOVANIYA (Space Research), volume XV, No 3.

3.27. Markov, M. N., et al, "Infrared Telescope-spectrometer of the Salyut-4 Station," PRIBORY I TEXHNIKA EKSPERIMENTA (Experimental Instruments and Equipment), No 4, 1976.

3.29. Markov, M. N., et al, "Infrared spectra of regulite by measurements from the "SALYUT-4 orbital station," KOSMICHESKIYE ISSLEDOVANIYA, Vol XV, No 3, 1977.

3.30. Moroz, V. I., FIZIKA PLANET (Planetary Physics), Moscow, Nauka, 1967.

4.1. NAUCHNOYE ISPOL'ZOZANIYE IS3 (Scientific Use of Artificial Earth Satellites), collection of articles Moscow, IL, 1960.

4.2. Soren, W., et al, "Camera Designed for Photography of Artificial Satellites," PHOTOGR. SCIENCE AND ENG., Vol 6, No 6, 1962.

4.3. INZHENERNYY SPRAVOCHNIK PO KOSMICHESKOY TEKHNIKE (Engineering Handbook on Space Engineering), Moscow, Voyeniizdat, 1977.

4.4 Aleksandrov, S. G., Fedorov, R. Ye. SOVETSKIYE SPUTNIKI I KOS-MICHESKIYE KORABLI (Soviet Satellites and Space Craft) Moscow, AN SSSR, 1962.

4.5. "ELECTRONICS," Vol 50, No 1, 1977, p 34, 36.

4.6. Favorskiy, O. N., Kadeaner, Ya. S., VOPROSY TEPLOBMENA V KOSMOSE (Problems of Heat Exchange in Space), Moscow Vysshaya shkola, 1967.

4.7. Hudson, R., INFRAKRASNYYE SISTEMY (Infrared Systems), Moscow, Mir, 1972.

4.8. SPACE WORKD, Vol L-3-135, 1975, p 32.

4.9. "Use of Space Engineering for Applied Purposes," ITOGI NAUKI I TEKHNIKI. SER. RAKETOSTROYENIYE, VINITI, Moscow, Vol 4, 1974.

4.10. Hall, F. E., Stanley, C. V., "infrared satellite radiometry," APPL. OPT., vol 1, No 97, 1962.

4.11. Swift, I. H., "Performance of background-limited systems for space use," INFRARED PHYS., Vol 2, No 19, 1962.

4.12. AVIATION WEEK, Vol 102, No 16, 1975, pp 18-20.

4.13. AVIATION WEEK, Vol 106, No 6, 1977, p 22.

4.14. AVIATION WEEK, Vol 106, No 7, 1977, p 9.

4.15. AIR ET COSMOS, Vol 14, No 617, 1976, pp 32-33.

4.16. AVIATION WEEK, Vol 105, No 12, 1976, pp 42-51.

4.17. SPACE AERONAUTICS, Vol 51, No 6, 1969, p 44.

4.18. AVIATION WEEK, Vol 96, No 18, 1972, p 27.

4.19. AVIATION WEEK, Vol 94, No 10, 1971, p 25.

4.20. AVIATION WEEK, Vol 90, No 18, 1969, p 19.

4.21. AVIATION WEEK, Vol 105, No 10, 1976, pp 30-34.

4.22. AVIATION WEEK, Vol 102, No 9, 1975, p 9.

4.23. AVIATION WEEK, Vol 106, No 4, 1977, p 19.

4.24. AVIATION WEEK, Vol 106, No 13, 1977, p 54.

4.25. Ammon G., Russel, S. R., "A laser tracking and ranging system,"
      APPL. OPT., Vol No 10, 1970.

4.26. Yusson, Zh., "Laser Experiment on the Lunokhod-1," ZEMLYA I VSELENNAYA
      (Earth and Universe), No 2, 1972.

4.27. Rosch, J., "Laser Measurements of the Earth-Moon Distances,"
      MOON, Vol 3, No 4, 1972.

4.28. AEROSPACE DAILY, Vol 76, No 33, 1975, pp 260-261.

4.29. AVIATION WEEK, Vol 102, No 9, 1975, pp 36-43.

4.30. PRAVDA, 20 August 1977.

4.31. Moss, S. J., Johnson, T. S., "Performance of the NASA Laser System
      in Satellite Tracking, IEEE TRANS., Vol GE-9, No 1, 1971.

4.32. Navara P., "The Laser Satellite Range Measurement of Ondrejow
      Observatory," STUDIA GEOPHYS. ET GEOD., Vol 15, No 3, 1971, p 4.

4.33. Pikus, I. M., "The Remote Measurement of Nitric Oxide from an Airplane
      or Space Platform, J. SPACECRAFT AND ROCK, Vol 10, No 3, 1971.

4.34. "2 kw cw Laser Radar Being Developed," MICROWAVES, Vol 11, No 10, 1972,
      p 14.

5.1. Kondrat'yev, K. Ya., KOSMICHESKAYA METEOROLOGIYA (Space Meteorology), Leningrad, Znaniye, 1966.

5.2. INZHENERNIY SPRAVOCHNIK PO KOSMICHESKOY TEKHNIKE (Engineering Handbook on Space Engineering), Edited by A. V. Solodov, Moscow, Voyenizdat, 1969.

5.3. Kondrat'yev, K. Ya., METEOROLOGICHESKIYE ISSLEDOVANIYA S POMOSHCH'YU RAKET I SPUTNIKOV (Meteorological Research Using Rockets and Satellites), Leningrad, Gidrometeoizdat, 1962.

5.4. "Round Up on Tiros 1," ASTRONAUTICS, Vol 5, No 2, 1960.

5.5. "Tiros Presages Long-Range Forecast," MISSILES AND ROCK., Vol 6, No 14, 1960.

5.6. Bandeen, W. R., and Manger, W. P., "Angular Motion of the Spin Axis of the Tiros I Meteorological Satellite to Magnetic and Gravitational Tourques," J. GEOPHYS. RES., Vol 65, No 9, 1960.

5.7. Kondrat'yev, K. Ya., LUCHISTYY TEPLOOBMEN V ATMOSFERE (Radiant Heat Exchange in the Atmosphere), Leningrad, Gidrometeoizdat, 1956.

5.8. HANDBOOK OF GEOPHYSIC., The McMillan Comp., New York, 1960.

5.9. Kaplan, L. D., "Inference of Atmospheric Structure from Remote Radiation Measurements, JOSA, Vol 49, No 10, 1959.

5.10. Kaplan, L. D., Spectroscope as Tool for Atmospheric Sounding by Satellites," FALL INSTRUM. AUTOM. CONF., Instr. Soc. Am., New York, Sept. 1960.

5.11. Kaplan, L. D., "Practicability of Stratospheric Sounding From Satellites," JUGG XII-TH GENERAL ASSEMBLY, Helsinki, 1960.

5.12. Wark, Q., "On Indirect Soundings of the Stratospheres from Satellites," J. GEOPHYS. RES., Vol 66, No 1, 1961.

5.13. Houghton, J. T., "The Meteorological Significance of Remote Measurements of Infrared Emission from Atmosphere Carbon Dioxide," QUART. J. R. MET. SOC., Vol 87, No 371, 1961.

5.14. Wexler, R., "Satellite Observations of Infrared Radiation," GEOPHYS. RES. DIRECT., CONTR. No AF19(604), 5968, 30 June, 1960.

5.15. Dreyfus, M. G., Hilleary, D. T., "Satellite Infrared Spectrometer," AEROSPACE ENG., Vol 21, No 22, 1962.

5.16. Jerome, C.; Thomas, John, R.; Weagant, Robert A., "Nimbus Limb Radiometer. Apollo Fin Sun Sensor and Skylab Multispectral Scanner," APPL. Opt., Vol 11, No 10, 1972.

5.17. Hanel, R. A.; Schlachman, B.; Clark, C,,Prolesh, H.; Taylor, J. B.; Wilson, W. M.; Channey, L., "The Nimbus 3 Michelson Interferometer," APPL. OPT., Vol 9, No 8, 1970.

5.18. Hanel, R. A.; Schlachman, B.; Rogers, D.; Vanoys, D., "Nimbus 4 Michelson Interferometer," APPL. OPT., Vol 10, No 6, 1970.

5.19. STAR, No 10, 1972, p 1352.

5.20. STAR, No 19, 1972, p 2549.

5.21. STAR, No 9, 1972, p 1195.

5.22. Taylor, F. W.; Houghton, J. T.; Peskett, G. D.; Rodgers, D. C.; Williamson, E. J., "Radiometer for Remote Sounding of the Upper Atmosphere," APPL. OPT., Vol 11, No 1, 1972.

5.23. Fink, D. E., "Budget Cuts Will Slow Pace of Space Shuttle Program," AVIATION WEEK, Vol 98, No 3, 1973.

5.24. "Nimbus Sensor Fails Skylab Checks," AVIATION WEEK, Vol 98, No 3, 1973.

5.25. ISSLEDOVANIYE KOSMICHESKOGO PROSTRANSTVA (Investigation of Outer Space), VINITI, 1972, Ref. I 8. 62. 254. p 34.

5.26. BULLETIN OF AMER. METEOROLOGICAL SOCIETY, Vol 53, No 6, 1972.

5.27. "Composition of Onboard Equipment for the Nimbus-3 Satellite," VOPROSY RAKETNOY TEKHNIKI (Problems of Rocket Engineering), No 10, 1969.

5.28. DESIGN NEWS, Vol 29, 1973, p 19.

5.29. AEROSPACE DAILY, No 21, 1971, p 165.

5.30. FLIGHT, Vol 100, No 3277, 1971, p 1049.

5.31 STAR, No 8, 1972, p 1041.

5.32. AVIATION WEEK, Vol 98, No 3, 1973, p 18.

5.33. Malkevich, M. S., OPTICHESKIYE ISSLEDOVANIYA ATMOSFERY SO SPUTNIKOV (Optical Studies of the Atmosphere from Satellites), Moscow, Nauka, 1973.

5.34. STAR, No 4, 1973, p 441.

6.1. Safronov, Yu. P., Tikhomirov, I. N., Ul'yanov, G. I., RASPOZNAYUSHIYE
USTROYSTVA (Recognition Devices), Moscow, Voyenizdat, 1970.

6.2. Barabash, Yu. L.; Varskiy, B. V.; Zinov'yev, V. T., et al, VOPROSY
STATISTICHESKOY TEORII RASPOZNAVANIYA (Problems of Statistical
Recognition Theory), Edited by B. V. Varskiy, Moscow, Sov radio, 1967.

6.3. Venttsel', Ye. S., TEORIYA VEROYATNOSTEY (Probability Theory), Moscow,
Fizmatgiz, 1962.

6.4. Krinov, Ye. L., SPEKTRAL'NAYA OTRAZHATEL'NAYA SPOSOBNOST' PRIRODNYKH
OBRAZOVANIY (Spectral Reflectivity of Natural Formations), AN SSSR,
Moscow-Leningrad, 1974.

6.5. Hovix, W. A.; Blaine, L. R.; Forman, M. L., "Infrared Reflectance of
High Altitude Clouds," APPL. OPT., Vol 9, No 3, 1970.

6.6. Plummer W. T., "Near Infrared Reflection Spectra of Artificial
Cumulus Clouds," APPL. OPT., Vol 8, No 10, 1969.

6.7. Myers, V. J., Allen, W. A., "Electrooptical Remote Sensing Methods
as Nondestructive Testing and Measuring Techniques in Agriculture,"
APPL. OPT., Vol 7, No 9, 1968.

6.8. "The Application of Pattern Recognition Techniques for Remote Sensing
Problem," 7TH SYMP. ON ADAPTIVE PROCESSES. UNIV. OF CAL., Los-Angles,
1968.

6.9. Coulson, K. L., "Effects of Reflection Properties of Natural Surfaces
in Aerial Reconnaissance," APPL. OPT., Vol 5, No 6, 1966.

6.10. AGRICULTURAL STATISTICS, U. S. Dept. of Agriculture, Washington, D.C.,
U. S. Govt. Printing Office, 1968.

6.11. Fu, K. S.; Landgrebe, D. A.; Phillips, T. L., "Information Processing
of Remotely Sensed Agricultural Data, " PROC. IEEE, Vol 59, No 4, 1969,
pp 300-315.

6.12. Marill, T. Green, "On the Effectiveness of Receptors in Recognition
Systems," IEEE TRANS., Vol IT-9, 1963, pp 11-17.

6.13. Guzhov, S. S., KAK ISHCHUT I DOBYVAYUT NEFT' I GAZ (How Oil and Gas
Are Found and Extracted), Moscow, Nedra, 1973.

6.14. Verbitskiy, V. A., "Infrared Radiometer for Geological Mapping,"
PRIBOROSTROYENIYE (Instrument Making), No 3, 1972.

6.15. Zaytsev, A. L., "Experimental 24-Channel System for Scanning the
      Earth's Surface," ZARUBEZHNAYA RADIOELEKTRONIKA (Foreign Radio
      Electronics), No 6, 1972.

6.16. Safronov, Yu. P., "Satellite Detects Forest Fires," LESNAYA PROMY-
      SHLENNOST' (Lumber Industry), No 4, 1973.

6.17. INTERNATIONAL AEROSPACE ABSTRACTS, Vol 10, No 18, 1970, Ref. A-70-
      36669.

6.18. Safronov, Yu. P., "Space Fire," LESNAYA PROMYSHLENNOST', 20 June, 1973,
      p 4.

6.19. Artsybashev, Ye. S., Mel'nikov, V. G., Shilin, B. V., "Infrared Aerial
      Photography of Forest Fires from High-Altitude Aircraft and Artificial
      Earth Satellites," LESNOYE KHOZYAYSTVA (Forestry), No 5, 1971.

6.20. Sotnik, Yu., "Elements Against Elements," NAUKA I ZHIZN' (Science and
      Life), No 3, 1971.

6.21. "Satellite Photographs Forest Fire Outbreak," AVIATION WEEK AND TECHN.,
      Vol 99, No 11, 1973.

6.22. "Sensor System Maintains Watch on Earth's Health," SPACE WORRLD, Vol
      J-2-110, 1973.

6.23. "Skylab S-192 Multispectral Scanner," SPACE WORLD, Vol J-3-111, 1973.

6.24. "Some 106 Principal Investigators Have Been Selected," INTERVIA,
      Vol 27, No 10, 1972, pp 1070-1071.

6.25. Artsybashev, Ye. S.; Safronov, Yu. P., "Study of the Infrared Radiation
      of Forest Fire Models," LESNOYE KHOZYAYSTVO, No 10, 1974.

7.1. Kraemer, A. R.; Cooke, C. R., "Optical Communication in Space," PROC. NAT.
      AEROSPACE ELECTRON. CONF., Dayton, Ohio, 1970, p 205-412.

7.2. "Laser Communications," PRIMENENIYA LAZEROV (Applications of Lasers),
      Moscow, Mir, 1974, p 318-402.

7.3. Pratt, V. K., LAZERNYYE SISTEMY SVYAZI (Laser Communication Systems),
      Moscow, Svyaz', 1972.

7.4. Elson, B. M., "Wideband Laser Link Test Planned," AVIATION WEEK, Vol 92,
      No 22, 1970.

7.5. McElroy, J. H. et al, "CO_2 Laser Communication Systems for Near-Earth
      Space Applications," PR. IEEE, Vol 65, No 2, 1977, p 221-255.

FOR OFFICIAL USE ONLY

7.6. Ross, M., "Jupiter Calling," LASER FOCUS, 1969, Vol 5, No 19, pp 32-38.

7.7. Foster, D. C., et al, "Wideband Laser Communication in Space, IEEE J. pt 2, 1972, v. QE-8, No 2, pp 263-272.

7.8. Sheremet'yev, A. G.; Tolparev, R. G., LAZERNAYA SVYAZ' (Laser Communications), Moscow, Svyaz', 1974.

7.9. Gudvin, F. Ye., "Operating Laser Communications Systems," TIIER, Vol 58, No 10, 1970, pp 365-372.

7.10. AEROSPACE DAILY, Vol 79, No 4, 1976, pp 25-26.

7.11. "Mars-to-Earth TV on a Laser Beam is now Feasible," INSTRUMENT NEWS: THE PERKIN-ELMER CORPORATION, Vol 19, No 3, 1969.

7.12. "Mars-Earth TV Link Possible with CO_2 Laser," PROC. DES. ENG., Vol 9, Aug, 1970, p 7.

8.1. DEYSTVIYE YADERNOGO ORUZHIYA (Effect of Nuclear Weaponry), translated from the English, Moscow, Voyenizdat, 1963.

8.2. ATOMNOYE ORUZHIYE (Nuclear Weapons), collection of articles, Moscow, Voyenizdat, 1955.

8.3. Ivanov, A,; Naumenko, I.; Pavlov, M. RAKETNO-YADERNOYE ORUZHIYE I EGO PORAZHAYUSHCHEYE DEYSTVIYE (Nuclear Missile Weapons and their Destructive Effect), Moscow, Voyenizdat, 1971.

8.4. "Investigation of the Radiation of Rocket Jets," VOPROSY RAKETNOY. TEKHNIKI (Problems of Rocket Engineering), No 10, 1969, pp 4-14.

8.5. "Thermal Radiation of the Jet Behind Solid-Fuel Jet Engines of the Titan-3C Booster Rocket," VOPROSY RAKETNOY TEKHNIKI (Problems of Rocket Engineering), No 2, 1971, pp 12-24.

8.6. "Study of the Rocket Jets by Optical Means," VOPROSY RAKETNOY TEKHNIKI, No 11, 1971, p 96.

8.7. Safronov, Yu. P., Sukhanov, Ya. A., "Samos, Midas, and So On," KRASNAYA ZVEZDA (Red Star), 26 October, 1972, p 3.

8.8 AVIATION WEEK, Vol 96, No 12, 1971, p 18.

8.9. AVIATION WEEK, Vol 95, No 12, 1971, p 19.

8.10. AVIATION WEEK, Vol 95, No 22, 1971, p 257.

8.11. AVIATION WEEK, Vol 101, No 2, 1974, pp 16-18.

8.12. AVIATION WEEK, Vol 105, No 2, 1976, pp 17-18.

10845
CSO: 8144/1744   END